Investigation of the Electrochemical Behavior of Catechol in Presence of Glycine, Aspartic acid and Glutamic acid

by

Md. Nazim Uddin

A thesis submitted in partial fulfillment of the requirements for the degree of

Master of Science in Chemistry

Khulna University of Engineering & Technology

Khulna 9203, Bangladesh.

July 2016

Declaration

This is to certify that the thesis work entitled "Investigation of the Electrochemical Behavior of Catechol in Presence of Glycine, Aspartic acid and Glutamic acid" has been carried out by Md. Nazim Uddin in the Department of Chemistry, Khulna University of Engineering & Technology, Khulna, Bangladesh. The above thesis work has not been submitted anywhere for the award of any degree or diploma.

Signature of Supervisor

Signature of Candidate

Acknowledgements

The author is extremely indebted to the Almightily Allah for the successful completion of the research work and the preparation of this dissertation.

The author expresses his deepest sense of gratitude and indebtedness to his respective and honorable supervisor **Dr. Md. Abdul Motin**, Professor and Head, Department of Chemistry, Khulna University of Engineering & Technology, Khulna for providing me the opportunity of working under his kind supervision. He had helped me at each and every point of the thesis work with his dedication, comments, suggestions and guidance which put me on the right path to fulfill the requirement, without which this situation was impossible to overcome. I learnt a lot of things from him, not only the academic knowledge, but also the way of research. This will be precious wealth in all my future academic life. Our communication is always flexible and efficient. He also friendly supported me a lot in my daily life which I am truly comprehended.

Again the author bestows thanks to his respective teacher **Md. Abdul Hafiz Mia**, Lecturer, Department of Chemistry, Khulna University of Engineering & Technology, Khulna for his lucid cooperation and necessary advice during the period of study.

The author wishes to offer deepest appreciation to all his friends and well-wishers especially **Palash Kumar Dhar** and **Md. Alim Uddin** for their continuous support and help.

The author feels proud to express his sincere appreciation and indebtedness to his parents, family members who always blessed, inspired and sacrificed a lot in the long process of building his academic career which can never be repaid.

Md. Nazim Uddin

Abstract

To monitor the electrochemical behavior of Catechol in presence of Glycine, L-Aspartic acid and L-Glutamic acid; cyclic voltammetry (CV), differential pulse voltammetry (DPV), controlled potential coulometry (CPC) and chronoamperometry (CA) techniques have been employed. A wide range of concentration (10mM to 150mM) of nucleophiles (Glycine, L-Aspartic acid and L-Glutamic acid), various pH media (5 to11), different electrodes ((Glassy carbon (GC), Gold (Au) and Platinum (P)) and successive scan rate (0.05 V/s to 0.5 V/s) have been used to find out the favorable condition.

Catechol is an electroactive substance which shows a pair of redox peak whereas Glycine, L-Aspartic acid and L-Glutamic acid are electroinactive, hence it shows no anodic and cathodic peak in the potential range (-0.6 to 0.9 V) of investigation.

By the addition of above nucleophiles in Catechol solution arises a new peak at lower potential, the corresponding redox peak shifts and peak current intensity of Catechol decreases with respect to the pure Catechol that indicates the participation of 1,4-Michael addition reaction of *o*-benzoquinone with mentioned nucleophiles. The formation of adducts from the reaction of Catechol with Glycine, L-Aspartic acid and L-Glutamic acid are assumed to be 2-((3,4-dihydroxyphenyl)amino)acetic acid, 2-((3,4-dihydroxy phenyl)amino)succinic acid and 2-((3,4-dihydroxyphenyl)amino)pentanedioic acid severally that go through electron transfer at more negative potentials than the Catechol.

The influence of pH of Catechol in presence of Glycine, L-Aspartic acid and L-Glutamic acid has been studied by varying pH from 5 to 11. It is seen that at pH 3, 5, 9 and 11 no new anodic peak appears after repetitive cycling. In the neutral media (pH 7), the *o*-benzoquinone undergoes nucleophilic attack by the above nucleophiles that voltammetric new anodic peak A_0 appears after repetitive cycling. The slopes of the peak potential was determined graphically from E_p vs pH plot as the anodic peaks of Catechol-glycine adducts (27 mV/pH) proceeded via one step $2e^-/2H^+$ process, Catechol-aspartic acid adducts (50 mV/pH) and Catechol-glutamic acid adducts (69 mV/pH) via two step $1e^-/1H^+$ process.

The reaction is strongly influenced by the different pH media as well as various compositions of nucleophiles. These reactions have been carried out wide range of concentration of nucleophiles. The optimum conditions for the formation of adducts such as Catechol-glycine (pH-7, Concentration 70 mM, GC electrode and Scan rate 0.1 V/s), Catechol-aspartic acid (pH-7, Concentration 70 mM, GC electrode and Scan rate 0.1 V/s) and Catechol-glutamic acid (pH-7, Concentration 30 mM, GC electrode and Scan rate 0.1 V/s) system are observed.

The effect of scan rates has been investigated on cyclic voltammogram of Catechol in presence of above nucleophile. The anodic and cathodic peak current increases proportionally with increasing square root of scan rates. This linear relationship indicates the reaction is controlled by diffusion process. The current function, $I_p/v^{1/2}$ decreases exponentially with increases scan rate which determine the reaction is controlled by ECE mechanism. The electro-synthesized adducts generated from the controlled potential coulometry of Catechol with Glycine, L-Aspartic acid and L-Glutamic acid was isolated and the generated adducts supported by FTIR spectra.

Contents

LIST OF TABLES

LIST OF FIGURES

CHAPTER I

Introduction

1.1 General

Electrochemistry is an active field of modern research. It is the study of interchange between chemical energy and electrical energy. Electrochemistry also offers precisely remarkable and useful means for the study of electro-synthesis and description of electro-active compounds [1, 2]. Electrochemical study of different organic compounds has been growing interest in the presence of various nucleophiles using different types of electrochemical methods [3].

Electrochemical methods are analytical techniques that use a measurement of potential, charges, or current to determine an analytes concentration or to characterize an analytes chemical activity. Those methods are divided into two major groups such as- (1) Bulk techniques, in which we measure a property of solution in the electrochemical cell; (2) Interfacial techniques, in which the potential, charge, or current depends on the species present at the interface between an electrode and the solution in which it sits [4].

The interfacial techniques are divided into static and dynamic techniques. In static techniques no current passes between the electrodes and the concentrations of species in the electrochemical cell remain static. Potentiometry is one of the most important quantitative electrochemical methods that measure the potential of a solution between two electrodes under static conditions. Dynamic methods are further subdivided by whether we choose to control the current or the potential. In controlled-current coulometry the analytes completely oxidize or reduce by passing a fixed current through the analytical solution. Controlled-potential methods are subdivided further into controlled-potential coulometry and amperometry, in which a constant potential is applied during the analysis, and voltammetry, in which the potential is systematically varied.

Electrochemical methods also classified as-Potentiometry, voltammetry, coulometry, conductometry and dielectrometry.

Voltammetric techniques have proved to be very excellent sensitivity with a very large useful range for both inorganic and organic species, drugs and related molecules in pharmaceutical dosages [5, 6], a large number of useful solvents and electrolytes, a wide range of temperatures, rapid analysis times (seconds), simultaneous determination of several analytes, the ability to determine kinetic and mechanistic parameters, a well-developed theory and thus the ability to reasonably estimate the values of unknown parameters, and the ease with which different potential waveforms can be generated and small currents measured.

Voltammetric techniques for the quantitative estimation of a variety of dissolved inorganic and organic substances have regularly used by analytical chemist. Inorganic, organic, physical, pharmaceutical and biological chemists comprehensively use voltammetric techniques for a series of intention, including fundamental studies of oxidation and reduction processes in various media, adsorption and/or diffusion processes on surfaces, electron transfer and reaction mechanisms, kinetics of electron transfer processes, transport, speciation, and thermodynamic properties of solvated species. Voltammetric methods are also used to the estimation of compounds of pharmaceutical interest and effective tools for the analysis of complex mixtures.

The most well-known characteristic of the Catechol is that they can be easily oxidized mainly due to their antioxidant activity and low oxidation potentials [7]. The products of oxidation are the corresponding reactive and electron-deficient *o*-quinones. There are many reports on electro-oxidation of Catechol to produce *o*-quinones as reactive intermediates that is susceptible for nucleophilic substitution in many useful homogeneous reactions which has attracted our attention for this research [3, 9]. The nucleophilic attacks that lead to the formation of Catechol derivatives with more or less positive oxidation potentials are followed by more E steps and C steps depends on the structure of intermediates by EC reaction [8]. Amino acids are very essential for human health any precursor for drug synthesis. The following drug or drug making compounds for example Nicotinamide, L-Aspartic acid, L-Glutamic acid, Glycine, Sulfanilic acid, Diethlylamine,

Metronidazole and Pyridoxine etc. may be used as nucleophiles. Due to weak alkaline nature of amino acids in neutral media it may act as a nucleophile and presence of one lone pair electron on nitrogen enables it to take participation in 1, 4-Michael addition reaction with *o*-benzoquinone.

The purpose of the recent study is thus a basic work to have better insight of the possible redox interactions of Catechol with Glycine, L-Aspartic acid and L-Glutamic acid compounds. These compounds go through redox reaction on the electrode surface within the potential range. The electro activeness of such compounds depends upon the pH of the medium, nature of the electrode and active moiety present in their structures. In this research work Cyclic voltammetry (CV), Differential pulse voltammetry (DPV), Controlled potential coulometry (CPC) and Chronoamperometry (CA) techniques have used to investigate the redox behavior of Catechol with Glycine, L-Aspartic acid and L-Glutamic acid.

1.2.1 Catechol

Catechol is an organic compound with the molecular formula $C_6H_4(OH)_2$. Catechol is also known as 1,2-dihydroxybenzene or pyrocatechol shown in Figure 1.1. It is a colorless crystal with a phenolic odor and soluble in water and most of organic solvents. It is easily sublimes and can react with oxidizing materials. It is the ortho isomer of benzenediols. This colorless compound occurs naturally in trace amounts. The cate skeleton occurs in a variety of natural products such as urushiols, which are the skin-irritating poisons are found in plants [9]. It occurs as feathery white crystals which are very rapidly soluble in water.

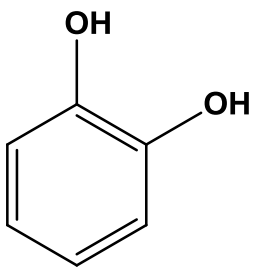

Figure 1.1: Structure of Catechol

1.2.2 Natural occurrence of Catechol

The natural occurrence of Catechol as a polyphenolic compounds. Catechol widely exists in various plants such as tea, vegetables, fruits, tobacco and in crude beet sugar coal and some traditional Chinese medicines, along with the enzyme polyphenol oxidase (also known as Catecholase or Catechol oxidase). Benzoquinone formed by mixing enzyme with substance and expose to oxygen. Those benzoquinone is said to be antimicrobial, which slows the spoilage of wounded fruits and other parts of plant. Catechol is also found in the leaves and branches of oak and willow trees. Catechol moieties are also found widely within the natural world. Arthropodcuticle consists of chitin linked by a Catechol moiety to protein. The cuticle may be strengthened by cross-linking, particularly in insects [10].

1.2.3 Use of Catechol

Catechol is mainly used as an intermediate for the synthesis of pharmaceuticals, agrochemicals and in formulation. Approximately 50% of the synthetic Catechol is consumed in the production of pesticides, the remainder being used as a precursor to fine chemicals such as perfumes and pharmaceuticals [11]. Several industrially significant flavors and fragrances such as vanillin or eugenol (synthetic "vanilla" aroma and flavor), piperonal (a flowery scent), guaiacol are prepared starting from Catechol that are used in food industry, perfumery, home and personal care products [12]. The Catechol route of vanillin synthesis is far more environmentally friendly than the o-nitrochlorobenzene route. Catechol also used as a black-and-white photographic developer.

1.2.4 Glycine

Glycine is a non-essential amino acid having no functional group in side chain whose isoelectric point is 6.0. Glycine (abbreviated as Gly or G) is the smallest of the 20 amino acids commonly found in proteins [13]. The formula Glycine is NH_2CH_2COOH shown in figure 1.2. It is a colorless, sweet-tasting crystalline solid. It is unique among the proteinogenic amino acids in that it is achiral. In aqueous solution, Glycine itself is amphoteric: at low pH the molecule can be protonated with a pK_a of about 2.4 and at high

pH it loses a proton with a pK_a of about 9.6. The principal function of Glycine is as a precursor to proteins, such as its periodically repeated role in the formation of the collagen helix in conjunction with hydroxyproline. It is also a building block to numerous natural products. Glycine is an inhibitory neurotransmitter in the central nervous system and as a biosynthetic intermediate [14].

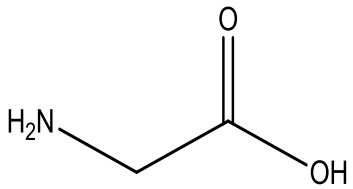

Figure 1.2: Structure of Glycine

1.2.5 Use of Glycine

The principal function of Glycine is as a precursor to proteins also a building block to numerous natural products. It acts as inhibitory neurotransmitter in the central nervous system and as a biosynthetic intermediate [15]. Pharmaceutical grade Glycine is produced for some pharmaceutical applications, such as intravenous injections, Technical grade Glycine is produced for some industrial applications such as an agent in metal complexing and finishing [16].

1.2.6 L-Aspartic acid

L-Aspartic acid (abbreviated as Asp or D) is an α-amino acid with the chemical formula $HOOCCH(NH_2)CH_2COOH$ shown in figure 1.3. Aspartate is non-essential in mammals, being produced from oxaloacetate by transamination. It can also be generated from ornithine and citrulline in the urea cycle. Aspartate is also a metabolite in the urea cycle and participates in gluconeogenesis. It carries reducing equivalents in the malate-aspartate shuttle, which utilizes the ready inter-conversion of aspartate and oxaloacetate, which is the oxidized (dehydrogenated) derivative of malic acid. Aspartate donates one nitrogen atom in the biosynthesis of inosine, the precursor to the purine bases. In addition, L-Aspartic acid acts as hydrogen acceptor in a chain of ATP synthase.

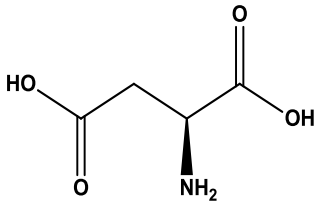

Figure 1.3: Structure of L-Aspartic acid

1.2.7 Use of L-Aspartic acid

L-Aspartic acid plays an important role for the synthesis of other amino acids and in the citric acid and urea cycles. L-Asparagine, L-Arginine, L-Lysine, L-Methionine, Isoleucine and some nucleotides are synthesized from L-Aspartic acid. It also serves as a neurotransmitter. To reduce ammonia blood levels and it can also promote energy production via its metabolism in the Krebs cycle [17, l8].

1.2.8 L-Glutamic acid

L-Glutamic acid (abbreviated as Glu or E) is an α-amino acid with chemical formula $C_5H_9NO_4$ shown in figure 1.4. It contains an α-amino group (which is in the protonated $-NH_3^+$ form under biological conditions), an α-carboxylic acid group (which is in the deprotonated $-COO^-$ form under biological conditions), and a side chain carboxylic acid, classifying it as a polar negatively charged (at physiological pH), aliphatic amino acid. It is non-essential in humans, meaning the body can synthesize it [19]. The side chain carboxyl of L-Aspartic acid is referred to as the β carboxyl group, while that of L-Glutamic acid is referred to as the γ carboxyl group. The pK_a of the γ carboxyl group for L-Glutamic acid in a polypeptide is about 4.3, significantly higher than that of L-Aspartic acid. This is due to the inductive effect of the additional methylene group. [21]

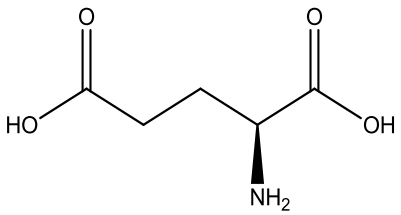

Figure 1.4: Structure of L-Glutamic acid

1.2.9 Use of L-Glutamic acid

L-Glutamic acid is used in the biosynthesis of proteins, plant growth, nutrients, and flavor enhancer. In neuroscience, its carboxylate anion L-glutamate is an important excitatory neurotransmitter that plays the principal role in neural activation [19]. In NMR spectroscopy a L-Glutamic acid derivative, poly-γ-benzyl-L-glutamate is often used as an alignment medium to control the scale of the dipolar interactions observed in NMR spectroscopy [18].

1.3 Electrochemical properties of Catechol derivatives

Investigation of the electrochemical behavior of Catechols in presence of some other nucleophiles such as benzenesulfinic acid, barbituric acid, indole, some Azacrown Ethers and Transition Metal Ions in Acetonitrile, benzoyl acetonitrile, dibuthylamine, diethylamine, thiourea, methanol, 4-hydroxycoumarin, ethanol, 2-thiobarbituric acid, β-diketones, 4-hydroxy-6-methyl-2-pyrone, 2-thiouracil, dimedone, 4,7-dihydroxycoumarin, 4,5,7-trihydroxycoumarin, 4-hydroxy-6-bromocoumarin, 3-hydroxycoumarin, 4-hydroxy-6-methyl-a-pyrone, 4-hydroxy-6-methyl-2-pyridone, 4-hydroxycarbostyrile, sulfonic acid, Dopamine and 4-amino-3-thio-1,2,4-triazole were studied [21-37].

Few works have been done on electrochemical oxidation of Catechols with amines [25]. They were studied the electrocatalytic effect of Catechol with amines in only GC electrode and limited concentration and pH. However, Aminoquinones are biologically important compounds in this direction, therefore, it demand detail electrochemical studies of Catechol in the presence of amines. In this research work, we have studied the electrocatalytic effect of Catechol in presence of Glycine, L-Aspartic acid L-Glutamic acid and their mixtures for three different electrodes (GC, Au and Pt) and various concentration ((Glycine (30-110mM), L-Aspartic acid (30-100mM) and L-Glutamic acid (30-100mM)) and different pH (5-11) at different scan rate. The primary aim of the present study is thus a fundamental realization to have better insight of the possible redox interactions of Catechol with Glycine, L-Aspartic acid and L-Glutamic acid compounds. To the best of our knowledge, comparison of electrochemical study of Catechol with

Glycine, L-Aspartic acid, L-Glutamic acid and their mixtures at different conditions has not been reported before this work.

1.4 Objectives of this Thesis

Attempt will be made in the present research work is systematic study of biologically important Catechol-amino acid adducts which may help to understand the role of amino drugs and their adducts in biological process.

The specific aims of this study are:

i) To synthesize electroactive Catechol-amino acid adducts electrochemically.
ii) To diagnose the mechanism of the redox processes of these compounds at different pH and different scan rate.
iii) To study the effect of pH, scan rate, concentration on the reaction.
iv) To identify the most favorable condition (concentration, pH) for the reaction.
v) To determine the electron transfer numbers of electro-synthesizing species with single step and/or multi-step electron transfer reaction.
vi) To know the redox interaction of the species by CV, DPV and CA techniques.
vii) To characterize the new features of the species by electrochemical and spectral analysis.

CHAPTER II

Theoretical Background

Electroanalytical chemistry encompasses a group of quantitative analytical methods that are based upon the electrical properties of an analyte solution when it is made part of an electrochemical cell. Electroanalytical methods study an analyte by measuring the potential (volts) and/or current (amperes) in an electrochemical cell containing the analyte. These methods can be broken down into several categories depending on which aspects of the cell are controlled and which are measured. The three main categories are potentiometry (the difference in electrode potentials is measured), coulometry (the cell's current is measured over time), and voltammetry (the cell's current is measured while actively altering the cell's potential). Voltammetry applies a constant and/or varying potential at an electrode's surface and measures the resulting current with a three electrode system. This method can reveal the reduction potential of an analyte and its electrochemical reactivity. This method in practical terms is nondestructive since only a very small amount of the analyte is consumed at the two-dimensional surface of the working and auxiliary electrodes. In practice the analyte solutions is usually disposed of since it is difficult to separate the analyte from the bulk electrolyte and the experiment requires a small amount of analyte. Electrodes are employed for electrochemical determination of organic molecules as well as metal ions. The electrode can act as a source (for reduction) or a sink (for oxidation) of electrons transferred to or from the species in solution:

$$O + ne \rightarrow R$$

Where, O and R are the oxidized and reduced species. In order for the electron transfer to occur, there must be a correspondence between the energies of the electron orbitals where transfer takes place in the donor and acceptor. In the electrode this level is the highest filled orbital, which in a metal is Fermi energy level. In the soluble species it is the orbital of the valence electron to be given or received. For reduction, there is a minimum energy that the transferable electrons from the electrode must have before the transfer can occur, which corresponds to a sufficiently negative potential. For an oxidation, there is a

maximum energy that the lowest unoccupied level in the electrode can have in order to receive electrons from the species in solution, corresponding to a sufficiently positive potential. In order to study electrode reactions, reproducible experimental conditions must be created which enable minimization of all unwanted factors that can contribute to the measurements and diminish their accuracy. That means to suppress migration effects, confine the interfacial region as close as possible to the electrode, and minimize solution resistance. These objectives are achieved by the addition of large amount of inert electrolyte, the electroactive species being at a concentration of 5 mM or less [38].

Since an electrode predominantly attracts positively and negatively charged species, which may or may not undergo reaction at the surface, it should be remembered that the species may adsorb at the electrode surface. This makes it clear that in the description of any electrode process we have to consider the transport of species to the electrode surface as well as the electrode reaction itself. This transport can occur by diffusion, convection or migration.

2.1 Mass transfer process in voltammetry

The movement of the electro-active substance through solution is referred as mass transfer at the electrode surface. In electrochemical systems, there are different types of mass transfer system by which a substance may be transferred to the electrode surface from bulk solution. Depended on the experimental conditions, any of these or more than one might be operating in a given experiment system.

A reacting species may be brought to an electrode surface by three types of mass transfer processes:

- Migration
- Diffusion
- Convection

2.1.1 Migration

Migration refers to movement of a charge particle in a potential field. It occurs by the movement of ions through a solution as a result of electrostatic attraction between the ions and the electrodes. In general, most electrochemical experiment it is unwanted but can be

eliminated by the addition of a large excess of supporting electrolytes. In the electrolysis solution, ions will move towards the charged electrode that means cations to the cathode and anions to the anode. This motion of charged particle through solution, induced by the charges on the electrodes is called migration [39]. This charge movement constitutes a current. This current is called migration current. The fraction of the current carried by a given cation and anion is known as its transport number. The larger the number of different kinds of ions in a given solution, the smaller is the fraction of the total charge that is carried by a particular species. Electrolysis is carried out with a large excess of inert electrolyte in the solution so the current of electrons through the external circuit can be balanced by the passage of ions through the solution between the electrodes, and a minimal amount of the electroactive species will be transported by migration. Migration is the movement of charged species due to a potential gradient. In voltammetric experiments, migration is undesirable but can be eliminated by the addition of a large excess of supporting electrolytes in the electrolysis solution. The effect of migration is applied zero by a factor of fifty to hundred ions excess of an inert supporting electrolyte.

2.1.2 Diffusion

The movement of a substance through solution by random thermal motion is known as diffusion. Whereas a concentration gradient exists in a solution, that is the concentration of a substance, is not uniform throughout the solution. There is a driving force for diffusion of the substance from regions of high concentration to regions of lower concentration. In any experiment in which the electrode potential is such that the electron transfer rate is very high, the region adjacent to the electrode surface will become depleted of the electro-active species, setting up a concentration in which this species will constantly be arriving at the electrode surface by the diffusion from points further away [40]. The one kind of mode of mass transfer is diffusion to an electrode surface in an electrochemical cell. The rate of diffusion is directly proportional to the concentration difference. When the potential is applied, the cations are reduced at the electrode surface and the concentration is decreased at the surface film. Hence a concentration gradient is produced. Finally, the result is that the rates of diffusion current become larger.

2.1.3 Convection

By mechanical way reactants can also be transferred to or from an electrode. Thus forced convection is the movement of a substance through solution by stirring or agitation. This will tend to decrease the thickness of the diffuse layer at an electrode surface and thus decrease concentration polarization. Natural convection resulting from temperature or density differences also contributes to the transport of species to and from the electrode [41]. At the same time a type of current is produced. This current is called convection current. Removing the stirring and heating can eliminate this current. Convection is a far more efficient means of mass transport than diffusion.

2.2 Electrochemical cell

An electrochemical cell is a device capable of either generating electrical energy from chemical reactions or facilitating chemical reactions through the introduction of electrical energy [42]. Electrolytic and galvanic cell are the mainly two types of electrochemical cells. This electrochemical cell may be either two or three electrode system. The electrochemical reaction of interest takes place at the working electrode and the electrical current at this electrode due to electron transfer is termed as faradic current.

Fig: The three electrode system consisting of a working electrode, a reference electrode and a counter electrode.

Electrodes

(1) **Working electrode:** The working electrode is an electrode where the redox reaction takes place. We measure the potential of the working electrode.

(2) **References electrode:** Ag|AgCl electrode used as references electrode. We measure the potential of working electrode with respect the reference electrode.

(3) **Counter electrode:** The counter electrode in the three-electrode system is made of an inert metal. The counter electrode used to complete the cell and reduce the resistances of the solution.

2.3 Cyclic voltammetry (CV)

There are several well established electrochemical techniques for the study of electrochemical reactions. We chose the CV technique to study and analyze the redox reactions occurring at the polarizable electrode surface. This technique helps us to understand the mechanism of electron transfer reaction of the compounds as well as the nature of adsorption of reactants or products on the electrode surface.

Cyclic voltammetry is a very versatile electrochemical technique which allows proving the mechanics of redox and transport properties of a system in solution. This is accomplished with a three electrode arrangement whereby the potential relative to some reference electrode is scanned at a working electrode while the resulting current flowing through a counter (or auxiliary) electrode is monitored in a quiescent solution. More precisely, the controlling electronic is designed such that the potential between the reference and the working electrodes can be adjusted but the big impedance between these two components effectively forces any resulting current to flow through the auxiliary electrode. Usually the potential is scanned back and forth linearly with time between two extreme values – the switching potentials using triangular potential waveform (see Figure 2.1). When the potential of the working electrode is more positive than that of a redox couple present in the solution, the corresponding species may be oxidized (i.e. electrons going from the solution to the electrode) and produce an anodic current. Similarly, on the return scan, as the working electrode potential becomes more negative than the reduction potential of a redox couple, reduction (i.e. electrons flowing away from the electrode) may occur to cause a cathodic current. By IUPAC convention, anodic currents are positive and cathodic currents negative.

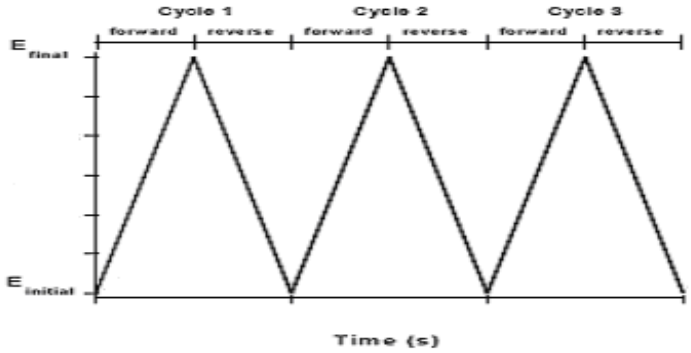

Figure 2.1: A cyclic voltammetry potential waveform with switching potentials

The magnitude of the observed faradaic current can provide information on the overall rate of the many processes occurring at the working electrode surface. As is the case for any multi–step process, the overall rate is determined by the slowest step. For an redox reaction induced at a working electrode, the rate determining step may be any one of the following individual step depending on the system: rate of mass transport of the electro-active species, rate of adsorption or de-sorption at the electrode surface, rate of the electron transfer between the electro-active species and the electrode, or rates of the individual chemical reactions which are part of the overall reaction scheme.

For the oxidation reaction involving *n* electrons

$$\mathrm{Red} \rightleftarrows \mathrm{Ox} + ne^-$$

the *Nernst Equation* gives the relationship between the potential and the concentrations of the oxidized and reduced form of the redox couple at equilibrium (at 298 K):

$$E = E^{0'} + \frac{0.059}{n} \log_{10} \frac{[\mathrm{Ox}]_s}{[\mathrm{Red}]}$$

where E is the applied potential and $E^{0'}$ the formal potential; [OX] and [Red] represent surface concentrations at the electrode/solution interface, *not* bulk solution concentrations. Note that the Nernst equation may or may not be obeyed depending on the system or on the experimental conditions.

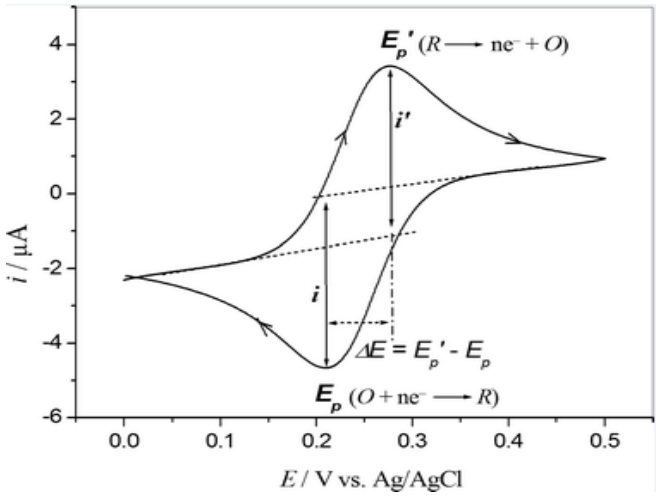

Figure 2.2: The expected response of a reversible redox couple during a single potential cycle

A typical voltammogram is shown in Figure 2.2. The current is first observed to peak at E_{pa} (with value i_{pa}) indicating that an oxidation is taking place and then drops due to depletion of the reducing species from the diffusion layer. During the return scan the processes are reversed (reduction is now occurring) and a peak current is observed at E_{pc} (corresponding value, i_{pc}).

Providing that the charge–transfer reaction is reversible, that there is no surface interaction between the electrode and the reagents, and that the redox products are stable (at least in the time frame of the experiment), the ratio of the reverse and the forward current i_{pr}/i_{pf} = 1.0 (in Figure 2.2 $i_{pa} = i_{pf}$ and $i_{pc} = i_{pr}$). In addition, for such a system it can be shown that:

- the corresponding peak potentials E_{pa} and E_{pc} are independent of scan rate and concentration
- the formal potential for a reversible couple $E^{0'}$ is centered between E_{pa} and E_{pc}: $E^{0'} = (E_{pa} + E_{pc})/2$
- the separation between peaks is given by $\Delta E_p = E_{pa} - E_{pc} = 59/n$ mV (for a n electron transfer reaction) at all scan rates (however, the measured value for a reversible process is generally higher due to uncompensated solution resistance and non-linear diffusion. Larger values of ΔE_p, which increase with increasing scan rate, are characteristic of slow electron transfer kinetics).

It is possible to relate the half-peak potential ($E_{p/2}$, where the current is half of the peak current) to the polarographic half-wave potential, $E_{1/2}$: $E_{p/2} = E_{1/2} \pm 29mV/n$ (The sign is positive for a reduction process.)

Simply stated, in the forward scan, the reaction is $O + e^- \rightarrow R$, R is electrochemically generated as indicated by the cathodic current. In the reverse scan, $R \rightarrow O + e^-$, R is oxidized back to O as indicated by the anodic current. The CV is capable of rapidly generating a new species during the forward scan and then probing its fate on the reverse scan. This is a very important aspect of the technique [43].

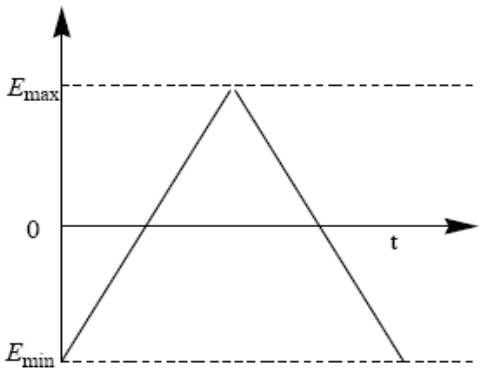

Figure 2.3: Variation of potential with time in cyclic voltammetry

A characteristic feature is the occurrence of peaks, identified by the peak potential E_p, which corresponds to electron transfer reactions. The repetitive triangular potential excitation signal for CV causes the potential of the working electrode to sweep backward and forward between two designate values (the switching potentials).

In cyclic voltammetry of reversible system, the product of the initial oxidation or reduction is then reduced or oxidized, respectively, on reversing the scan direction.

Adsorbed species lead to changes in the shape of the cyclic voltammogram, since they do not have to diffuse from the electrode surface. In particular, if only adsorbed species are oxidized or reduced, in the case of fast kinetics the cyclic voltammogram is symmetrical, with coincident oxidation and reduction peak potentials [44].

Cyclic voltammetry is one of the most versatile techniques for the study of electroactive species, as it has a provision for mathematical analysis of an electron transfer process at the electrode [45-48]. It is an electroanalytical tool for monitoring and recognition of many

electrochemical processes taking place at the surface of electrode and can be used to study redox processes in biochemistry and macromolecular chemistry [49].

2.3.1 Single electron transfer process

Based upon the values of electrochemical parameters, i.e., peak potential E_p, half peak potential ($E_{p/2}$), half wave potential ($E_{1/2}$), peak current (I_p), anodic peak potential E_{pa}, cathodic peak potential E_{pc} etc, it can be ascertained whether a reaction is reversible, irreversible or quasi-reversible. The electrochemical parameters can be graphically obtained from the voltammogram as shown in the Figure 2.3.

Three types of single electron transfer process can be studied.

a. Reversible process. b. Irreversible process and c. Quasi-reversible.

2.3.1(a) Reversible processes

The peak current for a reversible couple (at 25°C), is given by the Randles-Sevcik equation: $\boldsymbol{i}_p = (2.69 \times 10^5)\, n^{3/2} A C D^{1/2} v^{1/2}$

where n is the number of electrons, A the electrode area (in cm^2), C the concentration (in mol/cm^3), D the diffusion coefficient (in cm^2/s), and v the scan rate (in V/s). Accordingly, the current is directly proportional to concentration and increases with the square root of the scan rate. The ratio of the reverse-to-forward peak currents, $\boldsymbol{i}_{pr}/\boldsymbol{i}_{pf}$, is unity for a simple reversible couple. The current peaks are commonly measured by extrapolating the preceding baseline current. The position of the peaks on the potential axis (E_p) is related to the formal potential of the redox process. The formal potential for a reversible couple is centered between E_{pa} and E_{pc}:

$$E^\circ = (E_{pa} + E_{pc})/2$$

The separation between the peak potentials (for a reversible couple) is given by:

$$\Delta E_p = E_{pa} - E_{pc} = 59mV/n$$

Thus, the peak separation can be used to determine the number of electrons transferred, and as a criterion for a Nernstian behavior. Accordingly, a fast one-electron process exhibits a ΔE_p of about 59 mV. Both the cathodic and anodic peak potentials are independent of the scan rate. It is possible to relate the half-peak potential ($E_{p/2}$, where the current is half of the peak current) to the polarographic half-wave potential, $E_{1/2}$

$$E_{p/2} = E_{1/2} \pm 29mV/n$$

(The sign is positive for a reduction process.) For multi electron-transfer (reversible) processes, the cyclic voltammogram consists of several distinct peaks, if the E^o values for the individual steps are successively higher and are well separated. An example of such mechanism is the six-step reduction of the fullerenes C_{60} and C_{70} to yield the hexaanion products C_{60}^{6-} and C_{70}^{6-} where six successive reduction peaks can be observed.

The situation is very different when the redox reaction is slow or coupled with a chemical reaction. Indeed, it is these "nonideal" processes that are usually of greatest chemical interest and for which the diagnostic power of cyclic voltammetry is most useful. Such information is usually obtained by comparing the experimental voltammograms with those derived from theoretical (simulated) ones.

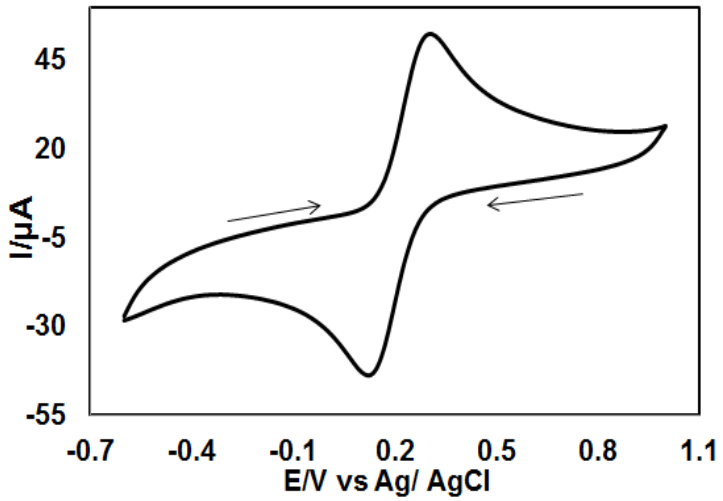

Figure 2.4: Reversible cyclic voltammogram of redox process

2.3.1(b) Irreversible processes

For irreversible processes (those with sluggish electron exchange), the individual peaks are reduced in size and widely separated. Totally irreversible systems are characterized by a shift of the peak potential with the scan rate:

$$E_p = E° - (RT/\alpha n_a F)[0.78 - \ln(k^o/(D)^{1/2}) + \ln(\alpha n_a F v/RT)^{1/2}]$$

where α is the transfer coefficient and n_a is the number of electrons involved in the charge-transfer step. Thus, E_p occurs at potentials higher than E°, with the overpotential related to k° and a. Independent of the value k°, such peak displacement can be compensated by an appropriate change of the scan rate. The peak potential and the half-peak potential (at

25°C) will differ by 48/αn mV. Hence, the voltammogram becomes more drawn-out as α**n** decreases.

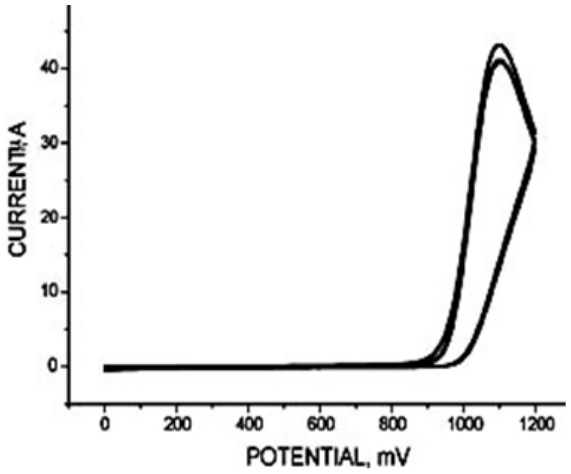

Figure 2.5: Cyclic voltammogram of irreversible redox process

2.3.1(c) Quasi-reversible process

Quasi-reversible process is termed as a process, which shows intermediate behavior between reversible and irreversible processes. In such a process the current is controlled by both the charge transfer and mass transfer.

Cyclic voltammogram for quasi-reversible process is shown in Figure 2.6 [50].

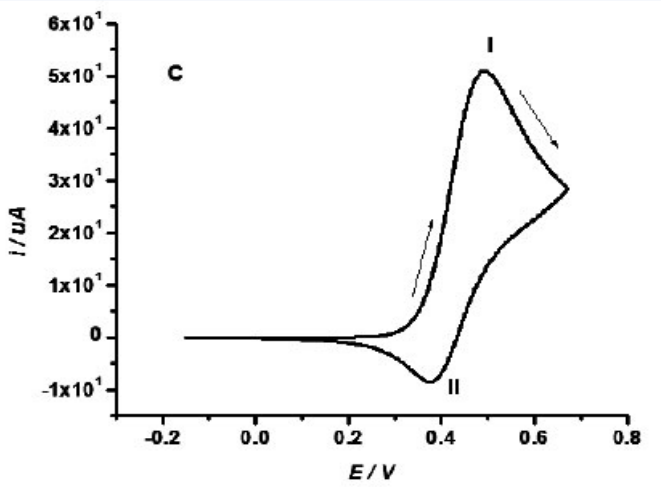

Figure 2.6: Cyclic voltammogram of quasi-reversible redox process

For quasi-reversible process the value of standard heterogeneous electron transfer rate constant, k_{sh}^{o} lies in the range of 10^{-1} to 10^{-5} cm sec^{-1} [51]. An expression relating the

current to potential dependent charge transfer rate was first provided by Matsuda and Ayabe [52].

$$I(t) = C_{o(0,t)} k_{sh}^{o} Exp\left[-\frac{\alpha nF}{RT}\left\{E(t) - E^{o}\right\}\right] - C_{R(0,t)} k_{sh}^{o} Exp\left[-\frac{\beta nF}{RT}\left\{E(t) - E^{o}\right\}\right] \ldots.2.1$$

where k_{sh}^{o} is the heterogeneous electron transfer rate constant at standard potential E^{0} of redox system. α is the transfer coefficient and β = 1- α. In this case, the shape of the peak and the various peak parameters are functions of α and the dimensionless parameter, Λ, defined as [53]

$$\Lambda = \frac{k_{s,h}}{D^{1/2}(nF/RT)^{1/2}\upsilon^{1/2}} \ldots\ldots\ldots\ldots\ldots\ldots\ldots\ldots\ldots\ldots\ldots..2.2$$

when $D_o = D_R = D$

D_o and D_R are the diffusion coefficients of oxidized and reduced species respectively.

For quasi-reversible process current value is expressed as a function of $\psi(E)$ [53].

$$I = nFAC_o^{*}\frac{k_{sh}^{o}}{\Lambda}\psi(E) \ldots\ldots\ldots\ldots\ldots\ldots\ldots\ldots\ldots\ldots\ldots..2.3$$

where $\psi(E)$ is expressed as

$$\psi(E) = \frac{I}{nFAC_o^{*}D_o^{1/2}(nF/RT)^{1/2}\upsilon^{1/2}} \ldots\ldots\ldots\ldots\ldots\ldots..2.4$$

It is observed that when $\Lambda \geq 10$, the behavior approaches that of a reversible system [54].

For three types of electrode processes, Matsuda and Ayabe [52] suggested following zone boundaries.

- Reversible (Nernstian)

  $k_{sh}^{o} \geq 0.3\upsilon^{1/2}$ cm s^{-1}
- Quasi-reversible

  $0.3\upsilon^{1/2} \geq k_{sh}^{o} \geq 2\times10^{-5}\upsilon^{1/2}$ cm s^{-1}
- Totally irreversible

  $k_{sh}^{o} \leq 2\times10^{-5}\upsilon^{1/2}$ cm s^{-1}

2.3.2 Multi electron transfer processes

Multi-electron transfer process usually takes place in different steps. A two-step mechanism each characterized by its own electrochemical parameters is called an "EE mechanism".

A two step reversible "EE mechanism" is represented as;

$$O + n_1 e \leftrightarrow R_1 \qquad (E_1^o) \ldots\ldots\ldots\ldots\ldots\ldots 2.5$$

$$R + n_1 e \leftrightarrow R_2 \qquad (E_2^o) \ldots\ldots\ldots\ldots\ldots\ldots 2.6$$

Each heterogeneous electron transfer step is associated with its own electrochemical parameters i.e., k_{sh}^o and α_i, where i = 1, 2 for the 1st and 2nd electron transfer respectively. The value of k_{sh}^o for first reversible electron transfer limiting case can be calculated as [55]:

$$k_{sh} = k_{sh}^o \exp\left[-\alpha 1 F \Delta E^o / 2RT\right] \ldots\ldots\ldots\ldots\ldots\ldots 2.7$$

where

$$\Delta E^o = E_2^o - E_1^o$$

For ΔE^0 greater than 180 mV, shape of wave does not dependent on the relative values of E^0, otherwise shapes of peak and peak currents depend upon ΔE^0 [56]. Based on the value of ΔE^0, we come across different types of cases as shown in the Figure 2.6.

Types of two electron transfer reactions

***Case 1*:** $\Delta E^0 \geq 150$ mV peaks separation

When $\Delta E^0 \geq 150$ mV the EE mechanism is termed as "disproportionate mechanism [57]. Cyclic voltammogram consists of two typical one-electron reduction waves. The heterogeneous electron transfer reaction may simultaneously be accompanied by homogenous electron transfer reaction, which in multi-electron system leads to disproportionation which can be described as:

$$R_1 \rightarrow O + n_1 e \ldots\ldots\ldots\ldots\ldots\ldots\ldots\ldots\ldots\ldots\ldots\ldots\ldots\ldots 2.8a$$

$$R_1 + n_2 e \rightarrow R_2 \ldots\ldots\ldots\ldots\ldots\ldots\ldots\ldots\ldots\ldots\ldots\ldots\ldots\ldots 2.8b$$

$$2R_1 \leftrightarrow O + R_2 \ldots\ldots\ldots\ldots\ldots\ldots\ldots\ldots\ldots\ldots\ldots\ldots\ldots\ldots 2.8c$$

$$k_{disp} = \frac{[O][R_2]}{[R_1]^2} \ldots\ldots\ldots\ldots\ldots\ldots\ldots\ldots\ldots\ldots\ldots\ldots\ldots\ldots 2.9$$

$$\ln k_{disp} = \left[\frac{nF}{RT}\right](E_2^o - E_1^o) \quad \text{.....2.10}$$

***Case 2*:** ΔE^0 < 100 mV ----- Peaks overlapped

In this case, the individual waves merge into one broad distorted wave whose peak height and shape are no longer characteristics of a reversible wave. The wave is broadened similar to an irreversible wave, but can be distinguished from the irreversible voltammogram, in that the distorted wave does not shift on the potential axis as a function of the scan rate.

***Case 3*:** ΔE^0 = 0 mV ----- Single peak

In this case, in cyclic voltammogram, only a single wave would appear with peak current intermediate between those of a single step one electron and two electron transfer reactions and E_p-$E_p/2$ = 56 mV.

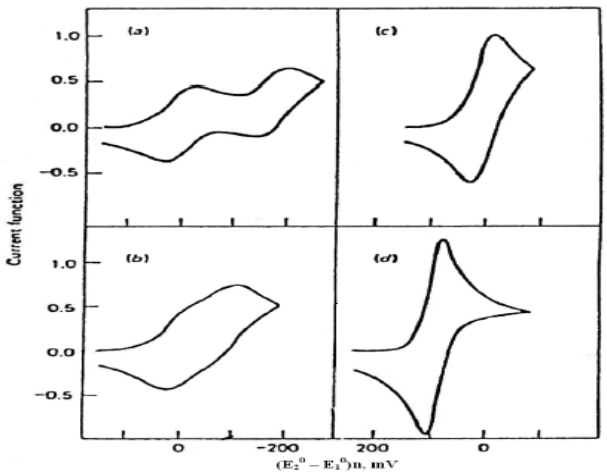

Figure 2.7 Cyclic voltammograms for a reversible two-step system (a) ΔE^0**= - 180 mV, (b)** ΔE^0 **= -90 mV, (c)** ΔE^0 **= 0 mV, (d)** ΔE^0 **= 180 mV.** (Taken from ref. [58])

Contrary to the convention the direction of the current in these voltammograms has been shown cathodic above the base line and anodic below the base line.

Case 4: $E^0_1 < E^0_2$ ----2nd Reduction is easy than 1st one

If the energy required for the second electron transfer is less than that for the first, one wave is observed, having peak height equal to $2^{3/2}$ times that of a single electron transfer

process. In this case, E_p-$E_p/2$ = 29 mV. The effective E^0 for the composite two electron wave is given by $\frac{(E_1^o + E_2^o)}{2}$ as reported in literature [58].

2.4 Pulse techniques

The basis of all pulse techniques is the difference in the rate of decay of the charging and the faradaic currents following a potential step (or pulse). The charging current decays considerably faster than the faradaic current. A step in the applied potential or current represents an instantaneous alteration of the electrochemical system. Analysis of the evolution of the system after perturbation permits deductions about electrode reactions and their rates to be made. The potential step is the base of pulse voltammetry. After applying a pulse of potential, the capacitive current dies away faster than the faradic one and the current is measured at the end of the pulse. This type of sampling has the advantage of increased sensitivity and better characteristics for analytical applications. At solid electrodes there is an additional advantage of discrimination against blocking of the electrode reaction by adsorption [44].

2.4.1 Differential pulse voltammetry (DPV)

Differential pulse voltammetry (DPV) is often used to make electrochemical measurements. It can be considered as a derivative of linear sweep voltammetry, with a series of regular voltage pulses superimposed on the potential linear sweep. The current is measured immediately before each potential change, and the current difference is plotted as a function of potential. By sampling the current just before the potential is changed, the effect of the charging current can be decreased [59].

The potential wave form for differential pulse voltammetry (DPV) is shown in Figure 2.8. The potential wave form consists of small pulses (of constant amplitude) superimposed upon a staircase wave form. Unlike Normal pulse voltammetry (NPV**)**, the current is sampled twice in each Pulse Period (once before the pulse, and at the end of the pulse), and the difference between these two current values is recorded and displayed.

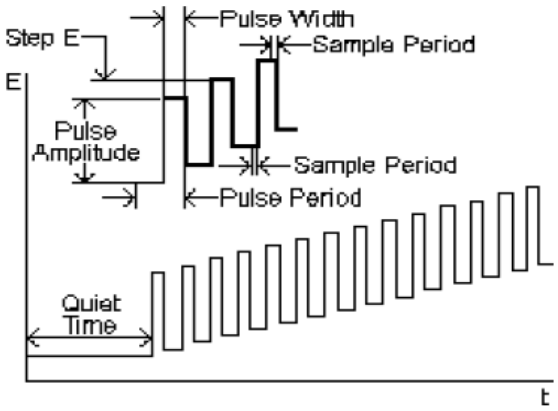

Figure 2.8: Scheme of application of potential

The important parameters for pulse techniques are as follows:

- Pulse amplitude is the height of the potential pulse. This may or may not be constant depending upon the technique.
- Pulse width is the duration of the potential pulse.
- Sample period is the time at the end of the pulse during which the current is measured.
- For some pulse techniques, the pulse period or drop time must also be specified. This parameter defines the time required for one potential cycle, and is particularly significant for polarography (i.e., pulse experiments using a mercury drop electrode), where this time corresponds to the lifetime of each drop (i.e., a new drop is dispensed at the start of the drop time, and is knocked off once the current has been measured at the end of the drop time - note that the end of the drop time coincides with the end of the pulse width).

2.5 Chronoamperometry (CA)

Chronoamperometry (CA) is an electrochemical technique in which potential of the working electrode is stepped and the resulting faradic current is monitored as a function of time. As with all pulsed techniques, chronoamperometry (CA) is one of the simplest potential wave forms. The potential is changed instantaneously from the Initial Potential to the First Step Potential, and it is held at this value for the First Step Time. This is a single potential step experiment. In CA, the current is monitored as a function of time. The

Faradaic current--which is due to electron transfer events and is most often the current component of interest--decays as described in the Cottrell equation. Since the current is integrated over relatively longer time intervals, CA gives a better signal to noise ratio in comparison to other amperometric technique. A chronoamperometric curve at a disk microelectrode varies from the Cottrell behavior to the steady state current. When potential is stepped to a diffusion-controlled potential domain at the disk electrode with radius, *a*, in the solution including electroactive species with the concentration, c^*, and the diffusion coefficient, *D*, the responding current, *I*, at the electrolysis time, *t*, has been expressed as [60, 61]

$$I = 4nFc^*Da\left(1+0.71835\tau^{-1/2}+0.05626\tau^{-3/2}-0.00646\tau^{-5/2}\right)\ldots..\ 2.12$$

$$I = 4nFc^*Da\left[\left(\pi/4\tau\right)^{1/2}+\pi/4+0.094\tau^{1/2}\right]\ldots\ldots\ldots\ldots\ldots\ldots 2.13$$

where $\tau = 4Dt/a^2$. Equations 2.12 and 2.13 are valid for $\tau > 1.44$ and $\tau < 0.82$, respectively. Some expressions for the chronoamperometric curves obtained by finite difference or the related methods [62-67] are closed to Equation (2.12) and (2.13). When τ is small enough to neglect the third term in Equation (2.13), the potential-depending current for the reversible case is expressed by

$$I = \left(\pi^{1/2}nFD^{1/2}a^2t^{-1/2}+\pi nFDa\right)c^*(1+\mathrm{e}^{-\varsigma})^{-1}\ldots\ldots\ldots 2.14$$

where $\varsigma = (F/RT)(E-E^{0'})$

The Cottrell plot (*I* vs. $t^{-1/2}$) gives the slope and the intercept, respectively

$$s = \pi^{1/2}nFD^{1/2}a^2c^*(1+\mathrm{e}^{-\varsigma})^{-1}$$

$$p = \pi nFDa\,c^*(1+\mathrm{e}^{-\varsigma})^{-1}$$

The ratio of the square of the slope to the intercept is

$$s^2/p = nFa^3\,c^*(1+\mathrm{e}^{-\varsigma})^{-1} \text{ or } n\left(1+\mathrm{e}^{-\varsigma}\right)^{-1} = s^2/pFa^3\,c^*\ldots 2.15$$

This equation does not include *D*, and hence is the basic equation of evaluating *n* without knowing *D* from the chronoamperometric curves.

CHAPTER III

Experimental

The electrochemical behavior of Catechol with Glycine, L-Aspartic acid and L-Glutamic acid in buffer solution at various pH has been investigated using Cyclic voltammetry (CV), Differential pulse voltammetry (DPV), Controlled potential coulometry (CPC) and Chronoamperometry (CA) at Glassy carbon (GC), Gold (Au) and Platinum (Pt) electrode. The instrumentation is given details in the following sections. The source of different chemicals, instruments and methods are briefly given below.

3.1 Chemicals

Analytical grade chemicals and solvents have been used in electrochemical synthesis and analytical work. The used chemicals were-

Sl. No.	Chemicals	Molecular formula	Molar mass	Reported purity	Producer
1.	Catechol	$C_6H_4(OH)_2$	110.11	99%	Fisher Scientific UK Ltd.
2.	Glycine	$C_2H_5NO_2$	75.05	99%	E-Merck, Germany
3.	Aspartic Acid	$C_4H_7NO_4$	133.10	99%	Merk Specialities Pvt. Ltd., India
4.	Glutamic acid	$C_5H_9NO_4$	147.13	99.5%	E-Merck, Germany
4.	Glacial Acetic Acid	CH_3COOH	60.05	99.5%	Loba Chemie Pvt. Ltd., India
5.	Sodium Acetate	$CH_3COONa.3H_2O$	136.08	99%	Merk Specialities Pvt. Ltd., India
6.	Potasium Chloride	KCl	74.60	99.5%	E-Merck, Germany

Sl. No.	Chemicals	Molecular formula	Molar mass	Reported purity	Producer
7.	Sodium Di-hydrogen Orthophosphate	$NaH_2PO_4.2H_2O$	156.01	98-100%	Loba Chemie Pvt. Ltd., India
8.	Di-sodium Hydrogen Orthophosphate	$Na_2HPO_4.2H_2O$	177.99	97-100%	Thermo Fisher Scientific India Pvt. Ltd.
9.	Sodium Hydroxide	NaOH	40.0	97%	E-Merck, Germany
10.	Sodium Bicarbonate	$NaHCO_3$	84.0	99%	E-Merck, Germany

3.2 Equipments

During this research work the following instruments were used-

- The electrochemical studies (CV, DPV) were performed with a computer controlled potentiostats/ galvanostats (μstat 400, Drop Sens, Spain)
- A Pyrex glass micro cell with teflon cap
- Glassy carbon (GC)/ Gold (Au)/ Platinum (Pt) as working electrode (BASi, USA)
- Three carbon rods (Local market Dhaka, Bangladesh)
- Ag/AgCl as reference electrode (BASi, USA)
- Liquid micro size (0.05um) polishing alumina (BAS Inc. Japan)
- Pt wire as counter electrode (Local market, Dhaka, Bangladesh)
- A HR 200 electronic balance with an accuracy of ± 0.0001g was used for weighting and
- A pH meter (pH Meter, Hanna Instruments, Italy) was employed for maintaining the pH of the solutions.

3.3 Cyclic voltammetry (CV)

There are many well developed electro-analytical techniques are used for the study of electrochemical reactions. Among these we have selected the CV technique to study and analyze the redox reactions occurring at the polarizable electrode surface. This technique provides suitable information to understand the mechanism of electron transfer reaction of

the compounds as well as the nature of adsorption of reactants or products on the electrode surface. CV is often the first experiment performed in an electrochemical study. CV consists of imposing an excitation potential nature on an electrode immersed in an unstirred solution and measuring the current and its potential ranges varies from a few millivolts to hundreds of millivolts per second in a cycle. This variation of anodic and cathodic current with imposed potential is termed as voltammogram [41].

The technique involves under the diffusion controlled mass transfer condition at a stationary electrode utilizing symmetrical triangular scan rate ranging from 1 mV/s to hundreds millivolts per second.

In CV the current function can be measured as a function of scan rate. The potential of the working electrode is controlled vs a reference electrode such as Ag/AgCl electrode. The electrode potential is ramped linearly to a more negative potential and then ramped is reversed back to the starting voltage. The forward scan produces a current peak for any analyte that can be reduced through the range of potential scan. The current will increase as the current reaches to the reduction potential of the analyte [68].

The current at the working electrode is monitored as a triangular excitation potential is applied to the electrode. The resulting voltammogram can be analyzed for fundamental information regarding the redox reaction. The potential at the working electrode is controlled vs a reference electrode, Ag/AgCl (standard NaCl) electrode. The excitation signal varies linearly with time. First scan positively and then the potential is scanned in reverse, causing a negative scan back to the original potential to complete the cycle. Signal on multiple cycles can be used on the scan surface. A cyclic voltammogram is plot of response current at working electrode to the applied excitation potential.

3.4 Important features of CV

An electrochemical system containing species ‘O’ capable of being reversibly reduced to ‘R’ at the electrode is given by,

$$O + ne^- = R \quad \text{.....3.1}$$

Nernst equation for the system is

$$E = E^0 + \frac{0.059}{n} \log \frac{C_0^s}{C_R^s} \quad \text{.....3.2}$$

Where,

E = Potential applied to the electrode

E^0 = Standard reduction potential of the couple versus reference electrode

n = Number of electrons in Equation (3.1)

C_0^s = Surface concentration of species 'O'

C_R^s = Surface concentration of species 'R'

A redox couple that changes electrons rapidly with the working electrode is termed as electrochemically reverse couple. The relation gives the peak current i_{pc}

$$i_{pc} = 0.4463\ nFA\ (D\alpha)^{1/2}C \quad \text{.....3.3}$$

$$\alpha = \left(\frac{nFv}{RT}\right) = \left(\frac{nv}{0.026}\right)$$

Where,

i_{pc} = peak current in amperes

F= Faraday`s constant (approximately 96500)

A = Area of the working electrode in cm^2

v= Scan rate in volt/ sec

C= Concentration of the bulk species in mol/L

D= Diffusion coefficient in cm^2 /sec

In terms of adjustable parameters, the peak current is given by the Randless- Sevcik equation,

$$i_{pc}=2.69\times10^5\times n^{3/2}AD^{1/2}Cv^{1/2} \quad \text{.....3.4}$$

The peak potential E_p for reversible process is related to the half wave potential $E_{1/2}$, by the expression,

$$E_{pc} = E_{1/2} - 1.11\left(\frac{RT}{nF}\right), \quad \text{at } 25^0\text{C} \text{ .....3.5}$$

$$E_{pc} = E_{1/2} - \left(\frac{0.0285RT}{n}\right) \text{.....3.6}$$

The relation relates the half wave potential to the standard electrode potential

$$E_{1/2} = E^0 - \frac{RT}{nF}\ln\frac{f_{red}}{f_{ox}}\left(\frac{D_{ox}}{D_{ox}}\right)^{1/2}$$

$$E_{1/2} = E^0 - \frac{RT}{nF}\ln\left(\frac{D_{ox}}{D_{red}}\right)^{1/2} \text{.....3.7}$$

Assuming that the activity coefficient f_{ox} and f_{red} are equal for the oxidized and reduced species involved in the electrochemical reaction.

From Equation (3.6), we have,

$$E_{pa} - E_{pc} = 2.22\left(\frac{RT}{nF}\right) \quad \text{at } 25^0\text{C} \ldots\ldots\ldots\ldots\ldots\ldots \quad 3.8$$

$$\text{or } E_{pa} - E_{pc} = \left(\frac{0.059}{n}\right) \quad \text{at } 25^0\text{C} \ldots\ldots\ldots\ldots\ldots\ldots \quad 3.9$$

This is a good criterion for the reversibility of electrode process. The value of i_{pa} should be close for a simple reversible couple,

$$i_{pa}/i_{pc} = 1 \ldots\ldots\ldots\ldots\ldots\ldots\ldots\ldots\ldots\ldots 3.10$$

And such a system $E_{1/2}$ can be given by,

$$E_{1/2} = \frac{E_{pa} + E_{pc}}{2} \ldots\ldots\ldots\ldots\ldots\ldots\ldots 3.11$$

For irreversible processes (those with sluggish electron exchange), the individual peaks are reduced in size and widely separated, Totally irreversible systems are characterized by a shift of the peak potential with the scan rate [69];

$$E_p = E^0 - (RT/\alpha n_a F)[0.78 - \ln(k^0/(D)^{1/2}) + \ln(\alpha n_a F\alpha/RT)^{1/2}] \ldots\ldots.. 3.12$$

Where α is the transfer coefficient and n_a is the number of electrons involved in the charge transfer step. Thus E_p occurs at potentials higher than E^0, with the over potential related to k^0 (standard rate constant) and α. Independent of the value k^0, such peak displacement can be compensated by an appropriate change of the scan rate. The peak potential and the half-peak potential (at 25^0 C) will differ by 48/ αn mV. Hence, the voltammogram becomes more drawn-out as αn decreases.

The peak current, given by

$$i_p = (2.99\times10^5)n(\alpha n_a)^{1/2}ACD^{1/2}v^{1/2} \ldots\ldots\ldots\ldots.. 3.13$$

is still proportional to the bulk concentration , but will be lower in height (depending upon the value of α) . Assuming α = 0.5, the ratio of the reversible–to–irreversible current peaks is 1.27 (i.e. the peak current for the irreversible process is about 80% of the peak for a reversible one). For quasi-reversible systems (with $10^{-1} > k^0 > 10^{-5}$ cm/s) the current is controlled by both the charge transfer and mass transport [70]. The shape of the cyclic voltammogram is a function of the ratio k^0 $(\pi vnFD/RT)^{1/2}$. As the ratio increases, the process approaches the reversible case. For small values of it, the system exhibits an irreversible behavior. Overall, the voltammograms of a quasi-reversible system are more

drawn out and exhibit a larger separation in peak potential compared to a reversible system.

Unlike the reversible process in which the current is purely mass transport controlled, currents due to quasi-reversible process are controlled by a mixture of mass transport and charge transfer kinetics [70, 71]. The process occurs when the relative rate of electron transfer with respect to that of mass transport is insufficient to maintain Nernst equilibrium at the electrode surface.

3.5 Differential pulse voltammetry (DPV)

Differential pulse voltammetry (DPV) is a technique in which potential is applied after certain period of time and measures the resulting faradic current as a function of applied potential either in oxidation or reduction. It is designed to minimize background charging currents. The waveform in DPV is a sequence of pulses, where a baseline potential is held for a specified period of time prior to the application of a potential pulse. Current is sampled just prior to the application of the potential pulse. The potential is then stepped by a small amount (typically < 100 mV) and current is sampled again at the end of the pulse. The potential of the working electrode is then stepped back by a lesser value than during the forward pulse such that baseline potential of each pulse is incremented throughout the sequence.

By contrast, in normal pulse voltammetry the current resulting from a series of ever larger potential pulse is compared with the current at a constant ‘baseline’ voltage. Another type of pulse voltammetry is square wave voltammetry, which can be considered a special type of differential pulse voltammetry in which equal time is spent at the potential of the ramped baseline and potential of the superimposed pulse. The potential wave form consists of small pulses (of constant amplitude) superimposed upon a staircase wave form [59]. Unlike NPV, the current is sampled twice in each pulse Period (once before the pulse, and at the end of the pulse), and the difference between these two current values is recorded and displayed.

3.6 Important features of DPV

Differential pulse voltammetry has following important features:

i) Current is sampled just prior to the application of the potential pulse.

ii) Reversible reactions show symmetrical peaks and irreversible reaction show asymmetrical peaks.

iii) The peak potential is equal to $E_{1/2}^{r}$-ΔE in reversible reactions, and the peak current is proportional to the concentration.

3.7 Chronoamperometry (CA)

Chronoamperometry is an electrochemical technique in which current is measured as a function of time. By applying this technique it is easily possible to find out the number of electron transfers during the course of redox reaction. It has advantage of without knowing a value of a diffusion coefficient [72]. When potential is stepped from a non-reacting domain to *E,* a Cottrell plot (*I* vs. $t^{-1/2}$) shows the slope by the linear diffusion.

$$s = \pi^{1/2} nFD^{1/2} a^2 c^*$$

together with the intercept for the edge effect

$$p = \pi nFDac^*$$

where *a* is the radius of the electrode, *c** is the concentration of the electroactive species, *D* is the diffusion coefficient. The ratio of the square of the slope, *s*, to the intercept, *p*, is

$$n = s^2 / pFa^3 c^* \quad \text{.....3.14}$$

Since this equation does not include *D*, values of *n* can be determined from *s* and *p* without knowing *D* values.

3.8 Computer controlled potentiostats (for CV, DPV and CA experiment)

Potentiostats/ Galvanostats (μStat 400, DropSens, Spain) is the main instrument for voltammetry, which has been applied to the desired potential to the electrochemical cell (i.e. between a working electrode and a reference electrode), and a current-to-voltage converter, which measures the resulting current, and the data acquisition system produces the resulting voltammogram.

3.9 Electrochemical cell

In this investigation three electrodes electrochemical cell has been used. It has advantages over two electrodes cell because of using 3rd electrode. It reduces the solvent resistance and ensures that no electron transfer through the reference electrode. The voltammetric cell also contains a Teflon cap. The electrochemical reaction of interest takes place at the working electrode and the electrical current at this electrode due to electron transfer is termed as faradic current. The counter electrode is driven by the potentiostatic circuit to balance the faradic process at the working electrode with an electron transfer of opposite direction.

3.10 Electrodes

Three types of electrodes are used in this research:

i) Working electrodes are Glassy carbon (GC) electrode with 3.0 mm diameter disc, Gold (Au) & Platinum (Pt) electrode with 1.6 mm diameter disc and three carbon rods (diameter 6.0 mm)

ii) Ag/AgCl (standard NaCl) electrode used as reference electrode from BASi, USA

iii) Counter electrode is a Pt wire

The working electrode is an electrode on which the reaction of interest is occurring. The reference electrode is a half-cell having a known electrode potential and it keeps the potential between itself and the working electrode. The counter electrode is employed to allow for accurate measurements to be made between the working and reference electrodes.

3.11 Preparation of electrodes

In this study, Glassy carbon (GC), Gold (Au) and Platinum (Pt) electrodes purchase from the BASi, USA are used as working electrode. Electrode preparation includes polishing and conditioning of the electrode. The electrode was polished with 0.05µm alumina powder on a wet polishing cloth. For doing so a part of the cloth was made wet with deionized water and alumina powder was sprinkled over it. Then the electrode was

polished by softly pressing the electrode against the polishing surface at least 10 minutes. The electrode surface would look like a shiny mirror after thoroughly washed with deionized water.

3.12 Removing dissolved Oxygen from solution

Dissolved oxygen can interfere with observed current response so it is needed to remove it. Experimental solution was indolent by purging for at least 5-10 minutes with 99.99% pure and dry nitrogen gas (BOC, Bangladesh). By this way, traces of dissolved oxygen were removed from the solution.

3.13 Electrode polishing

Materials may be adsorbed to the surface of a working electrode after each experiment. Then the current response will degrade and the electrode surface needs to clean. In this case, the cleaning required is light polishing with 0.05 μm alumina powder. A few drops of polish are placed on a polishing pad and the electrode is held vertically and the polish rubbed on in a figure-eight pattern for a period of 30 seconds to a few minutes depending upon the condition of the electrode surface. After polishing the electrode surface is rinsed thoroughly with deionized water.

3.14 Experimental procedure

The electrochemical cell filled with solution 50 mL of the experimental solution and the Teflon cap was placed on the cell. The working electrode together with reference electrode and counter electrode was inserted through the holes. The electrodes were sufficiently immersed. The solution system is deoxygenated by purging the nitrogen gas for about 10 minutes. The solution has been kept quiet for 10 seconds. After determination the potential window the voltammogram is taken at various scan rates, pH and concentrations from the Drop View Software.

3.15 Preparation of buffer solutions

Preparation of different kinds of buffer solution is discussed below:

Acetate Buffer Solution: To prepare acetate buffer (pH 3.0-5.0) solution definite amount of sodium acetate was dissolved in 0.5M acetic acid in a volumetric flask and the pH was measured. The pH of the buffer solution was adjusted by further addition of acetic acid and / or sodium acetate.

Phosphate Buffer Solution: Phosphate buffer solution (pH 6.0-8.0) was prepared by mixing a solution of 0.5M sodium dihydrogen ortho-phosphate ($NaH_2PO_4.2H_2O$) with a solution of 0.5M disodium hydrogen ortho-phosphate ($Na_2HPO_4.2H_2O$). The pH of the prepared solution was measured with pH meter.

Bicarbonate Buffer Solution: To prepare hydroxide buffer (pH 9.0-11.0) solution definite amount of sodium hydroxide was dissolved in 0.5M sodium bicarbonate in a volumetric flask. The pH of the prepared solution was measured with pH meter.

Figure 3.1: Experimental setup (Software controlled Potentiostats (µstat 400))

CHAPTER IV

Results and Discussion

Cyclic voltammetry (CV), differential pulse voltammetry (DPV), controlled potential coulometry (CPC) and chronoamperometry (CA) techniques were used to investigate the electrochemical behavior of Catechol in presence of Glycine, L-Aspartic acid and L-Glutamic acid in aqueous solution by using Glassy carbon (GC), Gold (Au) and Platinum (Pt) electrodes. In concordance with the experiment we have abstracted precious information considering nucleophilic substitution reaction of Catechol with Glycine, L-Aspartic acid and L-Glutamic acid which has been disputed elaborately in following section.

4.1.1 Electrochemical behavior of Catechol

Cyclic voltammogram of the first 15 cycles of 2 mM Catechol of GC (3 mm) electrode in neutral media shows in Fig. 4.1. According to this voltammogram it can be seen that at 0.1 V/s scan rate it shows one anodic peak at 0.38 V related to its transformation to *o*-quinone and corresponding cathodic peak at 0.03 V related to its transformation to Catechol from *o*-quinone (Scheme 1) within a quasi-reversible two-electron transfer process. In the overall cycle there is no new anodic peak observed. The anodic and corresponding cathodic peak current ratios at different scan rates are nearly unity at low scan rate which is tabulated in Table 4.1 it indicates that the redox reactions are quasi-reversible. It can be also considered as criteria for the stability of *o*-quinone produced at the surface of electrode under the experimental conditions [73]. In other words, any hydroxylation [74-77] or dimerization [78-80] reactions are too slow that can be observed in the time-scale of cyclic voltammetry [73].

4.1.2 Electrochemical nature of Catechol in presence of Glycine

Cyclic voltammogram of only Catechol (Green line), only Glycine (Blue line) and Catechol with Glycine (Red line) at GC (3 mm) electrode in buffer solution of pH 7 and scan rate 0.1 V/s in the second scan of potential shows in Fig. 4.2. The cyclic voltammogram of Catechol displays one redox pair at A_1 (0.26 V) and C_1 (0.05 V) related to its transformation to *o*-quinone and vice versa. Pure Glycine is electrochemically inactive amino acid hence no redox peak in the potential range investigated (Fig. 4.2, Blue line). Cyclic voltammogram of Catechol in the presence of Glycine in buffer solution at pH 7 shows one anodic peak in the first cycle of potential and on the reverse scan the corresponding cathodic peak slowly decreases and new peak C_0 is observed at less positive potential -0.34 V. In the second cycle of potential a new anodic peak A_0 is also observed at less positive potential at 0.04 V. Due to formation of new redox couple the current intensity of Catechol reduces. This phenomenon can be explained by the fact of nucleophilic attack of Glycine to *o*-benzoquinone. Due to the conduction of nucleophilic substitution reaction of Glycine with Catechol, the *o*-benzoquinone concentration in reaction layer reduces, subsequently the A_1 and C_1 peak reduces. Whereas in the same time Catechol-glycine adducts produces and consequently the new peak A_0 appears. The peak current ratio for the peaks A_1 and C_1 (I_{pa1}/I_{pc1}) decreased noticeably, which indicated the chemical reaction of Glycine (**2**) with the *o*-quinone (**1a**) produced at the surface of electrode. These observations may ascribe the formation of 2-((3,4-dihydroxy phenyl)amino)acetic acid through nucleophilic substitution reaction (Scheme 1). If the constituent is such that the potential for the oxidation of product is lower, then further oxidation of the product and further addition may occur [81]. According to this concept it can be drawn that, the oxidation of Catechol-glycine is easier than the oxidation of parent Catechol in the presence of excess amount of nucleophile and this substituted product can be further attacked by Glycine. However, it was not observed in cyclic voltammogram because of the low activity of *o*-quinone **4** toward **2**. This behavior is in agreement with that reported by other research groups for similar electrochemically generated compounds such as Catechol and different nucleophiles [21-23, 33, 34, 81-83]. In the absence of other nucleophiles, water or hydroxide ion often adds to the *o*-benzoquinone [76].

Fig. 4.3 shows the CV of second scan of potential of 2 mM Catechol with 70 mM Glycine at Platinum (Pt) (1.6 mm) electrode in pH 7 and at scan rate 0.1 V/s. This cyclic

voltammogram shows the comparison of only 2 mM Catechol (Green line), pure Glycine (Blue line) and Catechol (2 mM) with Glycine (70 mM) (Red line) in the second scan of potential at the same condition. A new reduction peak (C_0) appears at -0.29 V after the addition of 70 mM Glycine to the solution at first scan of potential. The peak current decreases significantly with respect to the only Catechol. In the second scan of potential Catechol with Glycine shows two anodic peaks at -0.03 V and 0.33 V and the corresponding two cathodic peaks at -0.29 V and 0.03 V, respectively. Upon addition of Glycine to Catechol solution, the cathodic peak C_1 decreases and a new cathodic peak C_o appears. Also, in the second scan of potential a new anodic peak A_0 appears and anodic peak A_1 decreases similar to GC electrode. This observation can be stated by considering nucleophilic attack of Glycine to *o*-benzoquinone. The nucleophilic attack of Glycine to *o*-benzoquinone reduces the *o*-benzoquinone concentration in reaction layer. Accordingly the A_1 and C_1 peak reduces, whereas in the same time produces Catechol-glycine adduct and consequently the peak A_0 and C_0 appears (Scheme 1).

A similar behavior is observed when we used a Gold (Au) electrode for the investigation of same solution in the same condition. Fig. 4.4 shows the CV of Catechol (2 mM) in the presence of Glycine (70 mM) at Au electrode in the second scan of potential. Upon addition of Glycine to Catechol solution at the Gold (Au) electrode it shows three anodic and three cathodic peaks for the second scan of potential. The newly appearance of A_0 and C_0 peak, and decrease of A_1 and C_1 peak, and also shifting of the positions of peaks A_1 and C_1 also indicates that it is due to follow up reaction of Catechol with Glycine (Scheme 1) at Au electrode. In case of GC and Pt electrodes, it shows two anodic and two cathodic peaks. The third peak of Au electrodes is due to the oxidation of Au in buffer solution. This unlike behavior has been discussed in the effect of electrode materials section.

4.1.3 Effect of scan rate of Catechol with Glycine

Fig. 4.5 demonstrates different scan rate comparison voltammogram of 2 mM Catechol in presence of 70 mM Glycine at pH 7. From this voltammogram it can be observed that the peak current intensity of newly appeared peak gradually increases with the increase of scan rates. The cathodic peaks shift towards left whereas the anodic peaks move to the right direction with increase of scan rate. Fig. 4.6 shows plot of the anodic and cathodic net peak

currents for second cycle against the square-root of the scan rates where the net current means the second peak subtracted from the first one by the scan-stopped method in the same condition [81]. The nearly proportional ratio in between redox couple specifies that the peak current of the reactant at each redox reaction is controlled by diffusion process (Table 4.2). It can be seen in Fig. 4.5, the cathodic peak for reduction of *o*-benzoquinone is almost disappeared in the scan rate of 0.05 V/s. By increasing the scan rate, the cathodic peak for reduction of *o*-benzoquinone starts to appear and increasing. The corresponding peak current ratio (I_{pa1}/I_{pc1}) vs scan rate for a mixture of Catechol and Glycine decreases with increasing scan rate firstly and then after 0.1 V/s, it remains almost unchanged (Fig. 4.7, left scale). The anodic peak current ratio (I_{pa0}/I_{pa1}) vs scan rate for a mixture of Catechol and Glycine firstly increases and then after 0.3 V/s scan rate the peak current remains constant (Fig. 4.7, right scale). On the other hand, the value of current function ($I_p/v^{1/2}$) is found to be decreased with increasing scan rate (Fig. 4.8). The exponential nature of the current function versus the scan rate plot is indicative of an Electron transfer-Chemical reaction- Electron transfer (ECE) mechanism for electrode reaction process [84]. This confirms the reactivity of *o*-benzoquinone (**1a**) towards Glycine (**2**) firstly increases at slow scan rate and then at higher scan rate it decreases.

The existence of a subsequent chemical reaction between *o*-benzoquinone **1a** and Glycine **2** is supported by the following evidence.

(i) In the presence of Glycine both I_{pc1} and I_{pa1} decreases during second cycle (Fig. 1), this could be indicative of the fact that electrochemically generated *o*-benzoquinone **1a** is removed partially by chemical reaction with Glycine (**2**).

(ii) Corresponding peak current ratio (I_{pa1}/I_{pc1}) varies with potential sweep rate. In this case, a well-defined cathodic peak C_1 is observed at highest sweep rate. For lower sweep rates, the peak current ratio (I_{pa1}/I_{pc1}) is less than one and increases with increasing sweep rate. This is indicative of departure from intermediate and arrival to diffusion region with increasing sweep rate [81].

(iii) Increase in the scan rate causes a decrease in the progress of the chemical reaction of **1a** with **2** during the period of recording the cyclic voltammogram and therefore, decease in peak current ratio (I_{pa0}/I_{pa1}) at higher scan rate.

(iv) The current function, $I_p/v^{1/2}$ for A_1 was found to be decreased exponentially with increasing scan rate. This indicates the reaction mechanism of the system was of ECE type (Scheme 1).

According to the results, it was assumed that Glycine (**2**) undergoes the 1,4-Michael addition reaction with *o*-benzoquinone (**1a**) leads to product **3**. The oxidation of this compound (**3**) was observed easier than the oxidation of parent molecule (**1**) by virtue of the presence of electron donating amine group. It is assumed that the product 3 can also undergo in addition reaction with 1b.

Reaction scheme 1

Step-1:

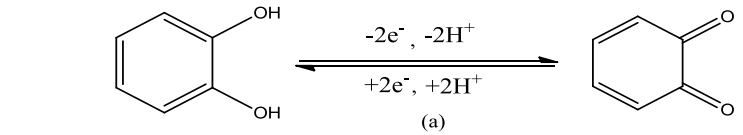

Catechol
1

o-benzoquinone
1a

Step-2:

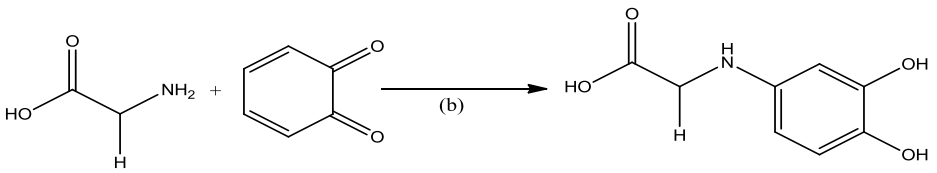

Glycine
2

o-benzoquinone
1a

2-((3,4-dihydroxyphenyl)amino)acetic acid
3

Step-3:

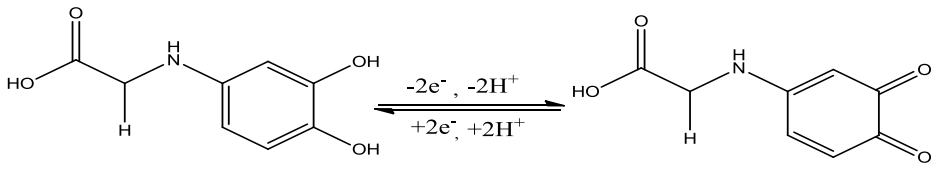

2-((3,4-dihydroxyphenyl)amino)acetic acid
3

2-((3,4-dioxocyclohexa-1,5-dien-1-yl)amino)acetic acid
4

Step-4:

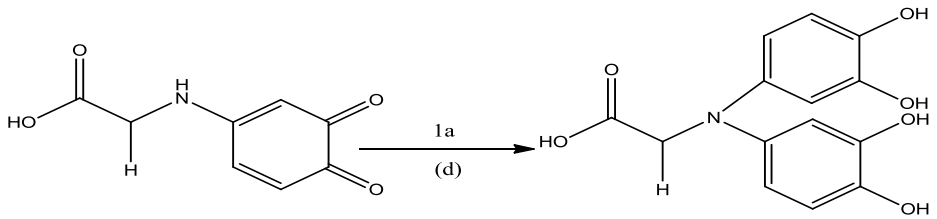

2-((3,4-dioxocyclohexa-1,5-dien-1-yl)amino)acetic acid
4

2-(bis(3,4-dihydroxyphenyl) amino)acetic acid

Fig. 4.9 shows the CV of second scan of potential at Pt electrode of 2 mM Catechol with 70 mM Glycine at pH 7 and different scan rate. The peak current of both the anodic and cathodic peaks increases with the increase of scan rate. The anodic peaks are shifted towards right direction and the cathodic peaks are to the left with increase in the scan rate. Fig. 4.10 shows plots of the anodic and cathodic peak currents for second scan of potential as a function of square-root of the scan rates. The proportionality of the anodic and the cathodic peaks ascribed that the peak current of the reactant at each redox reaction is controlled by diffusion process. The anodic and cathodic peak currents, peak potentials, corresponding peak potential differences and peak current ratio are tabulated in Table 4.3. Fig. 4.11 shows variation of peak current ratio of corresponding peak (I_{pa1}/I_{pc1}) and anodic peak (I_{pa0}/I_{pa1}) vs scan rate (v) of 2 mM Catechol with 70 mM Glycine in the same condition. The corresponding peak current ratio (I_{pa1}/I_{pc1}) vs scan rate for a mixture of Catechol and Glycine decreases with increasing scan rate firstly and then after 0.2 V/s, it remains almost unchanged (Fig. 4.11, left scale). The anodic peak current ratio (I_{pa0}/I_{pa1}) vs scan rate for a mixture of Catechol and Glycine firstly increases and then after 0.15 V/s scan rate the peak current starts to be decreased (Fig. 4.11, right scale). Beside this, the value of current function ($I_p/v^{1/2}$) is found to be decreased with increasing scan rate (Fig. 4.12). The exponential nature of the current function versus the scan rate plot indicates the ECE mechanism for the reaction system.

Similarly the voltammetric behavior of the above systems has been investigated at Au electrode. Fig. 4.13 shows the CV of Catechol with 70 mM Glycine for second cycle of potential at different scan rate in pH 7. This voltammogram is consistent with Fig. 4.5 and Fig. 4.9. According to Fig. 4.14 it can be seen that the anodic and cathodic net peak currents against the square-root of the scan rates is nearly proportional which suggests that the peak current of the reactant at each redox reaction is controlled by diffusion process (Table 4.4). Fig. 4.15 shows variation of peak current ratio of corresponding peak (I_{pa1}/I_{pc1}) and anodic peak (I_{pa0}/I_{pa1}) vs scan rate (v) in the same condition. The (I_{pa1}/I_{pc1}) peak current ratio gradually decreases up to 0.3 V/s and then it remains content (Fig. 4.15, left scale) whereas the anodic peak current ratio observed maximum at 0.15 V/s and after that is remains constant with increasing scan rates (Fig. 4.15, right scale). The exponentially decreasing nature with increasing scan rates in Fig. 4.16 indicates that the reaction is taken place by ECE mechanism. According to all system it can be said that, the nucleophilic

substitution reaction of Catechol in presence of Glycine is maximum favorable at slow scan rate by diffusion process.

4.1.4 Influence of pH on Catechol with Glycine

Cyclic voltammogram of Catechol in presence of 70 mM Glycine of GC (3 mm) electrode has been examined at pH from 5 to 11 (Fig. 4.17). The voltammetric behavior of Catechol at pH 5, 9 and 11 in the presence of 70 mM Glycine show no new anodic peak appeared after repetitive cycling indicating that the reaction between o-benzoquinone and Glycine has not forwarded. This can be clarified by the fact that at pH 5, the nucleophilic property of amine groups is diminished through protonation (Fig. 4.17) as well as at pH 5 or lowers; the amino group undergoes protonation by excess proton and form zwitterion. Whereas, in the higher pH range (e.g., pH 9-11), the cyclic voltammograms of Catechol show irreversible behavior. It was thus suggested that the oxidation of Catechol followed by an irreversible chemical reaction with hydroxyl ion, especially in alkaline solutions [85]. However amines in this condition can also act as nucleophiles. The peak position of the redox couple is found to be dependent upon pH.

Fig. 4.18 shows the plot of oxidation peak (A_0) current, I_p against pH of solution. From this figure it was seen that the maximum peak current was obtained at pH 7 (Table 4.5). At this pH, the difference between the peak current ratio (I_{pc0}/I_{pa0}) in the presence of Glycine is observed maximum. Consequently, pH 7 was selected as optimum condition for electrochemical study of Catechol, at which the electro oxidation was facilitated in neutral media and hence the rate of electron transfer was faster.

The anodic peak potential of Catechol shifted towards left with the increase of pH (Table 4.5). Figure 4.19 shows the plot of peak potential, E_p values against pH. As shown, the peak potential for A_0 and A_1 peak shifted to the negative potentials by increasing pH. This is expected because of participation of proton in the reaction of Catechol with Glycine. From the Figure 4.19, the slopes of the plot was determined graphically as the anodic peaks (27 mV/pH for oxidation peak A_1) at 0.1 V/s, which is close to the theoretical value for one step two electrons, two protons transfer process. This indicates that both the oxidation of the Catechol and Catechol-glycine adduct proceeded via the $2e^-/2H^+$ processes. This also suggests that during the reaction not only electron but also proton are released from the Catechol-glycine adduct.

CV of Catechol in presence of 70 mM Glycine at Platinum (Pt) (1.6 mm) electrode in the second scan of potential has been studied in pH 5 to 11 (Fig. 4.20). The voltammetric behavior of 2 mM Catechol at pH 5 in the presence of 70 mM Glycine shows one anodic peak and corresponding cathodic peak after repetitive cycling expressing that the reaction between *o*-quinone and Glycine has not occurred. This can be assigned to the fact that at acidic media, the nucleophilic property of amine groups is diminished through protonation. In the pH 7-9, the *o*-quinone undergoes Glycine attack by the amine through a Michael addition reaction suggests that voltammetric new anodic peak A_0 appeared after repetitive cycling. However amines in this condition can also act as nucleophiles. The peak position of the redox couple is found to be dependent upon pH. Fig. 4.21 shows the plot of oxidation peak current, I_p against pH solution. It is seen that the maximum peak current is obtained at pH 7 (Table 4.6). Fig. 4.22 shows the plot of peak potential, E_p vs pH. The slope value of the plot is obtained 69.5 mV/pH which is nearer to the value of two step one electron, one proton transfer process.

The effect of pH on the cyclic voltammogram of 2 mM Catechol in presence of 70 mM Glycine at Au (1.6 mm) electrode in the second scan of potential was studied at pH from 5 to 11 (Fig. 4.23). The influence of pH for Au electrode in the same systems, the voltammetric properties are slightly different from GC electrode. The voltammetric behavior of Catechol at pH 5 in the presence of Glycine shows no new peak in the second scan of potential. This can be indicated to the fact that in lower pH, the nucleophilic property of amine groups is diminished through protonation. In the pH 7-9, the *o*-benzoquinone undergoes Glycine attack by the amine through Michael addition reaction reflected that voltammetric new anodic peak A_0 appeared after repetitive cycling. In the higher pH (e.g., pH 11), no new anodic peak appeared in the second scan of potential. However, the peak position of the redox species is found to be dependent upon pH. Fig. 4.24 shows the plots of oxidation peak current, I_p against pH of solution. It is seen that the maximum peak current is obtained at pH 7 attributed that nucleophilic addition reaction is most favorable in neutral media (Table 4.7). Fig. 4.25 shows the plot of the peak potential, E_p against pH at second cycle in the same condition. The slopes of the plot were (50.5 mV/pH for anodic peak A_1) which is close to theoretical value for two step one electron, one proton transfer process.

4.1.5 Concentration effect of Glycine

The effect of composition change of Glycine has been studied by varying 30 mM to 110 mM with fixed composition of Catechol (2 mM) with the help of cyclic voltammetry of GC electrode at pH 7 and scan rate 0.1 V/s (Fig. 4.26). Upon addition of Glycine the anodic peaks moves positively and a new peak appears at ~ 0.04 V which suggests that the nucleophilic attack takes place and consequently Catechol-glycine adduct deposits on the electrode surface. The peak current intensity of the newly appeared anodic and cathodic peak increases with the increase of Glycine concentration up to 70 mM and after that the redox peak current is started to be decreased (Fig. 4.27). The nucleophilic substitution reaction of Catechol in presence of Glycine was maximum suitable up to 70 mM of Glycine at pH 7. The corresponding peak current ratio (I_{pc1}/I_{pa1}) changes with the concentration of Glycine. This is related to the increase of the homogenous reaction rate of following chemical reaction between *o*-benzoquinone **1a** and Glycine **2** with increasing concentration of Glycine up to 70 mM (Table 4.8). At higher concentration of Glycine (>70 mM), the excess electro-inactive Glycine may be deposited on the electrode surface and consequently the peak current decreased.

In addition of different concentration of Glycine (30, 50, 70, 90 and 110 mM) into fixed concentration of Catechol (2 mM) at Platinum (Pt) and Gold (Au) electrodes has been also examined in the same conditions (Fig. 4.28 and Fig. 4.30). In the first scan of potential a new cathodic peak (C_0) is appeared at -0.3 V and -0.19 V at Pt and Au electrodes respectively. Upon addition of Glycine in the second scan of potential, the anodic peaks shifted and a new anodic peak appeared at 0.03 V and - 0.1 V at Pt and Au electrodes respectively which suggests the formation of Catechol-glycine adduct. The net current intensity of the newly appeared anodic and cathodic peak increases with the increase of composition up to 30 to 70 mM of Glycine (Fig. 4.29 and 4.31). After further addition of Glycine (>70 mM), the anodic and cathodic peak current gradually decreases (Table 4.9 and 4.10). At higher concentration of Glycine (>70 mM), the excess electro inactive Glycine may be accumulated on the electrode surface and the peak current decreased. Therefore, the concentration effects of Glycine into the fixed concentration of Catechol (2 mM) for Au and Pt electrodes are few different from GC electrode.

4.1.6 Effect of electrode materials

The effect of electrode materials on the electrochemical nature of Catechol has been studied in absence and presence of 70 mM Glycine with the fixed composition of 2 mM Catechol with the help of both cyclic voltammetry (CV) and Differential pulse voltammetry (DPV) by using different electrodes like GC, Au and Pt at different pH at scan rate 0.1 V/s have displayed in Fig. 4.32 and Fig. 4.33. Due to the higher diameter size of GC electrode (3 mm) than Au and Pt (1.6 mm) the nature of voltammogram, the peak position and current intensity for the studied systems are different for different electrodes. The CV of Au electrode is significantly different from those of the GC and Pt electrodes. At the Au electrode it shows three anodic and three cathodic peaks for the second scan of potential (Fig. 4.32). In case of GC electrode it shows two anodic and two cathodic peaks for the second scan of potential whereas at Pt electrode it shows two anodic and corresponding cathodic peaks (Fig. 4.32). Voltammetric measurements performed at an Au electrode in only buffer solution of without Catechol and Glycine at pH 7, showed a peak at 1.1 V to the formation of Au (III) hydroxide. Consequently, the third peak (1.08 V) of Au electrode in presence of Catechol and Glycine at pH 7 is due to the oxidation of Au in buffer solution. Similar behavior of oxidation of Au electrode in different pH has been reported [86]. In the case of GC and Pt electrodes for the second cycle of potential a new oxidation and reduction peak appear at lower oxidation potential which can be attributed to the oxidation of adduct formed between the *o*-benzoquinone and Glycine. Electrochemical properties of Catechol with Glycine for example change of pH, concentration, scan rate etc. were studied in detail using Pt and Au electrodes. But among the electrodes, the voltammetric response of GC electrode was better than Pt and Au electrodes in the studied systems.

According to DPV electrode comparison graph (Fig. 4.33) it can be seen that GC electrode showed better voltammetric response and three anodic peak at -0.29 V, -0.2 V and 0.27 V. We considered the Catechol-adduct peak at -0.2 V and another peak at more lower potential -0.29 V could be due to side reaction like polymerization, further oxidation of Catechol-adduct or nucleophilic attract of hydroxyl ion. Among GC, Pt and Au electrode the peak current and voltammetric response of GC electrode was found much better than Pt electrode under this investigation. Therefore, GC electrode was chosen as electrode material for this investigation.

4.1.7 Subsequent cycles of CV of Catechol-glycine

Fig. 4.34 shows the cyclic voltammograms of the first 15 cycles of 2 mM Catechol with 70 mM Glycine of GC (3 mm) electrode in buffer solution of pH 7 for the potential range between - 0.6 V to 0.9 V. The voltammogram at the scan rate 0.1 V/s has one anodic peak at 0.25 V and two cathodic peaks at -0.29 V and 0.4 V when considered the first scan of potential (Red line). In the subsequent potential cycles a new anodic peak appeared at ~ 0.03 V and intensity of the first anodic peak current increased progressively on cycling but the second anodic peak current decreases and shifted positively on cycling. This can be attributed to produce of the Catechol-glycine adduct through nucleophilic substitution reaction in the surface of electrode (Scheme 1). The successive decrease in the height of the Catechol oxidation and reduction peaks with cycling can be ascribed to the fact that the concentrations of Catechol-glycine adduct formation increased by cycling leading to the decrease of concentration of Catechol or quinone at the electrode surface. The positive shift of the second anodic peak in the presence of Glycine is probably due to the formation of a thin film of product at the surface of the electrode, inhibiting to a certain extent the performance of electrode process. Along with the increase in the number of potential cycles the first anodic peak current increased up to 10 cycles and then the peak current almost unchanged with subsequent cycle (Fig. 4.34). This may be due to the block of electrode surface by the newly formed species after more cycling.

The effect of the cyclic voltammograms of the first 15 cycles of 2 mM Catechol with 70 mM Glycine of Platinum (Pt) electrode and Gold (Au) electrode in buffer solution of pH 7 were also studied in the same condition (Fig. 4.35-4.36). In Fig. 4.36 at Au electrode there were two anodic peaks at 0.19 V and 0.86 V and three cathodic peaks at - 0.17 V, 0.13 V and 0.44 V respectively in the first scan of potential (Red line). In the subsequent scan of potential Au electrode shows a new anodic peak at -0.1 V with another three anodic peaks (Blue line). But at Pt electrode there is one anodic peaks at 0.36 V and two cathodic peaks at - 0.29 V and - 0.03 V in the first scan of potential (Red line) (Fig. 4.35). In the subsequent potential cycles a new anodic peak appeared at -0.03 V and the first anodic peak current increased progressively on cycling but the second anodic peak current decreases and shifted positively on cycling. This can be suggested to produce the

Catechol-glycine adduct through nucleophilic substitution reaction in the surface of electrode (Scheme 1).

4.1.8 Controlled-potential coulometry of Catechol with Glycine

Controlled-potential coulometry has been performed to monitor the electrolysis progress containing 1 mM of Catechol and 35 mM of Glycine at 0.45 V in pH 7 by employing CV and DPV in aqueous solution which has been showed in Fig. 4.37-4.38. This voltammogram indicates that, during the course of coulometry the peak A_0 appears and the height of the A_0 peak increases to the advancement of coulometry, parallel to the decrease in height of anodic peak A_1. After some couples of hour both redox couple of appeared peak does not increase with the successive decrease of concentration of Catechol which has been showed by both CV and DPV (Fig. 4.37-4.38). This observation could lead us to draw a concept that the capacitive current was increased or side reactions were taken place. These observations allow us to propose the pathway in Scheme 1 for the electro-oxidation of Catechol (**1**) in the presence of Glycine (**2**). According to our results, it seems that the 1,4-addition reaction of **2** to *o*-quinone (**1a**) (reaction (2)) was faster than other secondary reactions, leading to the intermediate **3**. The oxidation of this compound (**3**) was easier than the oxidation of parent starting molecule (**1**) by virtue of the presence of electron-donating group. Like *o*-quinone **1a**, *o*-quinone **4** can also be attacked from the C-5 position by Glycine (**2**). However, no over reaction was observed during the voltammetric experiments because of the low activity of the *o*-quinone **4** toward 1,4-(Michael) addition reaction with Glycine (**2**).

4.1.9 pH effect of DPV of Catechol with Glycine

To understand the effect of pH on the Voltammogram obtained from 2 mM Catechol in the presence of 70 mM Glycine in second scan of potential in different pH (5, 7, 9 and 11) at GC electrode has been shown in Fig. 4.39. In the buffer solution of pH 7, Catechol shows three well-developed peaks at -0.28 V, 0.03 V and 0.26 V respectively in the presence of Glycine (Fig. 4.39). According to our observation the peak at -0.28 V could be due to the side reaction like polymerization or nucleophilic attack on newly appeared adduct which have been reported by a group of research worker [84]. As can be seen three completely

separated anodic peaks with high current intensity were observed in pH 7, which can be attributed to the oxidations of *o*-benzoquinone-glycine new compound and Catechol respectively.

The effect of pH on the DPV technique has also been employed to make clearer for Catechol-glycine addition reaction at Pt electrode in same condition. DPV of 2 mM Catechol in the presence of 70 mM Glycine in second scan of potential at different pH (5-11) were shown in Fig. 4.40 (E_{pulse}: 0.02 V, t_{pulse}: 20 ms and scan rate 0.1 V/s). It is noticed that the peak positions of the DPV of Catechol with Glycine shifts negatively this indicates that the nucleophilic reaction is easier at pH 7. But, in pH 3-5 no new peak appears in the second scan of potential and in pH 11, the species are totally electro inactive. High current intensity is observed at pH 7, which can be attributed to the formation of Catechol-glycine adduct.

Gold (Au) electrode is also used for the investigation of DPV of 2 mM Catechol with 70 mM Glycine in different buffer solution at 0.1 V/s. Fig. 4.41 shows the first and second scan of potential of Catechol with Glycine solution at different pH, respectively. However, in pH 7 new peak A_0 appeared which may be attributed to the formation of Catechol-glycine adduct. But, in lower and higher pH media no new anodic peak appeared. In the buffer solution of pH 7, the voltammogram shows two well-developed peak ascribed the formation of adduct. The DPV of Au and Pt electrodes are consistent with the GC electrode in the studied systems at the same condition.

4.1.10 Effect of deposition time change of DPV of Catechol with Glycine

Fig. 4.42, represents the DPV of deposition time changes (0, 10, 30, 60, 90, 120 and 150 s) of 2 mM Catechol with 70 mM Glycine at pH 7. According to this Fig.4.42, increasing of deposition time leads to develop a new peak at 0.0 V. At 10 s a new peak is observed and when the deposition time increases 30 s, more nucleophilic attack occurred and consequently more Catechol-glycine adduct was formed which leads to decreasing in the concentration of *o*-benzoquinone and increasing in the concentration of Catechol-glycine adduct at the surface of electrode. Maximum peak intensity was obtained up to 30 s. For further increase of deposition time from 60 s to 150 s, both first and second anodic peak

current decreases. This confirmed that with the increase of time decreases the concentration of *o*-benzoquinone due to follow up the reaction.

4.1.11 Effect of concentration of DPV of Catechol with Glycine

To justify the effect of different composition of Glycine on Catechol was studied by using the differential pulse voltammetry. DPV of 2 mM Catechol with 30 to 110 mM Glycine at pH 7 has been shown in Fig. 4.43. There we observed again three separated anodic peaks appeared after addition of different concentration of Glycine into Catechol similar to Fig. 4.26. In this case, the gradual increasing of the concentration of Glycine up to 70 mM leads to increasing of first anodic peak current. For further increase of concentration from 80 to 110 mM, all anodic peak decreases gradually. In lower concentration of Glycine (<60 mM), the nucleophilic substitution reaction take place in comparable degree, whereas increasing the concentration of Glycine (>60 mM) make favorable nucleophilic attack of Glycine toward *o*-benzoquinone generated at the surface of electrode. For further addition of Glycine (>70 mM) into Catechol solution, the excess electro inactive Glycine deposited on the electrode surface and hence the peak current decreases.

The effect of Glycine concentration on the DPV of Catechol was also studied by using Pt (1.6 mm) electrode in the same condition. Fig. 4.44 shows DPV for 2 mM of Catechol solution containing buffer (pH 7) in the presence of various concentration of Glycine from 30 mM to 110 mM at the surface of Pt electrode for the first and second scan of potential. As reported in Fig. 4.43, in the second scan there are two separated anodic peaks appeared after addition of Glycine into Catechol. In lower concentration of Glycine (< 70 mM), the nucleophilic substitution reaction take place in comparable degree, whereas increasing the concentration of Glycine (70 mM) make susceptible for nucleophilic attack of Glycine towards *o*-benzoquinone generated at the surface of electrode. For more addition of Glycine (> 70 mM) into Catechol solution, the excess electro inactive Glycine accumulated on the electrode surface and hence the peak current decreases.

Gold (Au) electrode was also used for the investigation on the DPV of fixed 2 mM Catechol with different concentration (30-110 mM) of Glycine in buffer solution pH 7 at

0.1 Vs^{-1}. Fig. 4.45 shows the second scan of potential of the studied systems at different concentration, respectively. In second scan of potential an appeared peak, A_0 was obtained which may be attributed the formation of Catechol-glycine adduct.

In this investigation different concentration 30-110 mM of Glycine was used to determine the optimum condition for the nucleophilic substitution reaction on Catechol. As the reaction was occurred at moderately high concentration of nucleophiles, consequently the voltammetric peaks (CV and DPV) for adduct appeared noticeably. In contrast, comparatively low concentration of Glycine was not favorable for the study of electrochemical oxidation of Catechol because the appearing peak was not so prominent.
From the experimental study it is noticeable that Glycine acts properly as a nucleophile at pH 7. When the pH is below 7 that is acidic media, the nucleophilic activity of Glycine reduces due to the protonation of amine. Whereas at basic condition, other nucleophiles such as –OH produce in solution, therefore, the activity of amines decreases and the oxidation of Catechol followed by an irreversible chemical reaction with hydroxyl ion [87].

Therefore, from the above discussion it was clear that the nucleophilic substitution reaction of Catechol in presence of Glycine is maximum favorable at 70 mM of Glycine and at pH 7 which is consistent with both CV and DPV. All above observations could be attributed to the reaction between Glycine and *o*-benzoquinone species produced at the surface of electrode, with the new anodic peak being attributed to the oxidation of newly formed Catechol- glycine adduct.

4.1.12 Spectral analysis of Catechol-glycine adduct

The FTIR spectrum of the vibrational modes of the Catechol-glycine adduct, Catechol and Glycine were taken (Figure 4.134). The Catechol showed the O-H stretching band at 3421 cm^{-1}. The Glycine showed the O-H stretching band at 3452 cm^{-1} and N-H stretching sharp band at 2879 cm^{-1}. The absorption peaks due to the O-H broad stretching vibration was appeared at 3460 cm^{-1}, C=O stretching at 1647 cm^{-1} and absorption peaks due to the N-H stretching vibration was disappeared at the wave number for the Catechol-glycine

adduct. Also the finger print region is different for adduct from pure Catechol and pure Glycine.

4.2.1 Electrochemical nature of Catechol in presence of Aspartic acid

Fig. 4.46 shows the cyclic voltammogram of only Catechol (Green line), only L-Aspartic acid (Blue line) and Catechol with L-Aspartic acid (Red line) at GC (3 mm) electrode in buffer solution of pH 7 and scan rate 0.1 V/s in the second scan of potential. The cyclic voltammogram of Catechol shows one anodic peak at A_1 (0.26 V) and corresponding cathodic peak at C_1 (0.05 V) related to its transformation to *o*-quinone and vice versa. Pure L-Aspartic acid is electrochemically inactive amino acid hence no redox couple was observed in the potential range investigated (Fig. 4.46, Blue line). Cyclic voltammogram of Catechol in the presence of L-Aspartic acid in buffer solution at pH 7 shows one anodic peak in the first cycle of potential and on the reverse scan the corresponding cathodic peak slowly decreases and new peak C_0 is observed at less positive potential -0.38 V. In the second cycle of potential a new anodic peak A_0 is also observed at less positive potential at 0.05 V. Due to formation of new redox couple the current intensity of Catechol reduces. This phenomenon can be explained by the fact of nucleophilic attack of L-Aspartic acid to o-benzoquinone. Due to the conduction of nucleophilic substitution reaction of L-Aspartic acid with Catechol, the *o*-benzoquinone concentration in reaction layer reduces, consequently the A_1 and C_1 peak reduces. Whereas in the same time Catechol-aspartic acid adduct produces and consequently the new peak A_0 appears. The peak current ratio for the peaks A_1 and C_1 (I_{pa1}/I_{pc1}) decreased noticeably, which indicated the chemical reaction of L-Aspartic acid (**2**) with the o-quinone (**1a**) produced at the surface of electrode. These observations may ascribe the formation of 2-((3,4-dihydroxyphenyl) amino) succinic acid through nucleophilic substitution reaction (Scheme 2). If the constituent is such that the potential for the oxidation of product is lower, then further oxidation of the product is lower, the further oxidation and further addition may occur [81]. According to this concept it can be drawn that, the oxidation of Catechol-aspartic acid is easier than the oxidation of parent Catechol in the presence of excess amount of nucleophile and this substituted product can be further attacked by L-Aspartic acid. However, it was not observed in cyclic voltammogram because of the low activity of *o*-quinone **4** toward **2**.

Fig. 4.47 shows the CV of second scan of potential of 2 mM Catechol with 70 mM L-Aspartic acid at Platinum (Pt) (1.6 mm) electrode in pH 7 and at scan rate 0.1 V/s. This cyclic voltammogram shows the comparison of only 2 mM Catechol (Green line), pure L-Aspartic acid (Blue line) and Catechol (2 mM) with L-Aspartic acid (70 mM) (Red line) in the second scan of potential at the same condition. A new reduction peak (C_0) appears at -0.32 V after the addition of 70 mM L-Aspartic acid to the solution at first scan of potential. The peak current decreases significantly with respect to the only Catechol. In the second scan of potential Catechol with L-Aspartic acid shows two anodic peaks at 0.0 V and 0.28 V and the corresponding two cathodic peaks at - 0.32 V and 0.07 V, respectively. Upon addition of L-Aspartic acid to Catechol solution, the cathodic peak C_1 decreases and a new cathodic peak C_o appears. Also, in the second scan of potential a new anodic peak A_0 appears and anodic peak A_1 decreases similar to GC electrode. This observation can be stated by considering nucleophilic attack of L-Aspartic acid to *o*-benzoquinone. The nucleophilic attack of L-Aspartic acid to *o*-benzoquinone reduces the *o*-benzoquine concentration in reaction layer. Accordingly the A_1 and C_1 peaks reduce, whereas in the same time produces Catechol-aspartic acid adduct and consequently the peak A_0 and C_0 appears (Scheme 2).

Reaction scheme 2

Step-1:

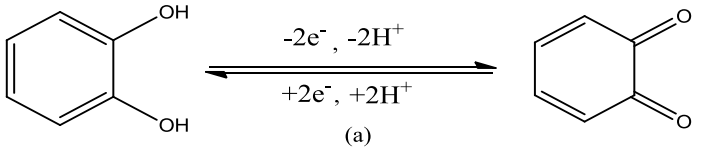

Catechol
1

o-benzoquinone
1a

Step-2:

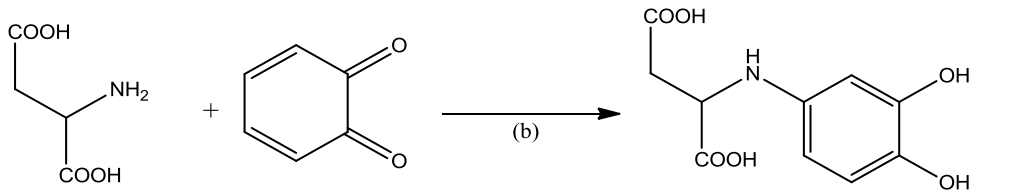

Aspartic acid
2

o-benzoquinone
1a

2-((3,4-dihydroxyphenyl)amino)succinic acid
3

Step-3:

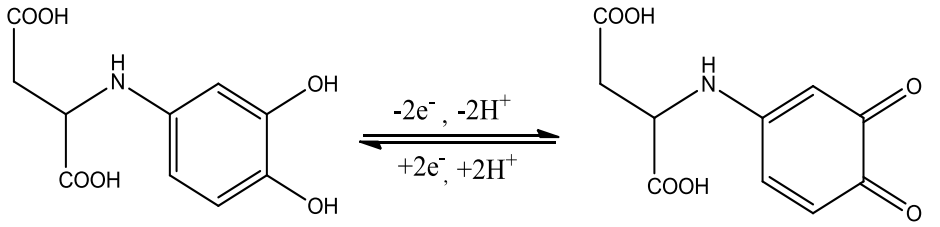

2-((3,4-dihydroxyphenyl)amino)succinic acid

3

2-((3,4-dioxocyclohexa-1,5-dien-1-yl)amino)succinic acid

4

Step-4:

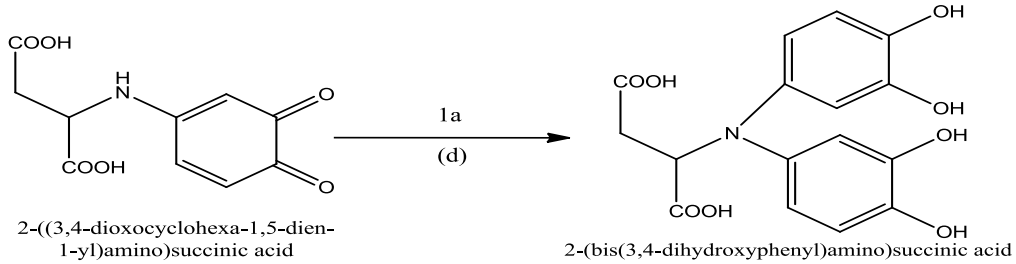

2-((3,4-dioxocyclohexa-1,5-dien-1-yl)amino)succinic acid

4

2-(bis(3,4-dihydroxyphenyl)amino)succinic acid

5

A similar behavior is observed when we used a Gold (Au) electrode for the investigation of same solution in the same condition. Fig. 4.48 shows the CV of Catechol (2 mM) in the presence of L-Aspartic acid (70 mM) at Au electrode in the second scan of potential. Upon addition of L-Aspartic acid to Catechol solution at the Gold (Au) electrode it shows three anodic and three cathodic peaks for the second scan of potential. The newly appearance of A_0 and C_0 peak, and decrease of A_1 and C_1 peak, and also shifting of the positions of peaks A_1 and C_1 also indicates that it is due to follow up reaction of Catechol with L-Aspartic acid (Scheme 2) at Au electrode. In case of GC and Pt electrodes, it shows two anodic and two cathodic peaks. The third peak of Au electrodes is due to the oxidation of Au in buffer solution. This unlike behavior has been discussed in the effect of electrode materials section.

4.2.2 Effect of scan rate of Catechol with L-Aspartic acid

According to the different scan rate comparison graph it can be seen that the peak current intensity of newly appeared peak gradually increases with the increase of scan rates (Fig. 4.49). The cathodic peaks shift towards left whereas the anodic peaks move to the right direction with increase of scan rate (Table 4.11). Fig. 4.50 shows plot of the anodic

and cathodic net peak currents for second cycle against the square-root of the scan rates where the net current means the second peak subtracted from the first one by the scan-stopped method in the same condition [81]. The nearly proportional ratio in between redox couple indicates that the peak current of the reactant at each redox reaction is controlled by diffusion process. It can be seen in Fig. 4.49, the cathodic peak for reduction of *o*-benzoquinone is almost disappeared in the scan rate of 0.05 V/s. By increasing the scan rate, the cathodic peak for reduction of *o*-benzoquinone starts to appear and increasing. The corresponding peak current ratio (I_{pa1}/I_{pc1}) vs scan rate for a mixture of Catechol and L-Aspartic acid decreases with increasing scan rate firstly and then after 0.2 V/s, it remains almost unchanged (Fig. 4.51, left scale). The anodic peak current ratio (I_{pa0}/I_{pa1}) vs scan rate for a mixture of Catechol and L-Aspartic acid firstly increases up to 0.1 V/s and then it starts to be decreased after 0.25 V/s scan rate the peak current remains almost constant in (Fig. 4.51, right scale). On the other hand, the value of current function ($I_p/v^{1/2}$) is found to be decreased with increasing scan rate (Fig. 4.52). The exponential nature of the current function versus the scan rate plot indicates the reaction occurred by ECE mechanism [84]. This confirms the reactivity of *o*-benzoquinone (**1a**) towards L-Aspartic acid (**2**) firstly increases at slow scan rate and then at higher scan rate it decreases.

According to the results, it was assumed that L-Aspartic acid (**2**) undergoes the 1,4-Michael addition reaction with *o*-benzoquinone (**1a**) leads to product **3**. The oxidation of this compound (**3**) was observed easier than the oxidation of parent molecule (**1**) by virtue of the presence of electron donating amine group.

Fig. 4.53 shows the CV of second scan of potential at Pt electrode of 2 mM Catechol with 70 mM L-Aspartic acid at pH 7 and different scan rate. The peak current of both the anodic and cathodic peaks increases with the increase of scan rate. The anodic peaks are shifted towards right direction and the cathodic peaks are to the left with increase in the scan rate. Fig. 4.54 shows plots of the anodic and cathodic peak currents for second scan of potential as a function of square-root of the scan rates. The proportionality of the anodic and the cathodic peaks ascribed that the peak current of the reactant at each redox reaction is controlled by diffusion process. The anodic and cathodic peak currents, peak potentials, corresponding peak potential differences and peak current ratio are tabulated in Tables 4.12.

Fig. 4.55 shows variation of peak current ratio of corresponding peak (I_{pa1}/I_{pc1}) and anodic peak (I_{pa0}/I_{pa1}) vs scan rate (v) of 2 mM Catechol with 70 mM L-Aspartic acid in the same condition. The corresponding peak current ratio (I_{pa1}/I_{pc1}) vs scan rate for a mixture of Catechol and L-Aspartic acid decreases with increasing scan rate firstly and then after 0.15-0.35 V/s it remains almost unchanged and finally it starts to be increased (Fig. 4.55, left scale). The anodic peak current ratio (I_{pa0}/I_{pa1}) vs scan rate for a mixture of Catechol and L-Aspartic acid firstly increases and then after 0.15 V/s scan rate the peak current starts to be decreased (Fig. 4.55, right scale). Beside this, the value of current function ($I_p/v^{1/2}$) is found to be decreased with increasing scan rate (Fig. 4.56). The exponential nature of the current function versus the scan rate plot indicates the ECE mechanism for electrode process.

Similarly the voltammetric behavior of the above systems has been investigated at Au electrode. Fig. 4.57 shows the CV of Catechol with 70 mM L-Aspartic acid for second cycle of potential at different scan rate in pH 7. This voltammogram is consistent with Fig. 4.49 and Fig. 4.53. According to Fig. 4.58 it can be seen that the anodic and cathodic net peak currents against the square-root of the scan rates is nearly proportional which suggests that the peak current of the reactant at each redox reaction is controlled by diffusion process. Fig. 4.59 shows variation of peak current ratio of corresponding peak (I_{pa1}/I_{pc1}) and anodic peak (I_{pa0}/I_{pa1}) vs scan rate (v) in the same condition. The (I_{pa1}/I_{pc1}) peak current ratio gradually decreases with increasing scan rate 0.5 V/s whereas anodic peak (I_{pa0}/I_{pa1}) gradually increases up to 0.2 V/s and then it starts to be decreased (Table 4.13). The exponentially decreasing nature with increasing scan rates in Fig. 4.60 indicates that the reaction is taken place by ECE mechanism. According to all system it can be said that, the nucleophilic substitution reaction of Catechol in presence of L-Aspartic acid is maximum favorable at slow scan rate by diffusion process.

4.2.3 Influence of pH on Catechol with L-Aspartic acid

Influence of pH has been investigated by means of cyclic voltammetry technique. Catechol in presence of 70 mM L-Aspartic acid of GC (3 mm) electrode was studied at different pH 5, 7, 9 and 11 (Fig. 4.61). The voltammetric behavior of Catechol at pH 9 and 11 in the presence of 70 mM L-Aspartic acid show no new anodic peak appeared after

repetitive cycling indicating that the reaction between *o*-benzoquinone and L-Aspartic acid has not occurred. This can be attributed to the fact that at pH 5, the nucleophilic property of amine groups is diminished through protonation that's why no new anodic peak observed (Fig. 4.61). Whereas, in the higher pH range (e.g., pH 9-11), the cyclic voltammograms of Catechol show irreversible behavior. It was thus suggested that the oxidation of Catechol followed by an irreversible chemical reaction with hydroxyl ion, especially in alkaline solutions [85]. However amines in this condition can also act as nucleophiles. The peak position of the redox couple is found to be dependent upon pH. Fig. 4.62 shows the plot of oxidation peak (A_0) current, I_p against pH of solution. From this Fig., it is seen that the maximum peak current was obtained at pH 7 (Table 4.14). At this pH, the difference between the peak current ratio (I_{pc0}/I_{pa0}) in the presence of L-Aspartic acid is observed maximum. Consequently, pH 7 was selected as optimum condition for electrochemical study of Catechol, at which the electro oxidation was facilitated in neutral media and hence the rate of electron transfer was faster. The anodic peak potential of Catechol shifted towards left with the increase of pH. Fig. 4.63 shows the plot of the peak potential, E_p against pH at second cycle in the same condition. The slopes of the plot were (50 mV/pH for anodic peak A_1) which is close to theoretical value for two step one electron, one proton transfer process.

CV of Catechol in presence of 70 mM L-Aspartic acid at Platinum (Pt) (1.6 mm) electrode in the second scan of potential has been studied in pH 5 to 11 (Fig. 4.64). The voltammetric behavior of 2 mM Catechol at pH 5 in the presence of 70 mM L-Aspartic acid shows two anodic peaks and one cathodic peak after repetitive cycling expressing that the reaction between *o*-quinone and L-Aspartic acid has started. In the pH 5-7, the *o*-quinone undergoes L-Aspartic acid attack by the amine through a Michael addition reaction suggests that voltammetric new anodic peak A_0 appeared after repetitive cycling. However amines in this condition can also act as nucleophiles. The peak position of the redox couple is found to be dependent upon pH. Fig. 4.65 shows the plot of oxidation peak current, I_p against pH solution. It is seen that the maximum peak current is obtained at pH 7 (Table 4.15). Fig. 4.66 shows the plot of peak potential, E_p vs pH. The slope value of the plot is obtained 74 mV/pH which is nearer to the value of two step one electron and one proton transfer process.

The effect of pH on the cyclic voltammogram of 2 mM Catechol in presence of 70 mM L-Aspartic acid at Au (1.6 mm) electrode in the second scan of potential was studied at pH from 5 to 11 (Fig. 4.67). The influence of pH for Au electrode in the same systems, the voltammetric properties are slightly different from GC electrode. The voltammetric behavior of Catechol at pH 5 in the presence of L-Aspartic acid shows no new peak in the second scan of potential. This can be indicated to the fact that in lower pH, the nucleophilic property of amine groups is diminished through protonation. In the pH 7, the *o*-benzoquinone undergoes L-Aspartic acid attack by the amine through Michael addition reaction reflected that voltammetric new anodic peak A_0 appeared after repetitive cycling. However, the peak position of the redox species is found to be dependent upon pH. Fig. 4.68 shows the plots of oxidation peak current, I_p against pH of solution. It is seen that the maximum peak current is obtained at pH 7 attributed that nucleophilic addition reaction is most favorable in neutral media (Table 4.16). Fig. 4.69 shows the plot of the peak potential, E_p against pH at second cycle in the same condition. The slopes of the plot were (56.5 mV/pH for anodic peak A_1) which is close to theoretical value for two step one electron, one proton transfer process.

4.2.4 Concentration effect of L-Aspartic acid

The nature of voltammogram, is strongly influenced by the composition of L-Aspartic acid. In the same condition (Fig. 4.70). Upon addition of L-Aspartic acid the anodic peaks shifts positively and a new peak appears at 0.06 V which suggests that the nucleophilic attack takes place and consequently Catechol-aspartic acid adduct deposits on the electrode surface. The peak current intensity of the newly appeared anodic and cathodic peak increases with the increase of L-Aspartic acid concentration up to 70 mM and after that the redox peak current is started to be decreased (Fig. 4.71). The nucleophilic substitution reaction of Catechol in presence of L-Aspartic acid was maximum favorable up to 70 mM of L-Aspartic acid at pH 7 (Table 4.17). The corresponding peak current ratio (I_{pc1}/I_{pa1}) changes with the concentration of L-Aspartic acid. This was related to the increase of the homogenous reaction rate of following chemical reaction between *o*-benzoquinone **1a** and L-Aspartic acid **2** with increasing concentration of L-Aspartic acid up to 70 mM. At higher concentration of L-Aspartic acid (>70 mM), the excess electro-inactive L-Aspartic acid may be deposited on the electrode surface and consequently the peak current decreased.

In addition of different concentration of L-Aspartic acid (30, 50, 70, 80 and 100 mM) into fixed concentration of Catechol (2 mM) at Platinum (Pt) and Gold (Au) electrodes has been also examined in the same conditions (Fig. 4.72 and Fig. 4.74). In the first scan of potential a new cathodic peak (C_0) is appeared at -0.32 V and -0.22 V/s at Pt and Au electrodes respectively. Upon addition of L-Aspartic acid in the second scan of potential, the anodic peaks shifted and a new anodic peak appeared at 0.01 V and -0.01 V at Pt and Au electrodes respectively which suggests the formation of Catechol-aspartic acid adduct. The net current intensity of the newly appeared anodic and cathodic peak increases with the increase of composition up to 70 mM of L-Aspartic acid (Table 4.18-4.19). After further addition of L-Aspartic acid (>70 mM), the anodic and cathodic peak current gradually decreases. At higher concentration of L-Aspartic acid (>70 mM), the excess electro inactive L-Aspartic acid may be accumulated on the electrode surface and the peak current decreased. Therefore, the concentration effects of L-Aspartic acid into the fixed concentration of Catechol (2 mM) for Au and Pt electrodes are few different from GC electrode.

4.2.5 Effect of electrode materials

Cyclic voltammetry (CV) and Differential pulse voltammetry (DPV) have been employed to study the effect of electrode materials in absence and presence of 70 mM L-Aspartic acid with the fixed composition of 2 mM Catechol by using different electrodes like GC, Au and Pt at different pH at scan rate 0.1 V/s has shown in Fig. 4.76 and Fig. 4.77. The nature of voltammogram, the peak position and current intensity for the studied systems are different for different electrodes although the diameter of GC electrode (3 mm) was higher than Au and Pt (1.6 mm). The CV of Au electrode is significantly different from those of the GC and Pt electrodes. Among them the peak current intensity of GC electrode is much higher than Au and Pt electrodes. In the case of second cycle of potential a new oxidation and reduction peak appear at lower oxidation potential which can be attributed to the oxidation of adduct formed between the *o*-benzoquinone and L-Aspartic acid. Electrochemical properties of Catechol with L-Aspartic acid for example change of pH, concentration, scan rate etc. were studied in detail using Pt and Au electrodes. But among the electrodes, the voltammetric response of GC electrode was better than Pt and Au electrodes in the studied systems.

According to DPV electrode comparison graph (Fig. 4.77) it can be seen that GC electrode showed better voltammetric response and three anodic peak at -0.27.5 V, 0.005 V and 0.3 V respectively. We considered the Catechol-aspartic acid adduct peak at 0.005 V and another peak at more lower potential -0.27.5 could be due to side reaction like polymerization, further oxidation of Catechol-adduct or nucleophilic attract of hydroxyl ion. Among GC, Pt and Au electrodes the peak current and voltammetric response of GC electrode was found much better than Pt and Au electrodes under this investigation. Therefore, GC electrode was chosen as electrode material for this investigation.

4.2.6 Subsequent cycles of CV of Catechol-aspartic acid

Cyclic voltammogram of the first 15 cycles of 2 mM Catechol with 70 mM L-Aspartic acid of GC (3 mm) electrode in buffer solution of pH 7 for the potential range between -0.6 V to 0.9 V has been shown in fig. 4.78. The voltammogram at the scan rate 0.1 V/s has one anodic peak at 0.32 V and two cathodic peaks at -0.38 V and 0.07 V when considered the first scan of potential (Red line). In the subsequent potential cycles a new anodic peak appeared at ~ 0.04 V and intensity of the first anodic peak current increased progressively on cycling but the second anodic peak current decreases and shifted positively on cycling. This can be attributed to produce of the Catechol-aspartic acid adduct through nucleophilic substitution reaction in the surface of electrode (Scheme 2). The successive decrease in the height of the Catechol oxidation and reduction peaks with cycling can be ascribed to the fact that the concentrations of Catechol-aspartic acid adduct formation increased by cycling leading to the decrease of concentration of Catechol or quinone at the electrode surface. The positive shift of the second anodic peak in the presence of L-Aspartic acid is probably due to the formation of a thin film of product at the surface of the electrode, inhibiting to a certain extent the performance of electrode process. Along with the increase in the number of potential cycles the first anodic peak current increased up to 10 cycles and then the peak current almost unchanged with subsequent cycle (Fig. 4.78). This may be due to the block of electrode surface by the newly formed species after more cycling.

The effect of the cyclic voltammograms of the first 15 cycles of 2 mM Catechol with 70 mM L-Aspartic acid of Platinum (Pt) electrode and Gold (Au) electrodes in buffer

solution of pH 7 were also studied in the same condition. At Pt electrode there is one anodic peak at 0.3 V and two cathodic peaks at - 0.33 V and 0.04 V in the first scan of potential (Red line) (Fig. 4.79). In the subsequent potential cycles a new anodic peak appeared at - 0.06 V and the first anodic peak current increased progressively on cycling but the second anodic peak current decreases and shifted positively on cycling. But in Fig. 4.80 at Au electrode there were two anodic peaks at 0.24 V and 1.03 V and three cathodic peaks at -0.33 V, 0.14 V and 0.43 V respectively in the first scan of potential (Red line). In the subsequent scan of potential Au electrode shows a new anodic peak at - 0.02 V with another three anodic peaks (Blue line). This can be suggested to produce the Catechol-aspartic acid adduct through nucleophilic substitution reaction in the surface of electrode (Scheme 2).

4.2.7 Controlled-potential coulometry of Catechol with L-Aspartic acid

To achieve deep information about the electrochemical oxidation, Controlled potential coulommetry technique has been employed to monitor the electrolysis progress with the help of CV and DPV in aqueous solution containing 1 mM of Catechol and 35 mM of L-Aspartic acid at 0.4 V in pH 7 which has been showed in Fig. 4.81-4.82. This voltammogram indicates that, during the course of coulometry the peaks A_0 appears and the height of the A_0 peak increases to the advancement of coulometry, parallel to the decrease in height of anodic peak A_1. After some couples of hour both redox couple of appeared peak does not increase with the successive decrease of concentration of Catechol which has been showed by both CV and DPV (Fig. 4.81 and 4.82). This observation could lead us to draw a concept that the capacitive current was increased or side reactions were taken place. These observations allow us to propose the pathway in Scheme 2 for the electro-oxidation of Catechol (**1**) in the presence of L-Aspartic acid (**2**). According to our results, it seems that the 1,4-addition reaction of **2** to *o*-quinone (**1a**) (reaction scheme-2) was faster than other secondary reactions, leading to the intermediate **3**. The oxidation of this compound (**3**) was easier than the oxidation of parent starting molecule (**1**) by virtue of the presence of electron-donating group. Like *o*-quinone **1a**, *o*-quinone **4** can also be attacked from the C-5 position by L-Aspartic acid (**2**). However, no over reaction was observed during the voltammetric experiments because of the low activity of the *o*-quinone **4** toward 1,4-(Michael) addition reaction with L-Aspartic acid (**2**).

4.2.8 pH effect of DPV of Catechol with L-Aspartic acid

It is worth to mention that, acidic, basic and neutral media play an important role in electrochemical characterization. Voltammogram obtained from 2 mM Catechol in the presence of 70 mM L-Aspartic acid in second scan in different pH (5-11) at GC electrode has shown in Fig. 4.83 to make clearer for the nucleophilic substitution reaction of L-Aspartic acid with Catechol. In the buffer solution of pH 7, Catechol gave three well-developed peaks at -0.29 V, - 0.06 V and 0.23 V respectively in the presence of L-Aspartic acid (Fig. 4.83). According to our observation the peak at -0.29 V could be due to the side reaction like polymerization or nucleophilic attack on newly appeared adduct which have been reported by a group of research worker [81]. It also can be seen that at pH 5 there are three oxidation peak observed at -0.9 V, 0.11 V and 0.52 V. As can be seen three completely separated anodic peaks with high current intensity were observed in pH 7, which can be attributed to the oxidations of Catechol-aspartic acid new compound and Catechol respectively.

The effect of pH on the DPV technique was also employed to make clearer for Catechol-aspartic acid addition reaction at Pt electrode in same condition. DPV of 2 mM Catechol in the presence of 70 mM L-Aspartic acid in second scan of potential at different pH (5-11) were shown in Fig. 4.84, (E_{pulse}: 0.02 V, t_{pulse}: 20 ms and scan rate 0.1 V/s). It is noticed that the peak positions of the DPV of Catechol with L-Aspartic acid shifts negatively this indicates that the nucleophilic reaction is easier at pH 7. But, in pH 5, pH 9 and pH 11 no new peak appears in the second scan of potential. High current intensity is observed at pH 7, which can be attributed to the formation of Catechol-aspartic acid adduct. Gold (Au) electrode is also used for the investigation of DPV of 2 mM Catechol with 70 mM L-Aspartic acid in different buffer solution at 0.1 V/s. Fig. 4.85 shows second scan of potential of Catechol with L-Aspartic acid solution at different pH. However, in pH 7 new peaks A_0 appeared which may be attributed to the formation of Catechol-aspartic acid adduct. But, in lower and higher pH media no new anodic peak appeared. In the buffer solution of pH 7, the voltammogram shows two well-developed peak ascribed the formation of adduct similar to GC electrode. The DPV of Au and Pt electrodes are consistent with the GC electrode in the studied systems at the same condition.

4.2.9 Effect of deposition time change of DPV of Catechol with L-Aspartic acid

The effect of deposition time change on the electrochemical behavior of Catechol has been summarized in fig.4.86. According to this Fig., increasing of deposition time leads to develop a new peak at - 0.01 V. At 10s a new peak is observed and when the deposition time increases 30s, more nucleophilic attack occurred and consequently more Catechol-aspartic acid adduct was formed which leads to decreasing in the concentration of *o*-benzoquinone and increasing in the concentration of Catechol-aspartic acid adduct at the surface of electrode. Maximum peak intensity was obtained up to 30s. For further increase of deposition time from 40s to 240s, both first and second anodic peak current decreases. This confirmed that with the increase of time decreases the concentration of *o*-benzoquinone due to follow up the reaction.

4.2.10 Effect of concentration of DPV of Catechol with L-Aspartic acid

According to above CV concentration comparison graph it was mentioned that the concentration of nucleophile strongly influence the electrochemical behavior of Catechol. To draw more information about the effect of different composition of L-Aspartic acid on Catechol was studied by using the differential pulse voltammetry (DPV). DPV of 2 mM Catechol with 30 to 100 mM L-Aspartic acid at pH 7 has been shown in Fig. 4.87. There we observed again three separated anodic peaks appeared after addition of different concentration of L-Aspartic acid into Catechol. In this case, the gradual increasing of the concentration of L-Aspartic acid up to 70 mM leads to increasing of first anodic peak current. For further increase of concentration from 80 to 100 mM, all anodic peak decreases gradually. In lower concentration of L-Aspartic acid (<70 mM), the nucleophilic substitution reaction take place in comparable degree, whereas increasing the concentration of L-Aspartic acid (>70 mM) make favorable nucleophilic attack of L-Aspartic acid toward *o*-benzoquinone generated at the surface of electrode. For further addition of L-Aspartic acid (>70 mM) into Catechol solution, the excess electro inactive L-Aspartic acid deposited on the electrode surface and hence the peak current decreases.

The effect of L-Aspartic acid concentration on the DPV of Catechol was also studied by using Pt (1.6 mm) electrode in the same condition. Fig. 4.88 shows DPV for 2 mM of

Catechol solution containing buffer (pH 7) in the presence of various concentration of L-Aspartic acid from 30 mM to 100 mM at the surface of Pt electrode for the second scan of potential. As reported in Fig. 4.88, in the second scan there are two separated anodic peaks appeared after addition of L-Aspartic acid into Catechol. In lower concentration of L-Aspartic acid (< 70 mM), the nucleophilic substitution reaction take place in comparable degree, whereas increasing the concentration of L-Aspartic acid (70 mM) make susceptible for nucleophilic attack of L-Aspartic acid towards *o*-benzoquinone generated at the surface of electrode. For more addition of L-Aspartic acid (> 70 mM) into Catechol solution, the excess electro inactive L-Aspartic acid accumulated on the electrode surface and hence the peak current decreases.

Gold (Au) electrode was also used for the investigation on the DPV of fixed 2 mM Catechol with different concentration (30-100 mM) of L-Aspartic acid in buffer solution pH 7 at 0.1 Vs^{-1}. Fig. 4.89 shows the second scan of potential of the studied systems at different concentration, respectively. In second scan of potential an appeared peak, A_0 was obtained which may be attributed the formation of Catechol-aspartic acid adduct.

In this investigation different concentration 30-100 mM of L-Aspartic acid was used to determine the optimum condition for the nucleophilic substitution reaction on Catechol. As the reaction was occurred at moderately high concentration of nucleophiles, consequently the voltammetric peaks (CV and DPV) for adduct appeared noticeably. In contrast, comparatively low concentration of L-Aspartic acid was not favorable for the study of electrochemical oxidation of Catechol because the appearing peak was not so prominent. From the experimental study it is noticeable that L-Aspartic acid acts properly as a nucleophile at pH 7. When the pH is below 7 that is acidic media, the nucleophilic activity of L-Aspartic acid reduces due to the protonation of amine. Whereas at basic condition, other nucleophiles such as –OH produce in solution, therefore, the activity of amines decreases and the oxidation of Catechol followed by an irreversible chemical reaction with hydroxyl ion [87].

Therefore, from the above discussion it was clear that the nucleophilic substitution reaction of Catechol in presence of L-Aspartic acid is maximum favorable at 70 mM of L-Aspartic acid and at pH 7 which is consistent with both CV and DPV. All above observations could be attributed to the reaction between L-Aspartic acid and

o-benzoquinone species produced at the surface of electrode, with the new anodic peak being attributed to the oxidation of newly formed *o*-benzoquinone- Aspartic acid adduct.

4.2.11 Spectral analysis of Catechol-aspartic acid adduct

The FTIR spectral assignments of the vibrational modes of the Catechol-aspartic acid adduct, Catechol and L-Aspartic acid were studied (Figure 4.135). The L-Aspartic acid showed the OH stretching band at 3450 cm^{-1} and N-H stretching band at 2911 cm^{-1}. Catechol showed the O-H stretching band at 3421 cm^{-1}. The absorption peaks due to the O-H broad stretching vibration was appeared at 3444 cm^{-1}, N-H stretching band at 3118 cm^{-1}, C=O stretching at 1624 cm^{-1} and aromatic C=C stretching at 1577 cm^{-1} for Catechol-aspartic acid adduct. In adduct the peaks at finger print region are different from pure Catechol and L-Aspartic acid.

4.3.1 Electrochemical nature of Catechol in presence of L-Glutamic acid

To investigate the electrochemical nature of Catechol in presence of L-Glutamic acid a comparison graph has shown in Fig. 4.90. This figure indicates the cyclic voltammogram of only 2 mM Catechol (Green line), only 30 mM L-Glutamic acid (Blue line) and Catechol with L-Glutamic acid (Red line) at GC (3 mm) electrode in buffer solution of pH 7 and scan rate 0.1 V/s in the second of potential. The cyclic voltammogram of Catechol shows one anodic peak at A_1 (0.26 V) and corresponding cathodic peak at C_1 (0.05 V) related to its transformation to *o*-quinone and vice versa. Pure L-Glutamic acid is electrochemically inactive amino acid hence no redox couple was observed in the potential range investigated (Fig. 4.90, Blue line). Cyclic voltammogram of Catechol in the presence of L-Glutamic acid in buffer solution at pH 7 shows one anodic peak in the first cycle of potential and on the reverse scan the corresponding cathodic peak slowly decreases and new peak C_0 is observed at less positive potential -0.44 V. In the second cycle of potential a new anodic peak A_0 is also observed at less positive potential at 0.04 V. Due to formation of new redox couple the current intensity of Catechol reduces. This phenomenon can be explained by the fact of nucleophilic attack of L-Glutamic acid to o-benzoquinone. Due to the conduction of nucleophilic substitution reaction of L-Glutamic acid with Catechol, the *o*-benzoquinone concentration in reaction layer reduces,

consequently the A_1 and C_1 peak reduces. Whereas in the same time Catechol-glutamic acid adduct produces and consequently the new peak A_0 appears. The peak current ratio for the peaks A_1 and C_1 (I_{pa1}/I_{pc1}) decreased noticeably, which indicated the chemical reaction of L-Glutamic acid (**2**) with the *o*-quinone (**1a**) produced at the surface of electrode. These observations may ascribe the formation of 2-((3,4-dihydroxyphenyl) amino)pentanedioic acid through nucleophilic substitution reaction (Scheme 3). If the constituent is such that the potential for the oxidation of product is lower, then further oxidation of the product is lower, the further oxidation and further addition may occur [81]. According to this concept it can be drawn that, the oxidation of Catechol-glutamic acid is easier than the oxidation of parent Catechol in the presence of excess amount of nucleophile and this substituted product can be further attacked by L-Glutamic acid. However, it was not observed in cyclic voltammogram because of the low activity of *o*-quinone **4** toward **2**.

Fig. 4.91 shows the CV of second scan of potential of 2 mM Catechol with 30 mM L-Glutamic acid at Platinum (Pt) (1.6 mm) electrode in pH 7 and at scan rate 0.1 V/s. This cyclic voltammogram shows the comparison of only 2 mM Catechol (Green line), pure L-Glutamic acid (Blue line) and Catechol (2 mM) with L-Glutamic acid (30 mM) (Red line) in the second scan of potential at the same condition. A new reduction peak (C_0) appears at -0.32 V after the addition of 30 mM L-Glutamic acid to the solution at first scan of potential. The peak current decreases significantly with respect to the only Catechol. In the second scan of potential Catechol with L-Glutamic acid shows two anodic peaks at -0.02 V and 0.27 V and the corresponding two cathodic peaks at -0.32 V and 0.06 V, respectively. Upon addition of L-Glutamic acid to Catechol solution, the cathodic peak C_1 decreases and a new cathodic peak C_o appears. Also, in the second scan of potential a new anodic peak A_0 appears and anodic peak A_1 decreases similar to GC electrode. This observation can be stated by considering nucleophilic attack of L-Glutamic acid to *o*-benzoquinone. The nucleophilic attack of L-Glutamic acid to o-benzoquinone reduces the *o*-benzoquinone concentration in reaction layer. Accordingly the A_1 and C_1 peaks reduce, whereas in the same time produces Catechol-glutamic acid adduct and consequently the peak A_0 and C_0 appears (Scheme 3).

A similar behavior is observed when we used a Gold (Au) electrode for the investigation of same solution in the same condition. Fig. 4.92 shows the CV of Catechol (2 mM) in the presence of L-Glutamic acid (30 mM) at Au electrode in the second scan of potential. Upon addition of L-Glutamic acid to Catechol solution at the Gold (Au) electrode it shows three anodic and three cathodic peaks for the second scan of potential. The newly appearance of A_0 and C_0 peak, and decrease of A_1 and C_1 peak, and also shifting of the positions of peaks A_1 and C_1 also indicates that it is due to follow up reaction of Catechol with L-Glutamic acid (Scheme 3) at Au electrode. In case of GC and Pt electrodes, it shows two anodic and two cathodic peaks. The third peak of Au electrodes is due to the oxidation of Au in buffer solution. This unlike behavior has been discussed in the effect of electrode materials section.

Reaction scheme 3

Step-1:

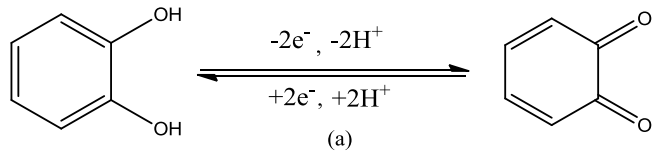

Catechol
1

o-benzoquinone
1a

Step-2:

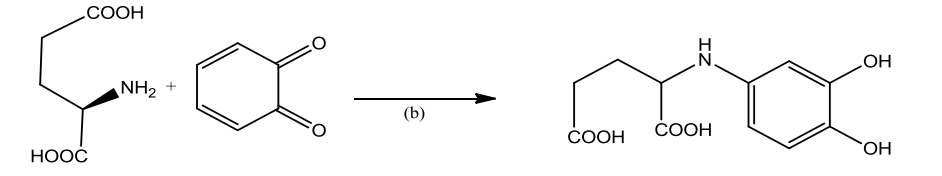

L-Glutamic acid
2

o-benzoquinone
1a

2-((3,4-dihydroxyphenyl)amino)pentanedioic acid
3

Step-3:

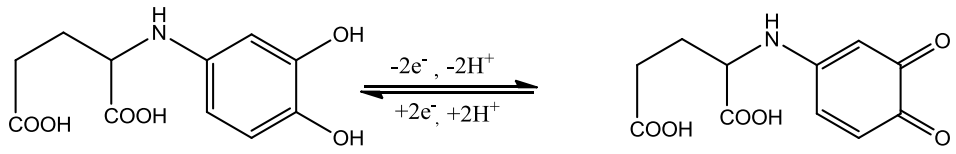

2-((3,4-dihydroxyphenyl)amino)pentanedioic acid
3

2-((3,4-dioxocyclohexa-1,5-dien-1-yl)amino)pentanedioic acid
4

Step-4:

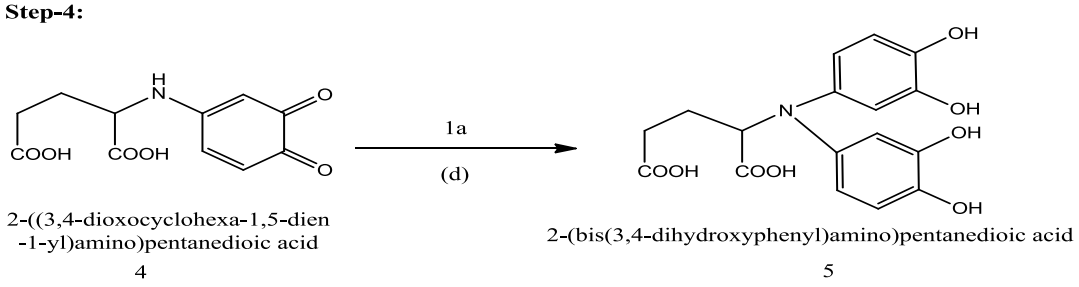

2-((3,4-dioxocyclohexa-1,5-dien -1-yl)amino)pentanedioic acid

4

2-(bis(3,4-dihydroxyphenyl)amino)pentanedioic acid

5

4.3.2 Effect of scan rate of Catechol with L-Glutamic acid

Scan rate effects on voltammogram obtained from electro-oxidation of 2 mM Catechol in presence of 30 mM Glutamic acid at pH 7 in the second scan of potential has been compared shows in Fig. 4.93. According to this voltammogram it can be seen that the peak current intensity of newly appeared peak gradually increases with the increase of scan rates. The cathodic peaks shift towards left whereas the anodic peaks move to the right direction with increase of scan rate. Fig. 4.94 shows plot of the anodic and cathodic net peak currents for second cycle against the square-root of the scan rates where the net current means the second peak subtracted from the first one by the scan-stopped method in the same condition [81]. The nearly proportional ratio in between redox couple indicates that the peak current of the reactant at each redox reaction is controlled by diffusion process. It can be seen in Fig. 4.93, the cathodic peak for reduction of o-benzoquinone is almost disappeared in the scan rate of 0.05 V/s. By increasing the scan rate, the cathodic peak for reduction of *o*-benzoquinone starts to appear and increasing (Table 4.20). The corresponding peak current ratio (I_{pa1}/I_{pc1}) vs scan rate for a mixture of Catechol and L-Glutamic acid decreases with increasing scan rate firstly and then after 0.25 V/s, it remains almost unchanged (Fig. 4.95, left scale). The anodic peak current ratio (I_{pa0}/I_{pa1}) vs scan rate for a mixture of Catechol and L-Glutamic acid firstly increases and then after 0.3 V/s scan rate the peak current remains constant in (Fig. 4.95, right scale). On the other hand, the value of current function ($I_p/v^{1/2}$) is found to be decreased with increasing scan rate (Fig. 4.96). The exponential nature of the current function versus the scan rate plot indicates the ECE mechanism for electrode process [84]. This confirms the reactivity of *o*-benzoquinone (**1a**) towards L-Glutamic acid (**2**) firstly increases at slow scan rate and then at higher scan rate it decreases.

According to the results, it was assumed that L-Glutamic acid (**2**) undergoes the 1,4-Michael addition reaction with o-benzoquinone (**1a**) leads to product **3**. The oxidation of this compound (**3**) was observed easier than the oxidation of parent molecule (**1**) by virtue of the presence of electron donating amine group.

Fig. 4.97 shows the CV of second scan of potential at Pt electrode of 2 mM Catechol with 30 mM L-Glutamic acid at pH 7 and different scan rate. The peak current of both the anodic and cathodic peaks increases with the increase of scan rates. The anodic peaks are shifted towards right direction and the cathodic peaks are to the left with increase in the scan rate Fig. 4.98 shows plots of the anodic and cathodic peak currents for second scan of potential as a function of square-root of the scan rates. The proportionality of the anodic and the cathodic peaks ascribed that the peak current of the reactant at each redox reaction is controlled by diffusion process. The anodic and cathodic peak currents, peak potentials, corresponding peak potential differences and peak current ratio are tabulated in Table 4.21. Fig. 4.99 shows variation of peak current ratio of corresponding peak (I_{pa1}/I_{pc1}) and anodic peak (I_{pa0}/I_{pa1}) vs scan rate (v) of 2 mM Catechol with 30 mM L-Glutamic acid in the same condition. The corresponding peak current ratio (I_{pa1}/I_{pc1}) vs scan rate for a mixture of Catechol and L-Glutamic acid decreases with increasing scan rate firstly and then after 0.15 V/s, it starts to be increased (Fig. 4.99, left scale). The anodic peak current ratio (I_{pa0}/I_{pa1}) vs scan rate for a mixture of Catechol and L-Glutamic acid firstly increases and then after 0.1 V/s scan rate the peak current starts to be decreased and after 0.26 V/s it remains nearly unchanged (Fig. 4.99, right scale). Beside this, the value of current function ($I_p/v^{1/2}$) is found to be decreased with increasing scan rate (Fig. 4.100). The exponential nature of the current function versus the scan rate plot indicates the reaction occurred by ECE mechanism.

Similarly the voltammetric behavior of the above systems has been investigated at Au electrode. Fig. 4.101 shows the CV of Catechol with 30 mM L-Glutamic acid for second cycle of potential at different scan rate in pH 7. This voltammogram is consistent with Fig. 4.93 and Fig. 4.97. According to Fig. 4.102 it can be seen that the anodic and cathodic net peak currents against the square-root of the scan rates is nearly proportional which suggests that the peak current of the reactant at each redox reaction is controlled by diffusion process. Fig. 4.103 shows variation of peak current ratio of corresponding peak (I_{pa1}/I_{pc1}) and anodic peak (I_{pa0}/I_{pa1}) vs scan rate (v) in the same condition. The (I_{pa1}/I_{pc1})

peak current ratio gradually decreases with increasing scan rate 0.5 V/s whereas the anodic peak current ratio observed maximum at 0.15 V/s and after that it starts to be decreased up to 0.4 V/s and then it remains constant with increasing scan rates (Table 4.22). The exponentially decreasing nature with increasing scan rates in Fig. 4.104 indicates that the reaction is taken place by ECE mechanism. According to all system it can be said that, the nucleophilic substitution reaction of Catechol in presence of L-Glutamic acid is maximum favorable at slow scan rate by diffusion process.

4.3.3 Influence of pH on Catechol with L-Glutamic acid

To study the effect of pH on the electrochemical behavior of Catechol in presence of 30 mM L-Glutamic acid; a comparison graph of pH ranging from 5-11 has displayed in (Fig. 4.105). The voltammetric behavior of Catechol at pH 5, 9 and 11 in the presence of 30 mM L-Glutamic acid show no new anodic peak appeared after repetitive cycling indicating that the reaction between *o*-benzoquinone and L-Glutamic acid has not occurred. This can be attributed to the fact that at pH 5, the nucleophilic property of amine group is diminished through protonation (Fig. 4.105). This can be explained by the fact that at pH 5 or lowers, the amino group undergoes protonation by excess proton. Whereas, in the higher pH range (e.g., pH 9-11), the cyclic voltammograms of Catechol show irreversible behavior. It was thus suggested that the oxidation of Catechol followed by an irreversible chemical reaction with hydroxyl ion, especially in alkaline solutions [85]. However amines in this condition can also act as nucleophiles. The peak position of the redox couple is found to be dependent upon pH. Fig. 4.106 shows the plot of oxidation peak (A_0) current, I_p against pH of solution. From this Fig., it is seen that the maximum peak current was obtained at pH 7 (Table 4.23). At this pH, the difference between the peak current ratio (I_{pc0}/I_{pa0}) in the presence of L-Glutamic acid is observed maximum. Consequently, pH 7 was selected as optimum condition for electrochemical study of Catechol, at which the electro oxidation was facilitated in neutral media and hence the rate of electron transfer was faster. The anodic peak potential of Catechol shifted towards left with the increase of pH. Fig. 4.107 shows the plot of the peak potential, E_p against pH at second cycle in the same condition. The slopes of the plot were (69 mV/pH for anodic peak A_1) which is close to theoretical value for two step one electron, one proton transfer process.

CV of Catechol in presence of 30 mM L-Glutamic acid at Platinum (Pt) (1.6 mm) electrode in the second scan of potential has been studied in pH 5 to 11(Fig. 4.108). The voltammetric behavior of 2 mM Catechol at pH 5 in the presence of 30 mM L-Glutamic acid shows one anodic peak and corresponding cathodic peak after repetitive cycling expressing that the reaction between *o*-quinone and L-Glutamic acid has not occurred. This can be assigned to the fact that at acidic media, the nucleophilic property of amine groups is diminished through protonation. In the pH 7-11, the *o*-quinone undergoes L-Glutamic acid attack by the amine through a Michael addition reaction suggests that voltammetric new anodic peak A_0 appeared after repetitive cycling. However amines in this condition can also act as nucleophiles. The peak position of the redox couple is found to be dependent upon pH. Fig. 4.109 shows the plot of oxidation peak current, I_p against pH solution. It is seen that the maximum peak current is obtained at pH 7 (Table 4.24). Fig. 4.110 shows the plot of peak potential, E_p vs pH. The slope value of the plot is obtained 68mV/pH which is nearer to the value of two step one electron, one proton transfer process.

The effect of pH on the cyclic voltammogram of 2 mM Catechol in presence of 30 mM L-Glutamic acid at Au (1.6 mm) electrode in the second scan of potential was studied at pH from 5 to 11 (Fig. 4.111). The influence of pH for Au electrode in the same systems, the voltammetric properties are slightly different from GC electrode. The voltammetric behavior of Catechol at pH 5 in the presence of L-Glutamic acid shows no new peak in the second scan of potential. This can be indicated to the fact that in lower pH, the nucleophilic property of amine groups is diminished through protonation. In the pH 7-11, the *o*-benzoquinone undergoes L-Glutamic acid attack by the amine through Michael addition reaction reflected that voltammetric new anodic peak A_0 appeared after repetitive cycling. However, the peak position of the redox species is found to be dependent upon pH. Fig. 4.112 shows the plots of oxidation peak current, I_p against pH of solution. It is seen that the maximum peak current is obtained at pH 7 attributed that nucleophilic addition reaction is most favorable in neutral media (table 4.25). Fig. 4.113 shows the plot of the peak potential, E_p against pH at second cycle in the same condition. The slopes of the plot were (55.5 mV/pH for anodic peak A_1) which is close to theoretical value for two step one electron, one proton transfer process.

4.3.4 Concentration effect of L-Glutamic acid

Concentration of nucleophile may affect the reaction environment. To understand the effect of composition change of L-Glutamic acid from 10 mM to 150 mM with fixed composition of Catechol at GC electrode in pH 7 and scan rate 0.1 V/s (Fig. 4.114) cyclic voltammetry method was employed. Upon addition of L-Glutamic acid the anodic peaks shifts positively and a new peak appears at 0.12 V which suggests that the nucleophilic attack takes place and consequently Catechol-glutamic acid adduct deposits on the electrode surface. The peak current intensity of the newly appeared anodic and cathodic peak increases with the increase of L-Glutamic acid concentration up to 30 mM and after that the redox peak current is started to be decreased (Fig. 4.115). The nucleophilic substitution reaction of Catechol in presence of L-Glutamic acid was maximum favorable up to 30 mM of L-Glutamic acid at pH 7 (Table 4.26). The corresponding peak current ratio (I_{pc1}/I_{pa1}) changes with the concentration of L-Glutamic acid. This was related to the increase of the homogenous reaction rate of following chemical reaction between *o*-benzoquinone **1a** and L-Glutamic acid **2** with increasing concentration of L-Glutamic acid up to 30 mM. At higher concentration of L-Glutamic acid (>30 mM), the excess electro-inactive L-Glutamic acid may be deposited on the electrode surface and consequently the peak current decreased.

In addition of different concentration of L-Glutamic acid (10, 30, 50, 100 and 150 mM) into fixed concentration of Catechol (2 mM) at Platinum (Pt) and Gold (Au) electrodes has been also examined in the same conditions (Fig. 4.116 and Fig. 4.118). In the first scan of potential a new cathodic peak (C_0) is appeared at -0.34 V and -0.22 V at Pt and Au electrodes respectively. Upon addition of L-Glutamic acid in the second scan of potential, the anodic peaks shifted and a new anodic peak appeared at 0.02 V and -0.02 V at Pt and Au electrodes respectively which suggests the formation of Catechol-glutamic acid adduct. The net current intensity of the newly appeared anodic and cathodic peak increases with the increase of composition up to 30 mM of L-Glutamic acid (Table 4.27-4.28). After further addition of L-Glutamic acid (>30 mM), the anodic and cathodic peak current gradually decreases. At higher concentration of L-Glutamic acid (>30 mM), the excess electro inactive L-Glutamic acid may be accumulated on the electrode surface and the peak current decreased. Therefore, the concentration effects of L-Glutamic acid into the fixed

concentration of Catechol (2 mM) for Pt and Au electrodes are few different from GC electrode.

4.3.5 Effect of electrode materials

Influence of electrode materials on the voltammogram have been carried out in absence and presence of 30 mM L-Glutamic acid with the fixed composition of 2 mM Catechol the by means of both cyclic voltammetry (CV) and Differential pulse voltammetry (DPV) by using different electrodes like GC, Au and Pt at different pH at scan rate 0.1 V/s has shown in Fig. 4.120 and Fig. 4.121. The nature of voltammogram, the peak position and current intensity for the studied systems are different for different electrodes although the diameter of GC electrode (3 mm) was higher than Au and Pt (1.6 mm). The CV of GC electrode is significantly different from those of the Au and Pt electrodes based on peak current consideration. All electrodes show two anodic and corresponding cathodic peaks in the potential range of investigation. Among them the peak current intensity of GC electrode is much higher than Au and Pt electrodes in Figures 4.120-4.121. In the case of second cycle of potential a new oxidation and reduction peak appear at lower oxidation potential which can be attributed to the oxidation of adduct formed between the *o*-benzoquinone and L-Glutamic acid. Electrochemical properties of Catechol with L-Glutamic acid for example change of pH, concentration, scan rate etc. were studied in detail using Pt and Au electrodes. But among the electrodes, the voltammetric response of GC electrode was better than Pt and Au electrodes in the studied systems.

According to DPV electrode comparison graph (Fig. 4.121) it can be seen that GC electrode showed better voltammetric response and three anodic peak at -0.29 V, -0.01 V and 0.28 V. We considered the Catechol-glutamic acid adduct peak at -0.01 V and another peak at more lower potential -0.29 V could be due to side reaction like polymerization, further oxidation of Catechol-glutamic acid adduct or nucleophilic attract of hydroxyl ion. Among GC, Pt and Au electrode the peak current and voltammetric response of GC electrode was found much better than Pt electrode under this investigation. Therefore, GC electrode was chosen as electrode material for this investigation.

4.3.6 Subsequent cycles of CV of Catechol-L-Glutamic acid

CV of first 15 cycles of both Catechol and Catechol-glutamic acid adduct has been displayed in Fig. 4.122 in optimum condition. The voltammogram at the scan rate 0.1 V/s has one anodic peak at 0.32 V and two cathodic peaks at -0.42 V and 0.04 V when considered the first scan of potential (Red line). In the subsequent potential cycles a new anodic peak appeared at ~ 0.06 V and intensity of the first anodic peak current increased progressively on cycling but the second anodic peak current decreases and shifted positively on cycling. This can be attributed to produce of the Catechol-glutamic acid adduct through nucleophilic substitution reaction in the surface of electrode (Scheme 3). The successive decrease in the height of the Catechol oxidation and reduction peaks with cycling can be ascribed to the fact that the concentrations of Catechol-glutamic acid adduct formation increased by cycling leading to the decrease of concentration of Catechol or quinone at the electrode surface. The positive shift of the second anodic peak in the presence of L-Glutamic acid is probably due to the formation of a thin film of product at the surface of the electrode, inhibiting to a certain extent the performance of electrode process. Along with the increase in the number of potential cycles the first anodic peak current increased up to 10 cycles and then the peak current almost unchanged with subsequent cycle (Fig. 4.122). This may be due to the block of electrode surface by the newly formed species after more cycling.

The effect of the cyclic voltammograms of the first 15 cycles of 2 mM Catechol with 30 mM L-Glutamic acid of Gold (Au) electrode and Platinum (Pt) electrode in buffer solution of pH 7 were also studied in the same condition. At Pt electrode there is one anodic peak at 0.27 V and two cathodic peaks at - 0.35 V and 0.04 V in the first scan of potential (Red line) (Fig. 4.123). In the subsequent potential cycles a new anodic peak appeared at -0.03 V and the first anodic peak current increased progressively on cycling but the second anodic peak current decreases and shifted positively on cycling. But in Fig. 4.124 at Au electrode there were two anodic peaks at 0.2 V and 1.03 V and three cathodic peaks at - 0.33 V, 0.12 V and 0.41 V respectively in the first scan of potential (Red line). In the subsequent scan of potential Au electrode shows a new anodic peak at - 0.04 V with another three anodic peaks (Blue line). This can be suggested to produce the Catechol-

Glutamic acid adduct through nucleophilic substitution reaction in the surface of electrode (Scheme 3).

4.3.7 Controlled-potential coulometry of Catechol with L-Glutamic acid

In this experiment we have introduced Controlled-potential coulommetry to monitor the electrolysis progress with the help of CV and DPV in aqueous solution containing 1 mM of Catechol and 15 mM of L-Glutamic acid at 0.40 V in pH 7 which has been showed in Fig. 4.125-4.126. This voltammogram indicates that, during the course of coulometry the peaks A_0 appears and the height of the A_0 peak increases to the advancement of coulometry, parallel to the decrease in height of anodic peak A_1. After some couples of hour both redox couple of appeared peak does not increase with the successive decrease of concentration of Catechol which has been showed by both CV and DPV. This observation could lead us to draw a concept that the capacitive current was increased or side reactions were taken place. These observations allow us to propose the pathway in Scheme 3 for the electro-oxidation of Catechol (**1**) in the presence of L-Glutamic acid (**2**). According to our results, it seems that the 1,4-addition reaction of **2** to *o*-quinone (**1a**) (reaction scheme-3) was faster than other secondary reactions, leading to the intermediate **3**. The oxidation of this compound (**3**) was easier than the oxidation of parent starting molecule (**1**) by virtue of the presence of electron-donating group. Like *o*-quinone **1a**, *o*-quinone **4** can also be attacked from the C-5 position by L-Glutamic acid (**2**). However, no over reaction was observed during the voltammetric experiments because of the low activity of the *o*-quinone **4** toward 1,4-(Michael) addition reaction with L-Glutamic acid (**2**).

4.3.8 pH effect of DPV of Catechol with L-Glutamic acid

Voltammogram attained from 2 mM Catechol in the presence of 30 mM L-Glutamic acid in second scan in different pH (5-11) at GC electrode has shown in Fig. 4.127 to make evidence for the nucleophilic substitution reaction of L-Glutamic acid with Catechol. In the buffer solution of pH 7, Catechol gave three well-developed peaks at -0.3 V, - 0.01 V and 0.25 V respectively in the presence of L-Glutamic acid (Fig. 4.127). According to our observation the peak at -0.3 V could be due to the side reaction like polymerization or nucleophilic attack on newly appeared adduct which have been reported by a group of

research worker [84]. It also can be seen that at pH 5 there are three oxidation peak observed at - 0.11 V, 0.125 V and 0.42 V. As can be seen three completely separated anodic peaks with high current intensity were observed in pH 7, which can be attributed to the oxidations of Catechol-glutamic acid new compound and Catechol, respectively.

The effect of pH on the DPV technique was also employed to make clearer for Catechol-glutamic acid addition reaction at Pt electrode in same condition. DPV of 2 mM Catechol in the presence of 30 mM L-Glutamic acid in second scan of potential at different pH (5-11) were shown in Fig. 4.128, (E_{pulse}: 0.02 V, t_{pulse}: 20 ms and scan rate 0.1 V/s). It is noticed that the peak positions of the DPV of Catechol with L-Glutamic acid shifts negatively this indicates that the nucleophilic reaction is easier at pH 7. But, in pH 5, pH 9 and pH 11 no new peak appears in the second scan of potential. High current intensity is observed at pH 7, which can be attributed to the formation of Catechol-glutamic acid adduct.

Gold (Au) electrode is also used for the investigation of DPV of 2 mM Catechol with 30 mM L-Glutamic acid in different buffer solution at 0.1 Vs^{-1}. Fig. 4.129 shows the first and second scan of potential of Catechol with L-Glutamic acid solution at different pH, respectively. However, in pH 7 new peaks A_0 appeared which may be attributed to the formation of Catechol-glutamic acid adduct. But, in lower and higher pH media no new anodic peak appeared. In the buffer solution of pH 7, the voltammogram shows two well-developed peak ascribed the formation of adduct. The DPV of Au and Pt electrodes are consistent with the GC electrode in the studied systems at the same condition.

4.3.9 Effect of deposition time change of DPV of Catechol with L-Glutamic acid

DPV of deposition time change (0, 10, 30, 60, 90, 120 and 150s) of 2 mM Catechol 30 mM L-Glutamic acid of pH 7 has been shown in Fig. 4.130. According to this Fig., a new peak develops at - 0.01 V with increasing deposition time. At 10s a new peak is observed and when the deposition time increases 30s, more nucleophilic attack occurred and consequently more Catechol-glutamic acid adduct is formed which leads to decreasing in the concentration of *o*-benzoquinone and increasing in the concentration of Catechol-glutamic acid adduct at the surface of electrode. Maximum peak intensity was obtained up

to 30s. For further increase of deposition time from 90s to 180s, both first and second anodic peak current decreases. This confirmed that with the increase of time decreases the concentration of *o*-benzoquinone due to follow up the reaction.

4.3.10 Effect of concentration of DPV of Catechol with L-Glutamic acid

The effect of different composition of L-Glutamic acid on Catechol was studied by using the differential pulse voltammetry (DPV). DPV of 2 mM Catechol with 10 to 150 mM L-Glutamic acid at pH 7 has been shown in Fig. 4.131. There we observed again three separated anodic peaks appeared after addition of different concentration of L-Glutamic acid into Catechol. In this case, the gradual increasing of the concentration of L-Glutamic acid up to 30 mM leads to increasing of first anodic peak current. For further increase of concentration from 50 to 150 mM, all anodic peak decreases gradually. In lower concentration of L-Glutamic acid (<30 mM), the nucleophilic substitution reaction take place in comparable degree, whereas increasing the concentration of L-Glutamic acid (>30 mM) make favorable nucleophilic attack of L-Glutamic acid toward *o*-benzoquinone generated at the surface of electrode. For further addition of L-Glutamic acid (>30 mM) into Catechol solution, the excess electro inactive L-Glutamic acid deposited on the electrode surface and hence the peak current decreases.

The effect of L-Glutamic acid concentration on the DPV of Catechol was also studied by using Pt (1.6 mm) electrode in the same condition. Fig. 4.132 shows DPV for 2 mM of Catechol solution containing buffer (pH 7) in the presence of various concentration of L-Glutamic acid from 10 mM to 150 mM at the surface of Pt electrode for the second scan of potential. As reported in Fig. 4.131, in the second scan there are two separated anodic peaks appeared after addition of L-Glutamic acid into Catechol. In lower concentration of L-Glutamic acid (< 30 mM), the nucleophilic substitution reaction take place in comparable degree, whereas increasing the concentration of L-Glutamic acid (30 mM) make susceptible for nucleophilic attack of L-Glutamic acid towards *o*-benzoquinone generated at the surface of electrode. For more addition of L-Glutamic acid (> 30 mM) into Catechol solution, the excess electro inactive L-Glutamic acid accumulated on the electrode surface and hence the peak current decreases.

Gold (Au) electrode was also used for the investigation on the DPV of fixed 2 mM Catechol with different concentration (10-150 mM) of L-Glutamic acid in buffer solution pH 7 at 0.1 V/s. Fig. 4.133 shows the second scan of potential of the studied systems at different concentration, respectively. In second scan of potential an appeared peak, A_0 was obtained which may be attributed the formation of Catechol-glutamic acid adduct.

In this investigation different concentration (10-150 mM) of L-Glutamic acid was used to determine the optimum condition for the nucleophilic substitution reaction on Catechol. As the reaction was occurred at moderately high concentration of nucleophiles, consequently the voltammetric peaks (CV and DPV) for adduct appeared noticeably. In contrast, comparatively low concentration of L-Glutamic acid was not favorable for the study of electrochemical oxidation of Catechol because the appearing peak was not so prominent. From the experimental study it is noticeable that L-Glutamic acid acts properly as a nucleophile at pH 7. When the pH is below 7 that is acidic media, the nucleophilic activity of L-Glutamic acid reduces due to the protonation of amine. Whereas at basic condition, other nucleophiles such as –OH produce in solution, therefore, the activity of amines decreases and the oxidation of Catechol followed by an irreversible chemical reaction with hydroxyl ion [87].

Therefore, from the above discussion it was clear that the nucleophilic substitution reaction of Catechol in presence of L-Glutamic acid is maximum favorable at 30 mM of L-Glutamic acid and at pH 7 which is consistent with both CV and DPV. All above observations could be attributed to the reaction between L-Glutamic acid and *o*-benzoquinone species produced at the surface of electrode, with the new anodic peak being attributed to the oxidation of newly formed Catechol-glutamic acid adduct.

Table 4.1: Peak potential (E_p), corresponding peak potential difference (ΔE), peak separation ($\Delta E_{1/2}$), peak current (I_p), corresponding peak current ratio (I_{pa}/I_{pc}) of 2 mM Catechol in aqueous buffer solution (pH 7) of GC electrode at different scan rate

v/Vs^{-1}	E_{pa1} /V	E_{pc1} /V	$\Delta E = E_{pc1} \sim E_{pa1}$	I_{pa1} /μA	I_{pc1} /μA	I_{pa1}/ I_{pc1}
0.05	0.37	0.04	0.33	5.23	-5.22	1.01
0.10	0.38	0.03	0.34	5.89	-5.75	1.03
0.15	0.38	0.04	0.34	3.78	-8.23	0.46
0.20	0.40	0.04	0.36	3.99	-7.46	0.53
0.25	0.42	0.03	0.39	5.27	-7.59	0.69
0.30	0.43	0.03	0.40	3.53	-7.64	0.46
0.35	0.50	0.01	0.49	3.64	-7.27	0.69
0.40	0.51	-0.03	0.54	3.52	-8.21	0.43
0.45	0.52	-0.04	0.56	4.61	-9.99	0.46

Table 4.2: Peak current (I_p), corresponding peak current ratio (I_{pa}/I_{pc}) of 2 mM Catechol with 70 mM Glycine in buffer solution (pH 7) of GC electrode at different scan rate (2nd cycle)

v/Vs^{-1}	I_{pa0} /μA	I_{pa1} /μA	I_{pc0}/μA	I_{pc1}/μA	I_{pa0}/I_{pa1}	I_{pa1}/I_{pc1}
0.05	2.93	17.66	-7.99	-6.68	0.17	2.21
0.10	4.39	19.67	-11.17	-6.73	0.22	1.76
0.15	5.89	27.25	-15.7	-9.63	0.21	1.73
0.20	7.03	33.78	-19.19	-12.53	0.20	1.76
0.25	7.87	37.98	-23.75	-12.58	0.20	1.59
0.30	8.89	40.98	-28.12	-12.64	0.21	1.45
0.35	10.87	42.65	-30.78	-16.24	0.25	1.38
0.40	12.05	44.31	-34.78	-19.65	0.27	1.27
0.45	12.66	49.99	-39.17	-20.68	0.25	1.27
0.50	13.17	53.97	-41.56	-21.71	0.24	1.29

Table 4.3: Peak current (I_p), corresponding peak current ratio (I_{pa}/I_{pc}) of 2 mM Catechol with 70 mM Glycine in buffer solution (pH 7) of Pt electrode at different scan rate (2nd cycle)

v/Vs^{-1}	I_{pa0} /μA	I_{pa1} /μA	I_{pc0}/μA	I_{pc1}/μA	I_{pa0}/I_{pa1}	I_{pa1}/I_{pc1}
0.05	1.25	4.56	-2.21	-1.98	0.27	2.30
0.10	2.01	6.62	-2.68	-3.83	0.30	1.72
0.15	2.35	7.71	-2.63	-4.04	0.30	1.90
0.20	2.53	9.78	-2.86	-7.19	0.25	1.36
0.25	2.78	12.98	-2.92	-11.75	0.21	1.10
0.30	2.89	14.98	-3.09	-13.12	0.19	1.14
0.35	3.01	16.65	-3.14	-15.78	0.18	1.05
0.40	3.1	18.31	-3.37	-17.78	0.16	1.02
0.45	3.23	21.99	-3.49	-19.17	0.14	1.14
0.50	3.45	23.97	-3.89	-21.56	0.14	1.11

Table 4.4: Peak current (I_p), corresponding peak current ratio (I_{pa}/I_{pc}) of 2 mM Catechol with 70 mM Glycine in buffer solution (pH 7) of Au electrode at different scan rate (2nd cycle)

ν/Vs^{-1}	I_{pa0} /μA	I_{pa1} /μA	I_{pc0}/μA	I_{pc1}/μA	I_{pa0}/I_{pa1}	I_{pa1}/I_{pc1}
0.05	2.57	8.09	-2.21	-3.11	0.31	2.60
0.10	3.38	11.19	-2.89	-3.9	0.30	2.86
0.15	3.78	14.33	-3.63	-4.04	0.26	3.54
0.20	4.22	17.53	-3.95	-9.67	0.24	1.81
0.25	4.37	21.23	-4.12	-11.75	0.20	1.80
0.30	4.53	25.44	-4.28	-13.12	0.17	1.93
0.35	4.89	26.57	-4.31	-15.78	0.18	1.68
0.40	5.22	28.67	-4.37	-19.46	0.18	1.47
0.45	5.4	29.78	-4.52	-19.17	0.18	1.55
0.50	5.67	31.14	-4.67	-21.56	0.18	1.44

Table 4.5: Peak Current I_p (μA), peak potential E_p (V) of 2 mM Catechol with 70 mM Glycine of GC electrode at scan rate 0.1V/s in different pH media (2nd cycle)

pH	Peak Current I_p (μA)	Peak potential E_p (V)	
	Oxidation, A_0	Oxidation, A_0	Oxidation, A_1
5	1.79	0.08	0.41
7	6.64	0.03	0.31
9	2.23	0.02	0.27
11	1.13	0.01	0.24

Table 4.6: Peak Current I_p (μA), peak potential E_p (V) of 2 mM Catechol with 70 mM Glycine of Pt electrode at scan rate 0.1V/s in different pH media (2nd cycle)

pH	Peak Current I_p (μA)	Peak potential E_p (V)
	Oxidation, A_0	Oxidation, A_0
5	0	0.08
7	3.26	0.03
9	1.23	0.02
11	0.23	0.01

Table 4.7: Peak Current I_p (µA), peak potential E_p (V) of 2 mM Catechol with 70 mM Glycine of Au electrode at scan rate 0.1V/s in different pH media (2^{nd} cycle)

pH	Peak Current I_p (µA)	Peak potential E_p (V)
	Oxidation, A_0	Oxidation, A_0
5	1.79	0.31
7	6.64	0.2
9	2.23	0.09
11	1.13	0.01

Table 4.8: Peak Current I_p (µA) of 2 mM Catechol with various concentration of Glycine of GC electrode at scan rate 0.1V/s in pH 7 (2^{nd} cycle)

Concentration	Peak Current I_p (µA)
	Oxidation, A_0
30	3.38
50	4.92
70	5.26
90	4.41
100	3.41

Table 4.9: Peak Current I_p (µA) of 2 mM Catechol with various concentration of Glycine of Pt electrode at scan rate 0.1V/s in pH 7 (2^{nd} cycle)

Concentration	Peak Current I_p (µA)
	Oxidation, A_0
30	1.79
50	2.02
70	3.27
90	1.42
100	1.30

Table 4.10: Peak Current I_p (μA) of 2 mM Catechol with various concentration of Glycine of Au electrode at scan rate 0.1V/s in pH 7 (2^{nd} cycle)

Concentration	Peak Current I_p (μA)
	Oxidation, A_0
30	2.44
50	3.49
70	4.01
90	2.88
100	2.07

Table 4.11: Peak current (I_p), corresponding peak current ratio (I_{pa}/I_{pc}) of 2 mM Catechol with 70 mM L-Aspartic acid in buffer solution (pH 7) of GC electrode at different scan rate (2^{nd} cycle)

v/Vs^{-1}	I_{pa0} /μA	I_{pa1} /μA	I_{pc0}/μA	I_{pc1}/μA	I_{pa0}/I_{pa1}	I_{pa1}/I_{pc1}
0.05	2.21	20.3	-6.62	-2.46	0.06	-7.00
0.10	2.65	32.12	-7.41	-13.75	0.15	-7.52
0.15	3.09	46.93	-8.2	-25.05	0.09	-2.33
0.20	3.45	54.34	-8.91	-30.35	0.06	-1.87
0.25	3.81	61.75	-9.62	-35.65	0.06	-1.79
0.30	4.05	66.96	-8.62	-41.71	0.06	-1.73
0.35	4.29	72.17	-7.63	-47.78	0.06	-1.60
0.40	4.66	76.9	-7.15	-54.65	0.05	-1.51
0.45	5.03	81.63	-6.68	-61.55	0.06	-1.40
0.50	2.21	20.3	-6.62	-2.46	0.06	-1.32

Table 4.12: Peak current (I_p), corresponding peak current ratio (I_{pa}/I_{pc}) of 2 mM Catechol with 70 mM L-Aspartic acid in buffer solution (pH 7) of Pt electrode at different scan rate (2^{nd} cycle)

v/Vs^{-1}	I_{pa0} /μA	I_{pa1} /μA	I_{pc0}/μA	I_{pc1}/μA	I_{pa0}/I_{pa1}	I_{pa1}/I_{pc1}
0.05	0.74	5.41	-0.98	-4.98	0.11	1.58
0.10	0.87	8.05	-1.12	-8.47	0.12	0.95
0.15	0.73	9.15	-1.07	-11.57	0.12	0.79
0.20	0.67	10.89	-1.04	-14.37	0.06	0.75
0.25	0.63	12.28	-0.88	-16.39	0.05	0.74
0.30	0.6	14.02	-0.78	-18.04	0.04	0.77
0.35	0.54	13.48	-0.69	-18.57	0.04	0.72
0.40	0.49	16.16	-0.63	-19.89	0.03	0.81
0.45	0.45	17.97	-0.54	-20.07	0.02	0.89
0.50	0.42	19.9	-0.49	-20.78	0.02	0.95

Table 4.13: Peak current (I_p), corresponding peak current ratio (I_{pa}/I_{pc}) of 2 mM Catechol with 70 mM L-Aspartic acid in buffer solution (pH 7) of Au electrode at different scan rate (2^{nd} cycle)

v/Vs^{-1}	I_{pa0} /μA	I_{pa1} /μA	I_{pc0}/μA	I_{pc1}/μA	I_{pa0}/I_{pa1}	I_{pa1}/I_{pc1}
0.05	1.15	9.07	-2.34	-5.38	0.12	1.68
0.10	0.93	12.38	-2.75	-9.02	0.07	1.37
0.15	0.84	16.89	-2.65	-11.03	0.04	1.53
0.20	0.78	19.41	-2.45	-12.94	0.04	1.51
0.25	0.7	23.04	-2.1	-14.59	0.03	1.51
0.30	0.63	25.21	-1.92	-17.74	0.02	1.42
0.35	0.59	28.79	-1.88	-21.85	0.02	1.31
0.40	0.54	33.14	-1.81	-25.25	0.01	1.31
0.45	0.46	34.45	-1.47	-26.22	0.01	1.31
0.50	0.39	35.67	-1.29	-27.59	0.01	1.29

Table 4.14: Peak Current I_p (μA), peak potential E_p (V) of 2 mM Catechol with 70 mM L-Aspartic acid of GC electrode at scan rate 0.1V/s in different pH media (2^{nd} cycle)

pH	Peak Current I_p (μA)	Peak potential E_p (V)	
	Oxidation, A_0	Oxidation, A_0	Oxidation, A_1
5	2.11	0.23	0.63
7	3.84	0.09	0.40
9	1.12	0.13	0.42
11	1.23	0.03	0.29

Table 4.15: Peak Current I_p (μA), peak potential E_p (V) of 2 mM Catechol with 70 mM L-Aspartic acid of Pt electrode at scan rate 0.1V/s in different pH media (2^{nd} cycle)

pH	Peak Current I_p (μA)	Peak potential E_p (V)
	Oxidation, A_0	Oxidation, A_0
5	0.00	0.51
7	0.84	0.29
9	0.43	0.19
11	0.23	0.05

Table 4.16: Peak Current I_p (µA), peak potential E_p (V) of 2 mM Catechol with 70 mM L-Aspartic acid of Au electrode at scan rate 0.1V/s in different pH media (2^{nd} cycle)

pH	Peak Current I_p (µA)	Peak potential E_p (V)
	Oxidation, A_0	Oxidation, A_0
5	0.00	0.37
7	1.43	0.20
9	1.02	0.09
11	0.55	0.03

Table 4.17: Peak Current I_p (µA) of 2 mM Catechol with various concentration of L-Aspartic acid of GC electrode at scan rate 0.1V/s in pH 7 (2^{nd} cycle)

Concentration	Peak Current I_p (µA)
	Oxidation, A_0
30	2.00
50	3.15
70	3.84
80	2.23
100	1.57

Table 4.18: Peak Current I_p (µA) of 2 mM Catechol with various concentration of L-Aspartic acid of Pt electrode at scan rate 0.1V/s in pH 7 (2^{nd} cycle)

Concentration	Peak Current I_p (µA)
	Oxidation, A_0
30	0.14
50	0.78
70	1.05
80	0.97
100	0.65

Table 4.19: Peak Current I_p (µA) of 2 mM Catechol with various concentration of L-Aspartic acid of Au electrode at scan rate 0.1V/s in pH 7 (2^{nd} cycle)

Concentration	Peak Current I_p (µA)
	Oxidation, A_0
30	0.20
50	1.01
70	1.27
80	0.89
100	0.24

Table 4.20: Peak current (I_p), corresponding peak current ratio (I_{pa}/I_{pc}) of 2 mM Catechol with 30 mM L-Glutamic acid in buffer solution (pH 7) of GC electrode at different scan rate (2nd cycle)

v/Vs^{-1}	I_{pa0} /μA	I_{pa1} /μA	I_{pc0}/μA	I_{pc1}/μA	I_{pa0}/I_{pa1}	I_{pa1}/I_{pc1}
0.05	2.62	14.91	-4.78	-2.02	0.17	7.38
0.10	3.14	26.5	-5.55	-7.45	0.11	3.55
0.15	3.06	34.97	-6.37	-12.22	0.08	2.86
0.20	3.18	43.44	-7.19	-16.99	0.07	2.55
0.25	3.32	45.87	-6.93	-22.85	0.07	2.00
0.30	2.96	55.51	-6.67	-27.72	0.05	2.00
0.35	3.08	61.34	-7.06	-35.26	0.05	1.73
0.40	3.4	74.36	-7.45	-40.8	0.04	1.82
0.45	3.02	76.98	-7.01	-45.88	0.03	1.67
0.50	2.63	81.61	-6.57	-49.8	0.03	1.63

Table 4.21: Peak current (I_p), corresponding peak current ratio (I_{pa}/I_{pc}) of 2 mM Catechol with 30 mM L-Glutamic acid in buffer solution (pH 7) of Pt electrode at different scan rate (2nd cycle)

v/Vs^{-1}	I_{pa0} /μA	I_{pa1} /μA	I_{pc0}/μA	I_{pc1}/μA	I_{pa0}/I_{pa1}	I_{pa1}/I_{pc1}
0.05	1.08	5.65	-1.56	-4.90	0.19	1.15
0.10	0.96	8.29	-1.74	-8.73	0.11	0.94
0.15	0.91	9.06	-1.81	-13.04	0.10	0.69
0.20	0.83	11.23	-1.83	-14.56	0.07	0.77
0.25	0.8	17.78	-1.82	-15.96	0.09	1.11
0.30	0.78	20.98	-1.81	-17.29	0.03	1.21
0.35	0.73	22.65	-1.78	-19.08	0.03	1.18
0.40	0.7	24.23	-1.73	-20.92	0.02	1.15
0.45	0.66	26.99	-1.65	-22.47	0.02	1.20
0.50	0.63	28.21	-1.54	-25.34	0.02	1.11

Table 4.22: Peak current (I_p), corresponding peak current ratio (I_{pa}/I_{pc}) of 2 mM Catechol with 30 mM L-Glutamic acid in buffer solution (pH 7) of Au electrode at different scan rate (2nd cycle)

v/Vs^{-1}	I_{pa0} /μA	I_{pa1} /μA	I_{pc0}/μA	I_{pc1}/μA	I_{pa0}/I_{pa1}	I_{pa1}/I_{pc1}
0.05	1.37	9.97	-3.09	-5.54	0.13	1.79
0.10	1.46	13.93	-3.19	-9.50	0.10	1.46
0.15	1.49	17.56	-3.78	-12.39	0.08	1.41
0.20	1.53	22.35	-4.39	-15.65	0.06	1.42
0.25	1.50	25.98	3.55	-19.03	0.05	1.36
0.30	1.42	28.88	-2.11	-23.22	0.04	1.24
0.35	1.23	33.04	-1.98	-27.28	0.03	1.21
0.40	1.10	35.07	-1.89	-31.23	0.03	1.12
0.45	0.93	37.17	-1.65	-32.79	0.02	1.13
0.50	0.9	39.78	-1.56	-34.89	0.02	1.14

Table 4.23: Peak Current I_p (µA), peak potential E_p (V) of 2 mM Catechol with 30 mM L-Glutamic acid of GC electrode at scan rate 0.1V/s in different pH media (2^{nd} cycle)

pH	Peak Current I_p (µA)	Peak potential E_p (V)
	Oxidation, A_0	Oxidation, A_1
5	0.00	0.50
7	2.94	0.39
9	0.33	0.27
11	0.00	0.08

Table 4.24: Peak Current I_p (µA), peak potential E_p (V) of 2 mM Catechol with 30 mM L-Glutamic acid of Pt electrode at scan rate 0.1V/s in different pH media (2^{nd} cycle)

pH	Peak Current I_p (µA)	Peak potential E_p (V)
	Oxidation, A_0	Oxidation, A_0
5	0.00	0.47
7	0.96	0.28
9	0.543	0.18
11	0.20	0.05

Table 4.25: Peak Current I_p (µA), peak potential E_p (V) of 2 mM Catechol with 30 mM L-Glutamic acid of Au electrode at scan rate 0.1V/s in different pH media (2^{nd} cycle)

pH	Peak Current I_p (µA)	Peak potential E_p (V)
	Oxidation, A_0	Oxidation, A_0
5	0.00	0.35
7	1.76	0.17
9	1.532	0.08
11	1.495	0.01

Table 4.26: Peak Current I_p (µA) of 2 mM Catechol with various concentration of L-Glutamic acid of GC electrode at scan rate 0.1V/s in pH 7 (2^{nd} cycle)

Concentration	Peak Current I_p (µA)
	Oxidation, A_0
10	1.34
30	2.84
50	2.65
100	1.29
150	0.89

Table 4.27: Peak Current I_p (µA) of 2 mM Catechol with various concentration of L-Glutamic acid of Pt electrode at scan rate 0.1V/s in pH 7 (2^{nd} cycle)

Concentration	Peak Current I_p (µA)
	Oxidation, A_0
10	1.26
30	1.69
50	0.90
100	0.78
150	0.65

Table 4.28: Peak Current I_p (µA) of 2 mM Catechol with various concentration of L-Glutamic acid of Au electrode at scan rate 0.1V/s in pH 7 (2^{nd} cycle)

Concentration	Peak Current I_p (µA)
	Oxidation, A_0
10	1.59
30	2.52
50	1.77
100	1.24
150	1.16

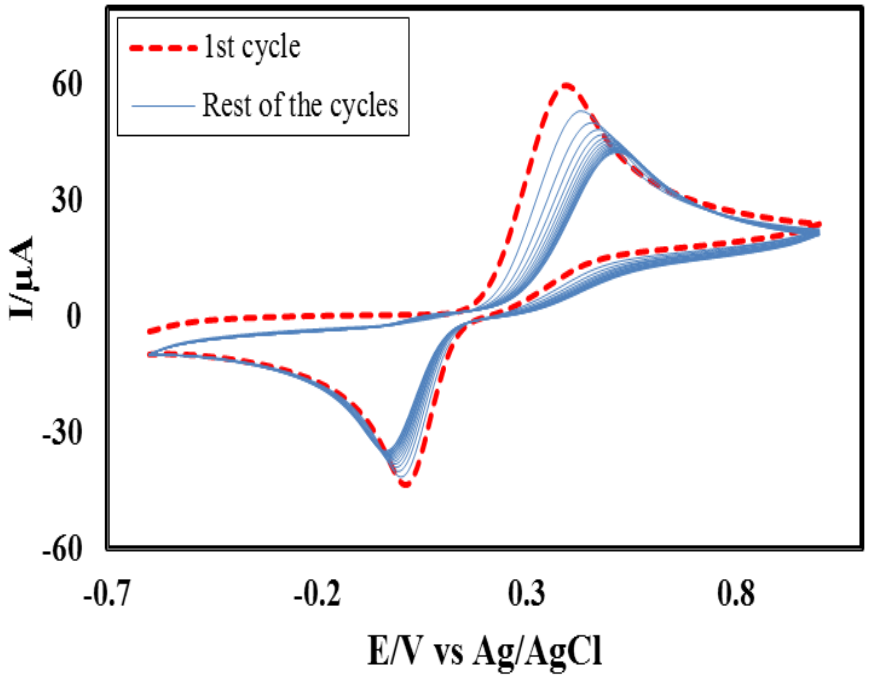

Fig. 4.1: Cyclic voltammogram (CV) of 2 mM Catechol of GC electrode in buffer solution (pH 7) at scan rate 0.1 V/s (15 cycles).

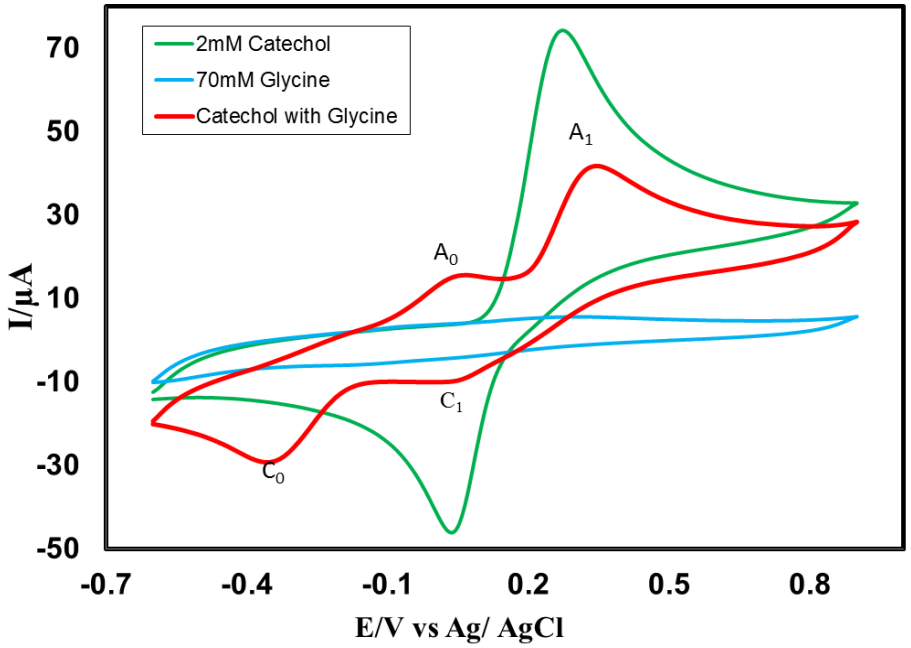

Fig. 4.2: Cyclic voltammogram of 2 mM Catechol (Green line), 70 mM Glycine (Blue line) and 2 mM Catechol with 70 mM Glycine (Red line) of GC electrode in buffer solution (pH 7) at scan rate 0.1 V/s (2nd cycle). (A_0 = appeared anodic peak)

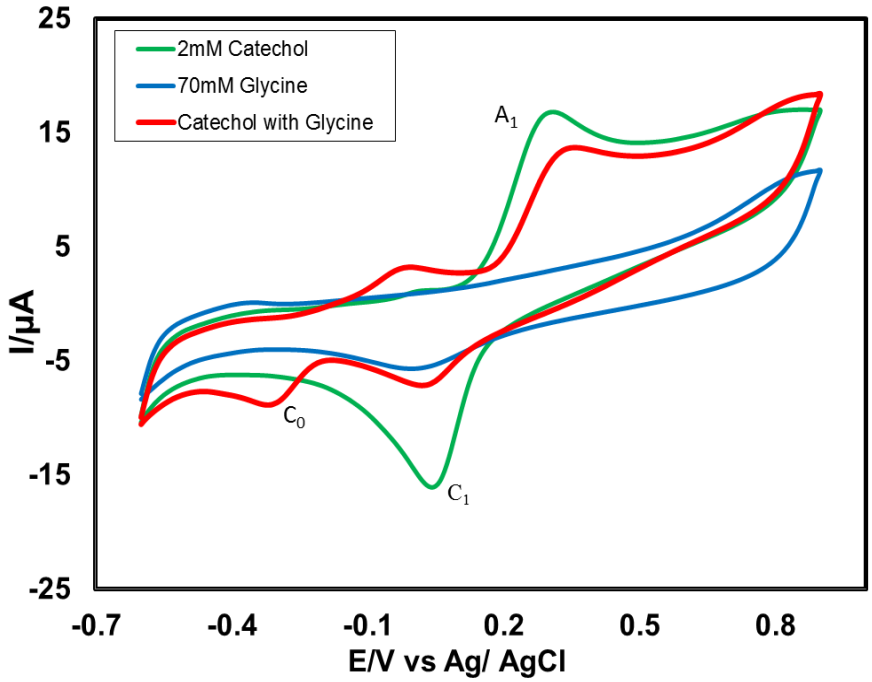

Fig. 4.3: Cyclic voltammogram of 2 mM Catechol (Green line), 70 mM Glycine (Blue line) and 2 mM Catechol with 70 mM Glycine (Red line) of Pt electrode in buffer solution (pH 7) at scan rate 0.1 V/s (2nd cycle). (A_0 = appeared anodic peak)

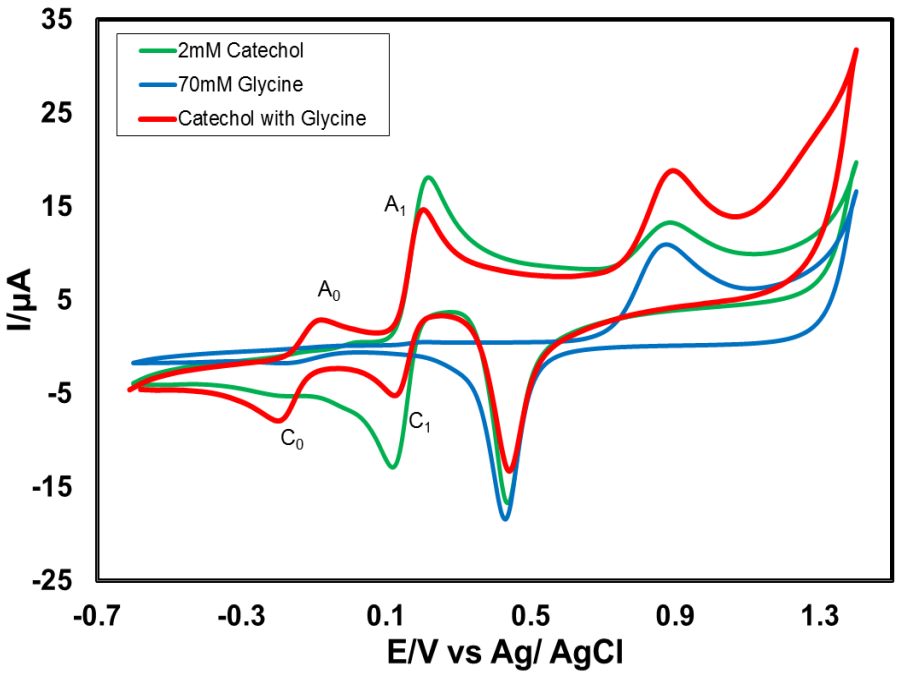

Fig. 4.4: Cyclic voltammogram of 2 mM Catechol (Green line), 70 mM Glycine (Blue line) and 2 mM Catechol with 70 mM Glycine (Red line) of Au electrode in buffer solution (pH 7) at scan rate 0.1 V/s (2nd cycle). (A_0 = appeared anodic peak)

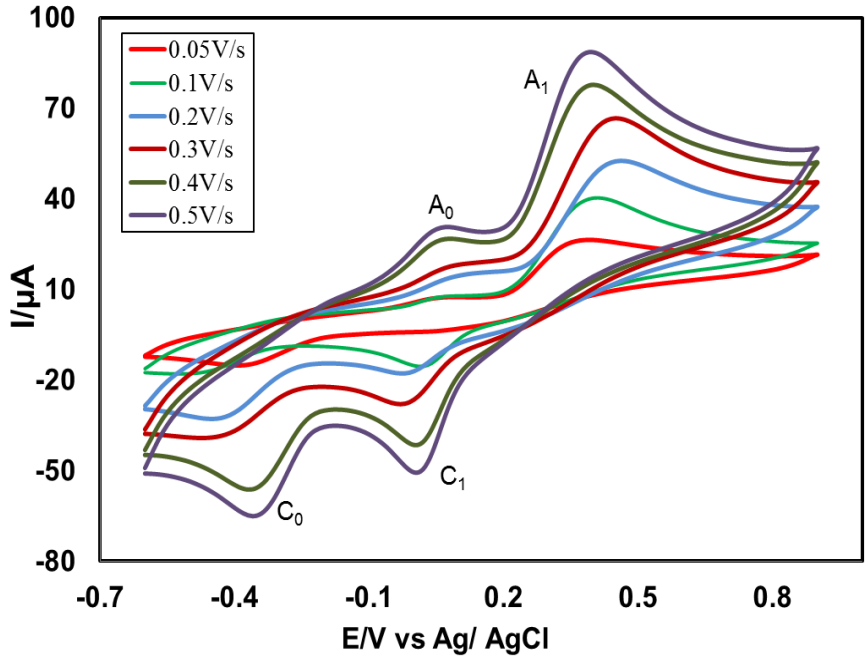

Fig. 4.5: Cyclic voltammogram of 2 mM Catechol with70 mM Glycine in the second scan of potential at GC electrode in buffer solution (pH 7) at scan rate 0.05 V/s to 0.5 V/s.

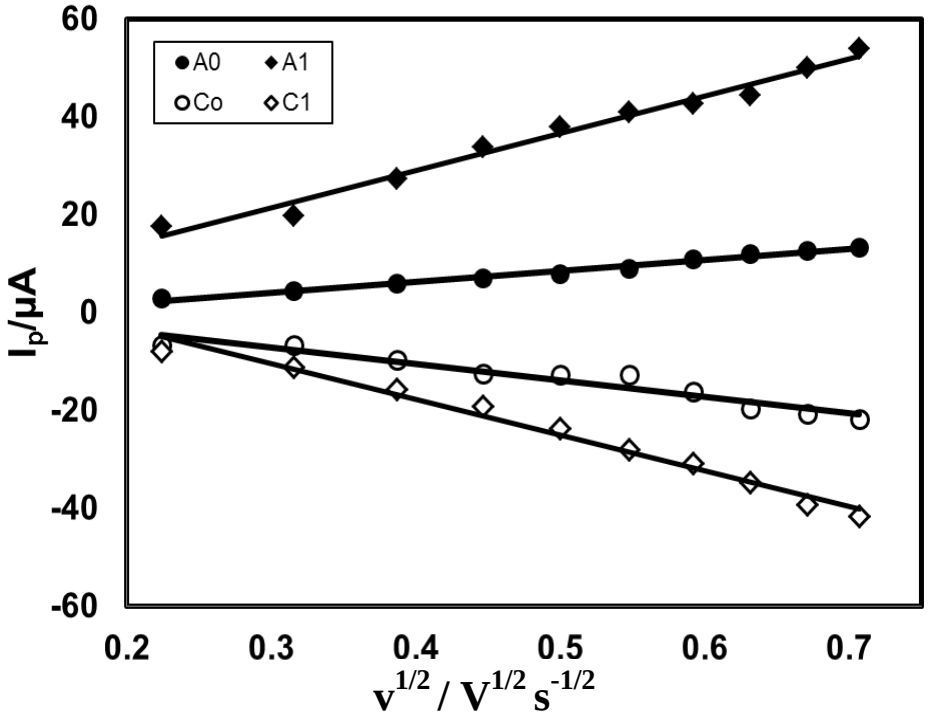

Fig. 4.6: Plots of peak current (I_p) versus square root of scan rate ($v^{1/2}$) of 2 mM Catechol with 70 mM Glycine of GC electrode in buffer solution (pH 7) (2^{nd} cycle).

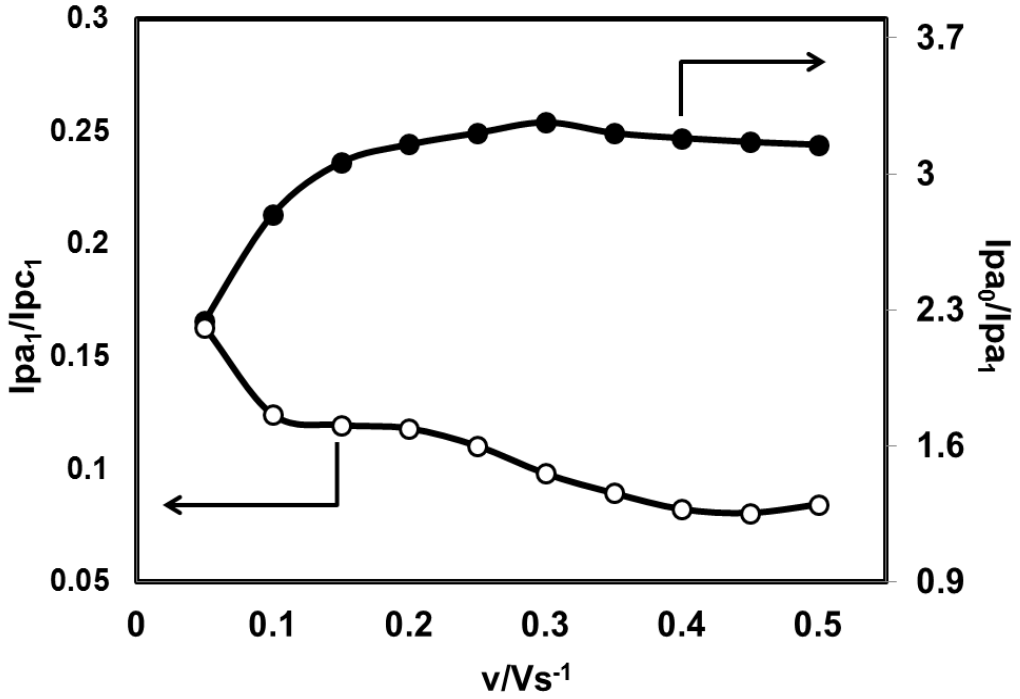

Fig. 4.7: Variation of peak current ratio of corresponding peak (I_{pa1}/I_{pc1}) and anodic peak (I_{pa0}/I_{pa1}) vs scan rate (v) of 2 mM Catechol with 70 mM Glycine of GC electrode in buffer solution (pH 7) at scan rate 0.1 V/s in the second scan of potential.

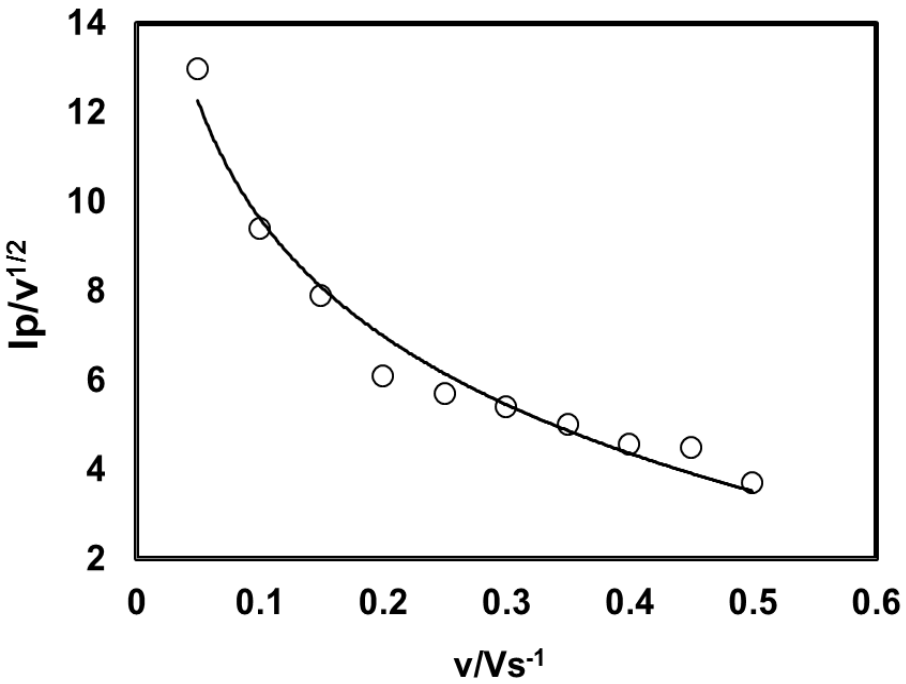

Fig. 4.8: Plot of current function ($I_p/v^{1/2}$) versus scan rate (v) of 2 mM Catechol with 70 mM Glycine of GC electrode in buffer solution (pH 7) of the Appeared anodic peak (A_0).

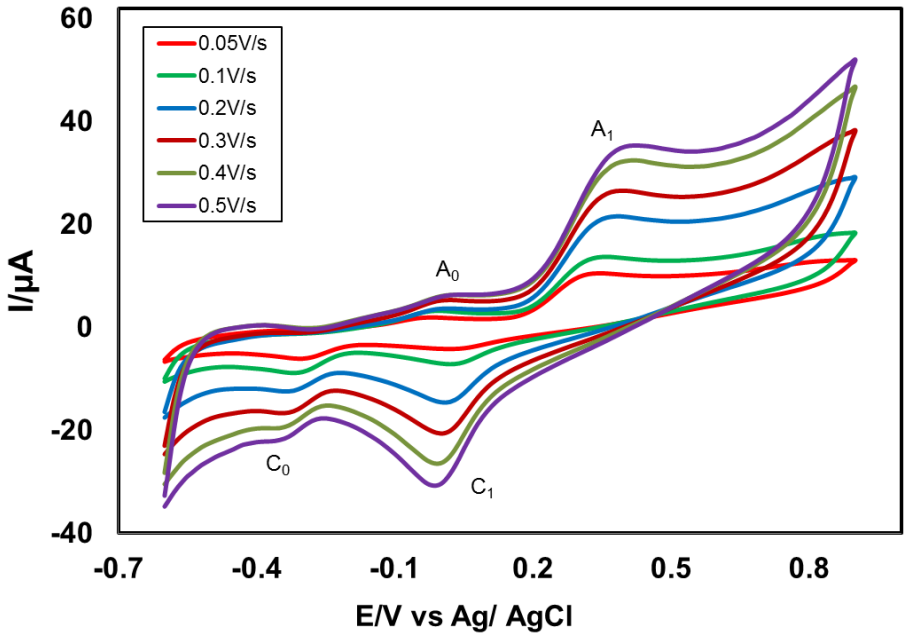

Fig. 4.9: Cyclic voltammogram of 2 mM Catechol with 70 mM Glycine in the second scan of potential at Pt electrode in buffer solution (pH 7) at scan rate 0.05 V/s to 0.5 V/s.

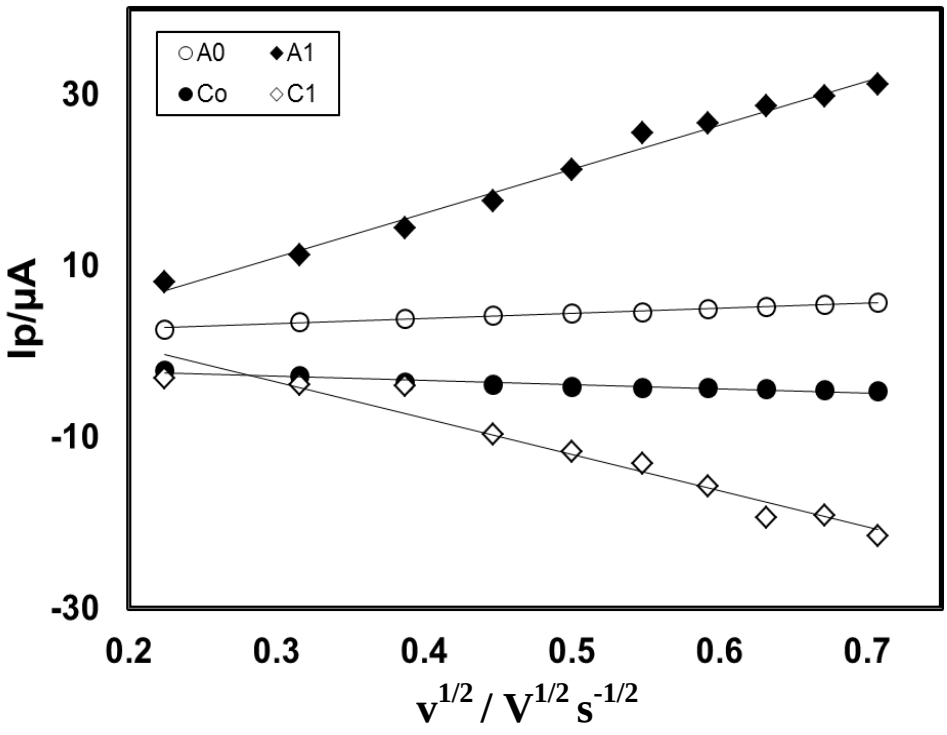

Fig. 4.10: Plots of peak current (I_p) versus square root of scan rate ($v^{1/2}$) of 2 mM Catechol with 70 mM Glycine of Pt electrode in buffer solution (pH 7) (2^{nd} cycle).

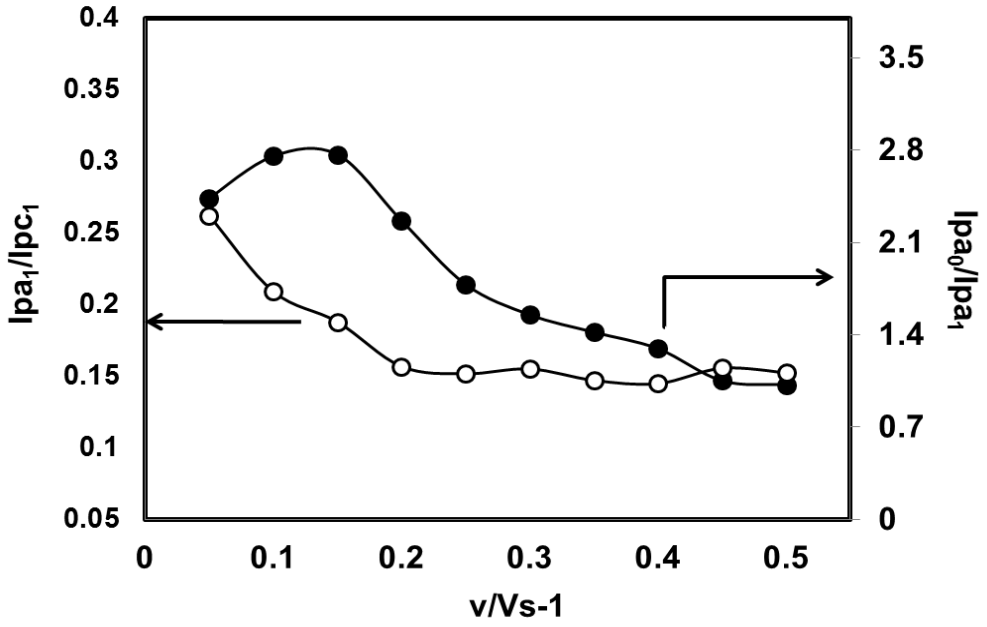

Fig. 4.11: Variation of peak current ratio of corresponding peak (I_{pa1}/I_{pc1}) and anodic peak (I_{pa0}/I_{pa1}) vs scan rate (v) of 2 mM Catechol with 70 mM Glycine of Pt electrode in buffer solution (pH 7) at scan rate 0.1 V/s in the second scan of potential.

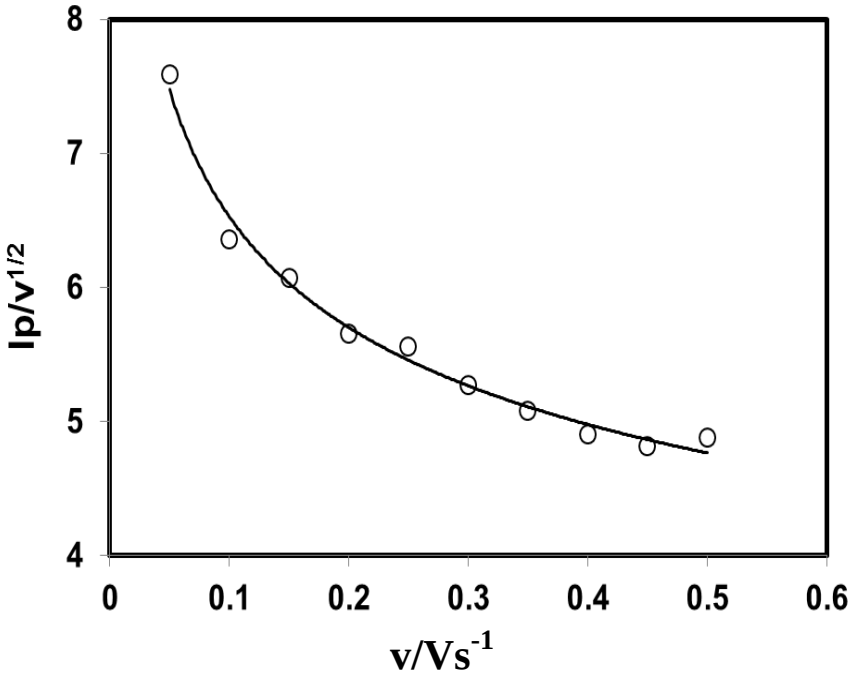

Fig. 4.12: Plots of current function ($I_p/v^{1/2}$) versus scan rate (v) of 2 mM Catechol with 70 mM Glycine of Pt electrode in buffer solution (pH 7) of the Appeared anodic peak (A_0).

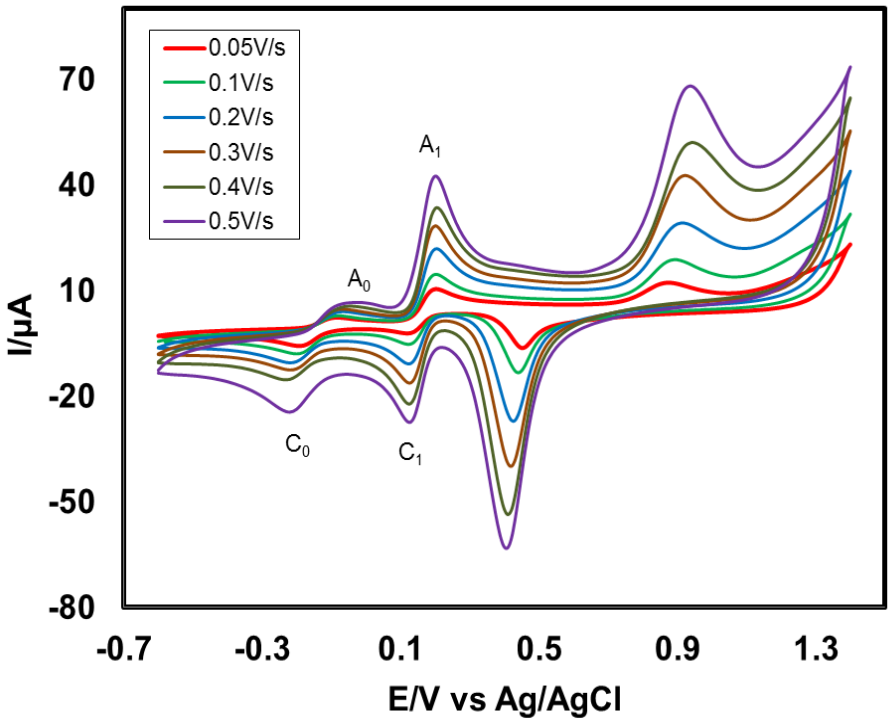

Fig. 4.13: Cyclic voltammogram of 2 mM Catechol with70 mM Glycine in the second scan of potential at Au electrode in buffer solution (pH 7) at scan rate 0.05 V/s to 0.5 V/s.

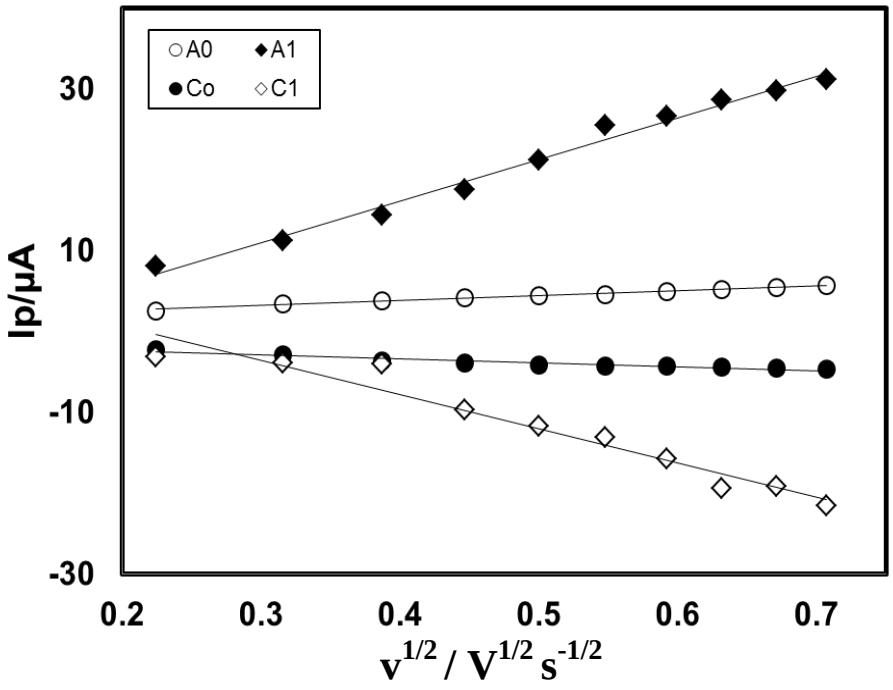

Fig. 4.14: Plots of peak current (I_p) versus square root of scan rate ($v^{1/2}$) of 2 mM Catechol with 70 mM Glycine of Au electrode in buffer solution (pH 7) (2^{nd} cycle).

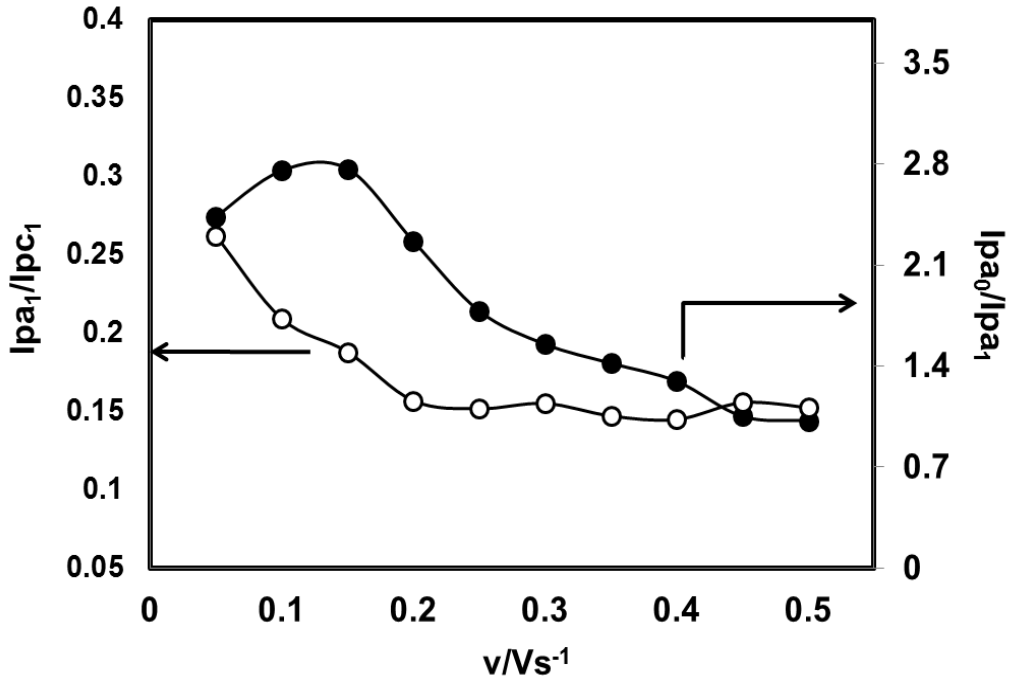

Fig. 4.15: Variation of peak current ratio of corresponding peak (I_{pa1}/I_{pc1}) and anodic peak (I_{pa0}/I_{pa1}) vs scan rate (v) of 2 mM Catechol with 70 mM Glycine of Au electrode in buffer solution (pH 7) at scan rate 0.1 V/s in the second scan of potential.

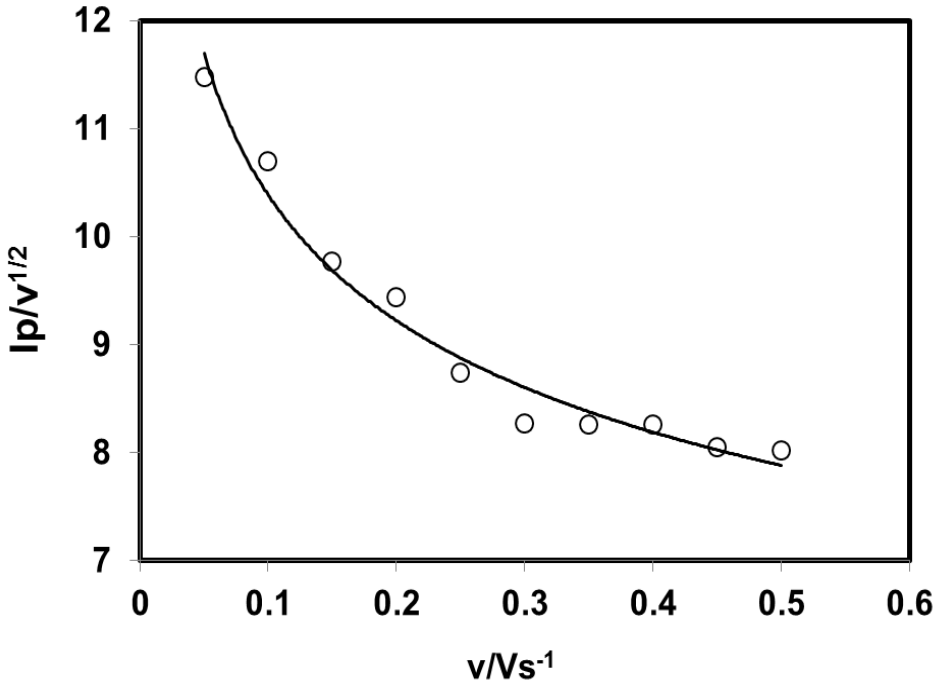

Fig. 4.16: Plots of current function ($I_p/v^{1/2}$) versus scan rate (v) of 2 mM Catechol with 70 mM Glycine of Au electrode in buffer solution (pH 7) of the Appeared anodic peak (A_0).

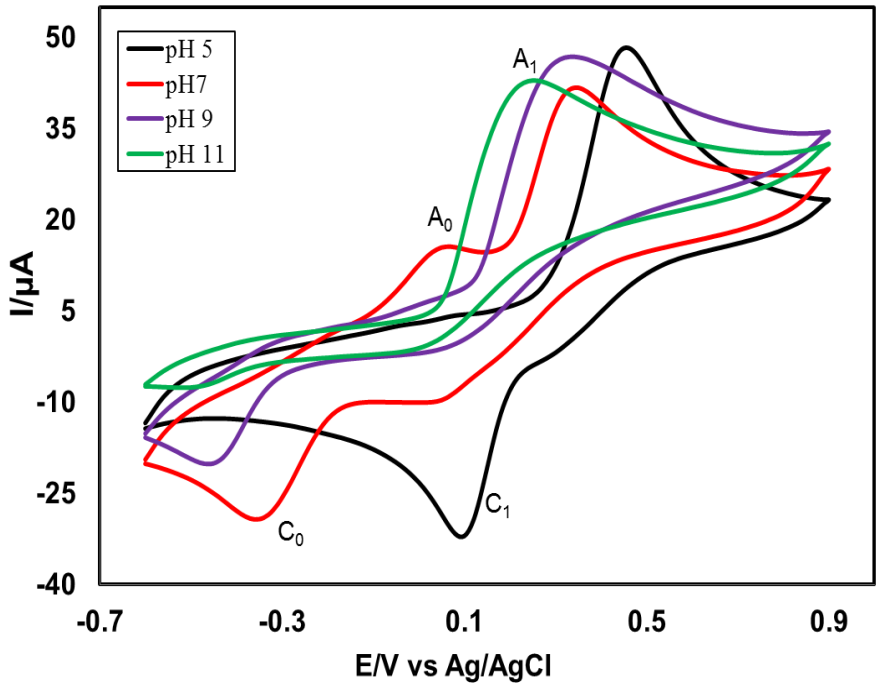

Fig. 4.17: Cyclic voltammogram of 2 mM Catechol with 70 mM Glycine of GC (3 mm) electrode in different pH (5, 7, 9 and 11) at scan rate 0.1 V/s.

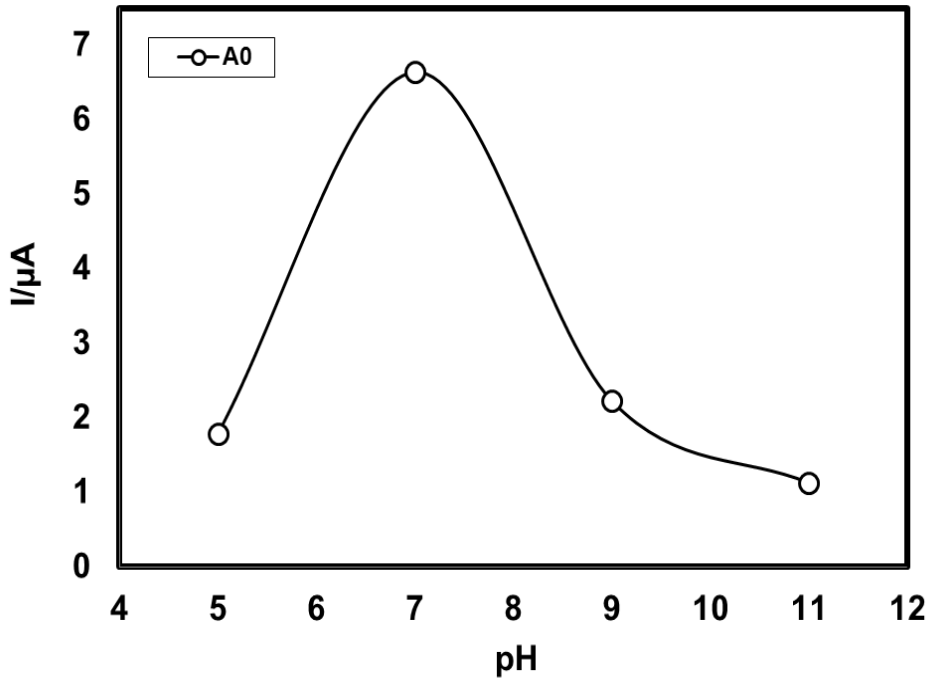

Fig. 4.18: Plot of peak current (I_p) versus pH (5, 7, 9 and 11) of 2 mM Catechol with 70 mM Glycine of GC electrode at scan rate 0.1 V/s (2^{nd} cycle).

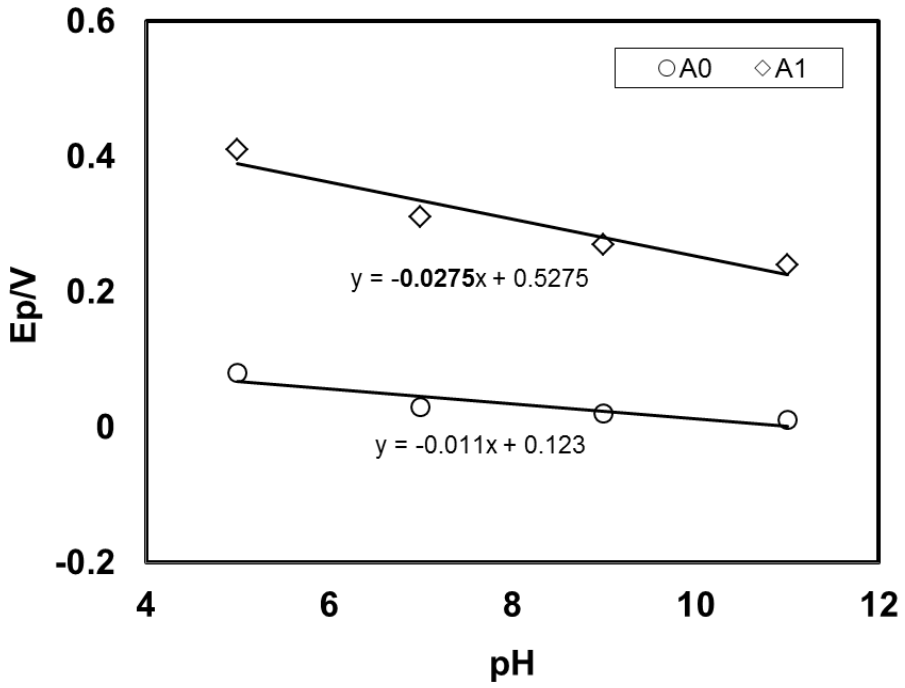

Fig. 4.19: Plots of peak potential (E_p) versus pH (5, 7, 9 and 11) of 2 mM Catechol with 70 mM Glycine of GC electrode at scan rate 0.1 V/s (2nd cycle).

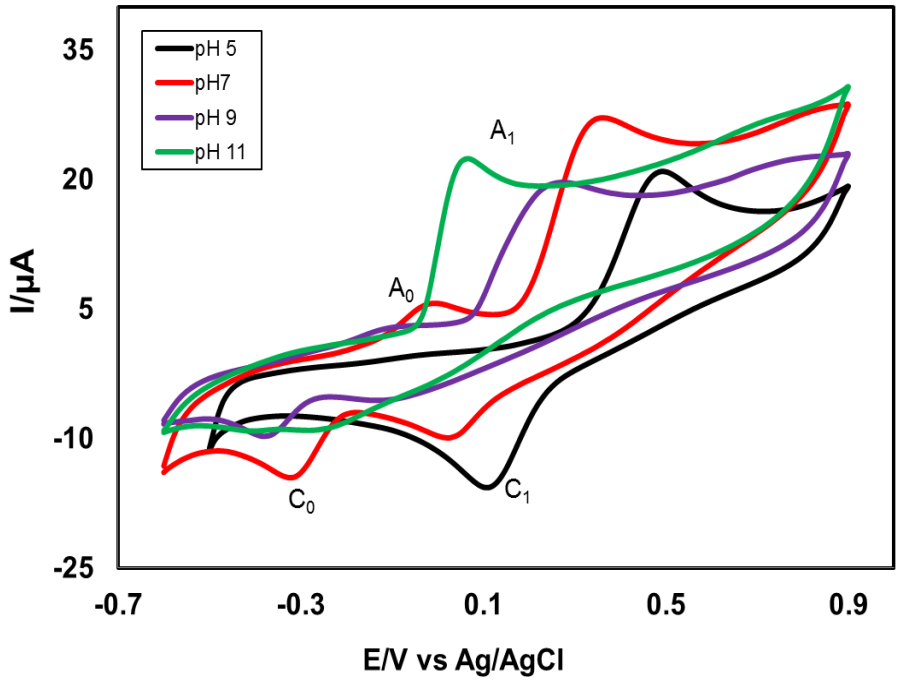

Fig. 4.20: Cyclic voltammogram of 2 mM Catechol with 70 mM Glycine of Pt electrode in different pH (5, 7, 9 and 11) at scan rate 0.1 V/s.

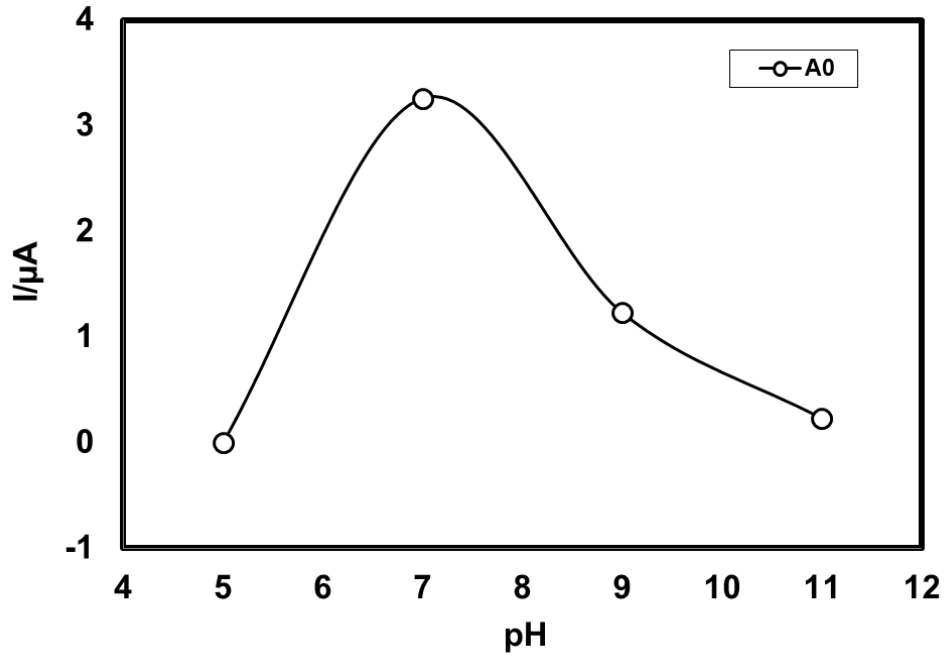

Fig. 4.21: Plots of peak current (I_p) versus pH (5, 7, 9 and 11) of 2 mM Catechol with 70 mM Glycine of Pt electrode at scan rate 0.1 V/s (2nd cycle).

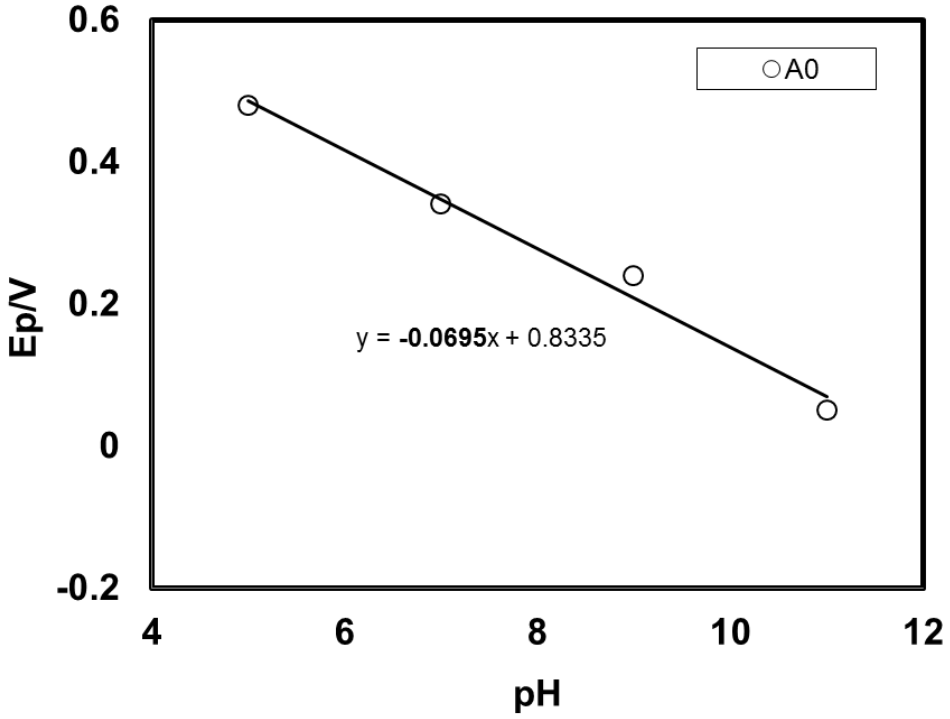

Fig. 4.22: Plot of peak potential (E_p) versus pH (5, 7, 9 and 11) of 2 mM Catechol with 70 mM Glycine of Pt electrode at scan rate 0.1 V/s (2nd cycle).

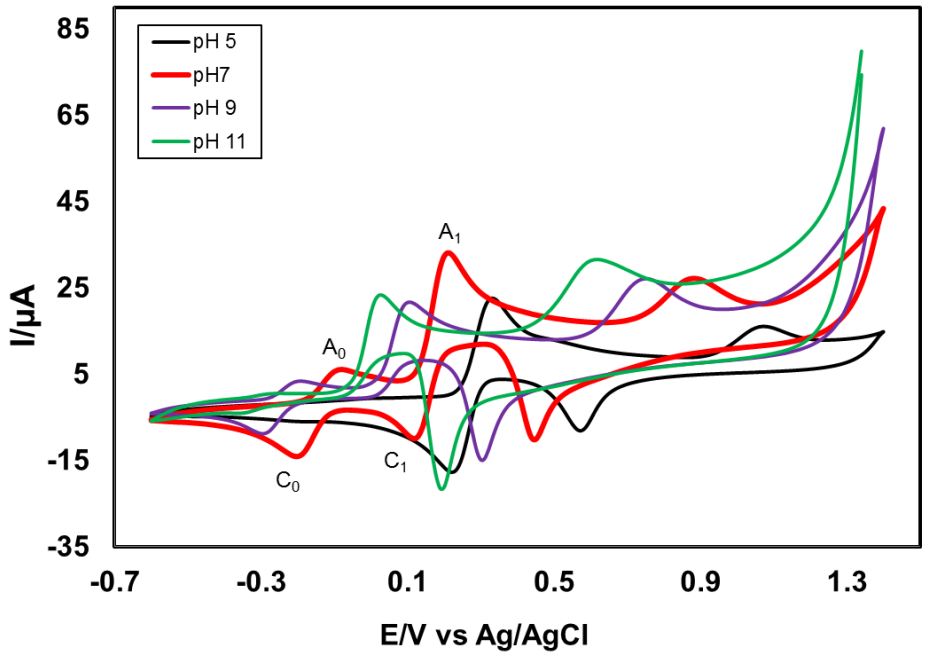

Fig. 4.23: Cyclic voltammogram of 2 mM Catechol with 70 mM Glycine of Au electrode in different pH (5, 7, 9 and 11) at scan rate 0.1 V/s.

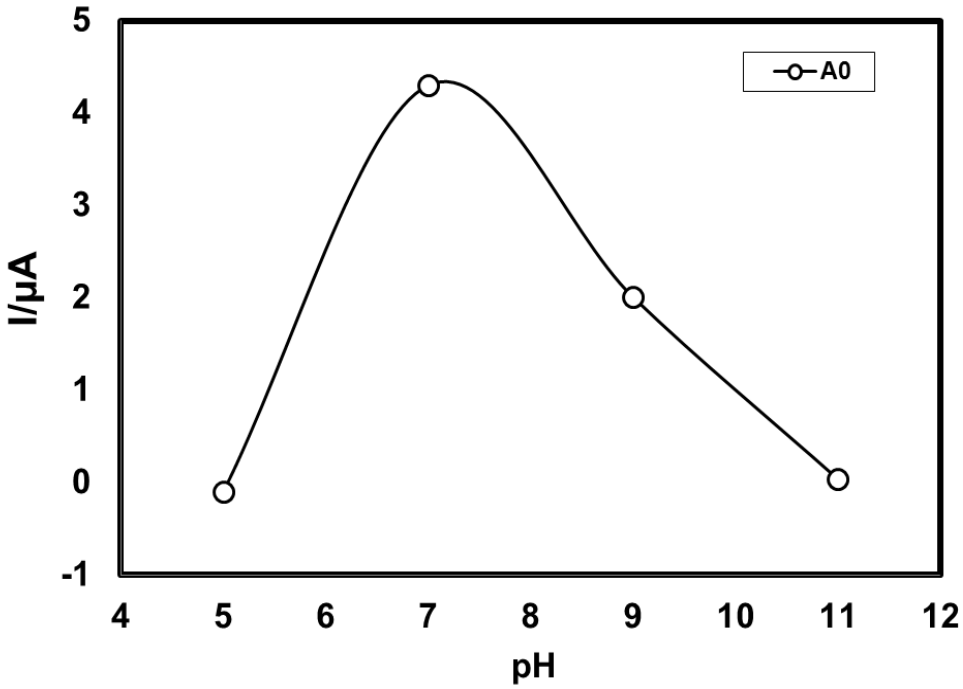

Fig. 4.24: Plots of peak current (I_p) versus pH (5, 7, 9 and 11) of 2 mM Catechol with 70 mM Glycine of Au electrode at scan rate 0.1 V/s (2^{nd} cycle).

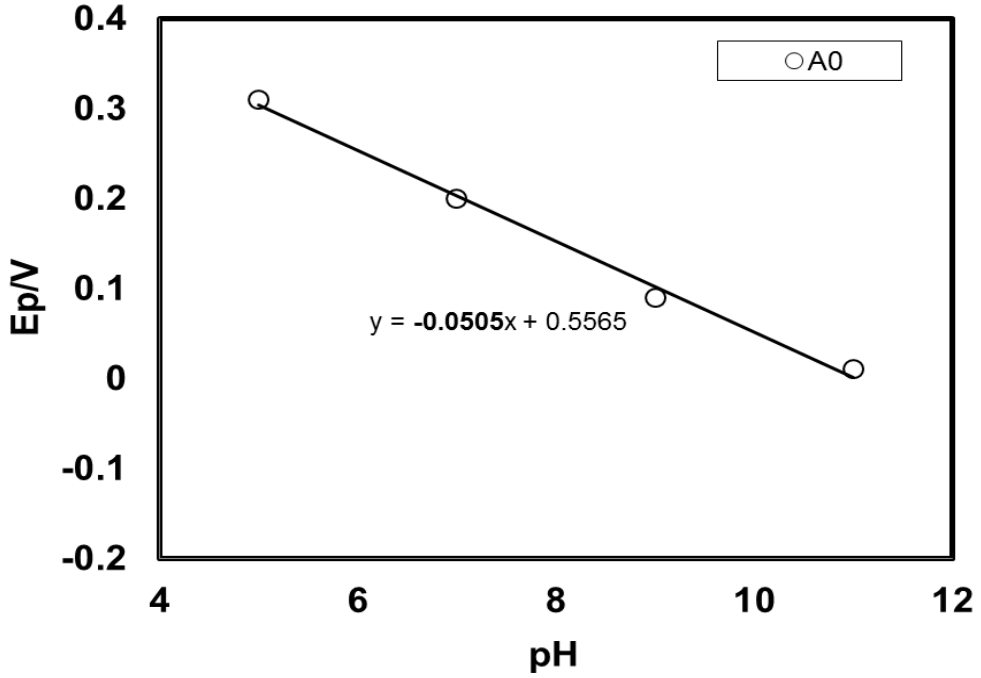

Fig. 4.25: Plot of peak potential (E_p) versus pH (5, 7, 9 and 11) of 2 mM Catechol with 70 mM Glycine of Au electrode at scan rate 0.1 V/s (2nd cycle).

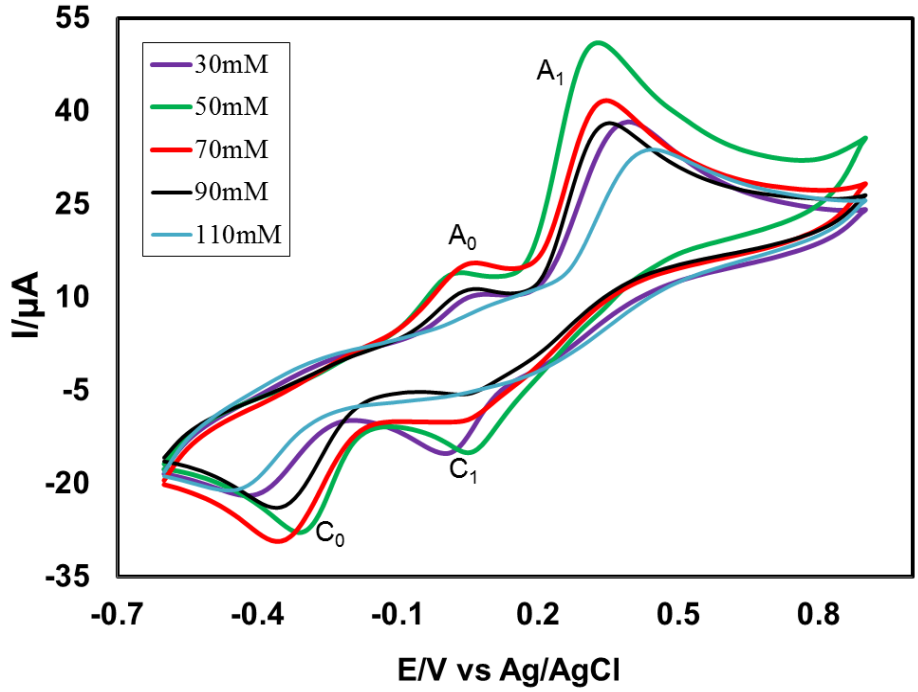

Fig. 4.26: CV of composition changes of Glycine (30, 50, 70, 90 and 110 mM) with fixed 2 mM Catechol of GC electrode at pH 7 and scan rate 0.1 V/s.

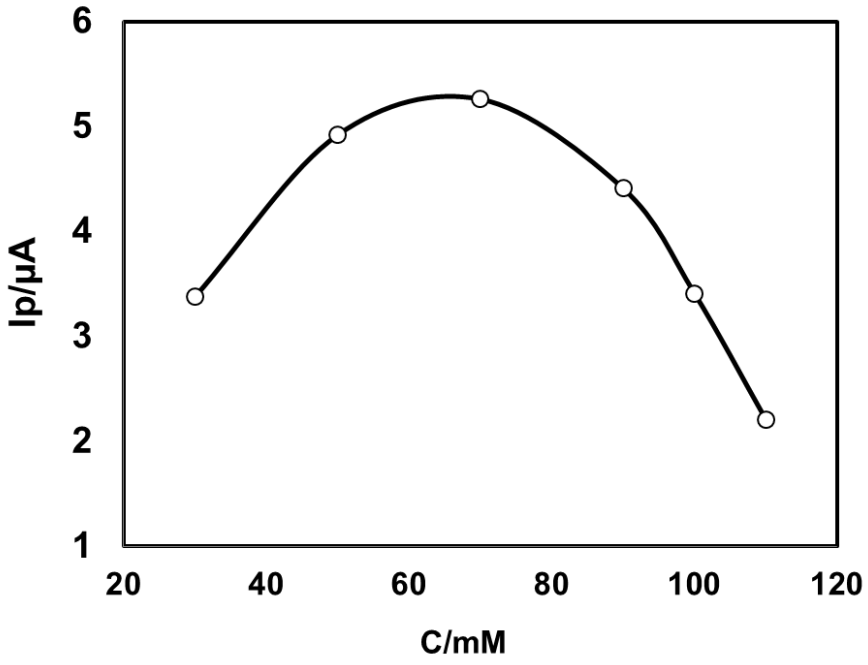

Fig. 4.27: Plots of peak current (I_p) versus concentration (C) of Glycine (30, 50, 70, 90 and 110 mM) with fixed 2 mM Catechol of GC electrode in buffer solution (pH) at 7 scan rate 0.1 V/s (2^{nd} cycle).

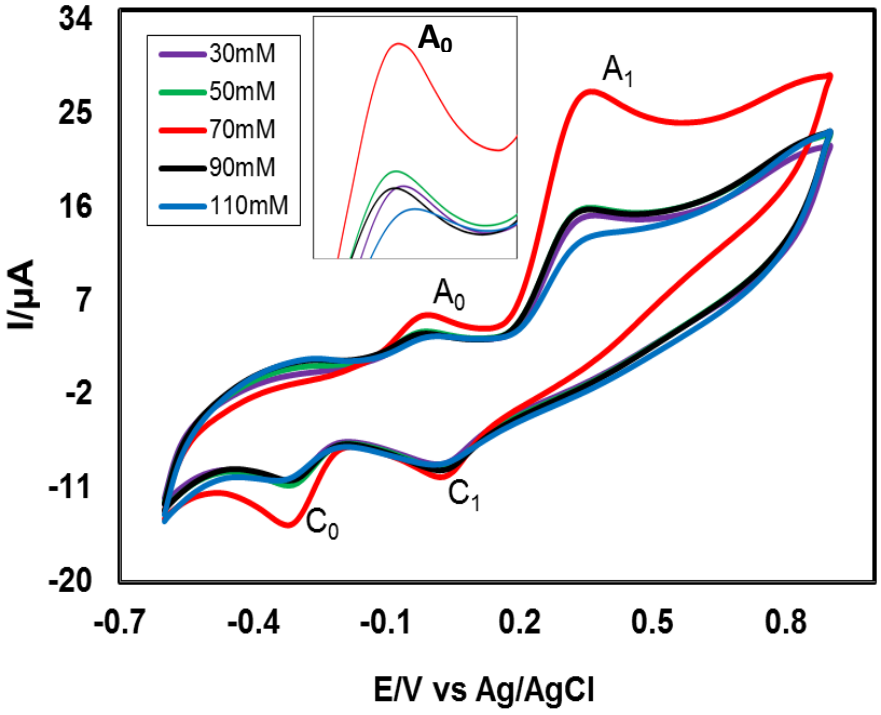

Fig. 4.28: CV of composition changes of Glycine (30, 50, 70, 90 and 110 mM) with fixed 2 mM Catechol of Pt electrode at pH 7 and scan rate 0.1 V/s. Insert: appeared anodic peak (A_0)

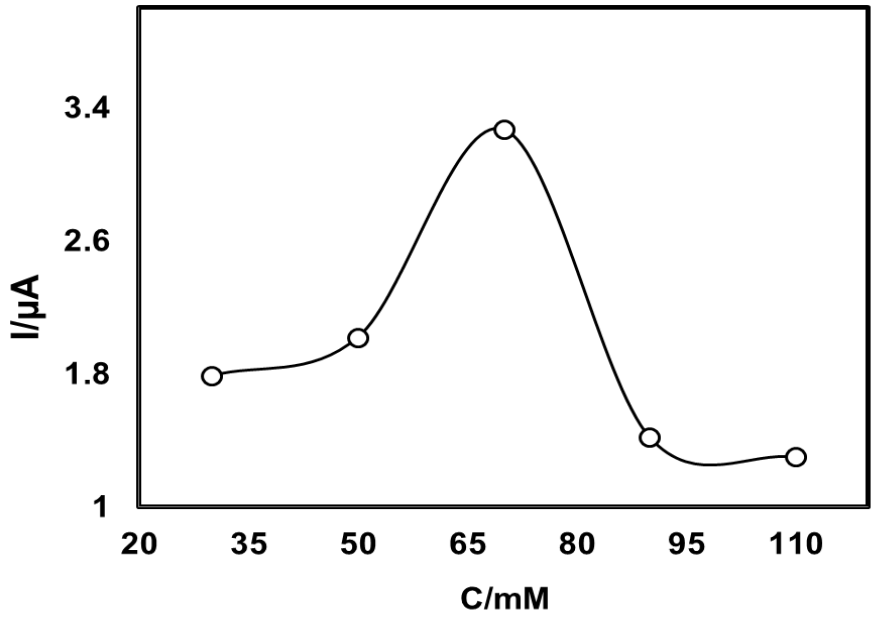

Fig. 4.29: Plots of peak current (I_p) versus concentration (C) of Glycine (30, 50, 70, 90 and 110 mM) with fixed 2 mM Catechol of Pt electrode in buffer solution (pH) at 7 scan rate 0.1 V/s (2nd cycle).

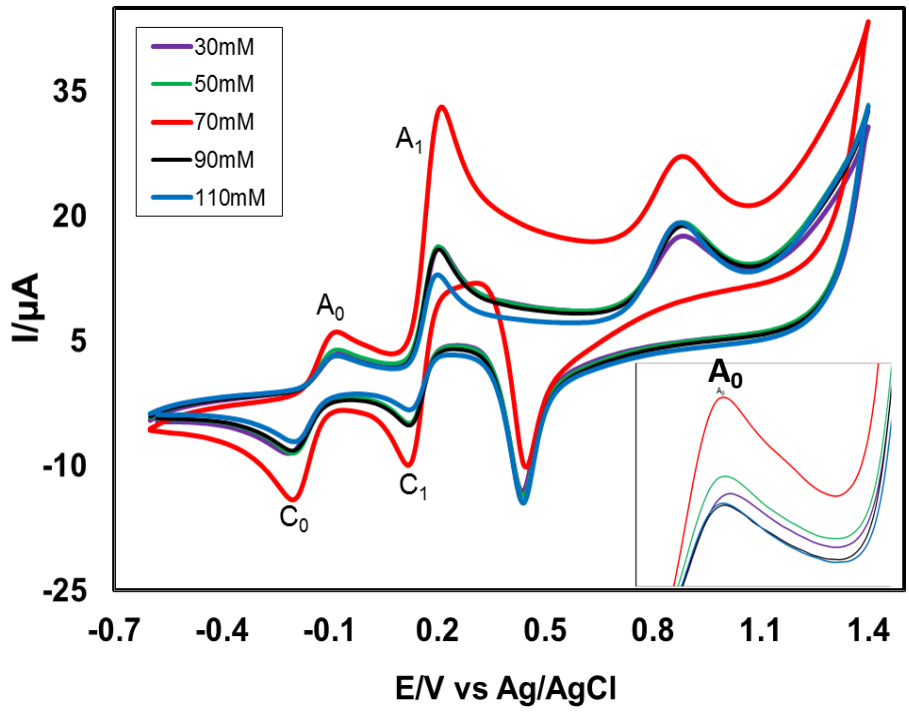

Fig. 4.30: CV of composition changes of Glycine (30, 50, 70, 90 and 110 mM) with fixed 2 mM Catechol of Au electrode at pH 7 and scan rate 0.1 V/s. Insert: appeared anodic peak (A_0)

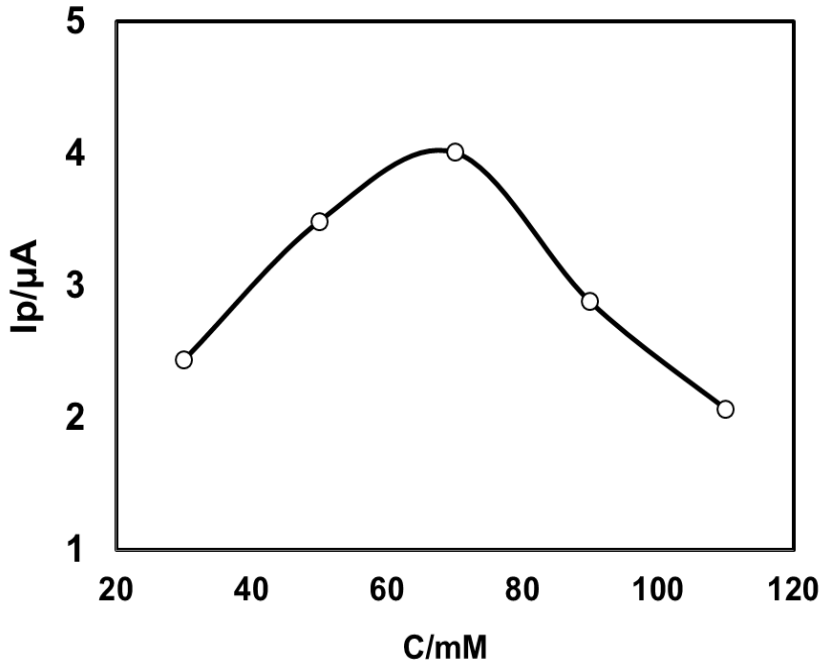

Fig. 4.31: Plots of peak current (I_p) versus concentration (C) of Glycine (30, 50, 70, 90 and 110 mM) with fixed 2 mM Catechol of Au electrode in buffer solution (pH 7) at scan rate 0.1 V/s (2^{nd} cycle).

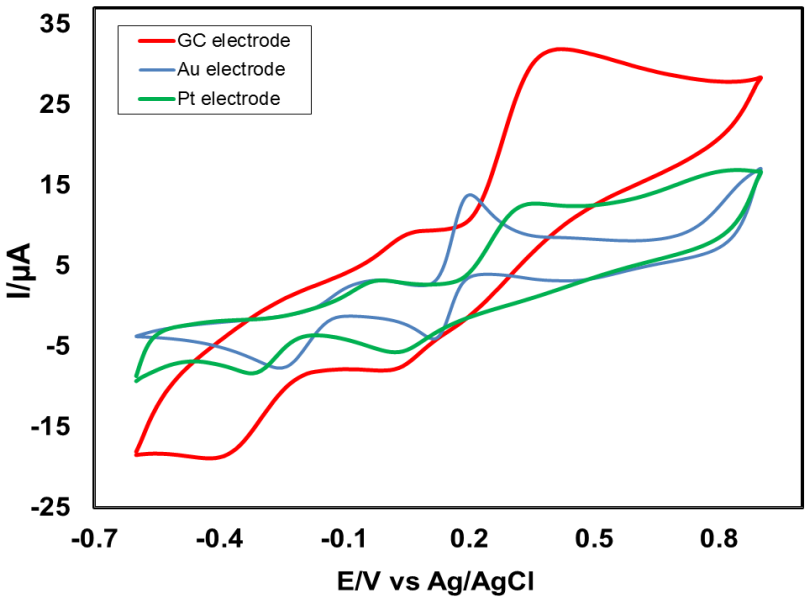

Fig. 4.32: Cyclic voltammogram (CV) of 2 mM catechol with 70 mM Glycine in GC electrode (3.0 mm), Gold electrode (1.6 mm) and Platinum electrode (1.6 mm) at pH 7 and scan rate 0.1 V/s.

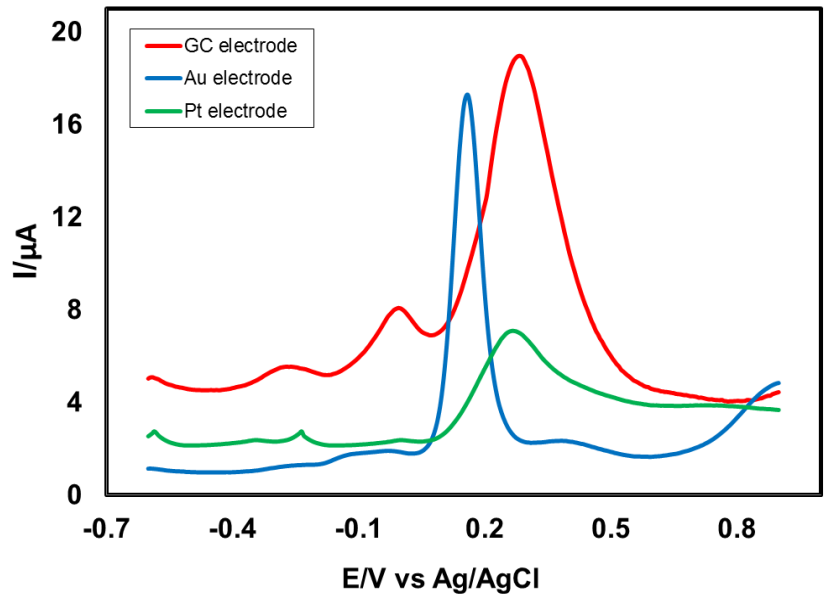

Fig. 4.33: Differential pulse voltammogram (DPV) of 2 mM catechol with 70 mM Glycine in GC electrode (3.0 mm), Gold electrode (1.6 mm) and Platinum electrode (1.6 mm) at pH 7 and scan rate 0.1 V/s.

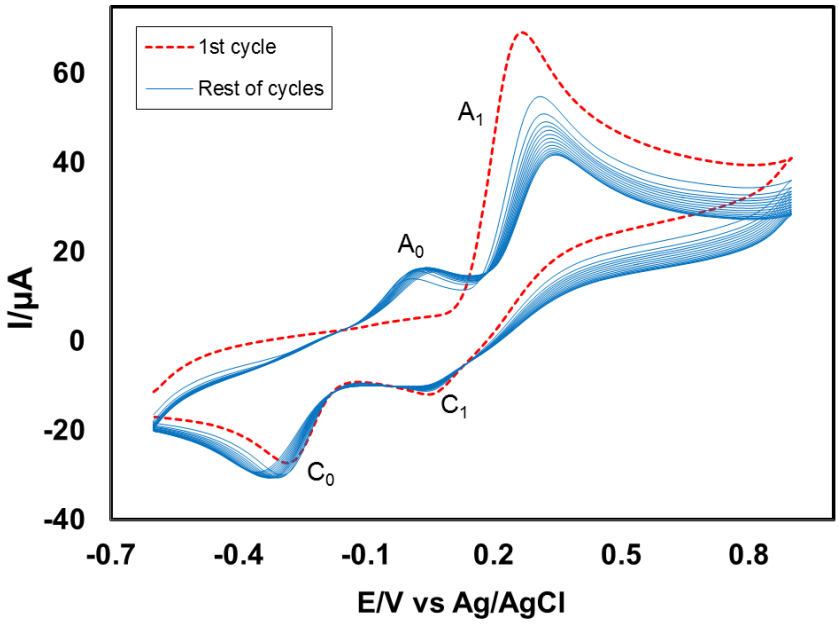

Fig. 4.34: Cyclic voltammogram of 2 mM Catechol with 70 mM Glycine of GC (3 mm) electrode in the buffer solution of pH 7 at scan rate 0.1 V/s (15 cycles). The appeared anodic peak current (A_0) and cathodic peak current (C_0) increased with the iteration scan from the first cycle.

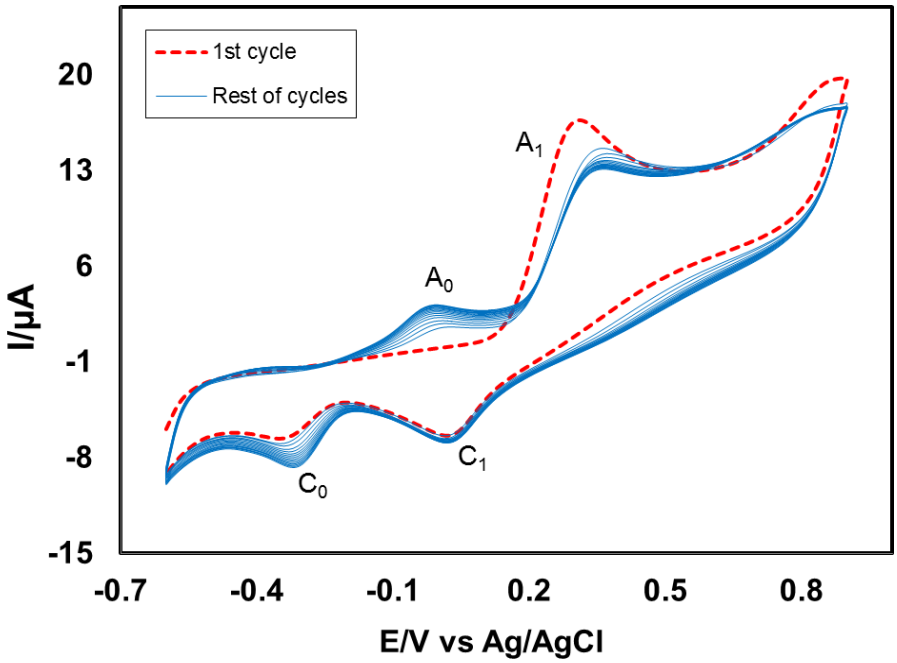

Fig. 4.35: Cyclic voltammogram of 2 mM Catechol with 70 mM Glycine of Pt electrode in the buffer solution of pH 7 at scan rate 0.1 V/s (15 cycles). The appeared anodic peak current (A_0) and cathodic peak current (C_0) increased with the iteration scan from the first cycle.

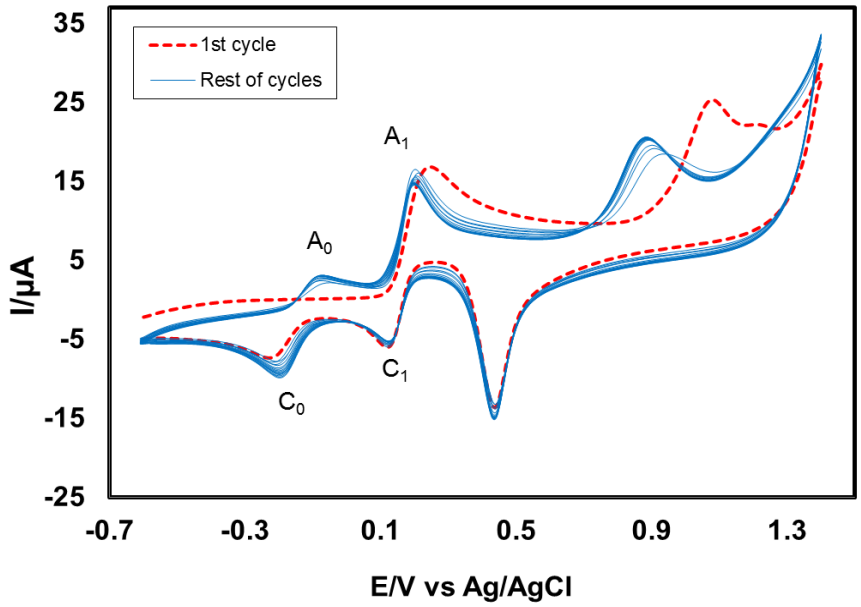

Fig. 4.36: Cyclic voltammogram of 2 mM Catechol with 70 mM Glycine of Au electrode in the buffer solution of pH 7 at scan rate 0.1 V/s (15 cycles). The appeared anodic peak current (A_0) and cathodic peak current (C_0) increased with the iteration scan from the first cycle.

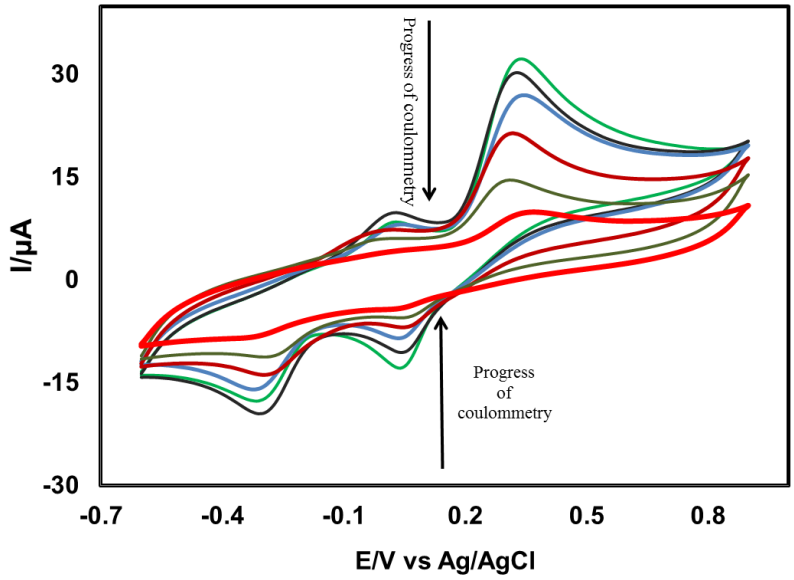

Fig. 4.37: Cyclic voltammogram and (CV) of 1 mM Catechol in presence of 35 mM Glycine of GC electrode during controlled potential coulometry at 0.45 V in pH 7 at scan rate 0.1 V/s.

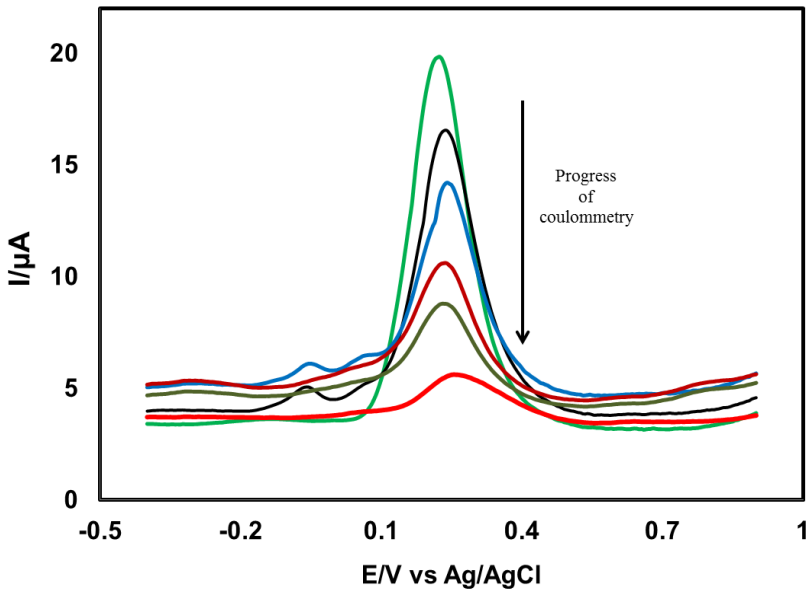

Fig. 4.38: Differential pulse voltammogram (DPV) of 1 mM Catechol in presence of 35 mM Glycine of GC electrode during controlled potential coulometry at 0.45 V in pH 7 at scan rate 0.1 V/s.

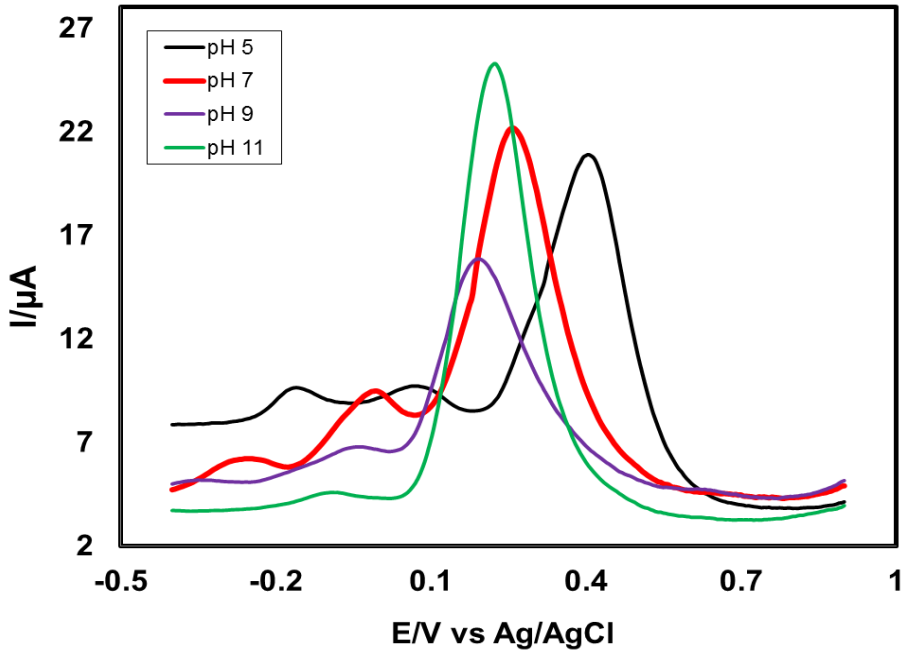

Fig. 4.39: Differential pulse voltammogram (DPV) of 2 mM Catechol with70 mM Glycine of GC electrode in second scan of different pH (5, 7, 9 and 11) and scan rate 0.1 V/s.

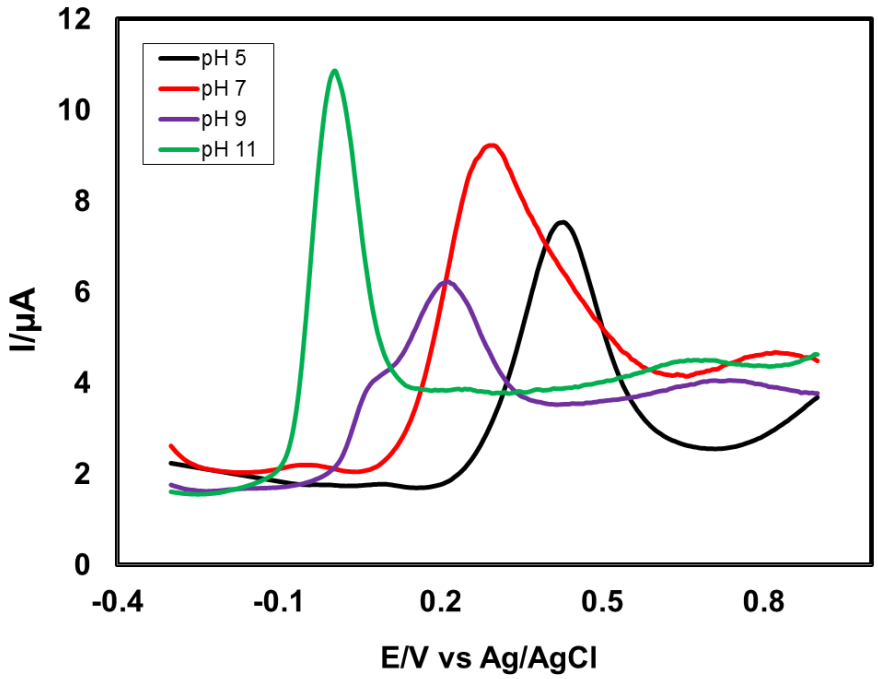

Fig. 4.40: Differential pulse voltammogram (DPV) of 2 mM Catechol with 70 mM Glycine of Pt electrode in second scans of different pH (5, 7, 9 and 11) and scan rate 0.1 V/s.

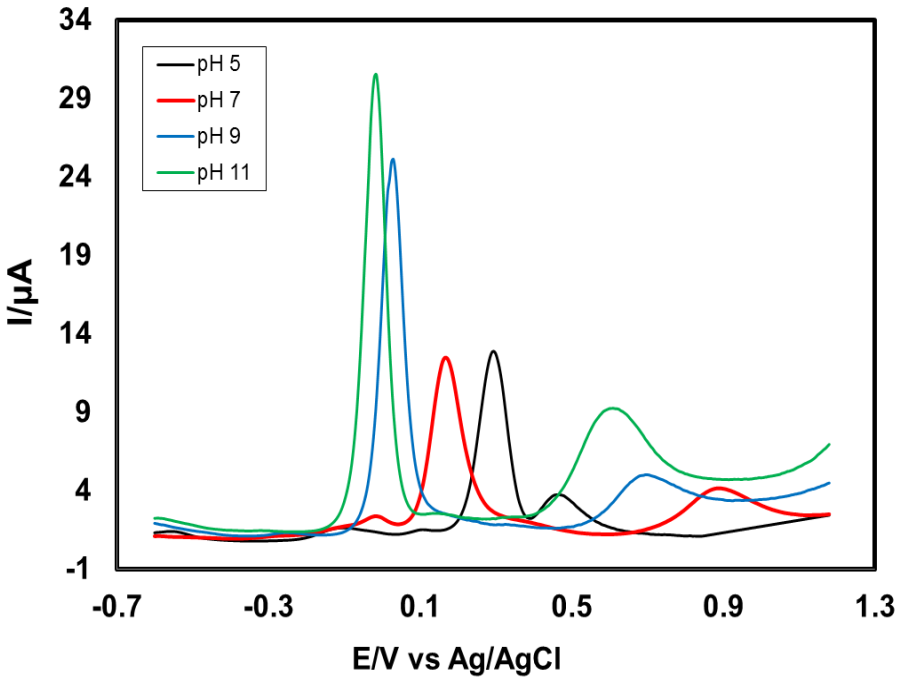

Fig. 4.41: Differential pulse voltammogram (DPV) of 2 mM Catechol with70 mM Glycine of Au electrode in second scans of different pH (5, 7, 9 and 11) and scan rate 0.1 V/s.

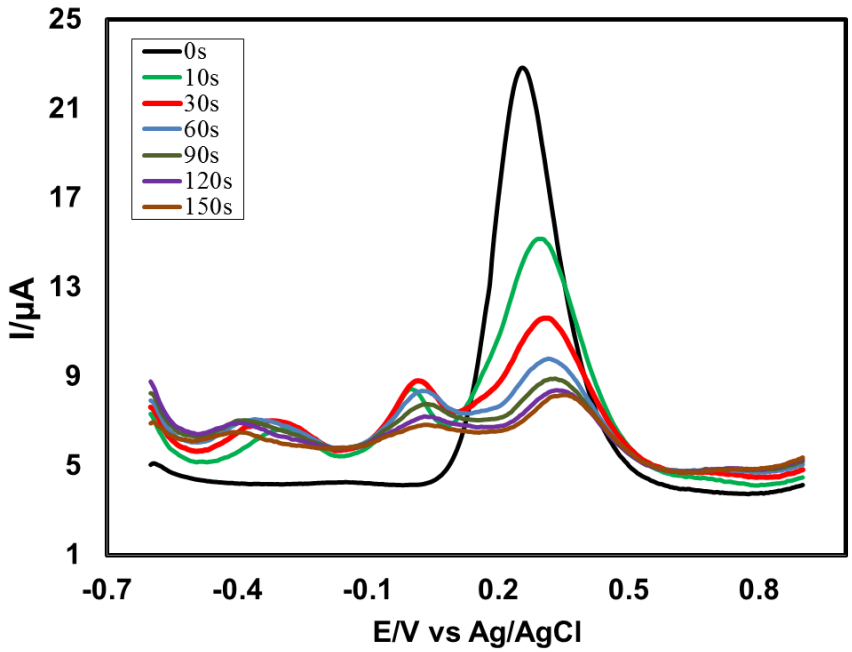

Fig. 4.42: Differential pulse voltammogram (DPV) of deposition time change (0, 10, 30, 60, 90, 120 and 150 s) of 2 mM Catechol with 70 mM Glycine of pH 7 at E_{puls} 0.02 V, t_{puls} 20ms and scan rate 0.1 V/s.

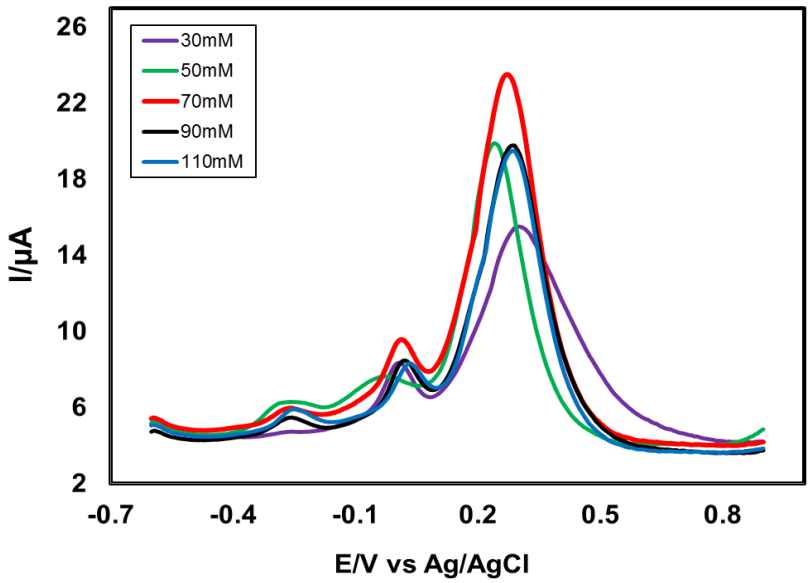

Fig. 4.43: Differential pulse voltammogram (DPV) of composition change of Glycine (30, 50, 70, 90 and 110 mM) with the fixed composition of 2 mM Catechol in second scan of pH 7 at *E*puls 0.02 V, tpuls 20ms of GC electrode and scan rate 0.1 V/s.

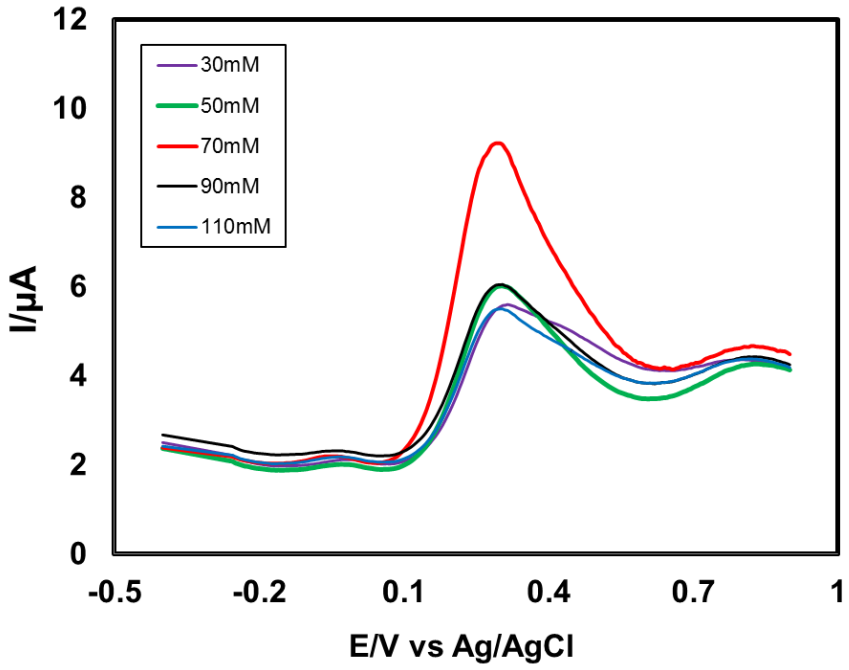

Fig. 4.44: Differential pulse voltammogram (DPV) of composition change of Glycine (30, 50, 70, 90 and 110 mM) with the fixed composition of 2 mM Catechol in second scan of pH 7 at *E*puls 0.02 V, tpuls 20ms of Pt electrode and scan rate 0.1 V/s.

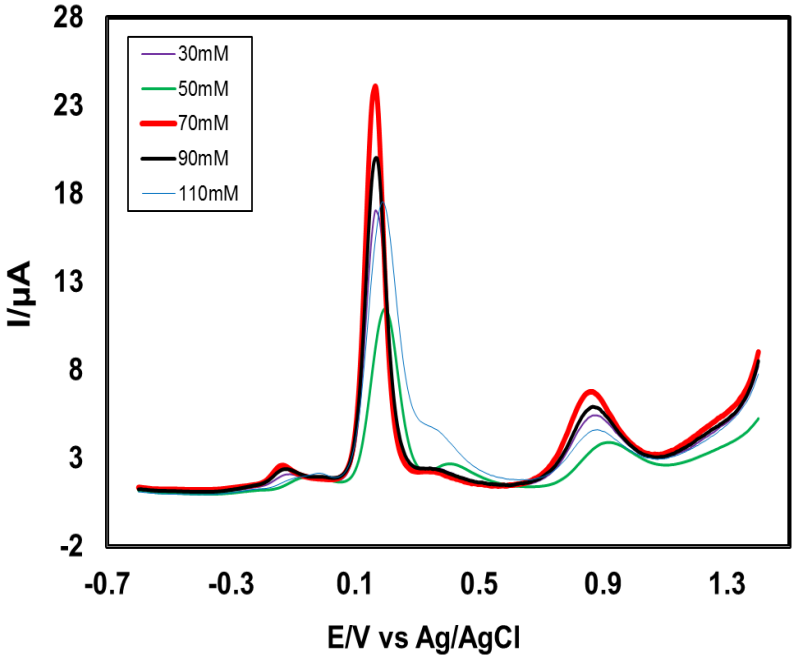

Fig. 4.45: Differential pulse voltammogram (DPV) of composition change of Glycine (30, 50, 70, 90 and 110 mM) with the fixed composition of 2 mM Catechol in second scan of pH7 at *E*puls 0.02 V, tpuls 20ms of Au electrode and scan rate 0.1 V/s.

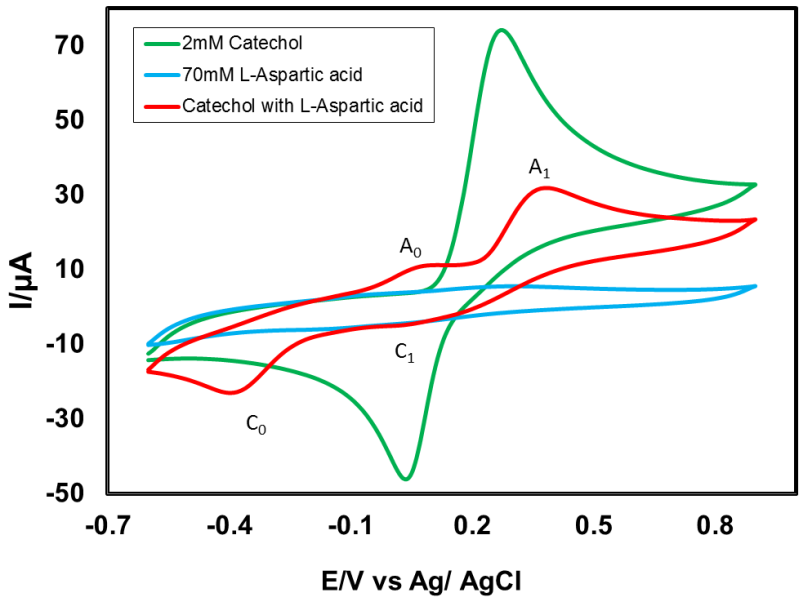

Fig. 4.46: Cyclic voltammogram of 2 mM Catechol (green line), 70 mM L-Aspartic acid (blue line) and 2 mM Catechol with 70 mM L-Aspartic acid (red line) of GC electrode in buffer solution (pH 7) at scan rate 0.1 V/s (2nd cycle). (A_0 = appeared anodic peak)

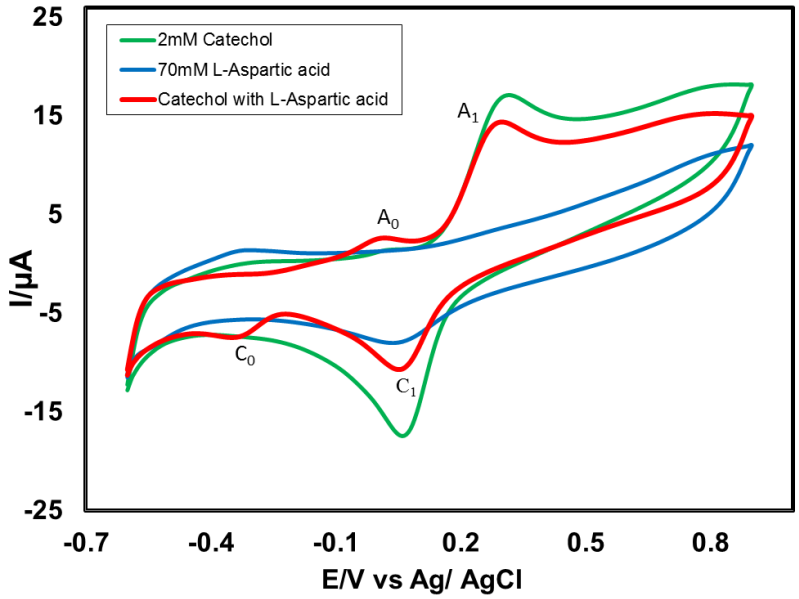

Fig. 4.47: Cyclic voltammogram of 2 mM Catechol (green line), 70 mM L-Aspartic acid (blue line) and 2 mM Catechol with 70 mM L-Aspartic acid (red line) of Pt electrode in buffer solution (pH 7) at scan rate 0.1 V/s (2nd cycle). (A_0 = appeared anodic peak)

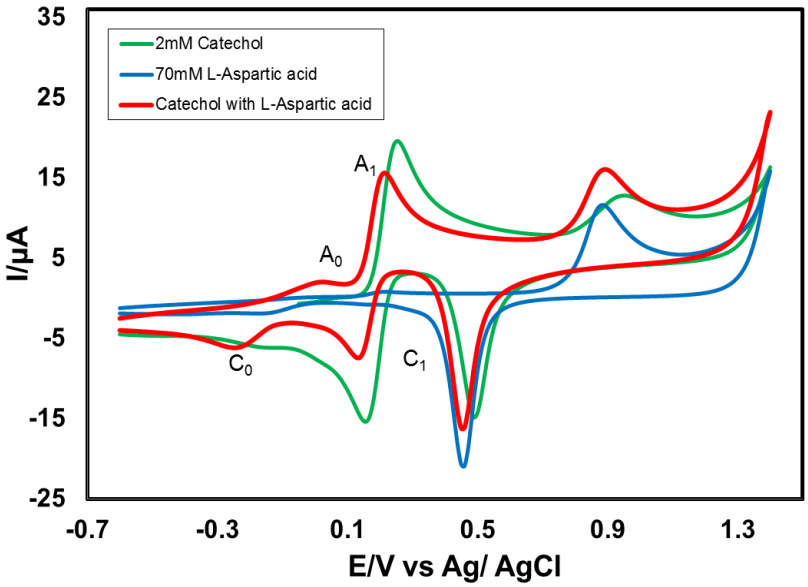

Fig. 4.48: Cyclic voltammogram of 2 mM Catechol (green line), 70 mM L-Aspartic acid (blue line) and 2 mM Catechol with 70 mM L-Aspartic acid (red line) of Au electrode in buffer solution (pH 7) at scan rate 0.1 V/s (2nd cycle). (A_0 = appeared anodic peak)

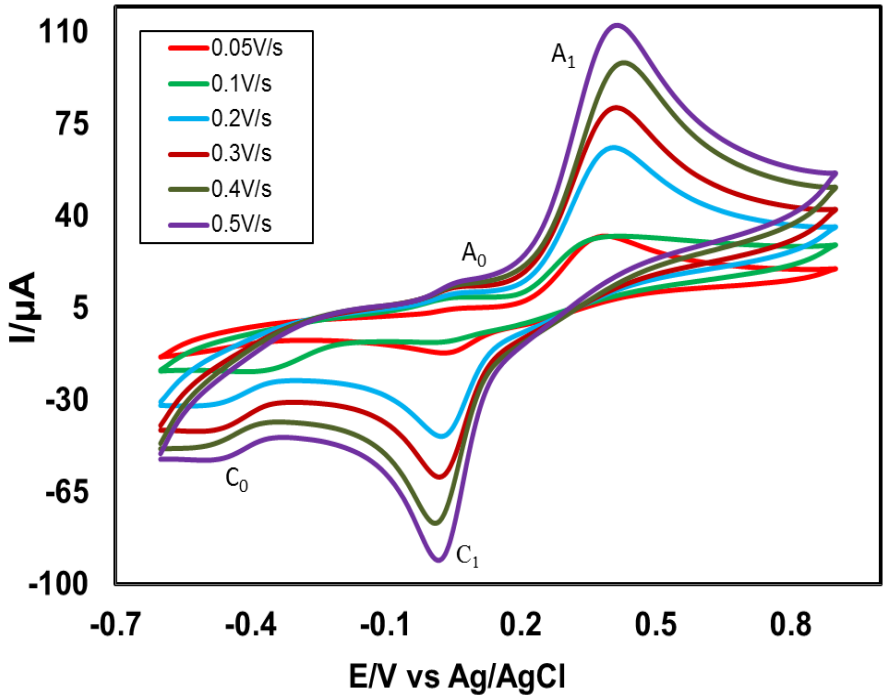

Fig. 4.49: Cyclic voltammogram of 2 mM Catechol with 70 mM L-Aspartic acid in the second scan of potential at GC electrode in buffer solution (pH 7) at scan rate 0.05 V/s to 0.5 V/s.

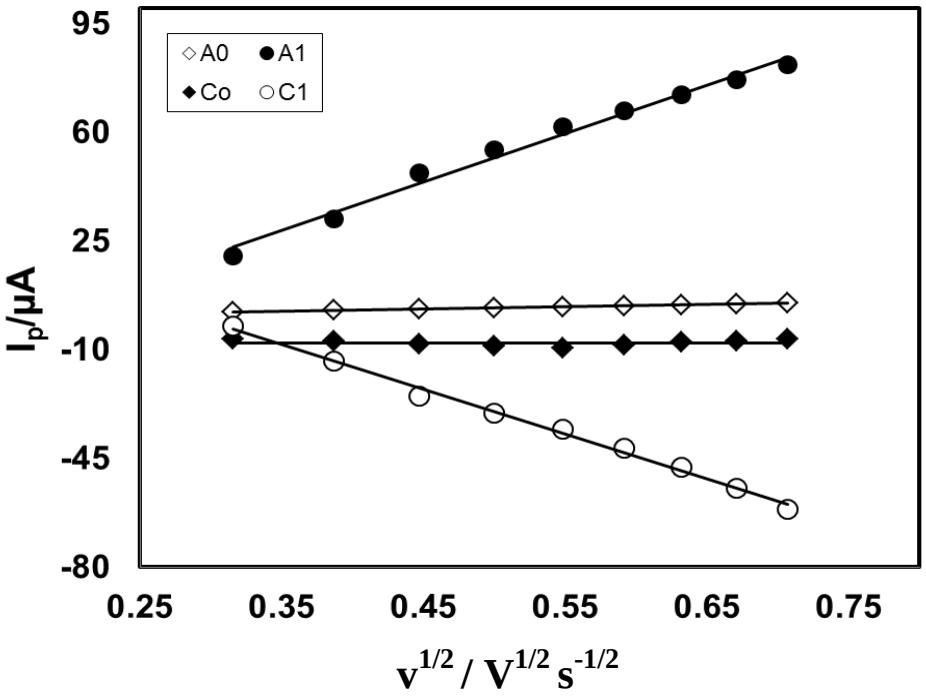

Fig. 4.50: Plots of peak current (I_p) versus square root of scan rate ($v^{1/2}$) of 2 mM Catechol with 70 mM L-Aspartic acid of GC electrode in buffer solution (pH 7) (2^{nd} cycle).

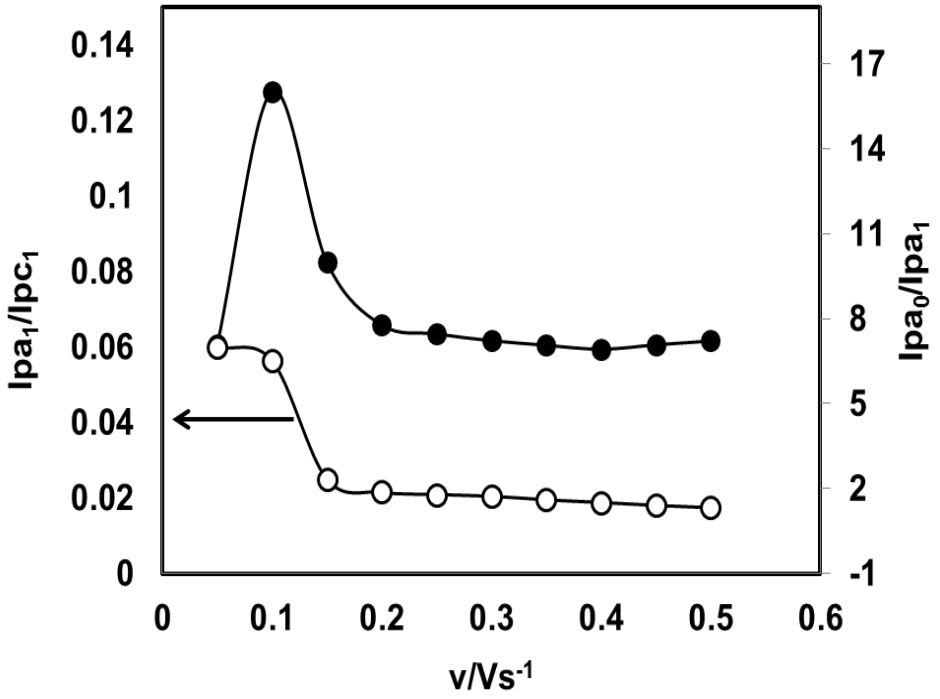

Fig. 4.51: Variation of peak current ratio of corresponding peak (I_{pa1}/I_{pc1}) and anodic peak (I_{pa0}/I_{pa1}) vs scan rate (v) of 2 mM Catechol with 70 mM L-Aspartic acid of GC electrode in buffer solution (pH 7) at scan rate 0.1 V/s in the second scan of potential.

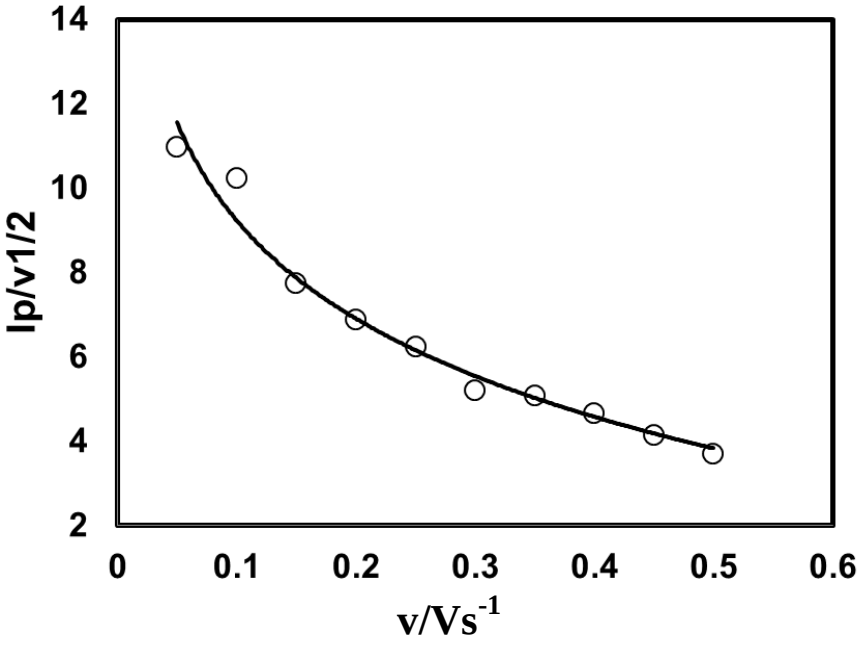

Fig. 4.52: Plot of current function ($I_p/v^{1/2}$) versus scan rate (v) of 2 mM Catechol with 70 mM L-Aspartic acid of GC electrode in buffer solution (pH 7) of the Appeared anodic peak (A_0).

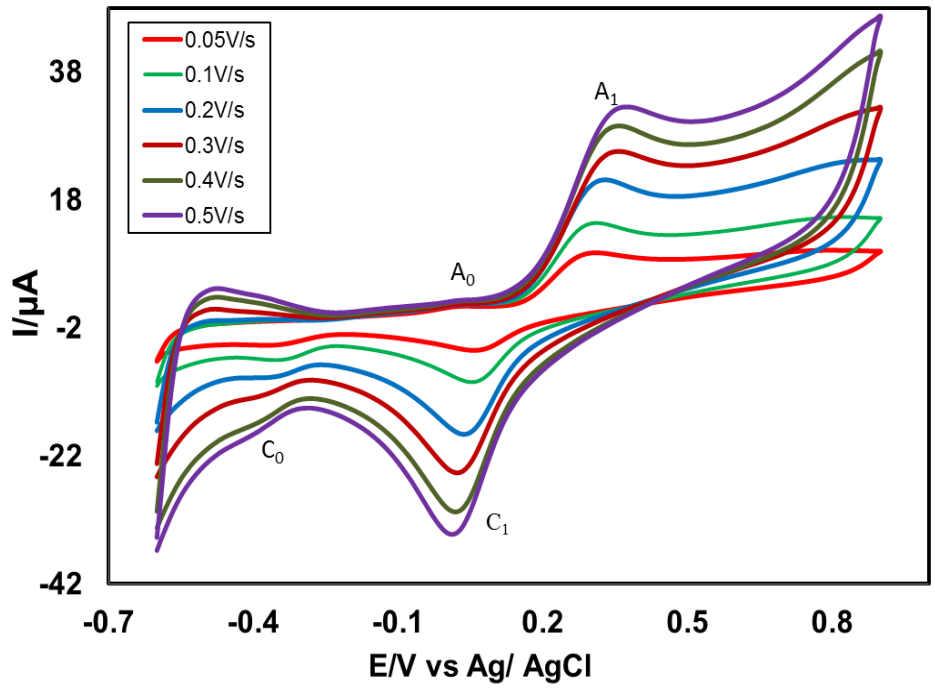

Fig. 4.53: Cyclic voltammogram of 2 mM Catechol with 70 mM L-Aspartic acid in the second scan of potential at Pt electrode in buffer solution (pH 7) at scan rate 0.05 V/s to 0.5 V/s.

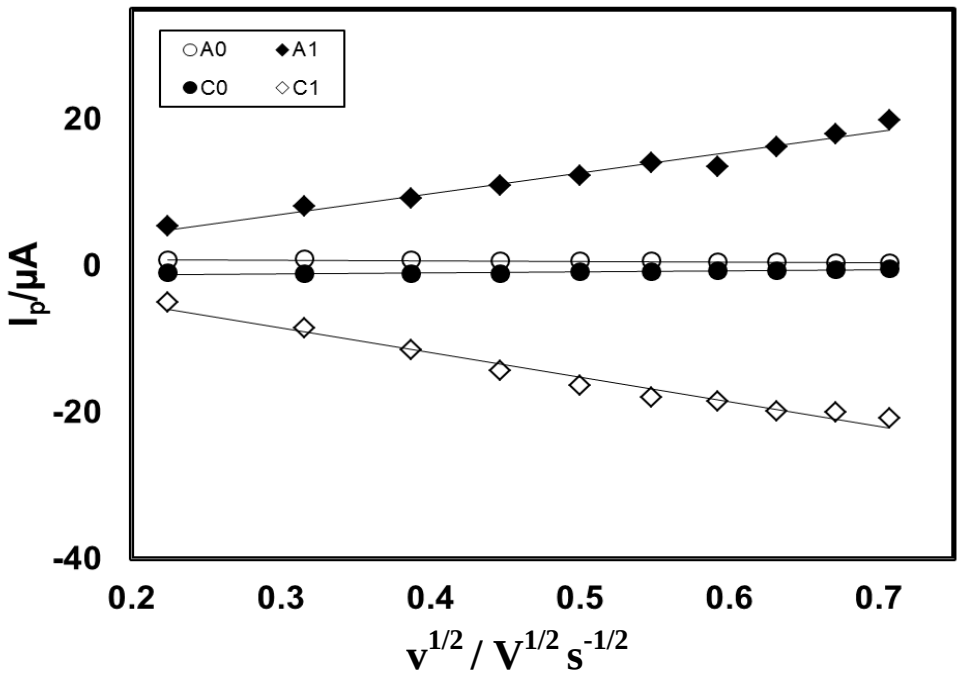

Fig. 4.54: Plots of peak current (I_p) versus square root of scan rate ($v^{1/2}$) of 2 mM Catechol with 70 mM L-Aspartic acid of Pt electrode in buffer solution (pH 7) (2^{nd} cycle).

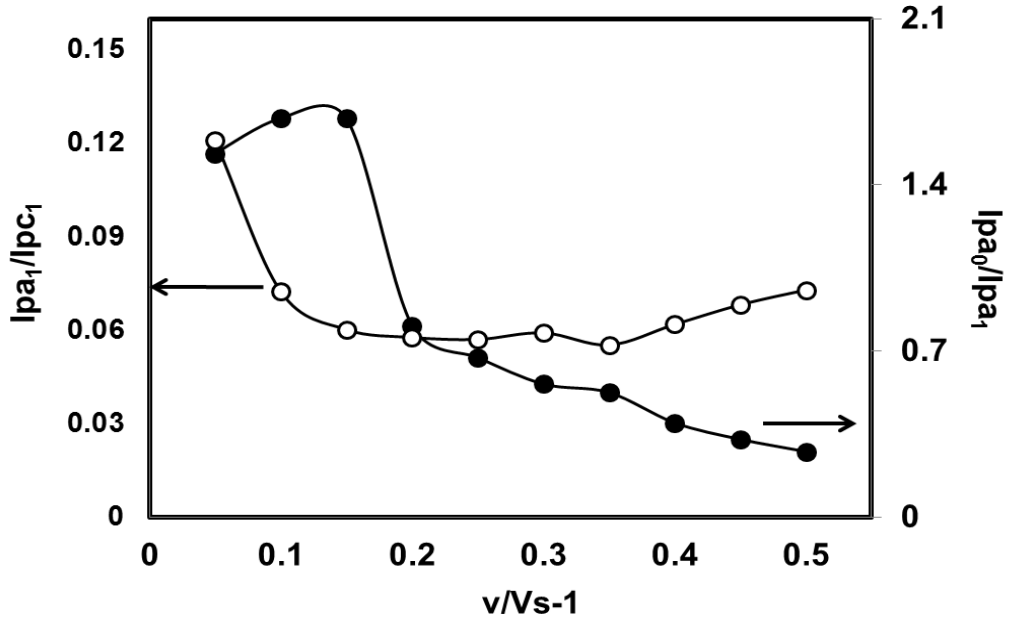

Fig. 4.55: Variation of peak current ratio of corresponding peak (I_{pa1}/I_{pc1}) and anodic peak (I_{pa0}/I_{pa1}) vs scan rate (v) of 2 mM Catechol with 70 mM L-Aspartic acid of Pt electrode in buffer solution (pH 7) at scan rate 0.1 V/s in the second scan of potential.

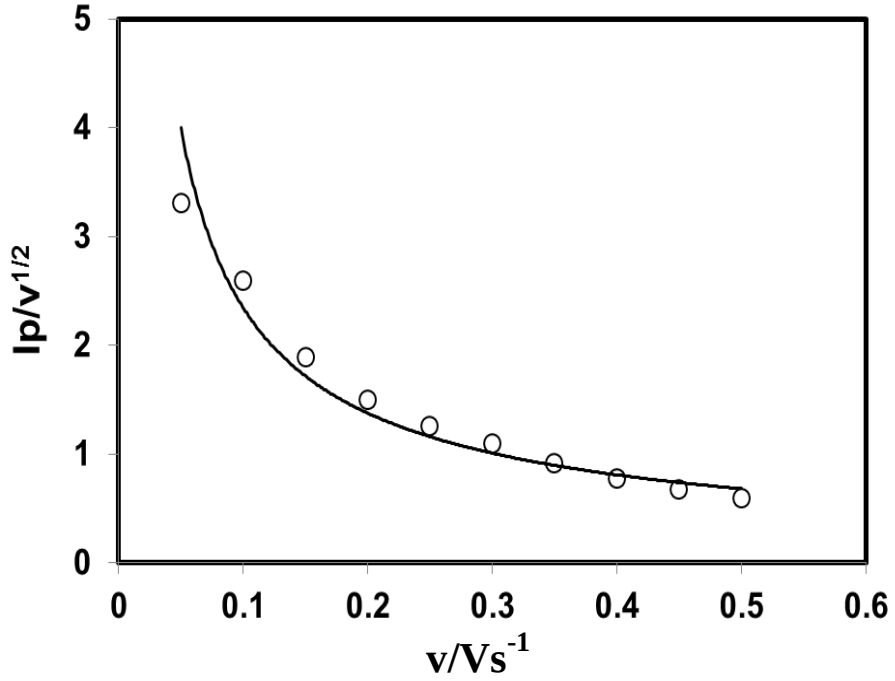

Fig. 4.56: Plots of current function ($I_p/v^{1/2}$) versus scan rate (v) of 2 mM Catechol with 70 mM L-Aspartic acid of Pt electrode in buffer solution (pH 7) of the Appeared anodic peak (A_0).

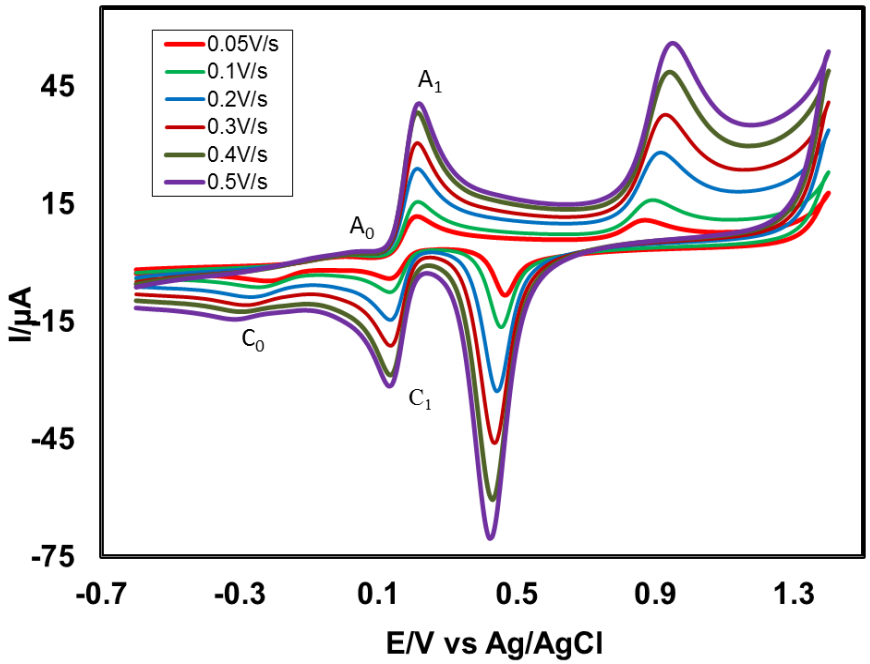

Fig. 4.57: Cyclic voltammogram of 2 mM Catechol with 70 mM L-Aspartic acid in the second scan of potential at Au electrode in buffer solution (pH 7) at scan rate 0.05 V/s to 0.5 V/s.

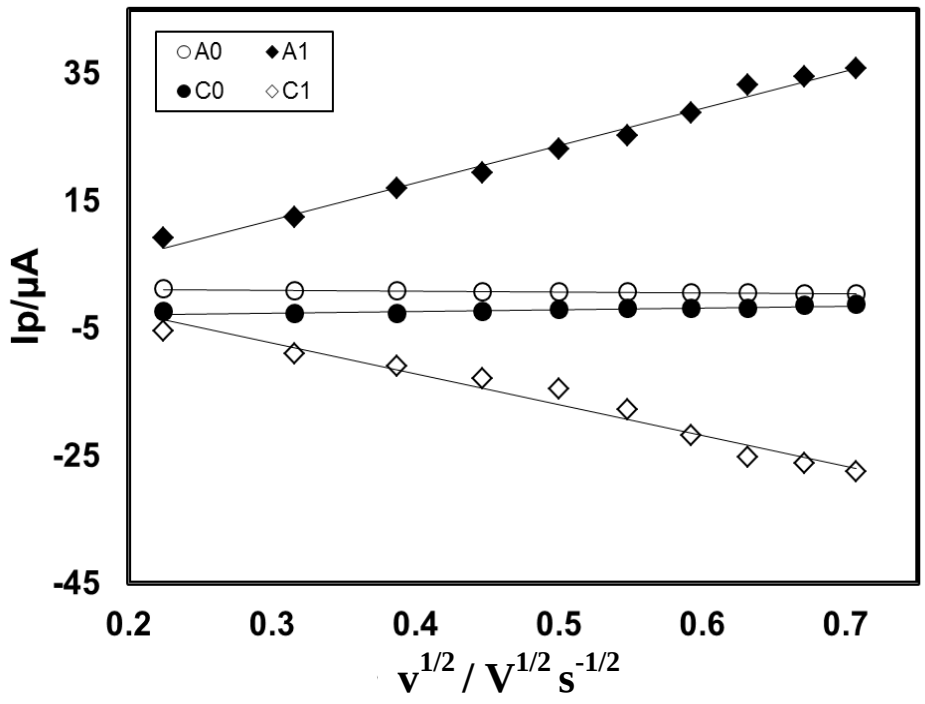

Fig. 4.58: Plots of peak current (I_p) versus square root of scan rate ($v^{1/2}$) of 2 mM Catechol with 70 mM L-Aspartic acid of Au electrode in buffer solution (pH 7) (2^{nd} cycle).

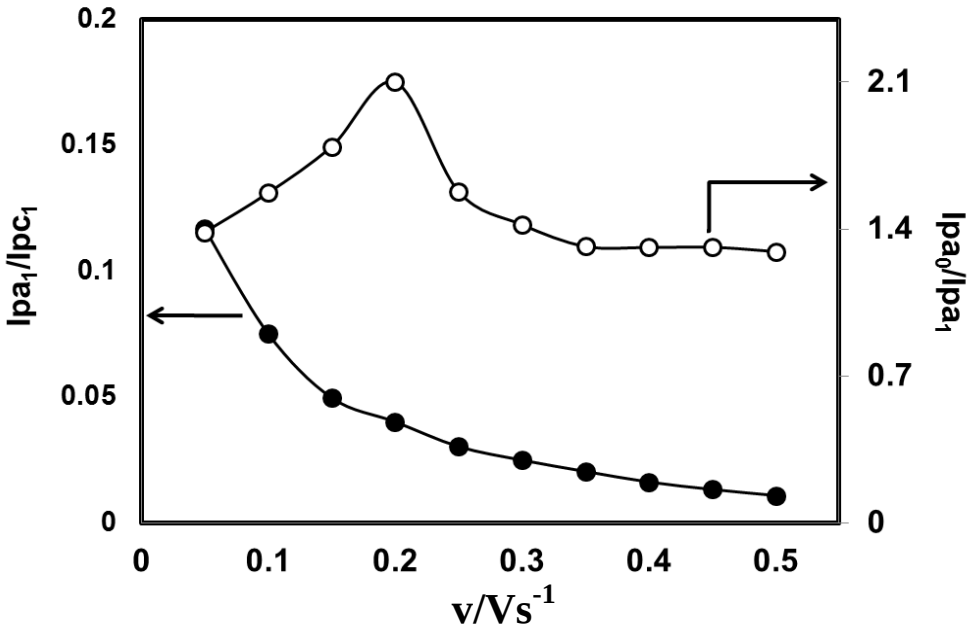

Fig. 4.59 : Variation of peak current ratio of corresponding peak (I_{pa1}/I_{pc1}) and anodic peak (I_{pa0}/I_{pa1}) vs scan rate (v) of 2 mM Catechol with 70 mM L-Aspartic acid of Au electrode in buffer solution (pH 7) at scan rate 0.1 V/s in the second scan of potential.

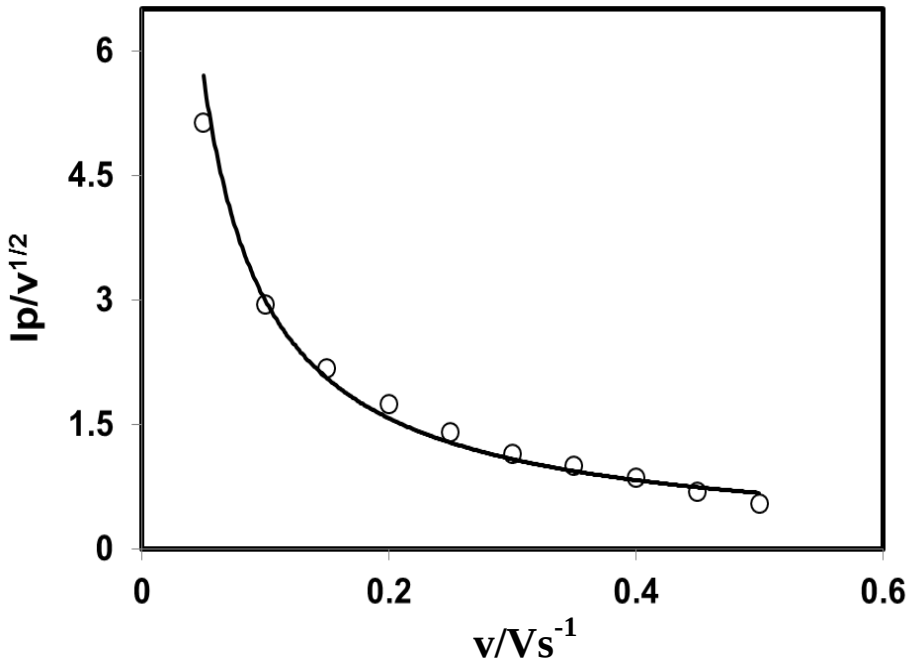

Fig. 4.60: Plots of current function ($I_p/v^{1/2}$) versus scan rate (v) of 2 mM Catechol with 70 mM L-Aspartic acid of Au electrode in buffer solution (pH 7) of the Appeared anodic peak (A_0).

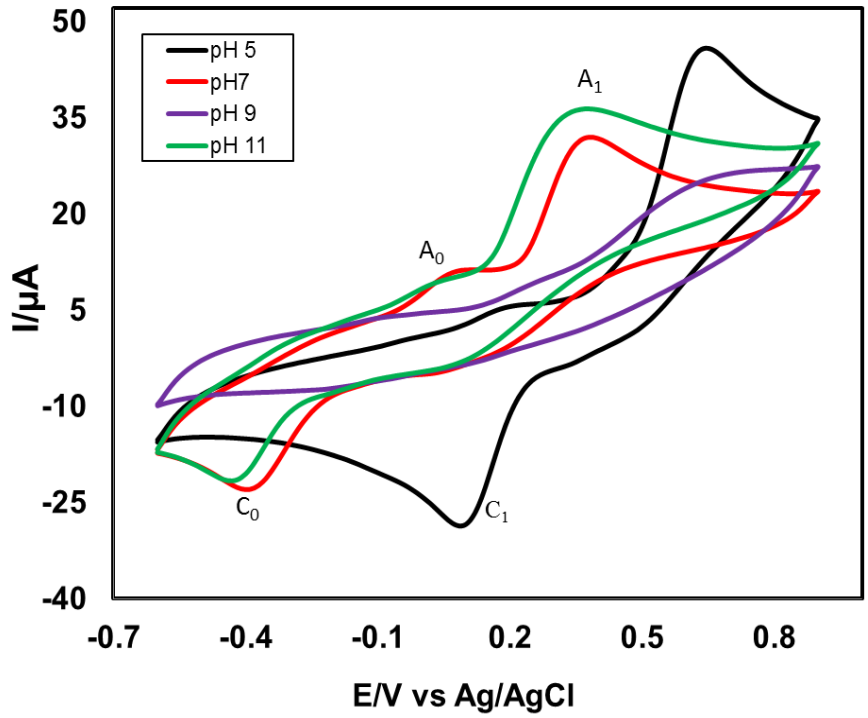

Fig. 4.61: Cyclic voltammogram of 2 mM Catechol with 70 mM L-Aspartic acid of GC (3 mm) electrode in different pH (5, 7, 9 and 11) at scan rate 0.1 V/s.

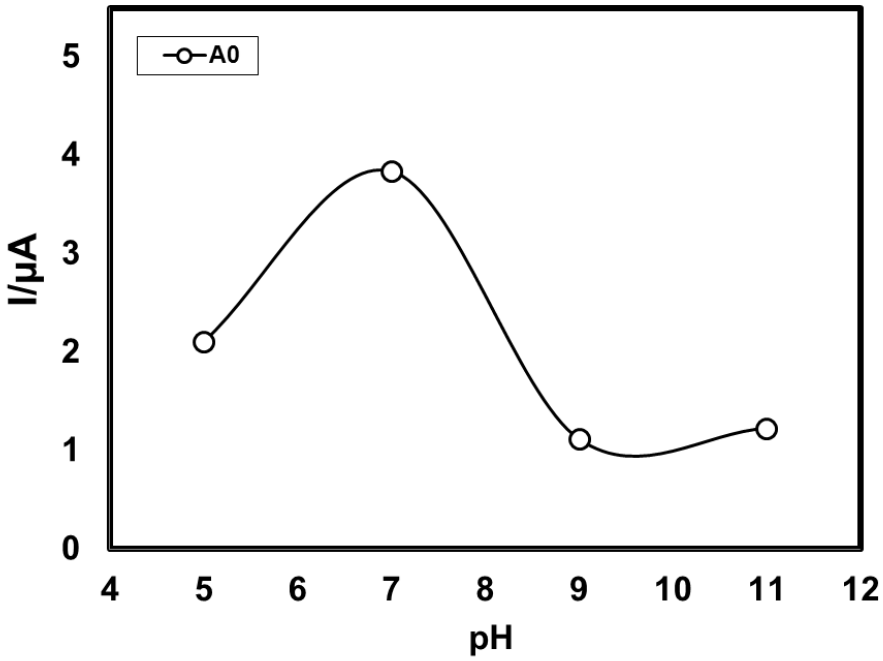

Fig. 4.62: Plot of peak current (I_p) versus pH (5, 7, 9 and 11) of 2 mM Catechol with 70 mM L-Aspartic acid of GC electrode at scan rate 0.1 V/s (2^{nd} cycle).

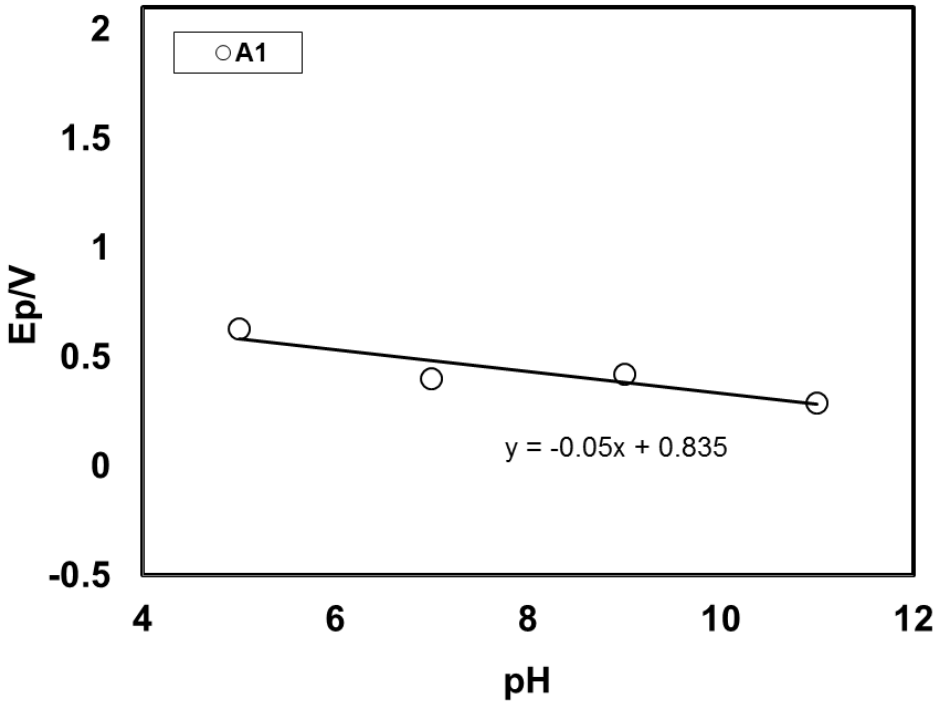

Fig. 4.63: Plots of peak potential (E_p) versus pH (5, 7, 9 and 11) of 2 mM Catechol with 70 mM L-Aspartic acid of GC electrode at scan rate 0.1 V/s (2nd cycle).

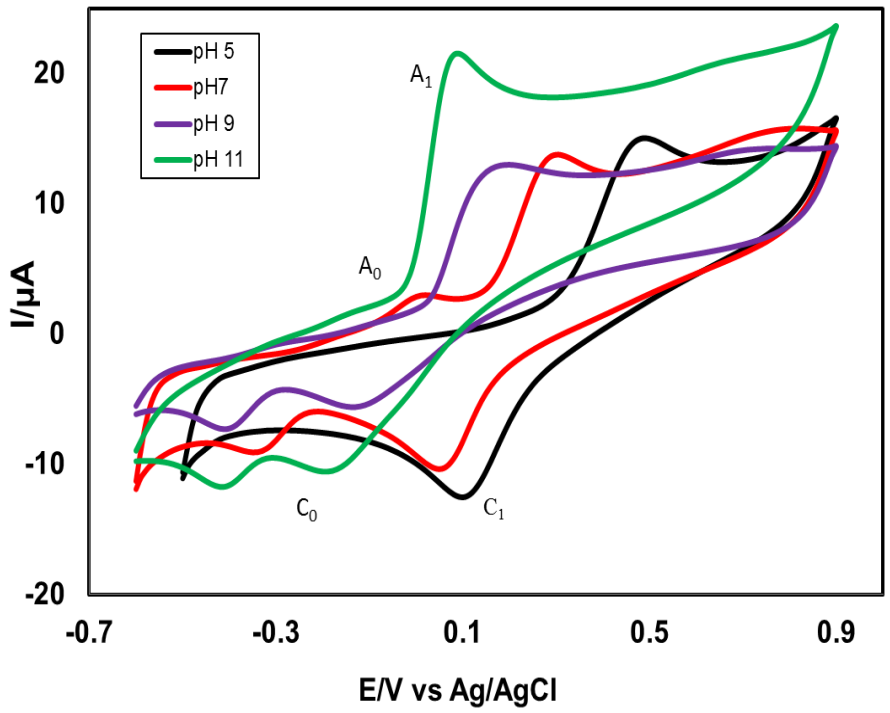

Fig. 4.64: Cyclic voltammogram of 2 mM Catechol with 70 mM L-Aspartic acid of Pt electrode in different pH (5, 7, 9 and 11) at scan rate 0.1 V/s.

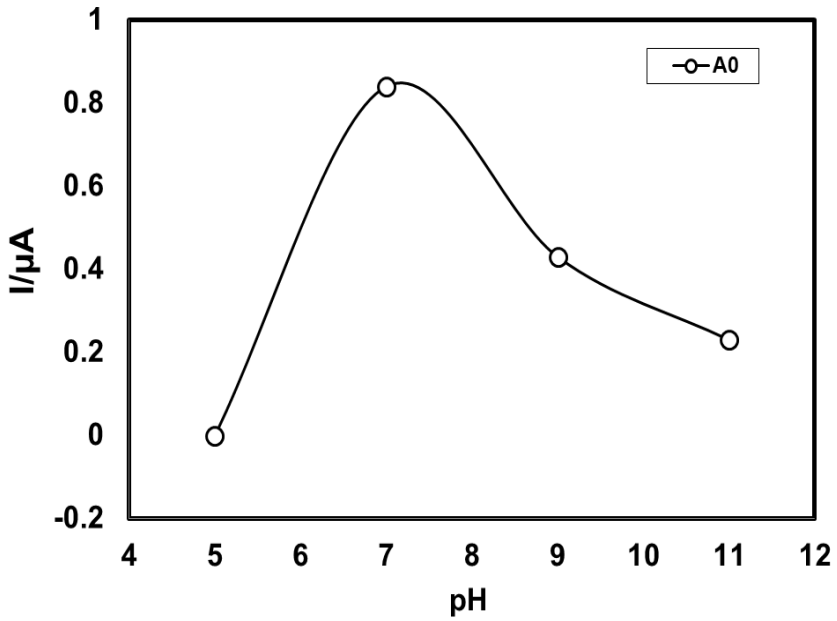

Fig. 4.65: Plots of peak current (I_p) versus pH (5, 7, 9 and 11) of 2 mM Catechol with 70 mM L-Aspartic acid of Pt electrode at scan rate 0.1 V/s (2nd cycle).

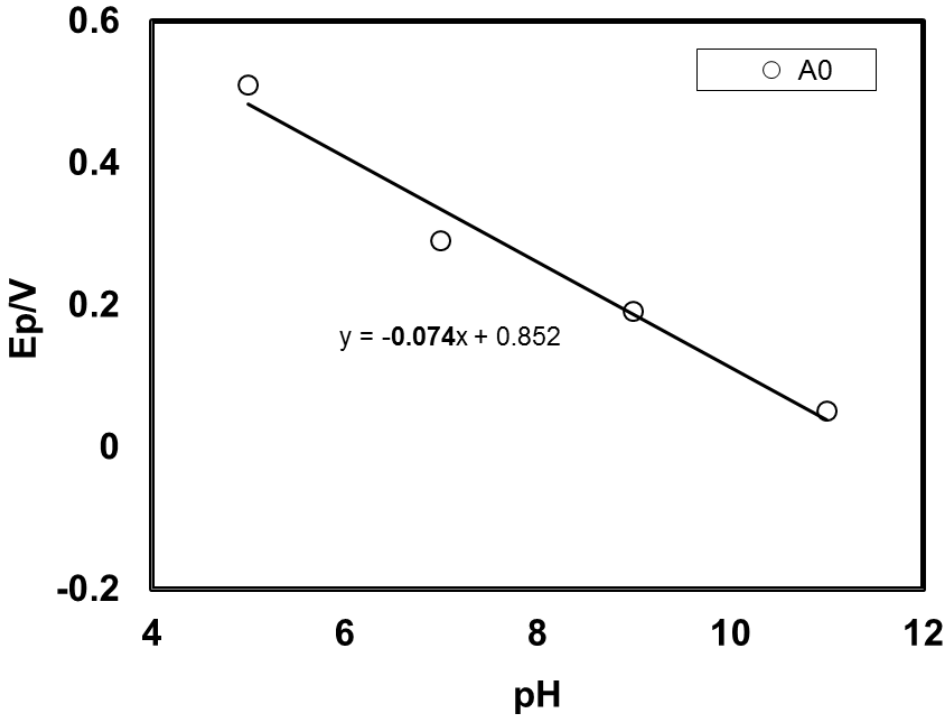

Fig. 4.66: Plot of peak potential (E_p) versus pH (5, 7, 9 and 11) of 2 mM Catechol with 70 mM L-Aspartic acid of Pt electrode at scan rate 0.1 V/s (2nd cycle).

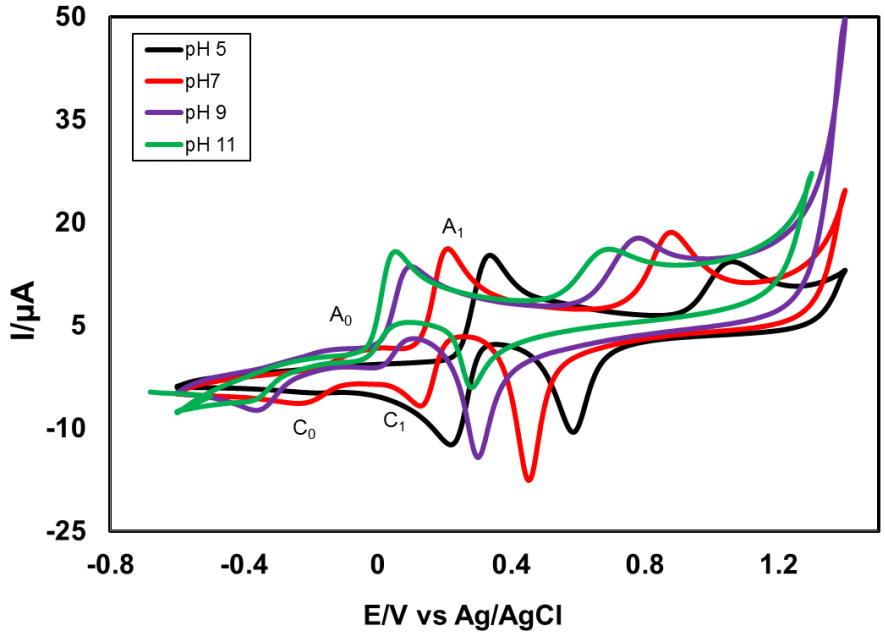

Fig. 4.67: Cyclic voltammogram of 2 mM Catechol with 70 mM L-Aspartic acid of Au electrode in different pH (5, 7, 9 and 11) at scan rate 0.1 V/s.

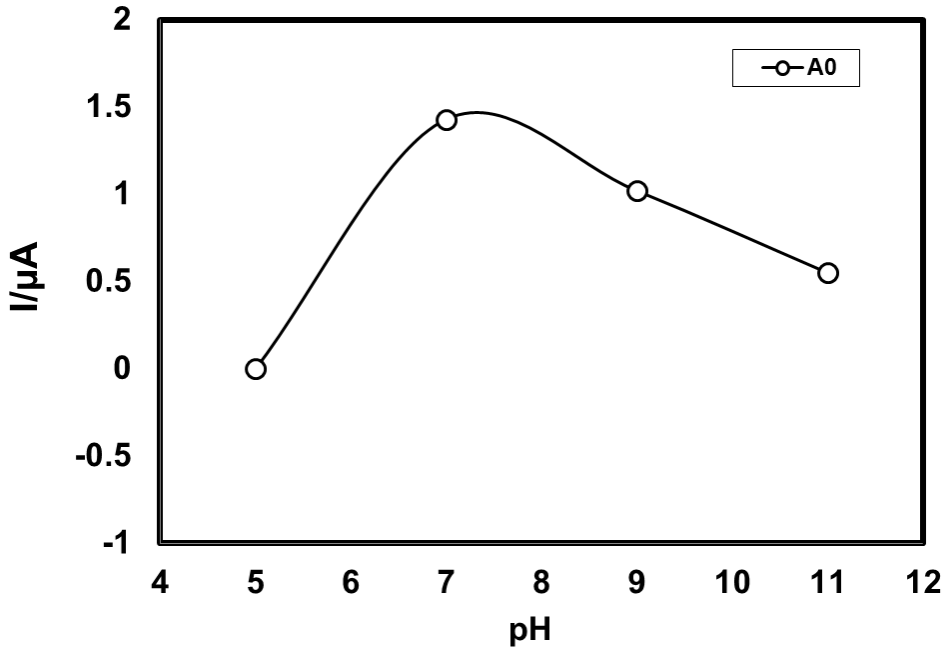

Fig. 4.68: Plots of peak current (I_p) versus pH (5, 7, 9 and 11) of 2 mM Catechol with 70 mM L-Aspartic acid of Au electrode at scan rate 0.1 V/s (2^{nd} cycle).

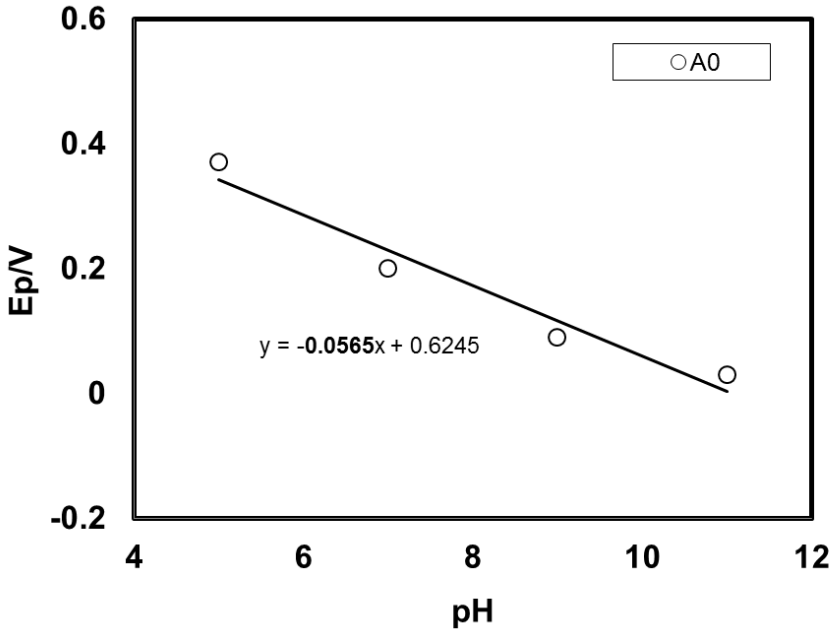

Fig. 4.69: Plot of peak potential (E_p) versus pH (5, 7, 9 and 11) of 2 mM Catechol with 70 mM L-Aspartic acid of Au electrode at scan rate 0.1 V/s (2nd cycle).

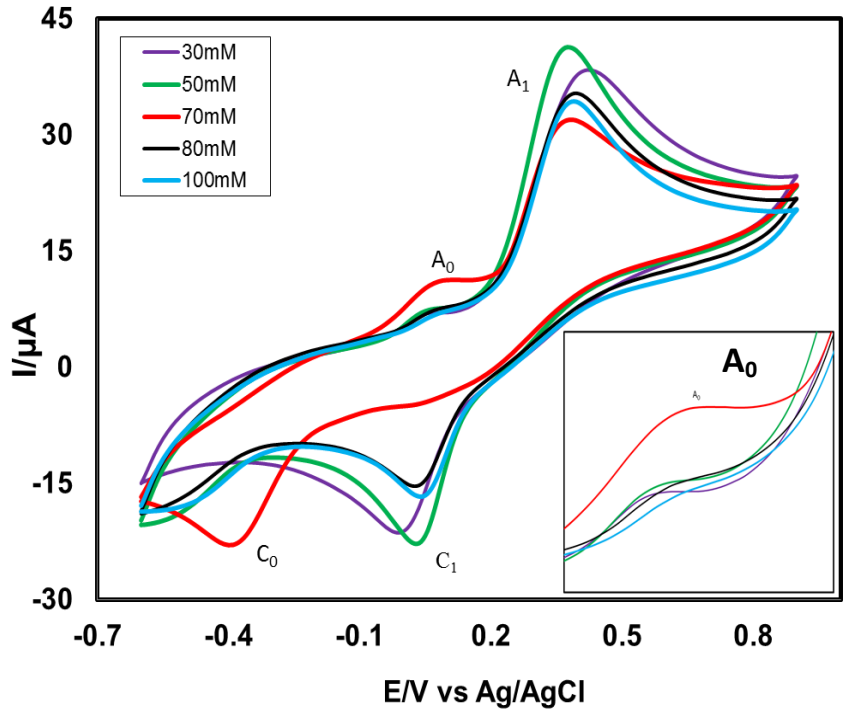

Fig. 4.70: CV of composition changes of L-Aspartic acid (30, 50, 70, 80 and 100 mM) with fixed 2 mM Catechol of GC electrode at pH 7 and scan rate 0.1 V/s. Insert: appeared anodic peak (A_0)

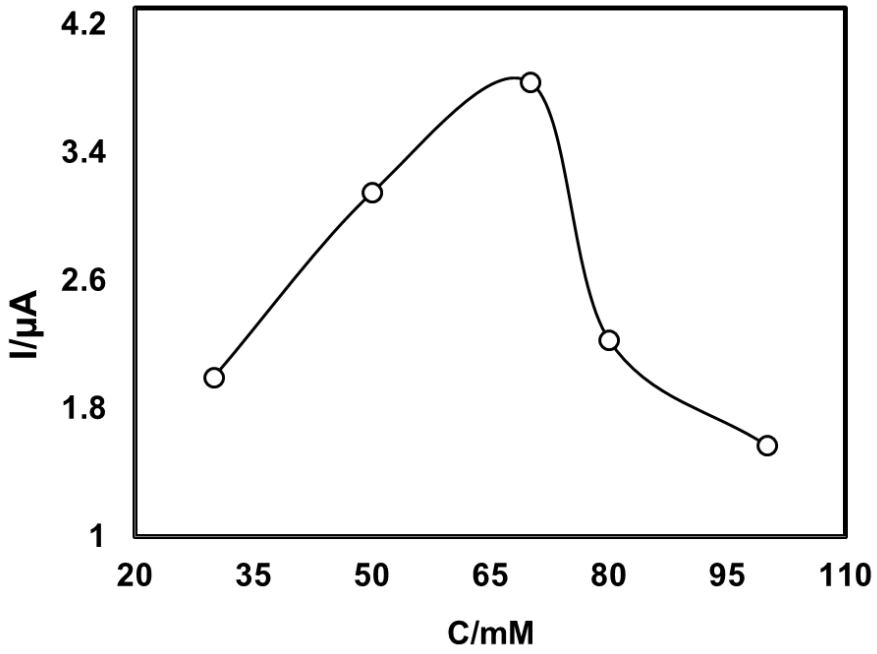

Fig. 4.71: Comparison of cyclic voltammogram of different concentration (30, 50, 70, 80 and 100 mM) of 2 mM Catechol with 70 mM L-Aspartic acid of GC electrode in buffer solution (pH 7) at scan rate 0.1 V/s (2nd cycle).

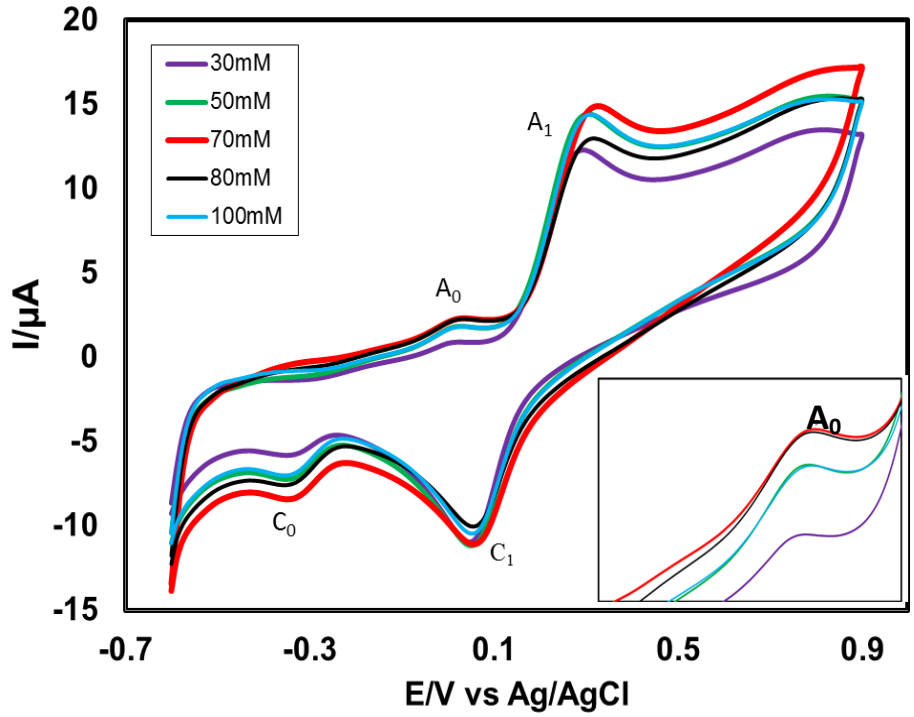

Fig. 4.72: CV of composition changes of L-Aspartic acid (30, 50, 70, 80 and 100 mM) with fixed 2 mM Catechol of Pt electrode at pH 7 and scan rate 0.1 V/s. Insert: appeared anodic peak (A_0)

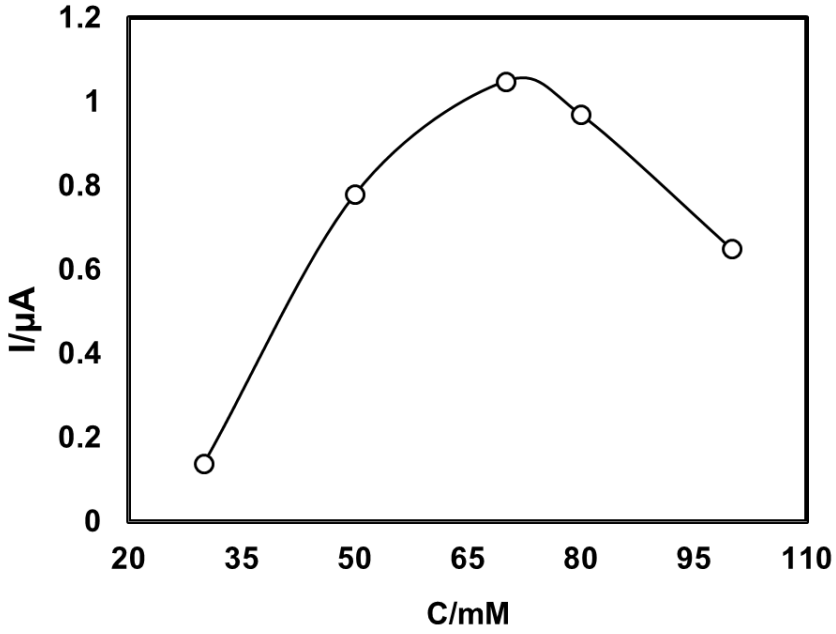

Fig. 4.73: Plots of peak current (I_p) versus concentration (C) of L-Aspartic acid (30, 50, 70, 80 and 100 mM) with fixed 2 mM Catechol of Pt electrode in buffer solution at pH 7 scan rate 0.1 V/s (2nd cycle).

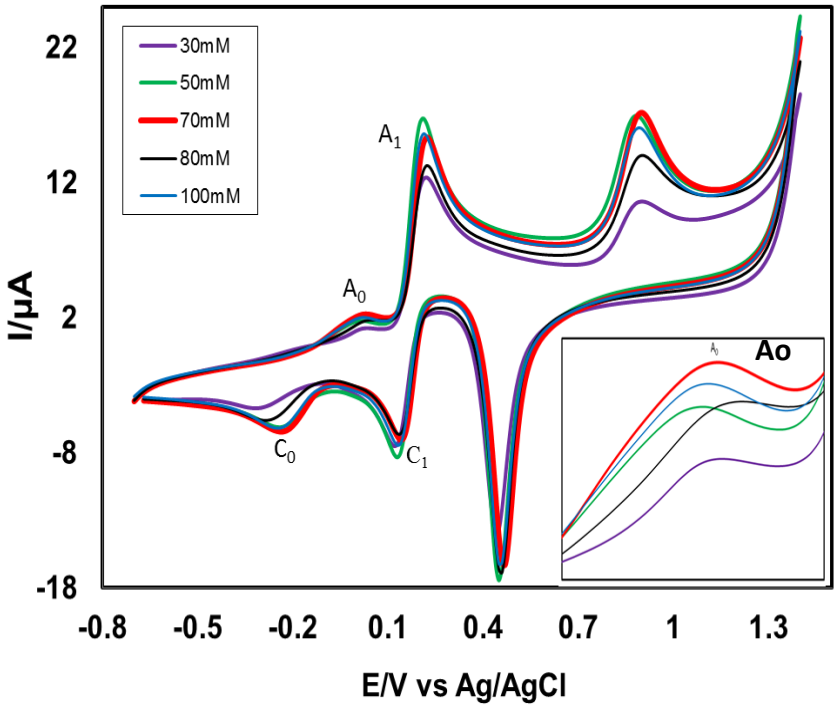

Fig. 4.74: CV of composition changes of L-Aspartic acid (30, 50, 70, 80 and 100 mM) with fixed 2 mM Catechol of Au electrode at pH 7 and scan rate 0.1 V/s. Insert: appeared anodic peak (A_0)

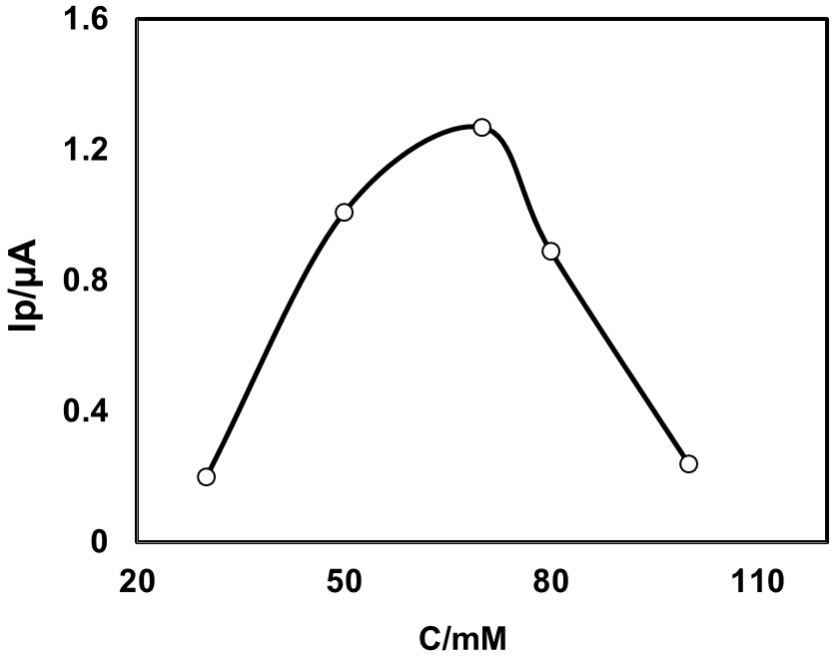

Fig. 4.75: Plots of peak current (I_p) versus concentration (C) of L-Aspartic acid (30, 50, 70, 80 and 100 mM) with fixed 2 mM Catechol of Au electrode in buffer solution (pH 7) at scan rate 0.1 V/s (2nd cycle).

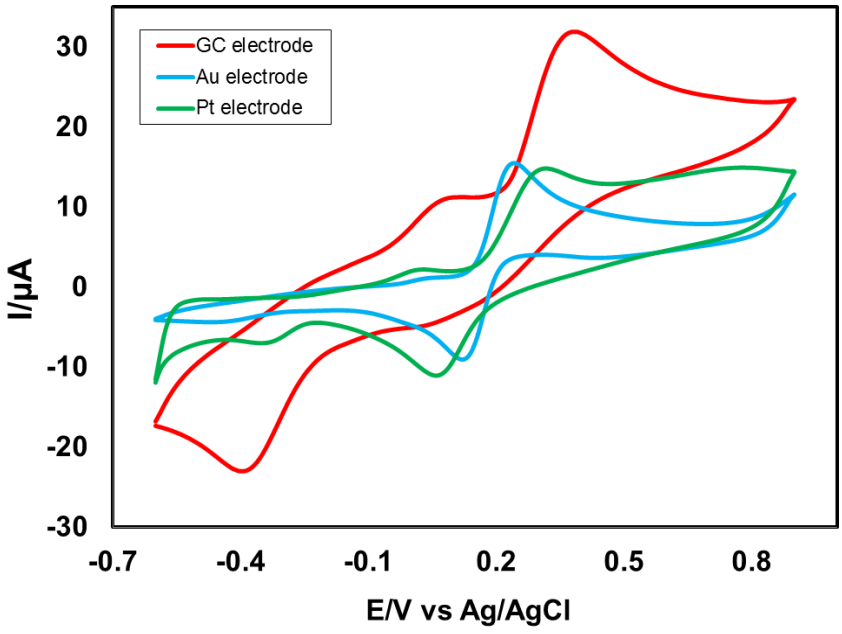

Fig. 4.76: Cyclic voltammogram (CV) of 2 mM catechol with 70 mM L-Aspartic acid in GC electrode (3.0 mm), Gold electrode (1.6 mm) and Platinum electrode (1.6 mm) at pH 7 and scan rate 0.1 V/s.

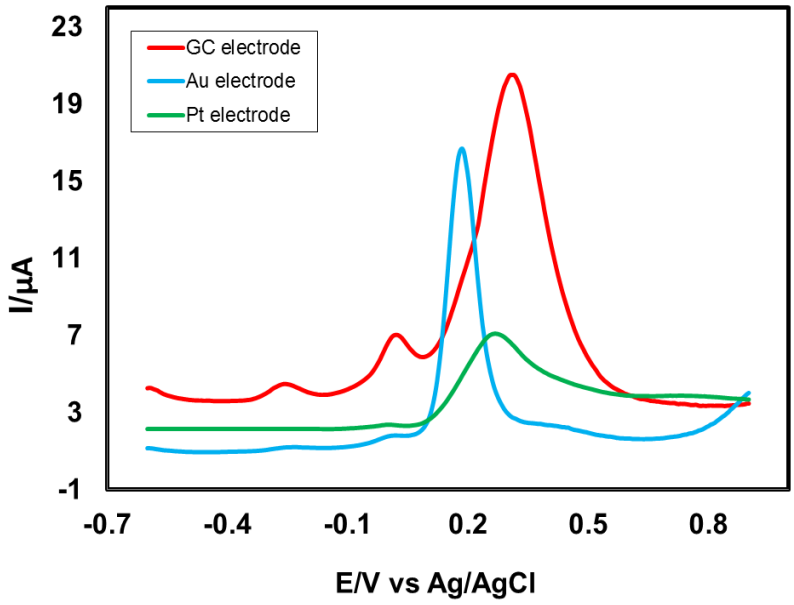

Fig. 4.77: Differential pulse voltammogram (DPV) of 2 mM catechol with 70 mM L-Aspartic acid in GC electrode (3.0 mm), Gold electrode (1.6 mm) and Platinum electrode (1.6 mm) at pH 7 and scan rate 0.1 V/s.

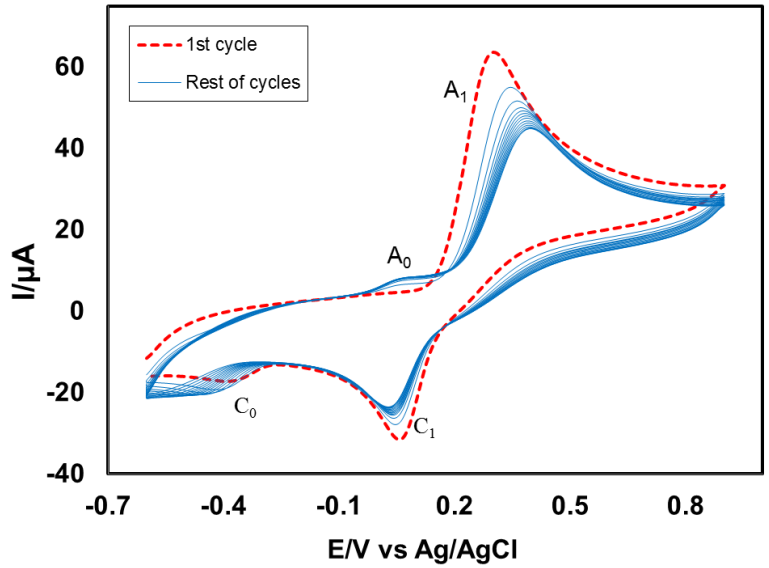

Fig. 4.78: Cyclic voltammogram of 2 mM Catechol with 70 mM L-Aspartic acid of GC (3 mm) electrode in the buffer solution of pH 7 at scan rate 0.1 V/s (15 cycles). The appeared anodic peak current (A_0) and cathodic peak current (C_0) increased with the iteration scan from the first cycle.

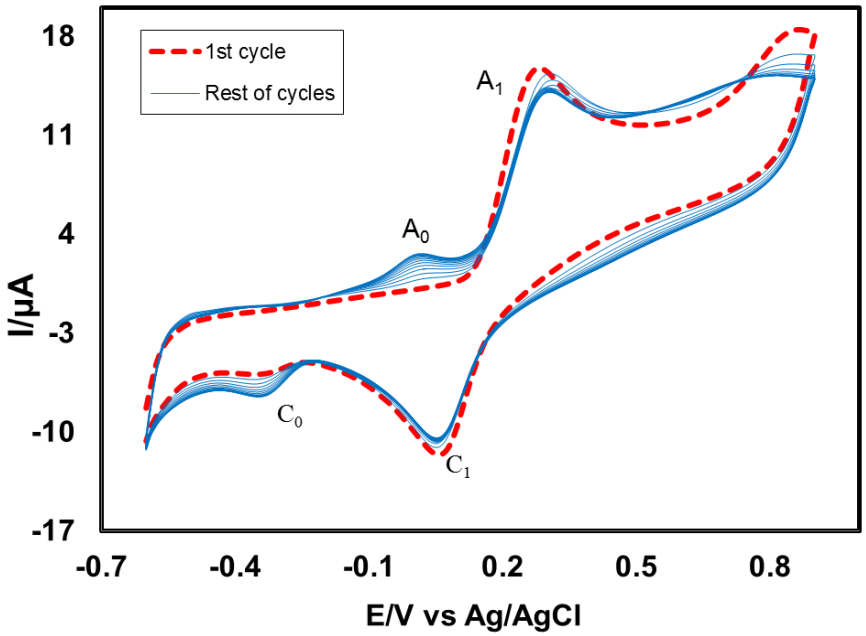

Fig. 4.79: Cyclic voltammogram of 2 mM Catechol with 70 mM L-Aspartic acid of Pt electrode in the buffer solution of pH 7 at scan rate 0.1 V/s (15 cycles). The appeared anodic peak current (A_0) and cathodic peak current (C_0) increased with the iteration scan from the first cycle.

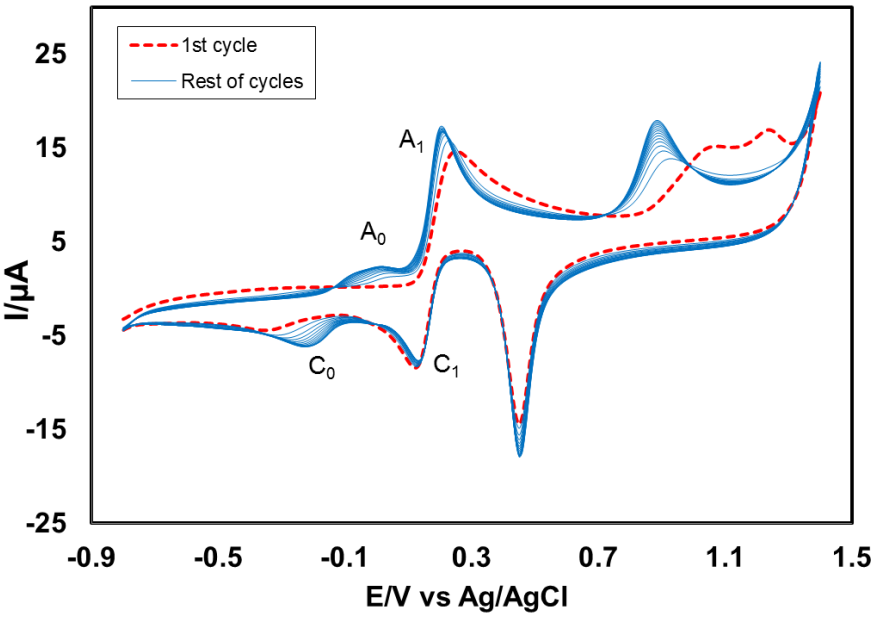

Fig. 4.80: Cyclic voltammogram of 2 mM Catechol with 70 mM L-Aspartic acid of Au electrode in the buffer solution of pH 7 at scan rate 0.1 V/s (15 cycles). The appeared anodic peak current (A_0) and cathodic peak current (C_0) increased with the iteration scan from the first cycle.

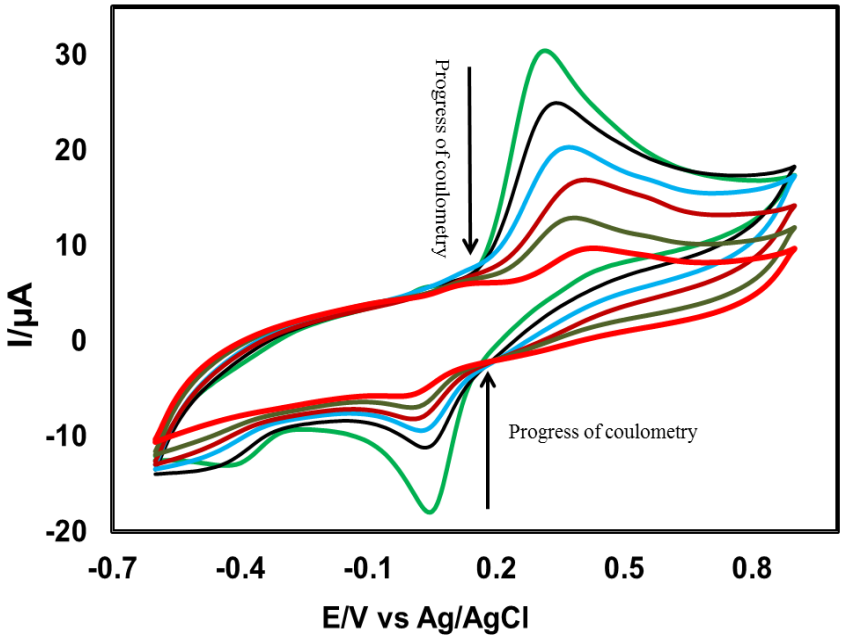

Fig. 4.81: Cyclic voltammogram and (CV) of 1 mM Catechol in presence of 50 mM L-Aspartic acid of GC electrode during controlled potential coulometry at 0.45 V in pH 7 at scan rate 0.1 V/s.

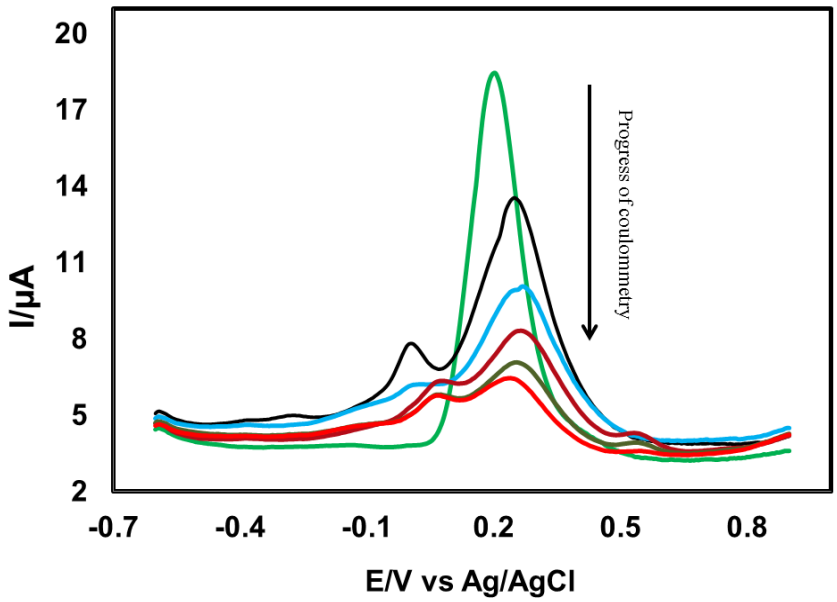

Fig. 4.82: Differential pulse voltammogram (DPV) of 1 mM Catechol in presence of 50 mM L-Aspartic acid of GC electrode during controlled potential coulometry at 0.45 V in pH 7 at scan rate 0.1 V/s.

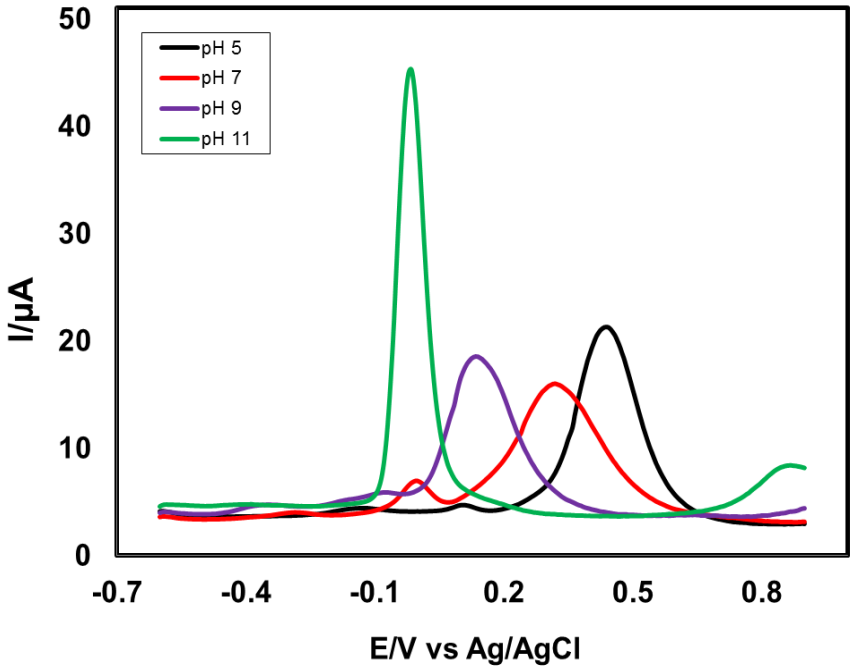

Fig. 4.83: Differential pulse voltammogram (DPV) of 2 mM Catechol with70 mM L-Aspartic acid of GC electrode in second scan of different pH (5, 7, 9 and 11) and scan rate 0.1 V/s.

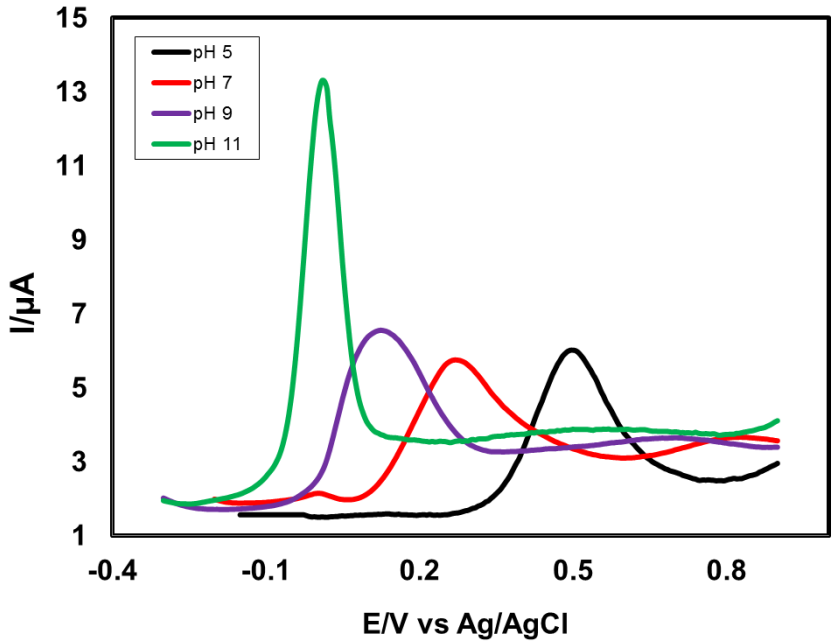

Fig. 4.84: Differential pulse voltammogram (DPV) of 2 mM Catechol with 70 mM L-Aspartic acid of Pt electrode in second scans of different pH (5, 7, 9 and 11) and scan rate 0.1 V/s.

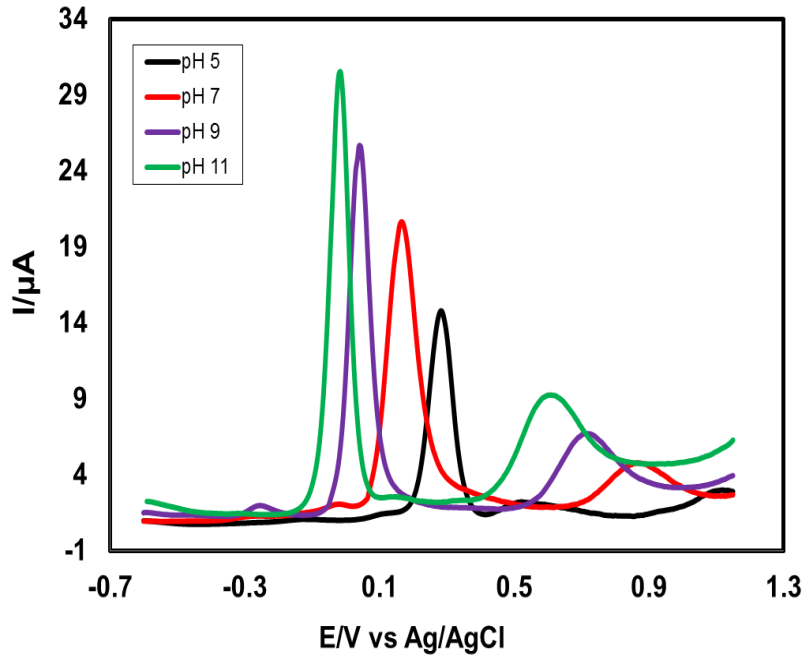

Fig. 4.85: Differential pulse voltammogram (DPV) of 2 mM Catechol with70 mM L-Aspartic acid of Au electrode in second scans of different pH (5, 7, 9 and 11) and scan rate 0.1 V/s.

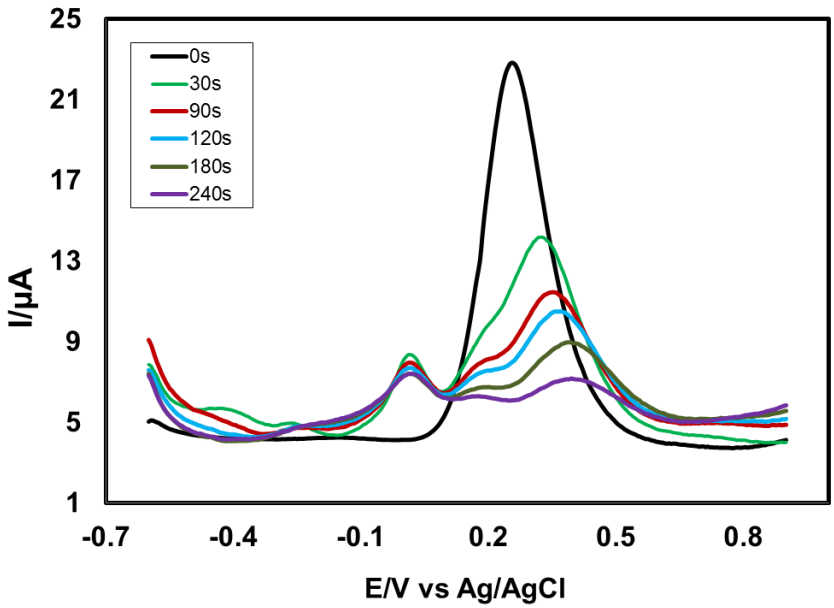

Fig. 4.86: Differential pulse voltammogram (DPV) of deposition time change (0, 30, 90, 120,180 and 240 s) of 2 mM catechol with 70 mM L-Aspartic acid of pH 7 at *E*puls 0.02 V, tpuls 20ms and scan rate 0.1 V/s.

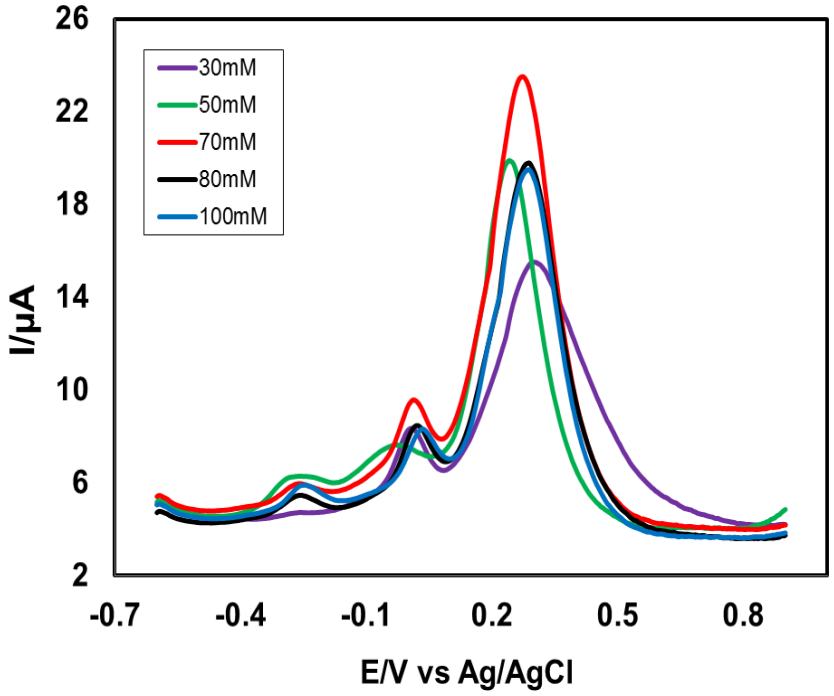

Fig. 4.87: Differential pulse voltammogram (DPV) of composition change of L-Aspartic acid (30, 50, 70, 80 and 100 mM) with the fixed composition of 2 mM Catechol in second scan of pH7 at E_{pulse} 0.02 V, t_{pulse} 20ms of GC electrode and scan rate 0.1 V/s.

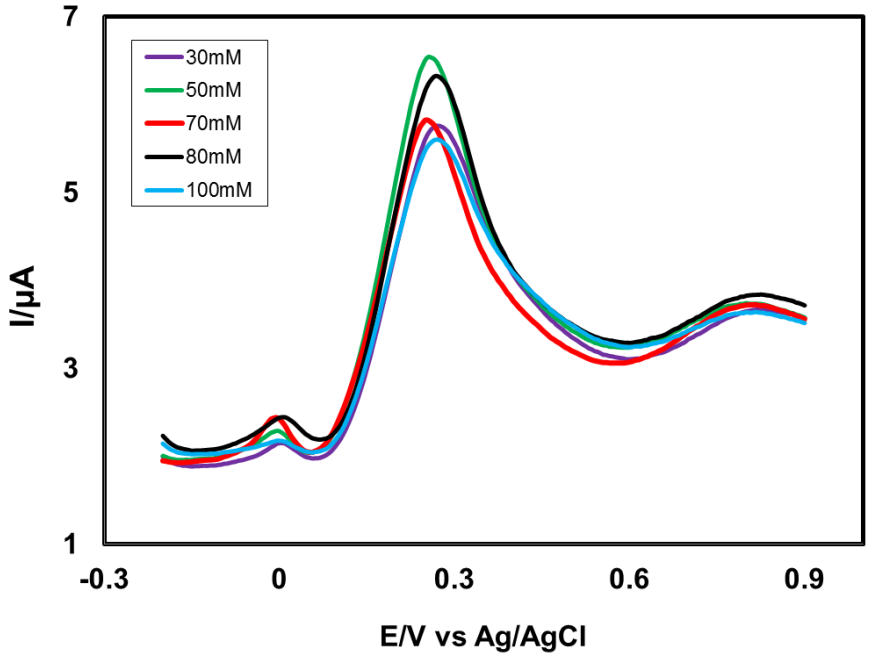

Fig. 4.88: Differential pulse voltammogram (DPV) of composition change of L-Aspartic acid (30, 50, 70, 80 and 100 mM) with the fixed composition of 2 mM Catechol in second scan of pH 7 at E_{pulse} 0.02 V, t_{pulse} 20ms of Pt electrode and scan rate 0.1 V/s.

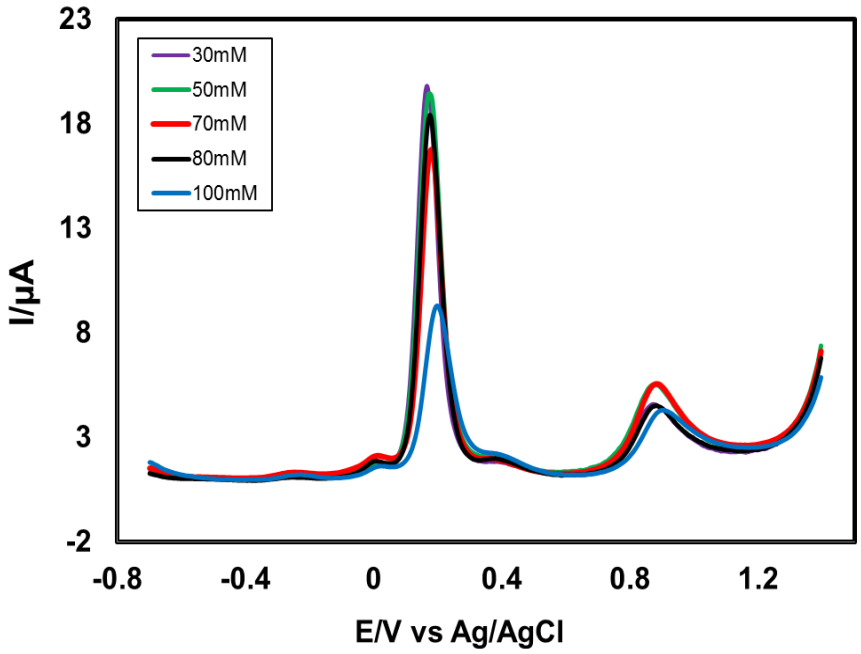

Fig. 4.89: Differential pulse voltammogram (DPV) of composition change of L-Aspartic acid (30, 50, 70, 80 and 100 mM) with the fixed composition of 2 mM Catechol in second scan of pH7 at E_{pulse} 0.02 V, t_{pulse} 20ms of Au electrode and scan rate 0.1 V/s.

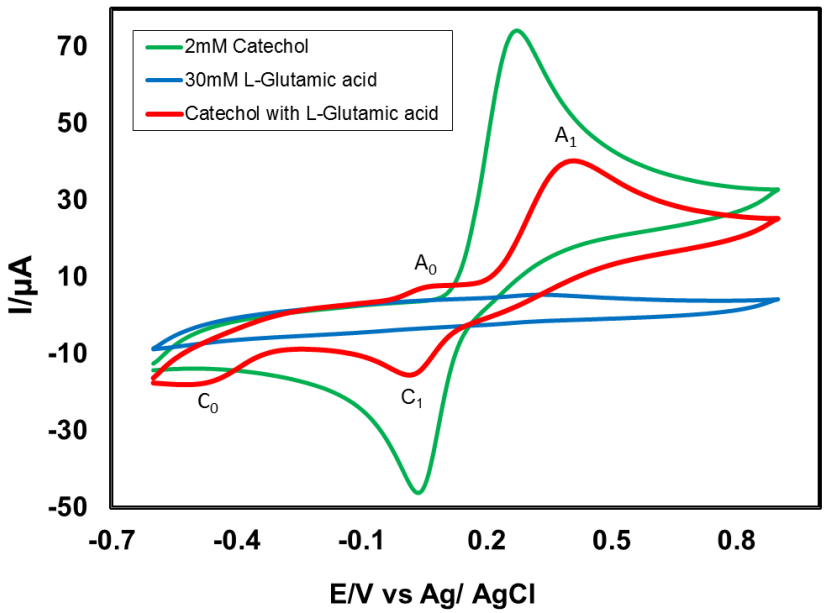

Fig. 4.90: Cyclic voltammogram of 2 mM Catechol (green line), 30 mM L-Glutamic acid (blue line) and 2 mM Catechol with 30 mM L-Glutamic acid (red line) of GC electrode in buffer solution (pH 7) at scan rate 0.1 V/s (2nd cycle). (A_0 = appeared anodic peak)

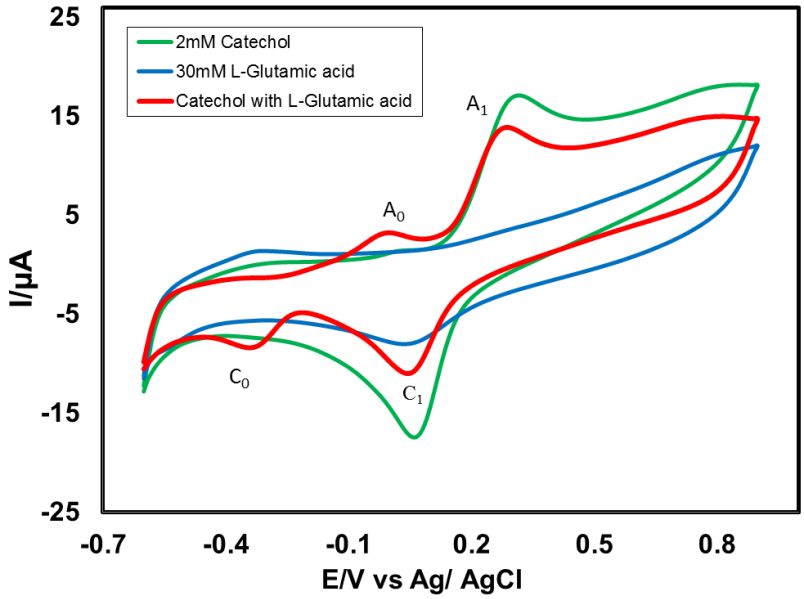

Fig. 4.91: Cyclic voltammogram of 2 mM Catechol (green line), 30 mM L-Glutamic acid (blue line) and 2 mM Catechol with 30 mM L-Glutamic acid (red line) of Pt electrode in buffer solution (pH 7) at scan rate 0.1 V/s (2nd cycle). (A_0 = appeared anodic peak)

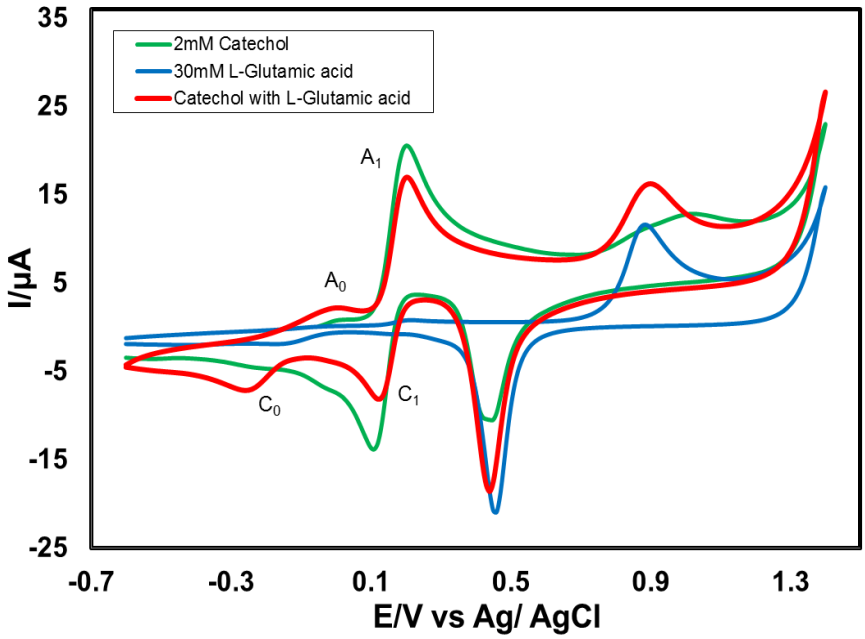

Fig. 4.92: Cyclic voltammogram of 2 mM Catechol (green line), 30 mM L-Glutamic acid (blue line) and 2 mM Catechol with 30 mM L-Glutamic acid (red line) of Au electrode in buffer solution (pH 7) at scan rate 0.1 V/s (2nd cycle). (A_0 = appeared anodic peak)

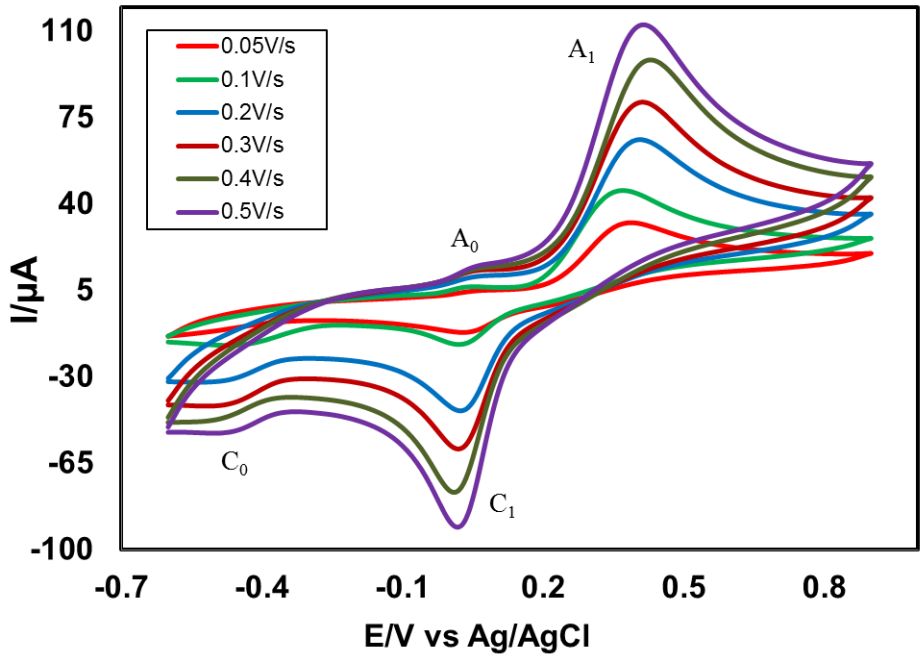

Fig. 4.93: Cyclic voltammogram of 2 mM Catechol with 30 mM L-Glutamic acid in the second scan of potential at GC electrode in buffer solution (pH 7) at scan rate 0.05 V/s to 0.5 V/s.

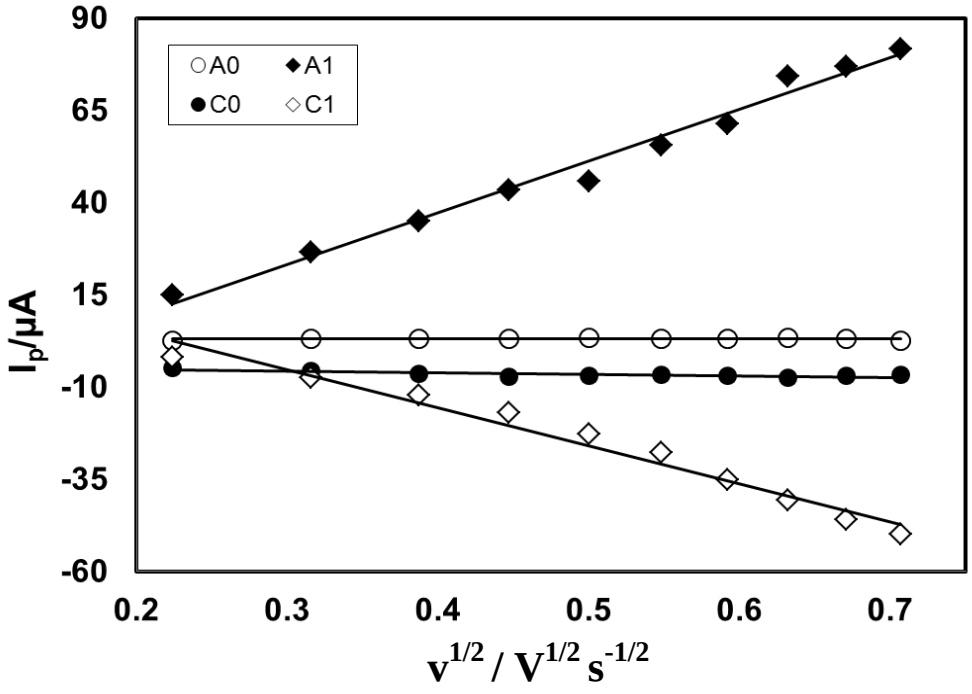

Fig. 4.94: Plots of peak current (I_p) versus square root of scan rate ($v^{1/2}$) of 2 mM Catechol with 30 mM L-Glutamic acid of GC electrode in buffer solution (pH 7) (2^{nd} cycle).

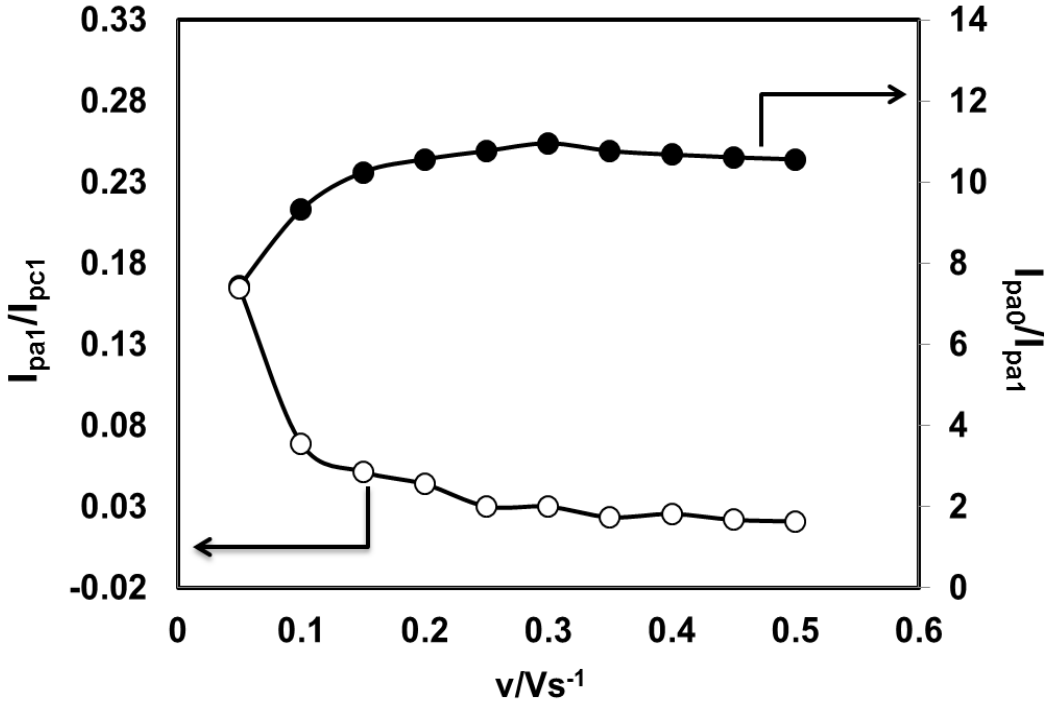

Fig. 4.95: Variation of peak current ratio of corresponding peak (I_{pa1}/I_{pc1}) and anodic peak (I_{pa0}/I_{pa1}) vs scan rate (v) of 2 mM Catechol with 30 mM L-Glutamic acid of GC electrode in buffer solution (pH 7) at scan rate 0.1 V/s in the second scan of potential.

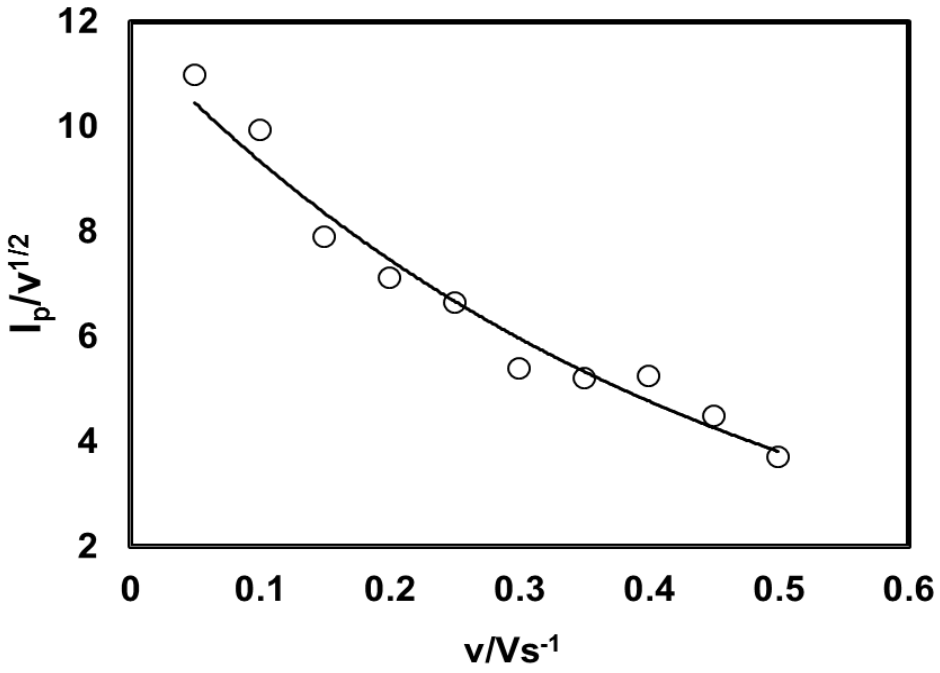

Fig. 4.96: Plot of current function ($I_p/v^{1/2}$) versus scan rate (v) of 2 mM Catechol with 30 mM L-Glutamic acid of GC electrode in buffer solution (pH 7) of the Appeared anodic peak (A_0).

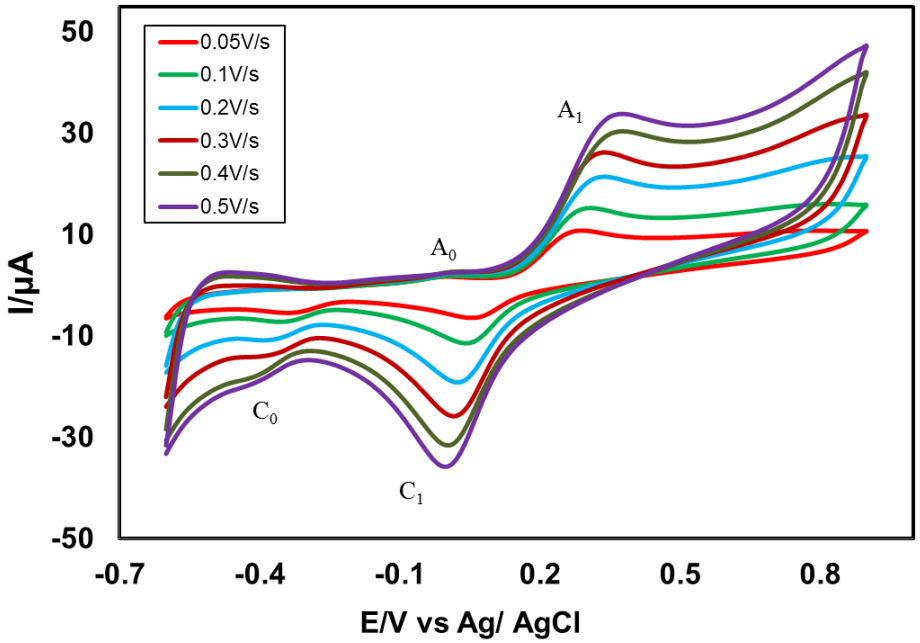

Fig. 4.97: Cyclic voltammogram of 2 mM Catechol with 30 mM L-Glutamic acid in the second scan of potential at Pt electrode in buffer solution (pH 7) at scan rate 0.05 V/s to 0.5 V/s.

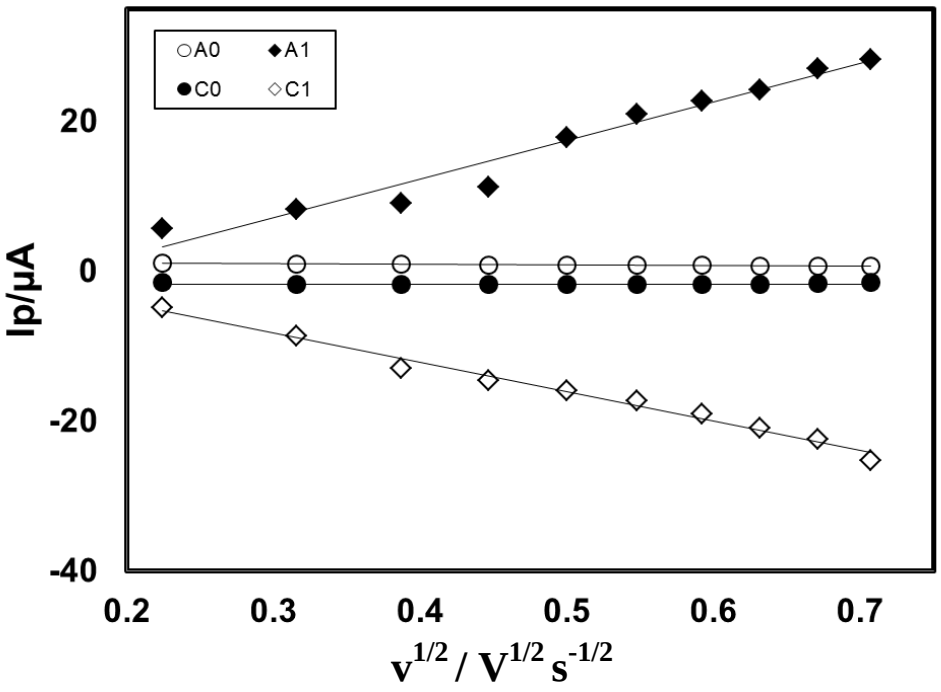

Fig. 4.98: Plots of peak current (I_p) versus square root of scan rate ($v^{1/2}$) of 2 mM Catechol with 30 mM L-Glutamic acid of Pt electrode in buffer solution (pH 7) (2^{nd} cycle).

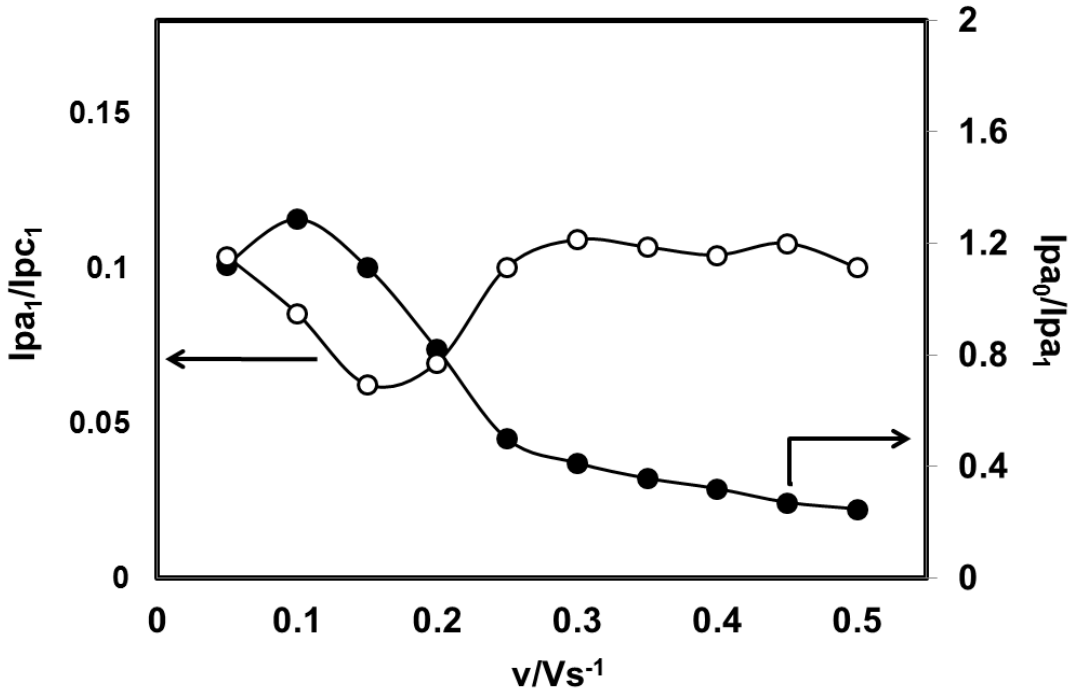

Fig. 4.99: Variation of peak current ratio of corresponding peak (I_{pa1}/I_{pc1}) and anodic peak (I_{pa0}/I_{pa1}) vs scan rate (v) of 2 mM Catechol with 30 mM L-Glutamic acid of Pt electrode in buffer solution (pH 7) at scan rate 0.1 V/s in the second scan of potential.

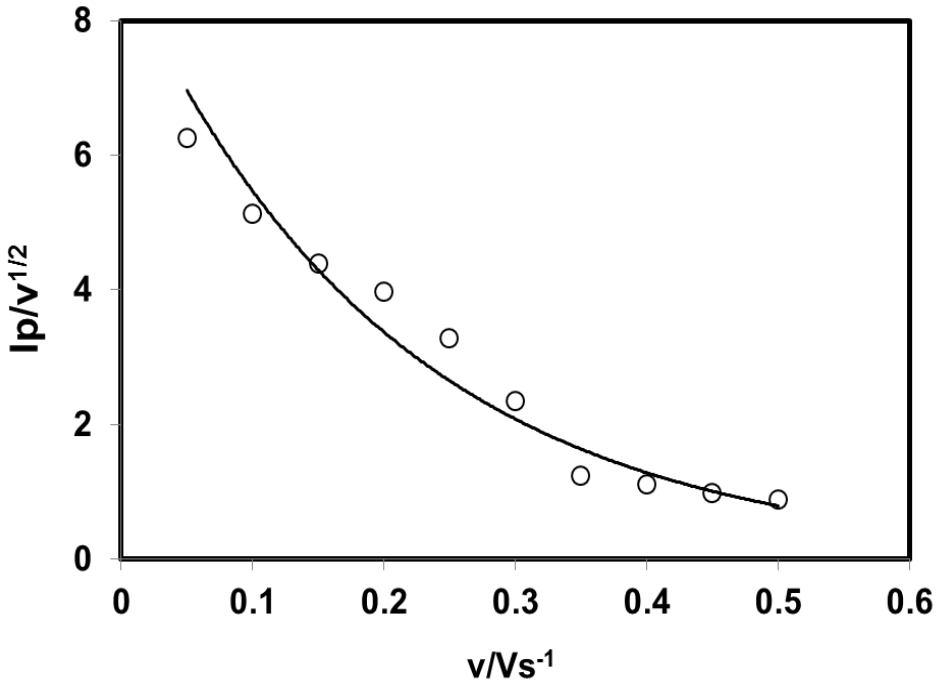

Fig. 4.100: Plots of current function ($I_p/v^{1/2}$) versus scan rate (v) of 2 mM Catechol with 30 mM L-Glutamic acid of Pt electrode in buffer solution (pH 7) of the Appeared anodic peak (A_0).

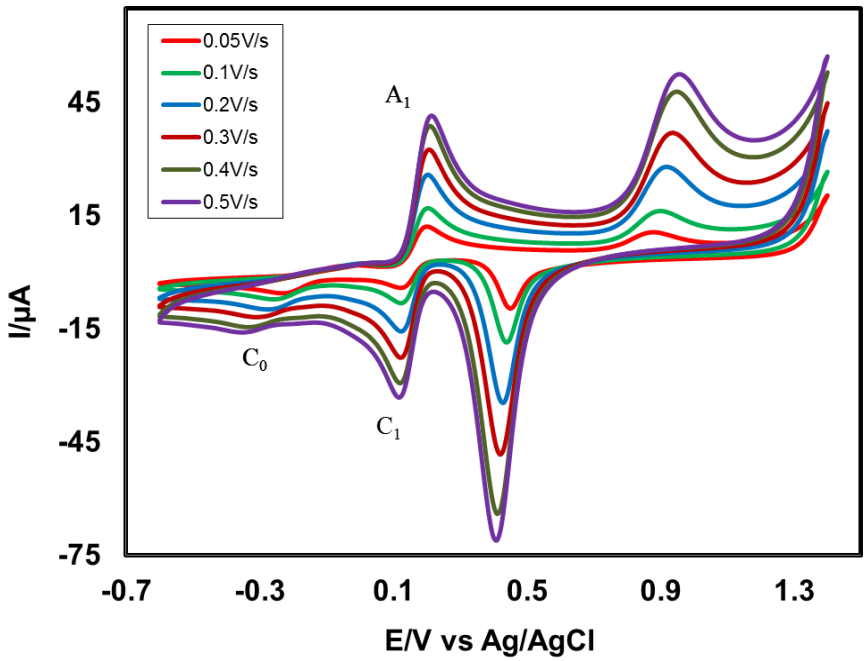

Fig. 4.101: Cyclic voltammogram of 2 mM Catechol with 30 mM L-Glutamic acid in the second scan of potential at Au electrode in buffer solution (pH 7) at scan rate 0.05 V/s to 0.5 V/s.

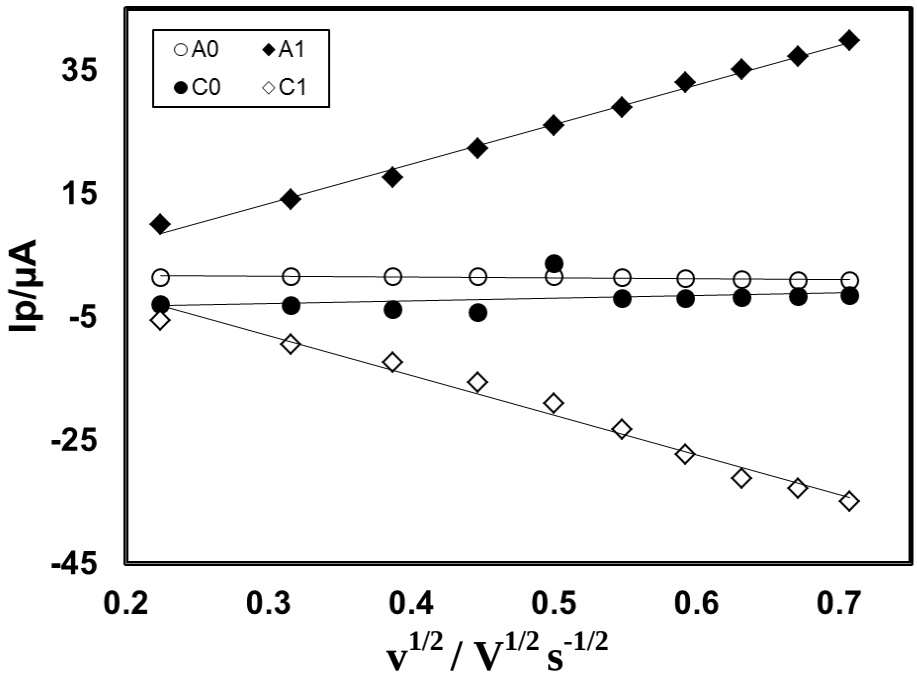

Fig. 4.102: Plots of peak current (I_p) versus square root of scan rate ($v^{1/2}$) of 2 mM Catechol with 30 mM L-Glutamic acid of Au electrode in buffer solution at pH 7 (2^{nd} cycle).

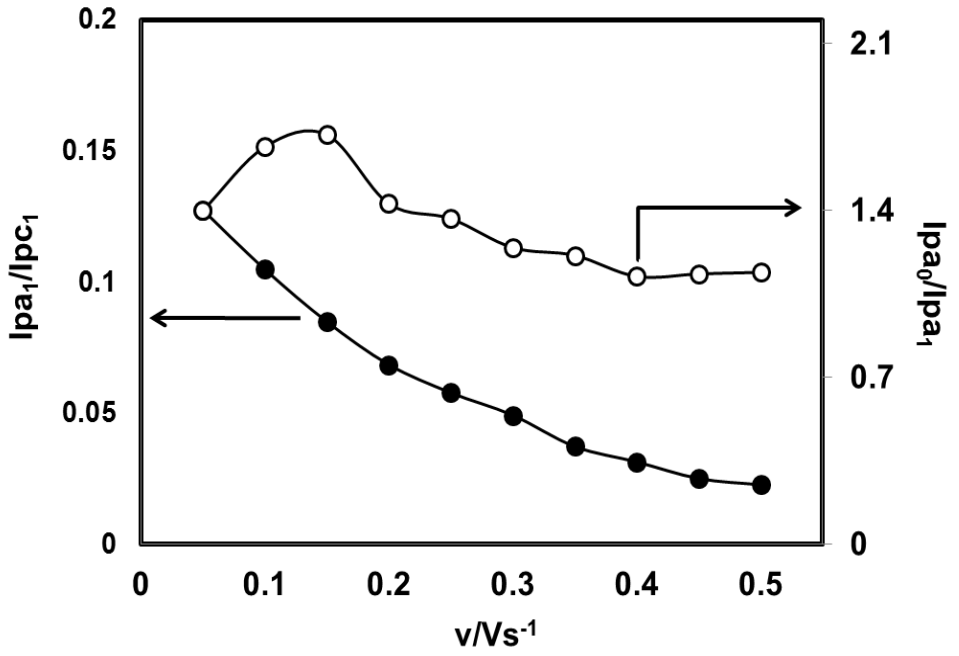

Fig. 4.103: Variation of peak current ratio of corresponding peak (I_{pa1}/I_{pc1}) and anodic peak (I_{pa0}/I_{pa1}) vs scan rate (v) of 2 mM Catechol with 30 mM L-Glutamic acid of Au electrode in buffer solution (pH 7) at scan rate 0.1 V/s in the second scan of potential.

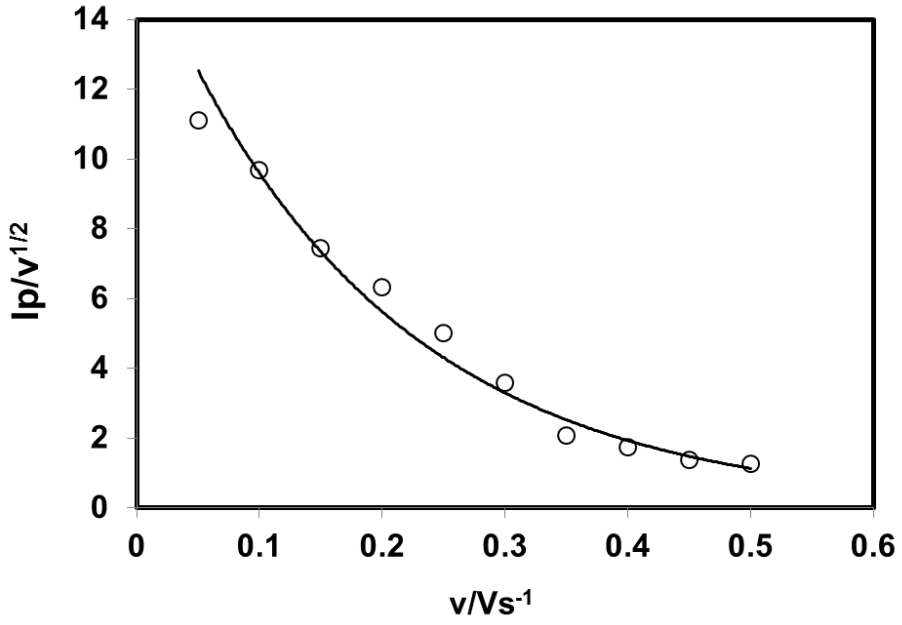

Fig. 4.104: Plots of current function ($I_p/v^{1/2}$) versus scan rate (v) of 2 mM Catechol with 30 mM L-Glutamic acid of Au electrode in buffer solution (pH 7) of the Appeared anodic peak (A_0).

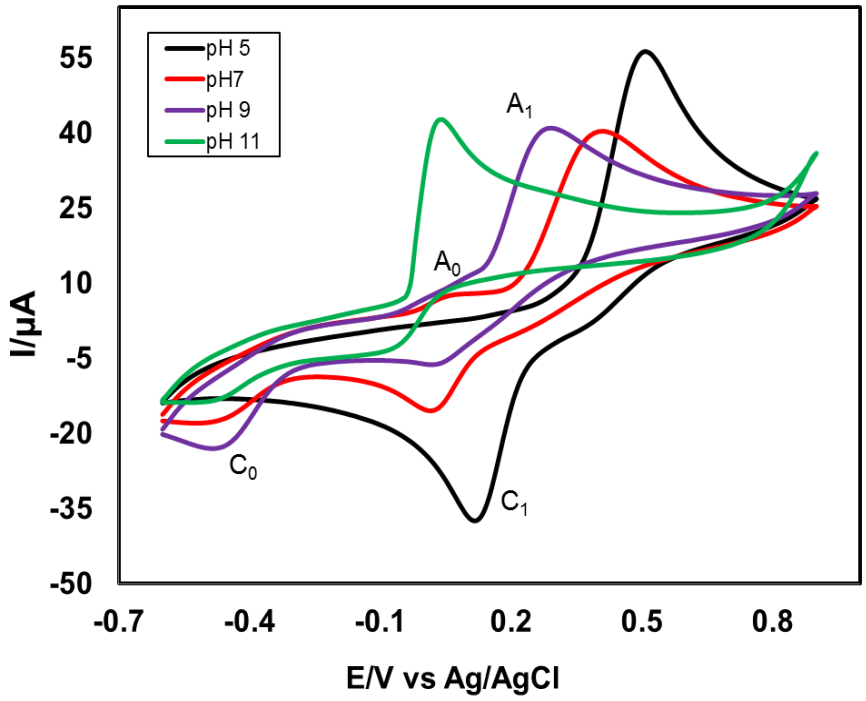

Fig. 4.105: Cyclic voltammogram of 2 mM Catechol with 30 mM L-Glutamic acid of GC (3 mm) electrode in different pH (5, 7, 9 and 11) at scan rate 0.1 V/s.

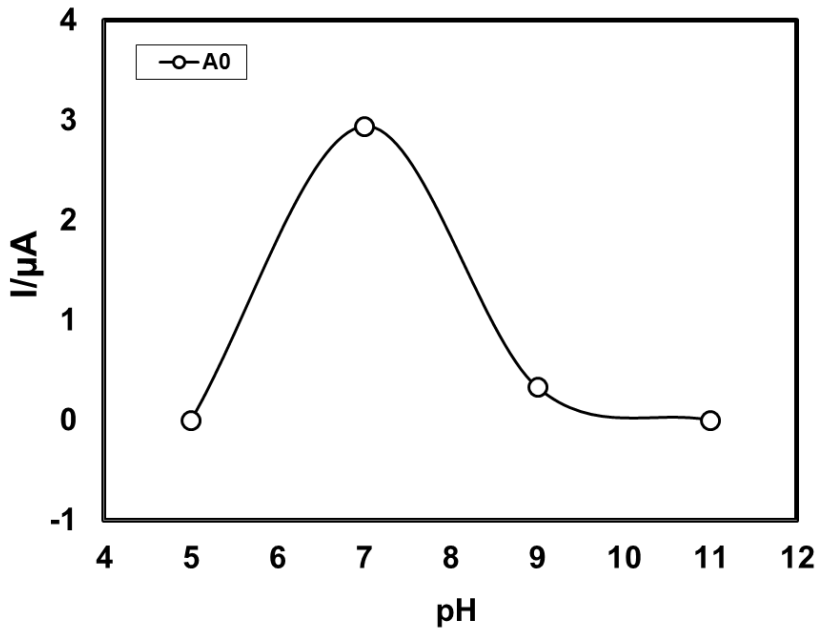

Fig. 4.106: Plot of peak current (I_p) versus pH (5, 7, 9 and 11) of 2 mM Catechol with 30 mM L-Glutamic acid of GC electrode at scan rate 0.1 V/s (2^{nd} cycle).

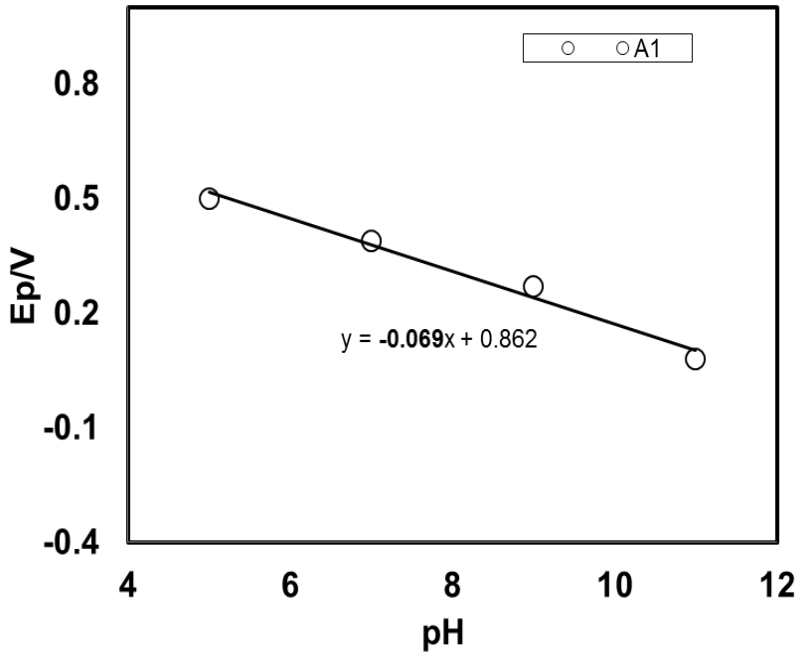

Fig. 4.107: Plots of peak potential (E_p) versus pH (5, 7, 9 and 11) of 2 mM Catechol with 30 mM L-Glutamic acid of GC electrode at scan rate 0.1 V/s (2nd cycle).

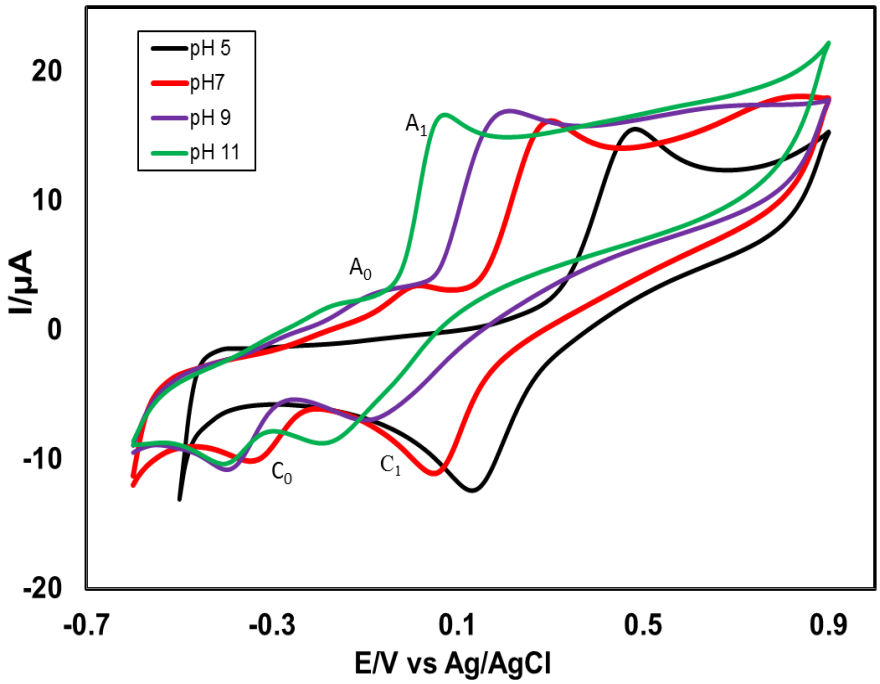

Fig. 4.108: Cyclic voltammogram of 2 mM Catechol with 30 mM L-Glutamic acid of Pt electrode in different pH (5, 7, 9 and 11) at scan rate 0.1 V/s.

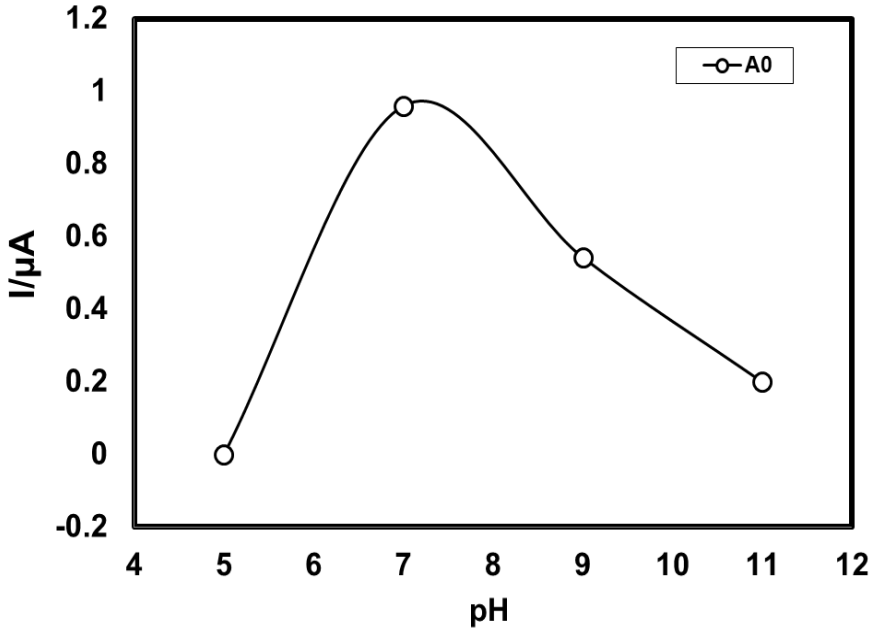

Fig. 4.109: Plots of peak current (I_p) versus pH (5, 7, 9 and 11) of 2 mM Catechol with 30 mM L-Glutamic acid of Pt electrode at scan rate 0.1 V/s (2nd cycle).

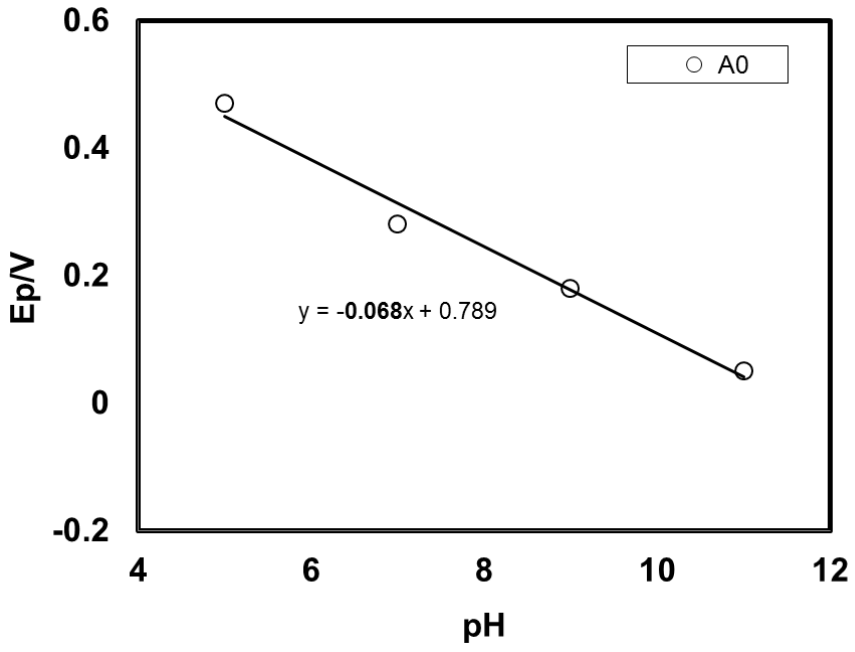

Fig. 4.110: Plot of peak potential (E_p) versus pH (5, 7, 9 and 11) of 2 mM Catechol with 30 mM L-Glutamic acid of Pt electrode at scan rate 0.1 V/s (2nd cycle).

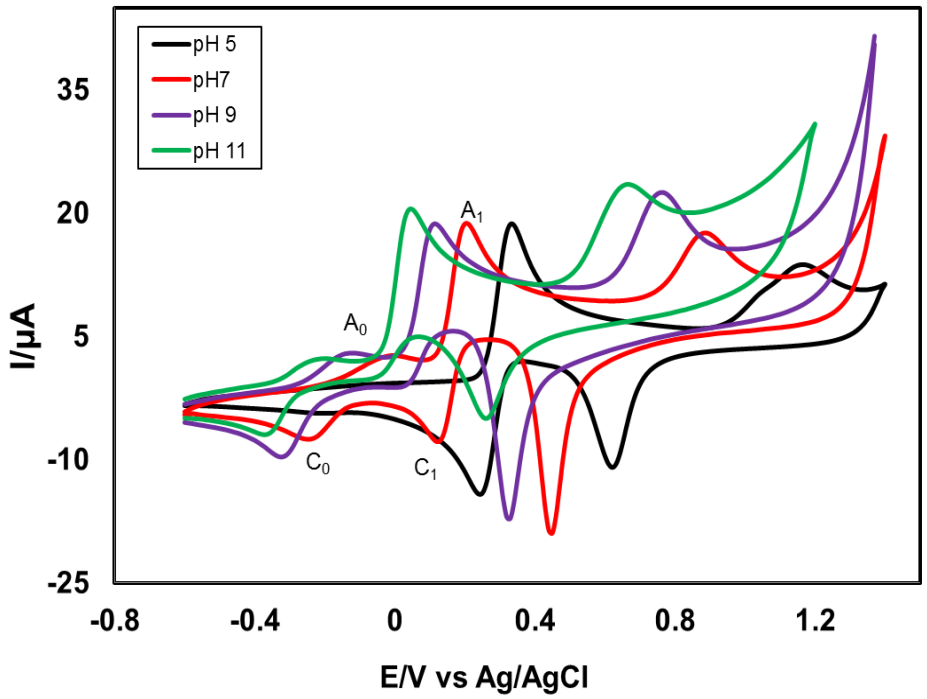

Fig. 4.111: Cyclic voltammogram of 2 mM Catechol with 30 mM L-Glutamic acid of Au electrode in different pH (5, 7, 9 and 11) at scan rate 0.1 V/s.

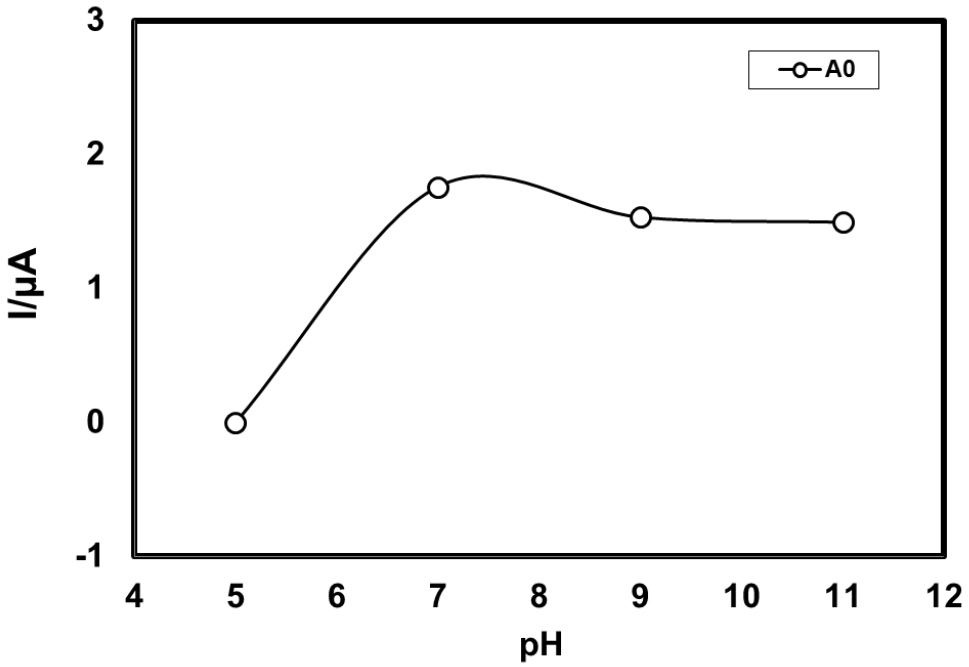

Fig. 4.112: Plots of peak current (I_p) versus pH (5, 7, 9 and 11) of 2 mM Catechol with 30 mM L-Glutamic acid of Au electrode at scan rate 0.1 V/s (2nd cycle).

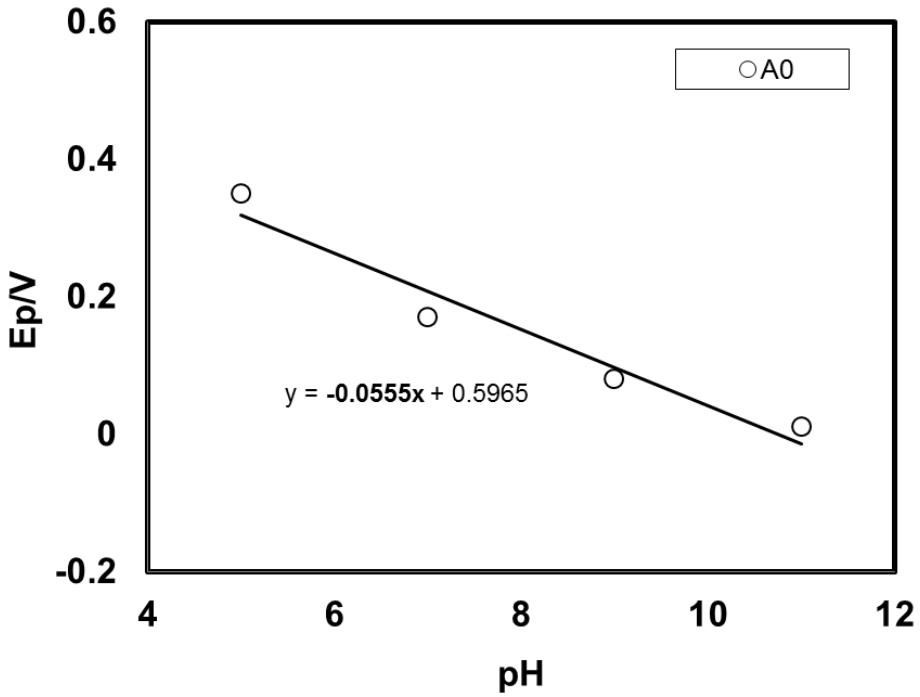

Fig. 4.113: Plot of peak potential (E_p) versus pH (5, 7, 9 and 11) of 2 mM Catechol with 30 mM L-Glutamic acid of Au electrode at scan rate 0.1 V/s (2nd cycle).

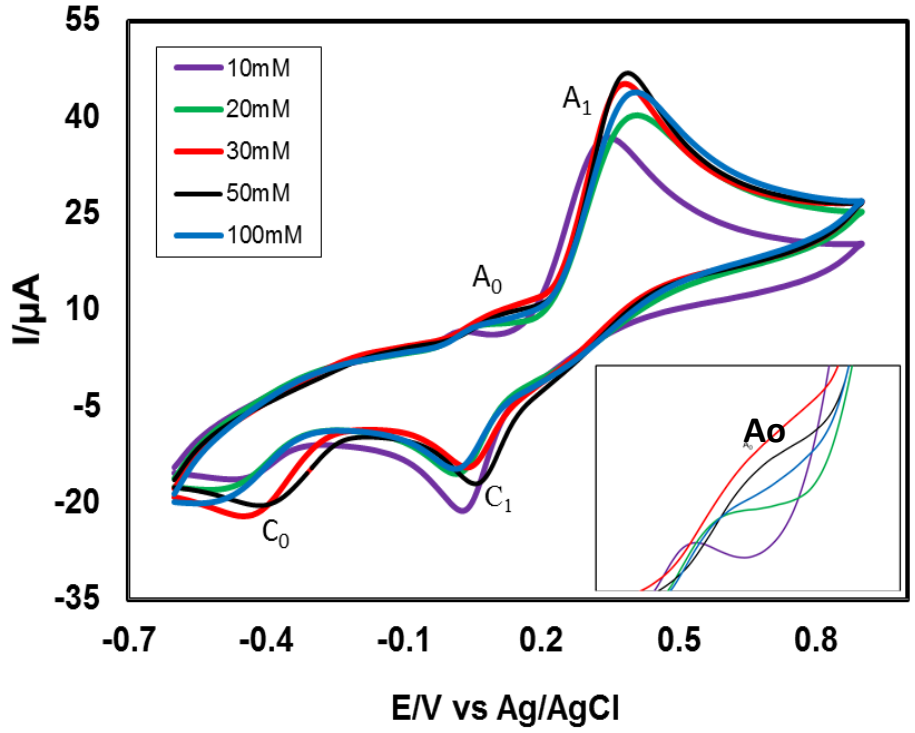

Fig. 4.114: CV of composition changes of L-Glutamic acid (10, 20, 30, 50 and 100 mM) with fixed 2 mM Catechol of GC electrode at pH 7 and scan rate 0.1 V/s. Insert: appeared anodic peak (A_0)

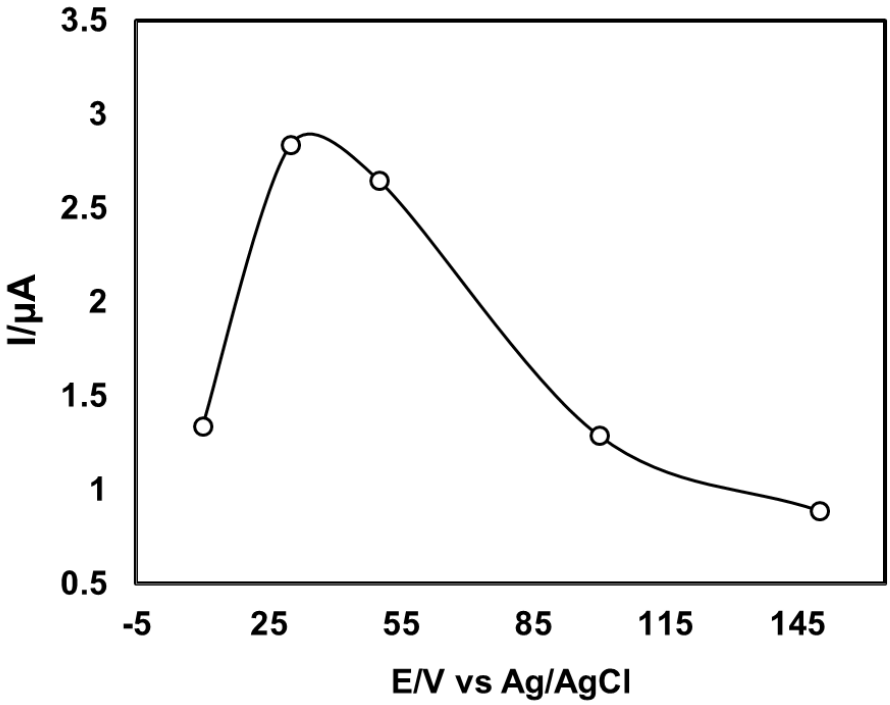

Fig. 4.115: Comparison of cyclic voltammogram of different concentration (10, 30, 50, 100 and 150 mM) of 2 mM Catechol with 30 mM L-Glutamic acid of GC electrode in buffer solution (pH 7) at scan rate 0.1 V/s (2nd cycle).

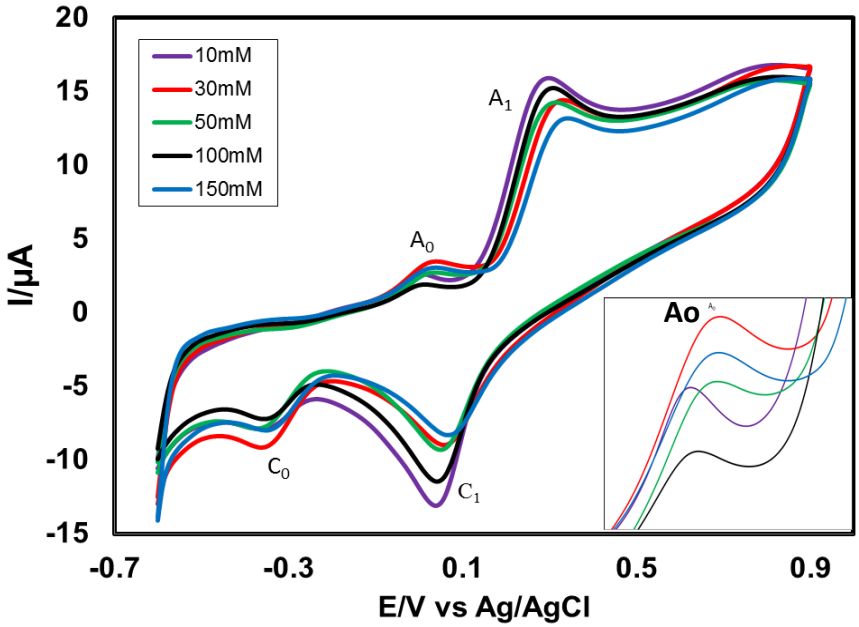

Fig. 4.116: CV of composition changes of L-Glutamic acid (10, 30, 50, 100 and 150 mM) with fixed 2 mM Catechol of Pt electrode at pH 7 and scan rate 0.1 V/s. Insert: appeared anodic peak (A_0)

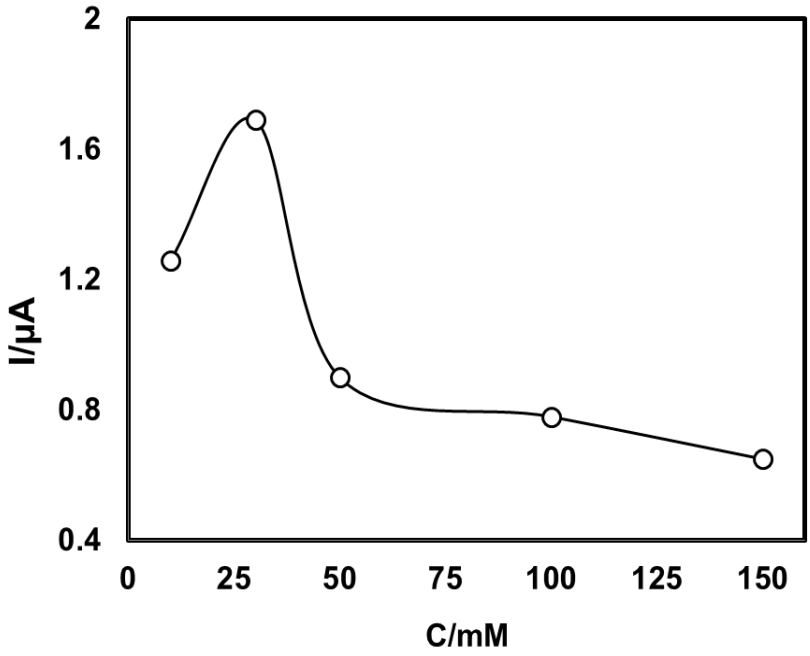

Fig. 4.117: Plots of peak current (I_p) versus concentration (C) of L-Glutamic acid (10, 30, 50, 100 and 150 mM) with fixed 2 mM Catechol of Pt electrode in buffer solution (pH) at 7 scan rate 0.1 V/s (2nd cycle).

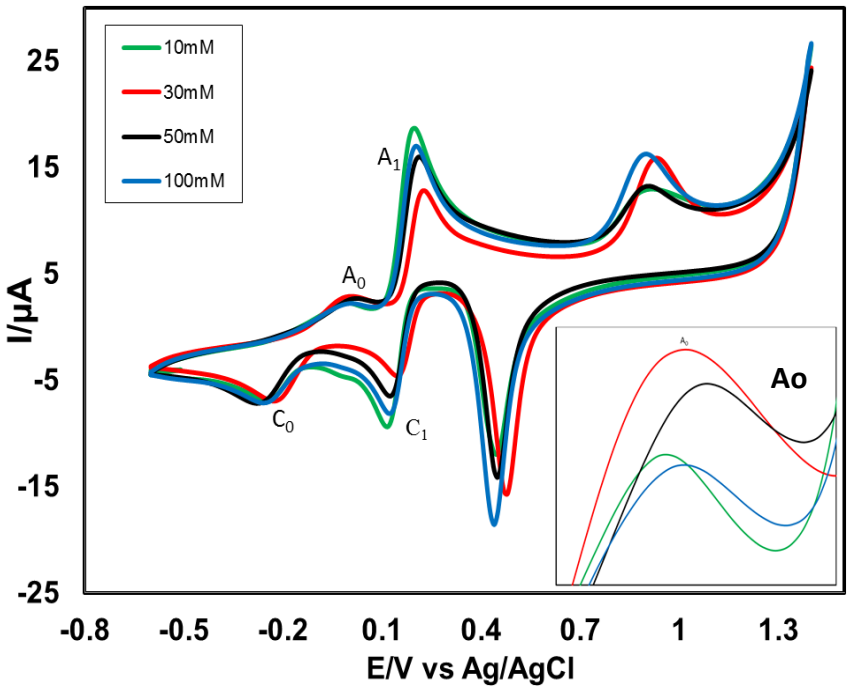

Fig. 4.118: CV of composition changes of L-Glutamic acid (10, 30, 50 and 100 mM) with fixed 2 mM Catechol of Au electrode at pH 7 and scan rate 0.1 V/s. Insert: appeared anodic peak (A_0)

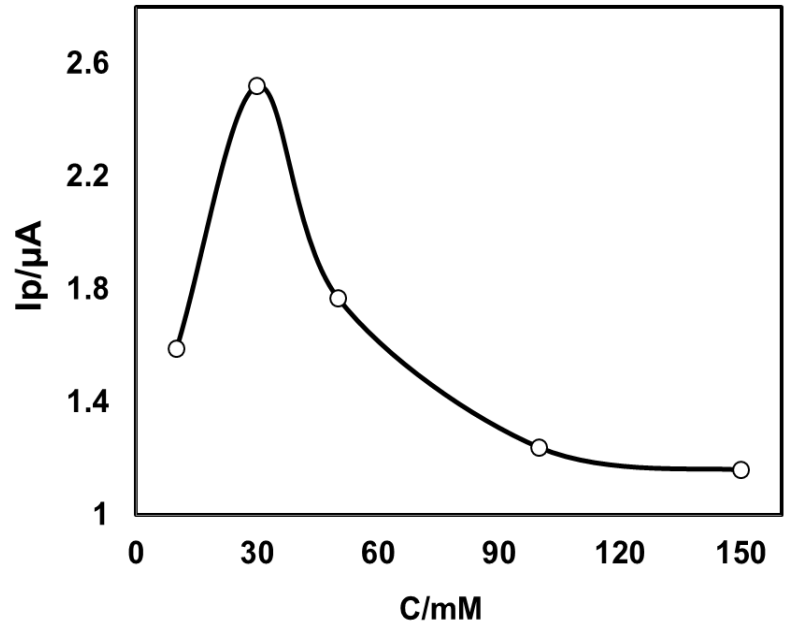

Fig. 4.119: Plots of peak current (I_p) versus concentration (C) of L-Glutamic acid (10, 30, 50, 100 and 150 mM) with fixed 2 mM Catechol of Au electrode in buffer solution (pH 7) at scan rate 0.1 V/s (2nd cycle).

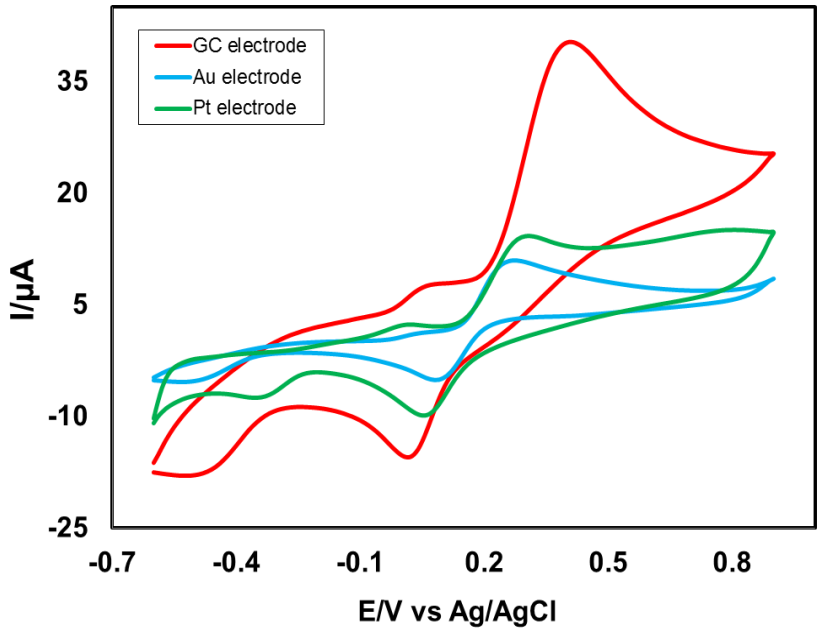

Fig. 4.120: Cyclic voltammogram (CV) of 2 mM catechol with 30 mM L-Glutamic acid in GC electrode (3.0 mm), Gold electrode (1.6 mm) and Platinum electrode (1.6 mm) at pH 7 and scan rate 0.1 V/s.

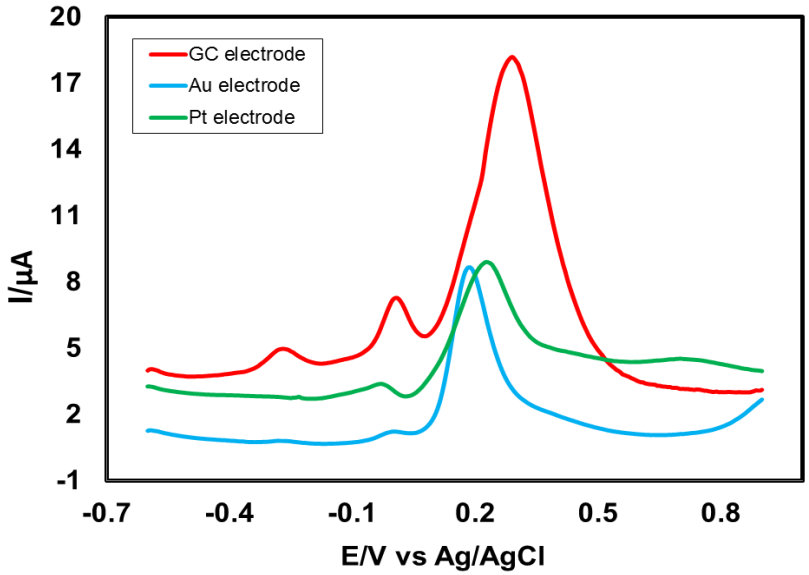

Fig. 4.121: Differential pulse voltammogram (DPV) of 2 mM catechol with 30 mM L-Glutamic acid in GC electrode (3.0 mm), Gold electrode (1.6 mm) and Platinum electrode (1.6 mm) at pH 7 and scan rate 0.1 V/s.

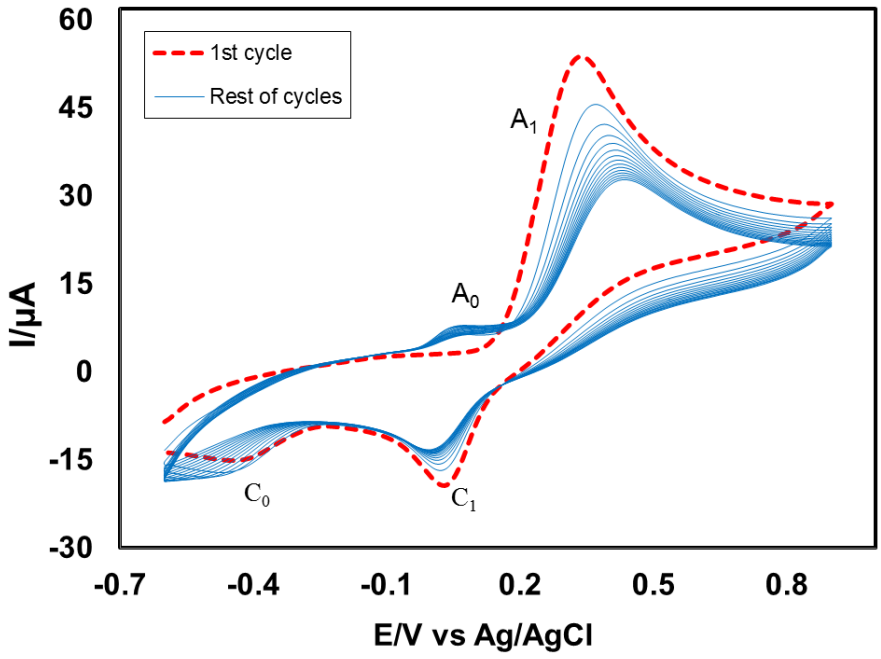

Fig. 4.122: Cyclic voltammogram of 2 mM Catechol with 30 mM L-Glutamic acid of GC (3 mm) electrode in the buffer solution of pH 7 at scan rate 0.1 V/s (15 cycles). The appeared anodic peak current (A_0) and cathodic peak current (C_0) increased with the iteration scan from the first cycle.

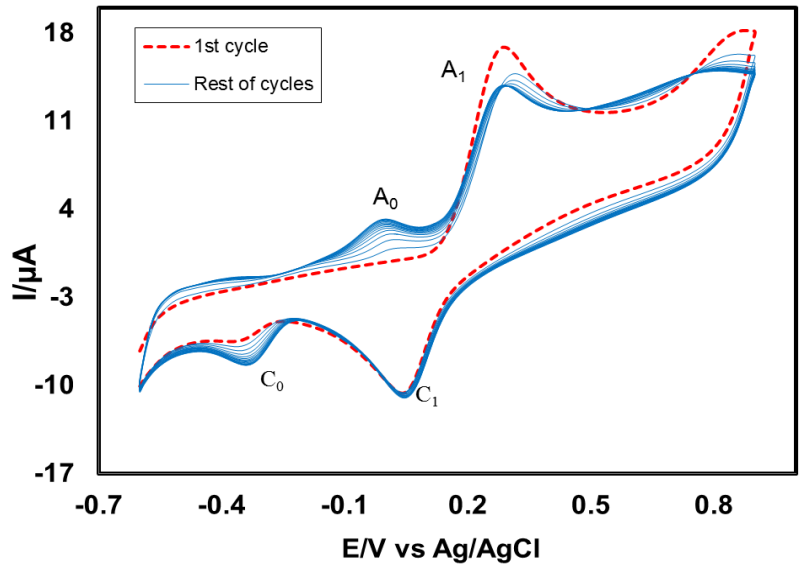

Fig. 4.123: Cyclic voltammogram of 2 mM Catechol with 30 mM L-Glutamic acid of Pt electrode in the buffer solution of pH 7 at scan rate 0.1 V/s (15 cycles). The appeared anodic peak current (A_0) and cathodic peak current (C_0) increased with the iteration scan from the first cycle.

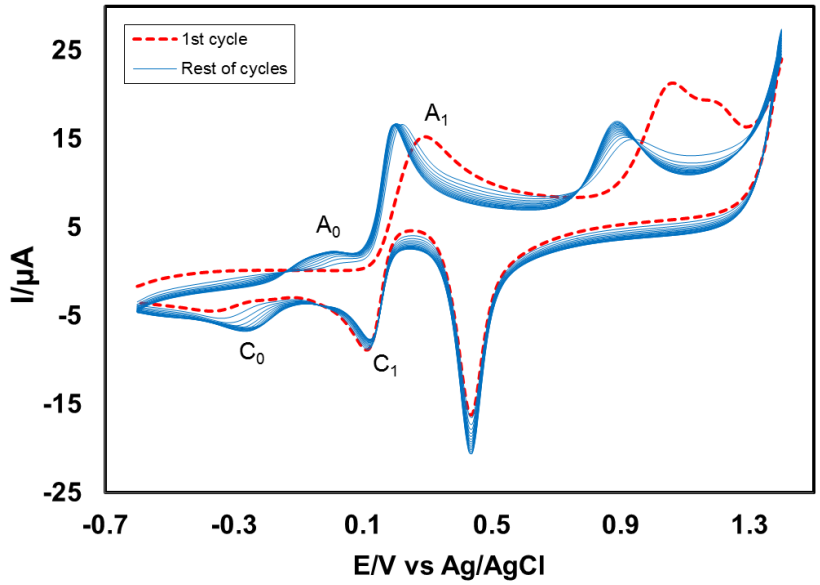

Fig. 4.124: Cyclic voltammogram of 2 mM Catechol with 30 mM L-Glutamic acid of Au electrode in the buffer solution of pH 7 at scan rate 0.1 V/s (15 cycles). The appeared anodic peak current (A_0) and cathodic peak current (C_0) increased with the iteration scan from the first cycle.

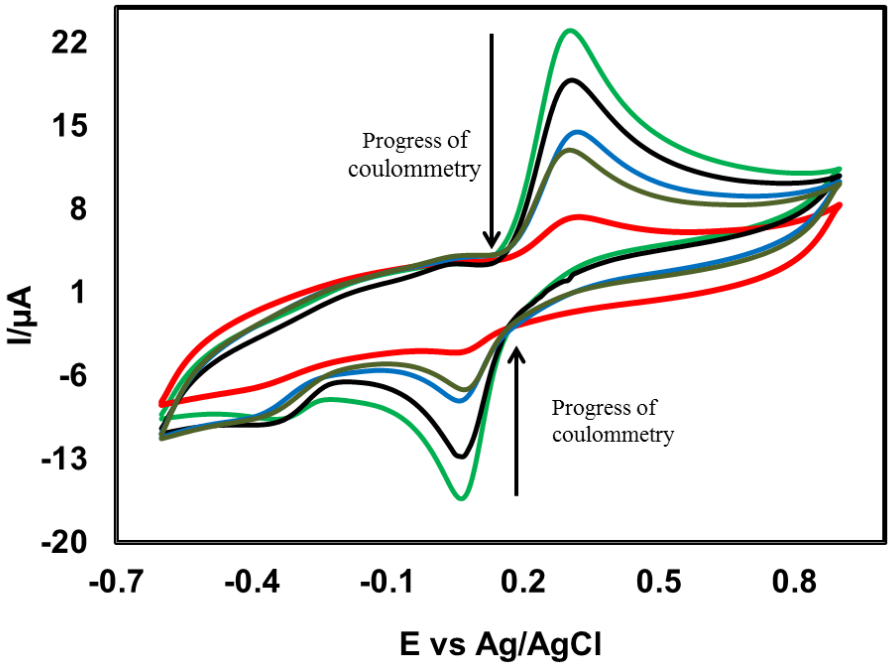

Fig. 4.125: Cyclic voltammogram and (CV) of 1 mM Catechol in presence of 50 mM L-Glutamic acid of GC electrode during controlled potential coulometry at 0.45 V in pH 7 at scan rate 0.1 V/s.

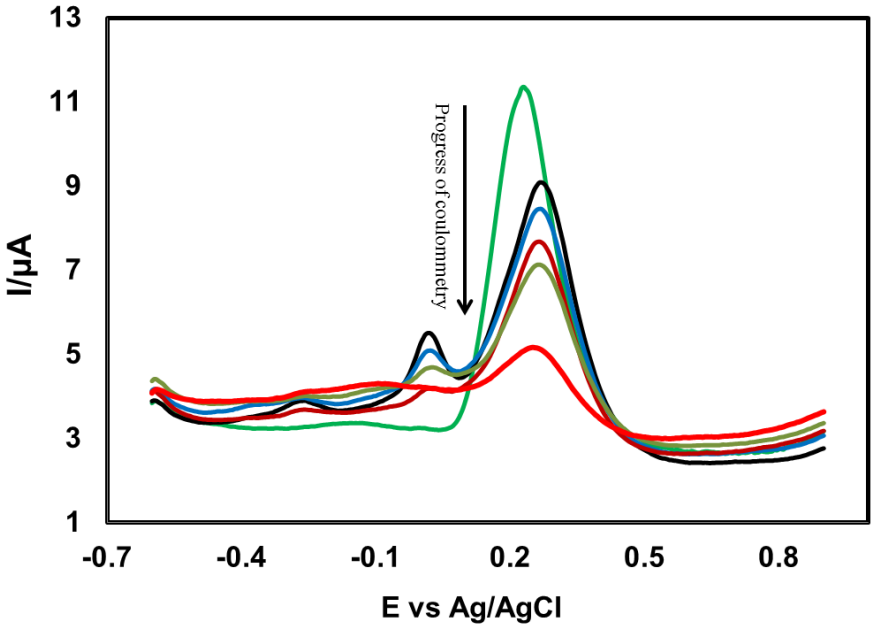

Fig. 4.126: Differential pulse voltammogram (DPV) of 1 mM Catechol in presence of 50 mM L-Glutamic acid of GC electrode during controlled potential coulometry at 0.45 V in pH 7 at scan rate 0.1 V/s.

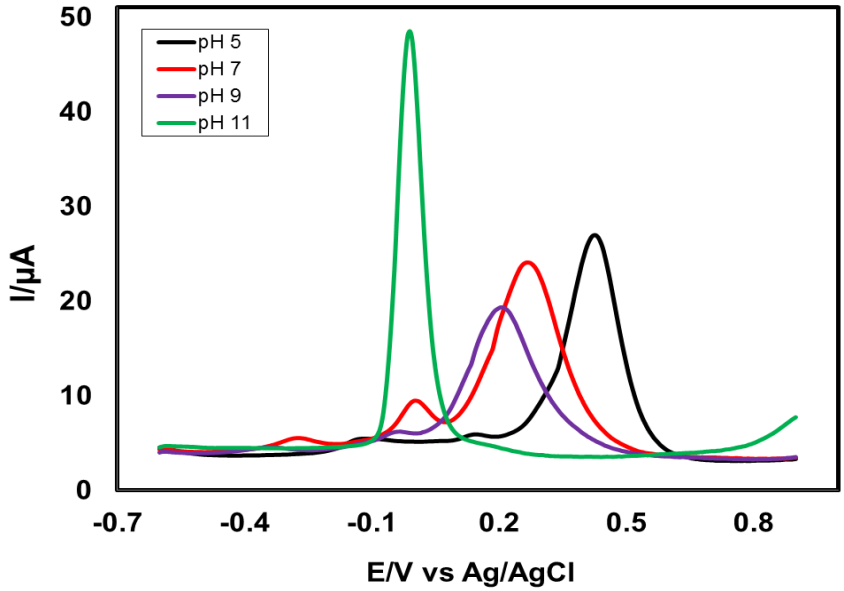

Fig. 4.127: Differential pulse voltammogram (DPV) of 2 mM Catechol with 30 mM L-Glutamic acid of GC electrode in second scan of different pH (5, 7, 9 and 11) and scan rate 0.1 V/s.

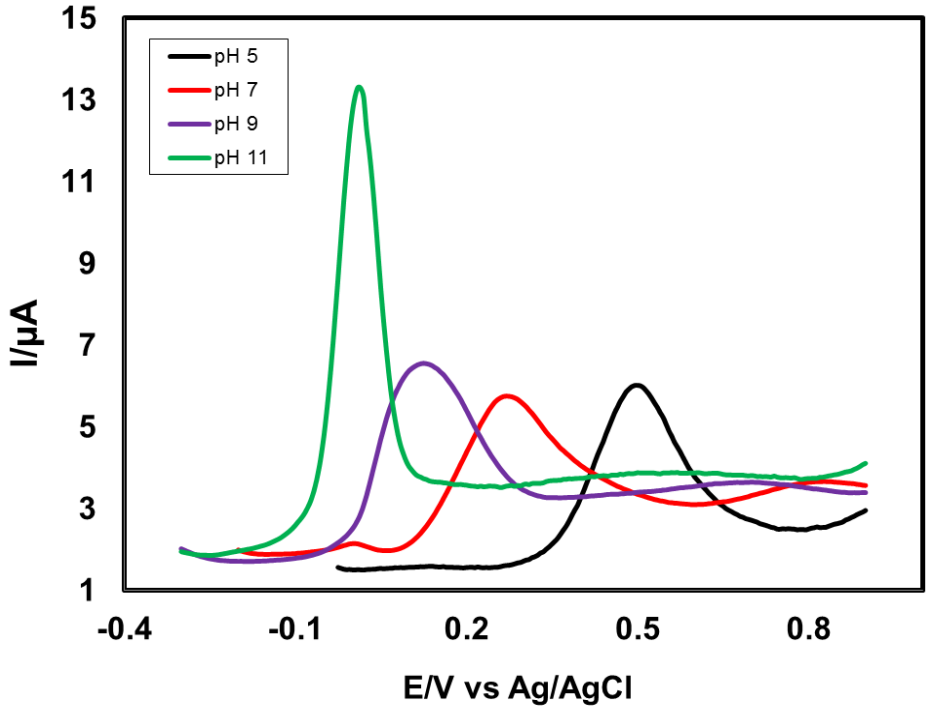

Fig. 4.128: Differential pulse voltammogram (DPV) of 2 mM Catechol with 30 mM L-Glutamic acid of Pt electrode in second scans of different pH (5, 7, 9 and 11) and scan rate 0.1 V/s.

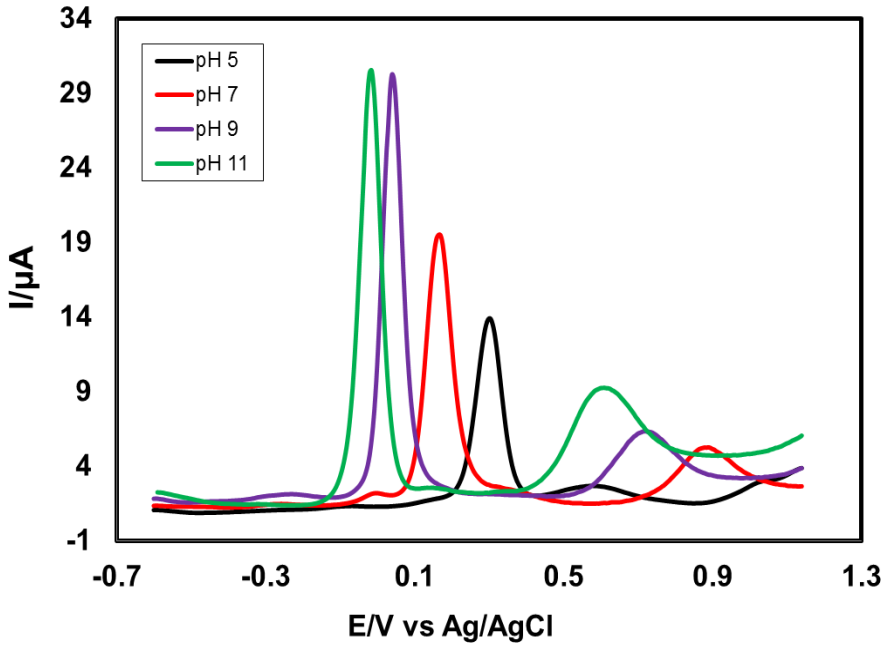

Fig. 4.129: Differential pulse voltammogram (DPV) of 2 mM Catechol with 30 mM L-Glutamic acid of Au electrode in second scans of different pH (5, 7, 9 and 11) and scan rate 0.1 V/s.

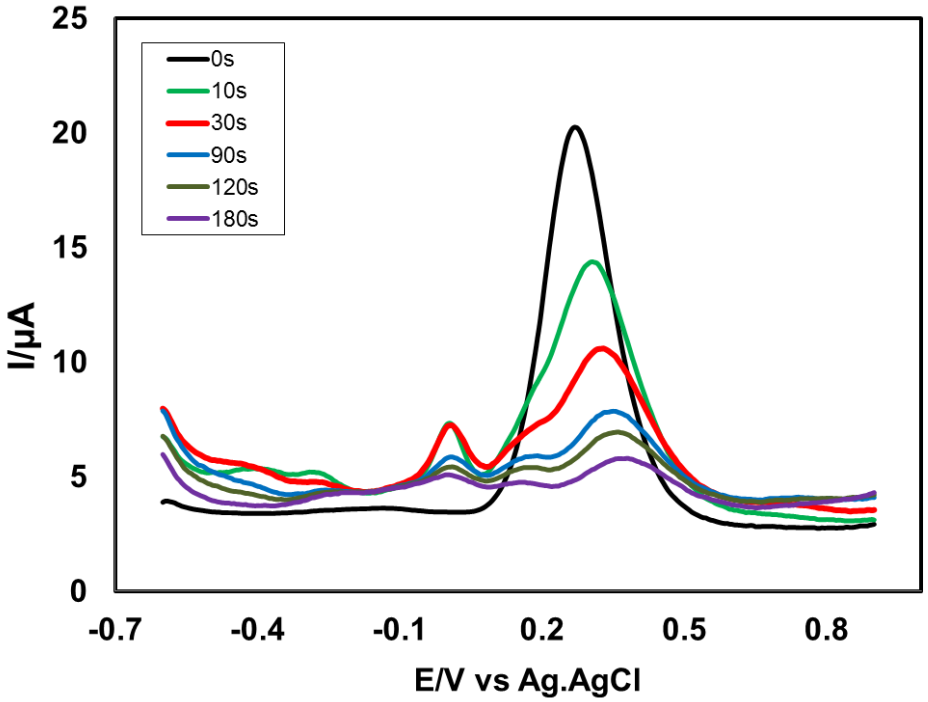

Fig. 4.130: Differential pulse voltammogram (DPV) of deposition time change (0, 10, 30, 90,120 and 180 s) of 2 mM catechol with 30 mM L-Glutamic acid of pH 7 at E_{pulse} 0.02 V, t_{pulse} 20ms and scan rate 0.1 V/s.

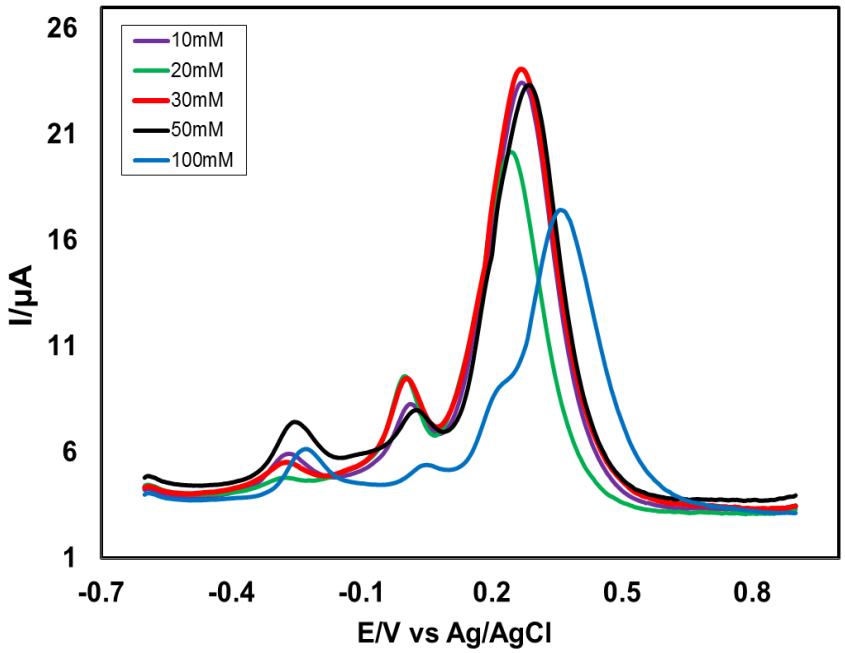

Fig. 4.131: Differential pulse voltammogram (DPV) of composition change of L-Glutamic acid (10, 20 30, 50 and 100 mM) with the fixed composition of 2 mM Catechol in second scan of pH7 at E_{pulse} 0.02 V, t_{pulse} 20ms of GC electrode and scan rate 0.1 V/s.

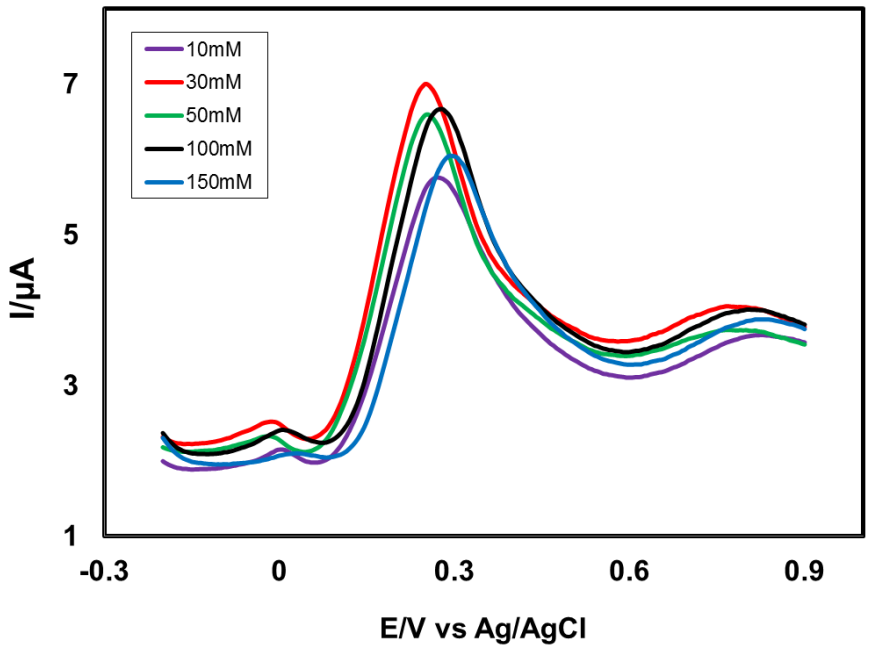

Fig. 4.132: Differential pulse voltammogram (DPV) of composition change of L-Glutamic acid (10, 30, 50, 100 and 150 mM) with the fixed composition of 2 mM Catechol in second scan of pH 7 at E_{pulse} 0.02 V, t_{pulse} 20ms of Pt electrode and scan rate 0.1 V/s.

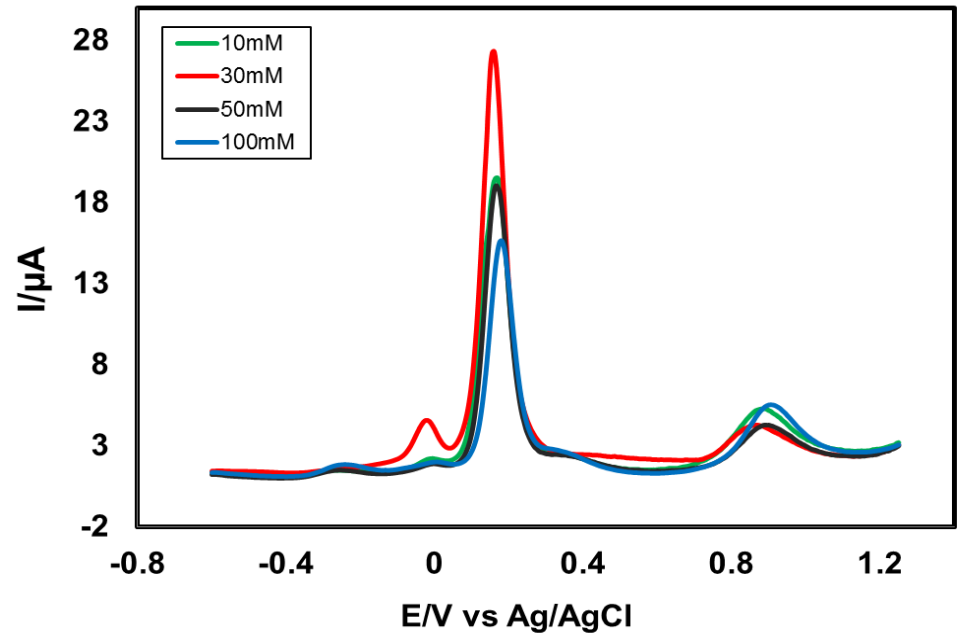

Fig. 4.133: Differential pulse voltammogram (DPV) of composition change of L-Glutamic acid (10, 30, 50 and 100 mM) with the fixed composition of 2 mM Catechol in second scan of pH 7 at E_{pulse} 0.02 V, t_{pulse} 20ms of Au electrode and scan rate 0.1 V/s.

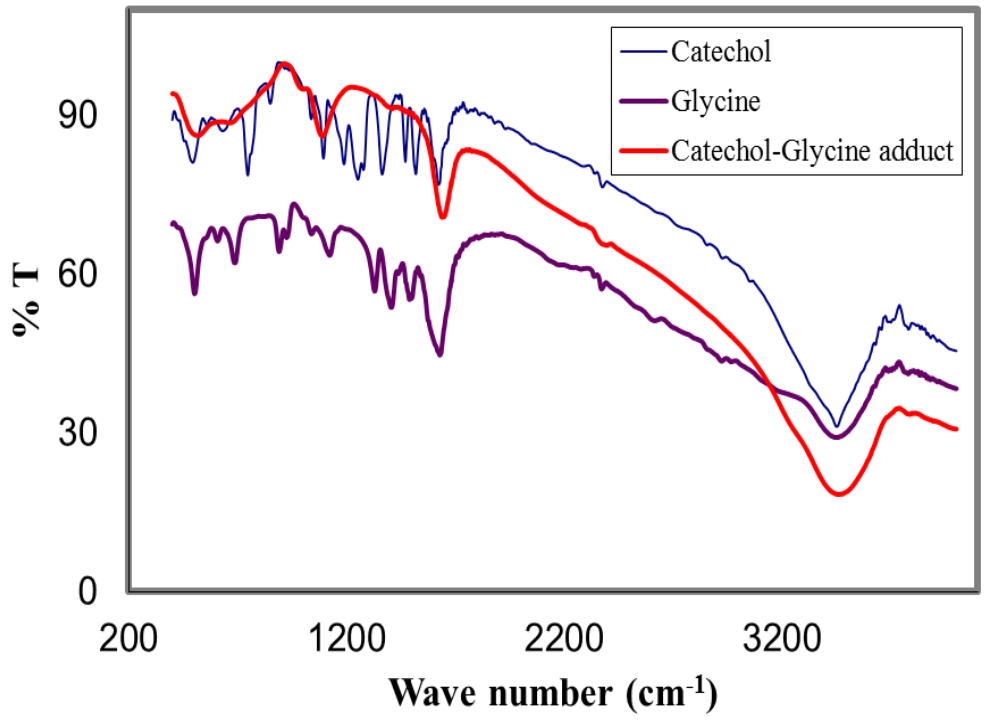

Fig. 4.134: Comparison of FTIR spectra of only Catechol, only Glycine and Catechol-glycine adduct.

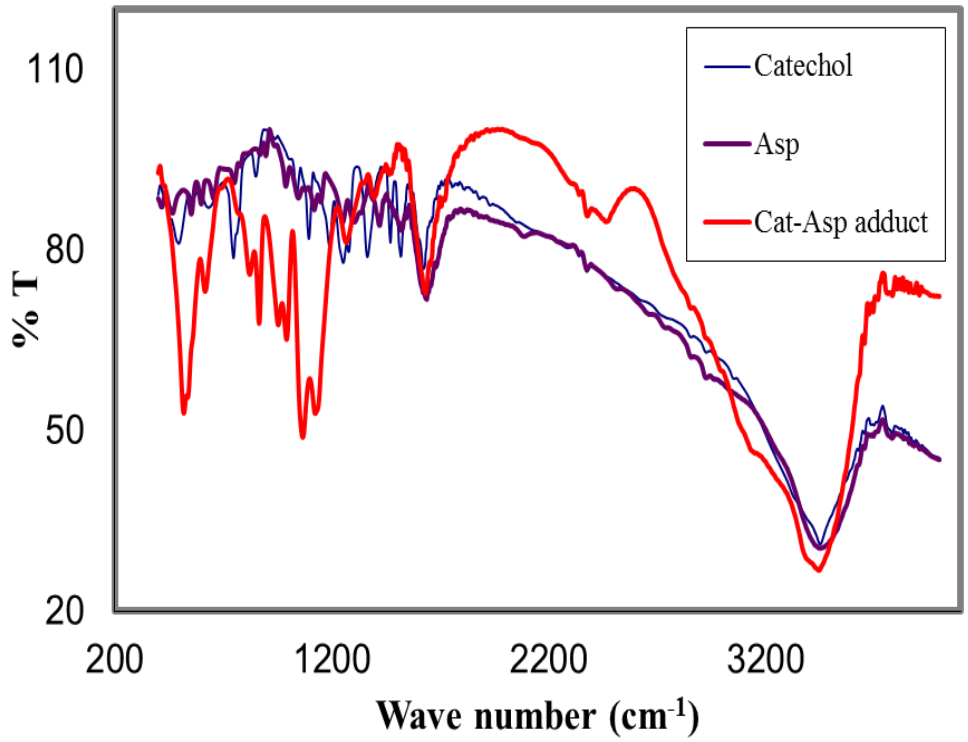

Fig. 4.135: Comparison of FTIR spectra of only Catechol, only L-Aspartic acid (Asp) and Catechol-aspartic acid (Cat-Asp) adduct.

CHAPTER V

Conclusions

Cyclic voltammetry (CV), differential pulse voltammetry (DPV), controlled potential coulometry (CPC) and chronoamperometry (CA) were used to investigate the reaction of electrochemically produced *o*-benzoquinone from the oxidation of Catechol as Michael acceptors with Glycine, L-Aspartic acid and L-Glutamic acid in aqueous solution with various pH, different electrodes and different concentration.

The redox reactions of Catechol are quasi-reversible. The substrate Catechol is electro-active but the studied three nucleophiles are electro-inactive. The products generated from the reaction that undergo electron transfer at more negative potentials than the pure Catechol. The nucleophilic substitution reactions are concentration, pH and electrode dependent. The reaction was mostly favorable in 70 mM Glycine, 70 mM L-Aspartic acid and 30 mM L-Glutamic acid with fixed 2 mM of Catechol in pH 7 of GC electrode at 0.1V/s scan rate. The oxidation reaction of Catechol-amino acid adduct produced via the one step $2e^{-}/2H^{+}$ or two step $1e^{-}/1H^{+}$ process. This also suggests that during the reaction not only electron but also proton are released from the Catechol-amino acid adduct this type of reaction is called proton coupled electron transfer reaction (PCET). For different electrode systems the nature of voltammogram, peak position and current intensity are different. The voltammetric response of GC electrode is better than Au and Pt electrodes.

All the investigated system shows that peak current of both the anodic and the corresponding cathodic peak enhance with the increase of scan rates. The nearly proportionality of the anodic and corresponding cathodic peak suggests that the peak current of the reactant at each redox reaction is controlled by diffusion process. The current function exponentially decreases with enhance of scan rate is ascribed that the nucleophilic addition of Glycine, L-Aspartic acid and L-Glutamic acid occurs through ECE mechanism. During the course of coulometry the electrosynthesized products were generated from Catechol with Glycine, L-Aspartic acid and L-Glutamic acid and the generated products supported by FTIR spectra.

REFERENCES

1. P. Atkines and J. de Paul, 2010, "Physical Chemisty", W. H. Freeman and Co., New York, 9th Ed.

2. R. Banerjee, D. Becker, M. Dickman, V. Gladyshev and S. Ragsdale, 2007, "Redox Biochemistry", willey, New York, 2nd Ed.

3. Golabi, S.M. and Nematollahi, D.P., 1992, Journal of Pharmaceutical and Biomedical Analysis, Vol. 10, p. 1035.

4. http://www.slideshare.net/SihamAbdallaha/electrochemical-method-of-analysis-31352857.

5. Vermeulen, N. P., Bessems, J. G. and Van de Straat, R., 1992, "Drug Metab. Rev", Vol. 24, p. 367.

6. Prescott, L. F., 1996, "Paracetamol (Acetaminophen) a Critical Bibliographic Review", Taylor & Francis Ltd., London, pp. 285–351.

7. Bisby, R.H., Brooke, R. and Navaratnam, S., 2008, Food Chem., Vol. 108, p. 1002.

8. Testa, A. C. and Reinmuth, W.H., 1961, Anal. Chem., Vol. 33, p. 1320.

9. Khalafi, L., and Rafiee, M., 2010, Journal of Hazardous Materials, Vol. 174, p. 801.

10. Briggs, D. E. G., 1999, "Molecular taphonomy of animal and plant cuticles: selective preservation and diagenesis". Biochemical Science, Vol. 7, p. 354.

11. http://en.wikipedia.org/wiki/Catechol.

12. Fahlbusch, K. G., Hammerschmidt, F. J. and panten, J., 2005, "Horst Surburg Flavours and Fragrances" in Ullmann's Encyclopedia of Industrial Chemistry, Wiley-VCH.

13. U. Satyanarayana and U. Chakrapanni, 2006, Biochemistry, Arunabha Sen, books and allied (P) Lro. 3rd Ed, pp. 43-52.

14. Nelson, D. L. and Cox, M. M., 2005, Principles of Biochemistry New York: W. H. Freeman, 4th ed., pp. 127, 675–77, 844, 854.

15. M. Michael, "Principles of Biochemistry", New York: W. H. Freeman, 4th Ed., p. 127

16. "Glycine From Japan and Korea" Retrieved, 2014-06-13.

17. Rossoff, I.S., 1974, “Handbook of Veterinary Drugs”, New York, Springer Publishing Company, p. 28.

18. Physicians’ Desk Reference (PDR) for Nutritional Supplements, 2001, “Medical Economics”, Thomson Healthcare Montvale NJ, 1st Ed., p. 255

19. R. Sapolsky, 2005, "Biology and Human Behavior: The Neurological Origins of Individuality, 2nd edition". The Teaching Company. pp. 19-20

20. http://www.biology.arizona.edu/biochemistry/problem_sets/aa/glutamate.html.

21. Nematollahi, D. and Golabi, S.M., 2000, Journal of Electroanalytical Chemistry, Vol. 481, p. 208.

22. Nematollahi, D. and Forooghi, Z., 2002, Tetrahedron Letters, Vol. 58, p. 4949.

23. Nematollahi, D. and Golabi, S.M., 2001, Journal of Electroanalytical Chemistry, Vol. 13, p. 1008.

24. Nematollahi, D. and Golabi, S.M., 1997, Journal of Electroanalytical Chemistry, Vol. 420, p. 127.

25. Kiani, A., Raoof, J.B. and Ojani, R., 2005, Electroanalysis, Vol. 17, No. 19, pp. 1755–1760.

26. Dowlati, B. and Othman M. R. B., 2011, Int. J. Electrochem. Sci., Vol. 6, pp. 5767 – 5778.

27. Nematollahi, D. and Golabi, S.M., 1996, Journal of Electroanalytical Chemistry, Vol. 405, p. 133.

28. Nematollahi, D. and Golabi, S.M., 1997, Journal of Electroanalytical Chemistry, Vol. 430, p. 141.

29. Nematollahi, D. and Golabi, S.M., 1998, Bulletin of Electrochemistry, Vol. 14, p. 97.

30. Nematollahi, D. and Goodarzi, H., 2001, Iran Journal of Electroanalytical Chemistry, Vol. 510, p. 108.

31. Nematollahi, D. and Goodarzi, H., 1997, Iran Journal of Science and Technology, Vol. 21, p. 121.

32. Shahrokhian, S. and Hamzehloei, A., 2003, Electrochemistry Communications, Vol. 5, p. 706.

33. Grujic, Z., Tabakovic, I. and Trkovnic, M., 1976, Tetrahedron Letters, Vol. 52, p. 4823.

34. Tabakovic, I., Grujic, Z. and Bejtovic, Z., 1983, Journal of Heterocyclic Chemistry, Vol. 20, p. 635.

35. Golabi, S.M, Nourmohammadi, F. and Saadnia, A., 2002, Journal of Electroanalytical Chemistry, Vol. 529, p. 12.

36. Fotouhi, L., Kiani, S.T., Nematollahi, D. and Heravi, M.M., 2007, Journal of Electroanalytical Chemistry, Vol. 10, p. 1002.

37. Colin-Orozco, E., Corona-Avendano, S. and Ramirez-Silva, M. T., 2012, International Journal of Electroanalytical Science, pp. 6097-6105.

38. C.M.A. Brett and A.M.O. Brett, 1993, "Electrochemistry Principles, Methods and Applications", Oxford University Press.

39. M. E. Hossain, 2014, "Electrochemical sensor simultaneous detection and estimation of environmental toxic pollutants", M.Phil Thesis, KUET.

40. http://www.drhuang.com/science/chemistry/electrochemistry/polar.doc.htm.

41. D.A. Skoog, F.J. Holler and T.A. Nieman, 2007, "Principles of Instrumental Analysis", Thomson Brooks/ Cole, 6th Ed., pp. 349-351.

42. https://www.google.com/?gws_rd=ssl#q=Definition+of+electrochemical+cell.

43. P.T. Kissinger and W.R. Heineman, 1996, "Laboratory Techniques in Electroanalytical Chemistry", Marcel Dekker, Inc.

44. C.M.A. Brett and A.M.O. Brett, 1998, "Electroanalysis", Oxford University Press.

45. Chaires, J.B., Dattagupta, N. and Crothers, D.M., 1982, Biochemistry, Vol. 21, p. 3933.

46. Randles, J.E.B., 1948, Transactions of the Faraday Society, Vol. 44, p. 327.

47. Sevcik, A., 1948, Collection of Czechoslovak Chemical Communications, Vol. 13, p. 349.

48. Bott, A.W., 1994, Curr. Seps., Vol. 13, p. 49.

49. Klinger, R.J. and Kochi, J.K., 1981, Journal of Physical Chemistry, Vol. 85, p. 12.

50. Afzal Shah, 2010, "Redox Behavior and DNA Binding Studies of Some Electroactive Compounds", Ph.D Thesis, Department of Chemistry, Quaid-i-Azam University, Islamabad.

51. Nicholson, R.S., 1965, Analytical Chemistry, Vol. 37, p. 135.

52. Matsuda, H. and Ayabe, Y.Z., 1955, Electrochimica Acta, Vol. 59, p. 494.

53. Andrews, L.J., 1954, Chem. Revs., Vol. 54, p. 713.

54. A.J. Bard and L.R. Faulkner, 1980, "Electrochemical Methods, Fundamentals and Applications", John Wiley, New York.

55. Eyring, H., Glasstone, S. and Laidler, K.J., 1939, The Journal of Chemical Physics, Vol. 7, p. 1053.

56. Reinmuth, W.H., 1962, Analytical Chemistry, Vol. 34, p. 144.

57. Laviron, E., 1983, J. Electrochim. Interfac. Electrochim., Vol. 1, p. 148.

58. Polcyn, D.S. and Shain, I., 1966, Analytical Chemistry, Vol. 38, p. 370.

59. Armada, P. G., Losada, J. and Perez, S. V., 1996, "Cation analysis scheme by differential pulse polarography", Vol. 73(6), pp. 544-546.

60. Aoki, K. and Osteryoung, J., 1981, Journal of Electroanalytical Chemistry, Vol. 122, p. 19.

61. Aoki, K. and Osteryoung, J., 1984, Journal of Electroanalytical Chemistry, Vol. 160, p. 335.

62. Flanagan, J.B. and Marcoux, L., 1973, Journal of Physical Chemistry, Vol. 77, p. 1051.

63. Heinze, J., 1981, Journal of Electroanalytical Chemistry, Vol. 124, p. 73.

64. Shoup, D. and Szabo, A., 1982, Journal of Electroanalytical Chemistry, Vol. 140, p. 237.

65. Gavaghan, D.J. and Rollett, J.S., 1990, Journal of Electroanalytical Chemistry, Vol. 295, p. 1.

66. Qian, W., Jin, B., Diao, G., Zhang, Z. and Shi, H., 1996, Journal of Electroanalytical Chemistry, Vol. 414, p. 1.

67. Ikeuchi, H. and Kanakubo, M., 2000, Journal of Electroanalytical Chemistry, Vol. 493, p. 93.

68. Jr. D.K. Gosser, 1993, "Cyclic Voltammetry (Simulation and analysis of reaction mechanisms)", Wiley-VCH, Inc.

69. F.M. Hawkridgein, P.T. Kissinger and W.R.(Eds.) Heieman, 1996, "Laboratory Techniques in Electroanalytical chemistry", Marcel Dekker Inc., New York. 2nd Ed.

70. J. Wang, 1994, "Analytical Electrochemistry", VCH Publishers Inc., New York.

71. E.R. Brown, R.F. Larg, A. Weissberger and B.(Eds.) Rossiter, 1971, Physical Methods of chemistry, Vol.1-Part IIA, Wiley-Interscience, New York.

72. Zhang, J., 1972, Journal of Electroanalytical Chemistry, Vol. 331, p. 945.

73. Nematollahi, D., Afkhami, A., Mosaed, F. and Rafiee, M., 2004, "Research on Chemical Intermediates", Vol. 30, p. 299.

74. Papouchado, L., Petrie, G. and Adams, R. N., 1972, Journal of Electroanalytical Chemistry, Vol. 38, p. 389.

75. Papouchado, L., Petrie, G., Sharp, J.H. and Adams, R.N., 1968, Journal of the American Chemical Society, Vol. 90, p. 5620.

76. Young, T.E., Griswold, J.R. and Hulbert, M.H., 1974, Journal of Organic Chemistry, Vol. 39, p. 1980.

77. Brun, A. and Rosset, R., 1974, Journal of Electroanalytical Chemistry, Vol. 49, p. 287.

78. Stum, D.I. and Suslov, S.N., 1979, Bio. Zika, Vol. 21, p. 40.

79. Rayn, M.D., Yueh, A. and Yu, C.W., 1980, Journal of Electrochemical Society, Vol. 127, p. 1489.

80. Md. Matiar Rahman, 2014, “Electrochemical characterization of biologically important electroactive metal ligand complexes with multi-electron transfer reaction”, M.Phil Thesis, KUET.

81. Kiani A., Raoof, J.B., Nematollahi, D. and Ojania R., 2005, Electroanalysis, Vol. 17 p. 1755.

82. Shahrokhian, S. and Hamzehloei, A., 2003, Electrochem. Commun. Vol. 5, p. 506.

83. Golabi, S.M., Nourmohammadi, F. And Saadnia, A., 2002, J. Electroanal. Chem., Vol. 529, p. 12.

84. Nematollahi, D. and Golabi, S.M., 2000, J. Electroanal. Chem., Vol. 481, p. 208.

85. Mazzini, S., Monderelli, R., Ragg, E. and Scaglioni L., 1995, J. Chem. Soc. Perkin Trans., Vol. 2, p. 285.

86. Pasta, M., Mantia, F.L. and Cui, Y., 2010, Electrochimica Acta, Vol. 55, p. 5561.

87. Rayn, M.D., Yueh, A. and. Yu, C.W., 1980, J. Electrochem. Soc., Vol. 127, p. 1489.